STOCHASTIC MODELLING OF CENTRAL HEATING SYSTEMS

Lars Henrik Hansen

LYNGBY 1997
IMM-PHD-1997-34
ATV Erhvervsforskerprojekt EF 528

IMM

GRUNDFOS

ISSN 0909-3102.
ISBN 87-88306-26-7.

Trykt af IMM - DTU.
Bogbinder Hans Meier.

Preface

This thesis has been prepared at the Department for Mathematical Modelling (IMM, Institut for Matematisk Modellering) at the Technical University of Denmark (DTU, Danmarks Tekniske Universitet), and at Grundfos A/S in partial fulfillment of the requirements for the degree of *Ph.D. in engineering* and the degree *Erhvervsforsker* (a special Danish degree, equivalent to "Industrial Ph.D.").

The thesis is mainly concerned with experimental design and system identification for individual components in water based central heating systems. The main contribution to this field is on the nonlinear dynamic modelling of the following components: pipe, radiator, thermostatic valve and house. Each model is based on prior knowledge, on physical properties and experimental conditions. The estimated parameters are directly the physical model parameters. The model performance of each model has been assessed based on a number of validation methods.

Lyngby, June 16'th, 1997.

Lars Henrik Hansen.

Acknowledgements

This thesis concludes 3 years of research at the Department of Mathematical Modelling at the Technical University of Denmark and at Grundfos A/S in Bjerringbro, Denmark. A lot of people have been involved in one way or another due to the interdisciplinary contents of my work.

First of all I would like to thank my four supervisors, Assoc. Prof., Ph. D. Henrik Madsen, IMM, DTU; Prof., Techn. Dr. Jan Holst, Department of Mathematical Statistics, Lund Institute of Technology, Sweden; Senior Engineer, Ph. D. Pierré Vadstrup and Ph. D. Niels Bidstrup, both from Research and Development, Grundfos A/S, Bjerringbro, Denmark, for guidance and constructive criticism during this work. Further, I would like to thank my supervisor during my stay at the Institute for Systems Engineering and Informatics, Joint Research Center, Ispra, Italy, Hans Bloem for his promotion of physical aspects in relation to the heat dynamics in buildings.

I also want to thank all my colleagues, both at IMM and Grundfos, for a pleasant scientific and social environment, especially the people (former and present) of the Time Series Group at IMM, the Energy Group at Grundfos and my two Grundfos colleagues at DTU, Christian Wolf and Gert Eriksen. I would also like to thank my two Master students Mads R. Schmidt and

Klaus K. Andersen for good discussions, and especially Klaus for his great interest in my test house experiment.

Moreover, I want to thank the people at the Department of Buildings and Energy for their cooperation in connection with the test house experiment, especially Bjarne Saxhof and Jørgen M. Schultz.

Furthermore, I wish to thank the staff at the ISEI, especially Mr. Faedo, for their support during my stay at JRC in Ispra, and Hans Bloem, Anders Lindfors and Bjarke Rasmussen for providing good social experiences.

During my residences at Grundfos, I found good accommodation at "bondegården". For that I wish to thank the Møller family.

As many other authors, I will permanently remember the special support and encouragement of the person closest to me during the final writing; I am deeply indebted to my lovely wife Anca Daniela Hansen, for her patience, willingness to listen, read and for carefully typing large parts of this thesis. Special thank to our four months daughter Bianca Laura for not interfering too much.

Finally, I want to acknowledge the Danish Academy of Technical Sciences (ATV, Akademiet for Tekniske Videnskaber) and Grundfos A/S for the financial support of this work.

Summary

The main objective of the present thesis is to enhance insight into the dynamic properties of water based central heating systems. The procedure is to identify, estimate and verify dynamic models, which can be used for clarification of the level of information in the water based central heating system in a single family house. This will be accomplished through the development of models of the individual components as well as models of combinations of some components with respect to acknowledged physical regularity and observable variations. Special attention is laid on variations linked to the thermal properties of the system.

The central heating system is by nature a nonlinear system. Therefore, the Grey Box modelling method is selected as modelling method. In the second chapter, the theoretical basis for the Grey Box modelling method is presented, including model formulation, estimation method and validation tools. The considerations on experimental design in the third chapter are close related to the modelling method.

To get well defined experimental conditions, two experimental setups are constructed, one of a pipe system and one of a central heating system. The pipe system and the heating system forms together with a low energy test

house the frames for the dynamic modelling. The experimental setups are the main subject of Chapter 4.

The central heating system can be divided into a number of standard components. The thesis is focused on the dynamic modelling and identification of water pipes, radiators, thermostatic valves and of the low energy test house. The formulation of models for these components is based on prior knowledge, e.g. mass and momentum conservation, heat balance and experimental conditions. The formulation of the model, estimation results and model validations for these components are described in Chapter 5, Chapter 6, Chapter 7 and Chapter 8, respectively. The type of the resulting models are lumped parameter models. The modelling of the pipe is based on the fundamental principles of conservation of mass and momentum for incompressible one-dimensional flow in a straight circular pipe. The dynamic radiator model is derived from a partial differential equation, which describes the heat transfer process from the water to the ambient air as the cooling of a one-dimensional water flow. The dynamic model of the thermostatic valve is based on a macroscopic modelling approach, since the microscopic modelling approach (i.e. using the second law of Newton) yields an model with ambiguous number of parameters. Finally, the modelling of the test house is concentrated on thermal dynamics. The test house model contains two rooms with a water based central heating system as heating installation.

Considerations on system simulation of the central heating system are presented in Chapter 9. Moreover, a solution to a particular simulation problem for the selected simulation tool is described.

Sammenfatning

Hovedformålet med nærværende Ph.D.-afhandling er at udvide indsigten i de dynamiske egenskaber for vandbaserede centralvarmeanlæg. Proceduren er at identificere, estimere og verificere dynamiske modeller, som kan anvendes ved afklaring af informationsinholdet i det vandbaserede centralvarmeanlæg for énfamiliehuse. Dette vil blive gjort gennem udviking af modeller for de enkelte komponenter såvel som modeller for kombinationer af nogle komponenter med hensyn til erkendte fysiske lovmæssigheder og de observerbare variationer. Speciel opmærksomhed tillægges de variationer, som hidrører fra systemets termiske egenskaber.

Centralvarmeanlægget er i sin natur et uliniært system. Derfor er Grey Box modelleringsmetoden valgt som modelleringsmetode. Det teoretiske grundlag for Grey Box modelleringsmetoden er præsenteret i Kapitel 2, inklusiv model formulering, estimationsmetode og valideringsværktøjer. Betragtningerne angående eksperimentelt design i tredie kapitel er tæt relateret til identifikationsmetoden.

For at sikre veldefinerede eksperimentelle betingelser er to forsøgsopstillinger konstrueret, en for et rørsystem og en for et centralvarmeanlæg. Rørsystemet og varmeanlægget udgør sammen med et lavenergitesthus rammerne

for den dynamiske modellering. Forsøgsopstillingerne er hovedgenstand for Kapitel 4.

Centralvarmeanlægget kan opdeles i et antal standardkomponenter. Afhandlingen er fokuseret på den dynamiske modellering og identifikation af vandrør, radiatorer, termostatventiler og på lavenergitesthuset. Modelformuleringen for disse komponenter er baseret på a priori viden, for eksempel masse- og momentbevarelse, varmebalance og eksperimentelle betingelser. Modelformuleringen, estimationsresultater og modelvalidering af disse komponenter er beskrevet i henholdsvis Kapitel 5, Kapitel 6, Kapitel 7 og Kapitel 8. Typen af de opstillede modeller er konsentrerede parametermodeller. Modelleringen af vandrøret er baseret på de fundamentale principper om bevarelse af masse og moment for inkompressibelt endimensionelt flow i et lige cirkulært rør. Den dynamiske radiatormodel er afledt fra en partiel differentialligning, der beskriver varmetransporten fra vandet i radiatoren til omgivelserne som afkølingen af et endimensionelt vand flow. Den dynamiske model af radiatortermostatventilen er baseret på en makroskopisk modelleringsmetodik, idet den mikroskopiske modelleringsmetodik (dvs. ved brug af Newtons 2. lov) fører til en model med et omfattende antal parametre. Modelleringen af lav energi huset er konsentreret omkring de termiske dynamikker. Husmodellen består af to rum med et vandbaseret centralvarmeanlæg som varmningssystem.

Betragtninger angående systemsimulering af centralvarmeanlægget er præsenteret i Kapitel 9. Endvidere er en løsning til et specifikt simuleringsproblem for det valgte simuleringsværktøj beskrevet.

Parts of this thesis have been/will be published in:

- Hansen, L. H., Bidstrup, N., Madsen, H., Vadstrup, P., and Holst, J. (1995). A hydraulic simulink model of the heating system in a single family house. In Langemyr, L., editor, *Nordic Matlab Conference '95*, volume II, pages 114–118. Computer Solutions Europe AB, Sweden.
- Hansen, L. H. (1996). Dynamic Analysis of a low Energy Test House and a Central Heating System. Technical Report No. 20, Department of Mathematical Modelling, the Technical University of Denmark.
- Hansen, L. H., Madsen, H., Holst, J., Bidstrup, N., and Vadstrup, P. (1997a). A Dynamic Nonlinear Model of a Thermostatic Valve. In *Clima 2000.*
- Sadegh, P., Hansen, L. H., Madsen, H., and Holst, J. (1997). Maxmin Input Design for Linear Dynamic Systems. *Journal of Information & Optimization Sciences.* Accepted and in print.
- Hansen, L. H., Madsen, H., Holst, J., Bidstrup, N., and Vadstrup, P. (1997b). A Dynamic Nonlinear Model of Turbulent Flow a Pipe. *Building and Environment.* Submitted.

Contents

Glossary

This section contains the most important symbols and abbreviations used in this thesis.

Abbreviations

CTLSM : Continuous Time Linear Stochastic Modelling.
CV : Control Volume.
EC : Electric Cooker.
mWc : Meter Water column, alias 0.1 Bar.
PRBS : Pseudo Random Binary Sequence.
PRUS : Pseudo Random Uniformly distributed Sequence.

Operators

B Backward shift operator.
d Differential operator.
∂ Partial differential operator.
Δ Difference operator.
s Laplace operator.

Notation

A vector will be denoted by underlining and a matrix by bold face.

$\{\cdot\}$	Sequence.
$C(\cdot)$	Auto or crosscovariance function.
$\mathcal{D}_{\mathcal{M}}$	Closed subset of values over which the parameter vector $\underline{\theta}$. ranges in the model structure $\mathcal{M}$.
$I(\cdot)$	Periodogram.
$\mathcal{I}(\cdot)$	Cumulated periodogram.
$J(\cdot)$	Scalar valued loss function.
$\ell(\cdot)$	Scalar valued criterion function.
$\Lambda(B)$	Stable linear filter.
k	Sample number at time $t = kT_s$.
$\mathcal{L}(\cdot)$	Likelihood function.
$\mathcal{M}(\underline{\theta})$	Particular model corresponding to $\underline{\theta}$.
$\mathcal{M}^*$	Set of models.
$p(\cdot)$	Probability density function.
$\rho(\cdot)$	Auto or crosscorrelation function.
T_{op}	Operation point of state T.
$\overline{T}$	Deviation of state T from the operation point T_{op}.
$\tilde{\mathcal{Z}}$	Auxiliary thermal zone.

Symbols

a	Characteristic parameter for the thermostatic valve.
α	Heat diffusivity.
A	Area.
$\boldsymbol{A}$	System matrix.
b	Characteristic parameter for the thermostatic valve.
β	Angle.
$\boldsymbol{B}$	Input matrix.
c	Specific heat capacity.
C	Thermal capacity.
$\boldsymbol{C}$	Output matrix.
$\mathcal{C}$	Overall thermal capacity.
d	Diameter or distance/width.
$\boldsymbol{D}$	Direct output matrix.

$\mathcal{D}$	Data set.
e	Measurement noise or pipe roughness.
ε	Prediction error.
E	Energy.
f	Frequency.
F	Force.
F	Function describing the evaluation of the state variables.
g	Acceleration of gravity.
G	Function describing the entrance of noise into a system.
$\mathcal{G}$	Transfer function from input to output.
$\boldsymbol{G}$	System noise input matrix.
h	Convective or conductive coefficient.
H	Heat transmittance.
H	Function describing the observed output of a system.
$\mathcal{H}$	Transfer function from noise to output.
$\boldsymbol{H}$	Hessian matrix.
$\mathbf{I}$	Identity matrix.
K	Valve constant or gas constant.
$\boldsymbol{K}$	Kalman gain matrix.
κ	Exponent of flow.
l	Length or height.
λ	Friction factor or heat conductivity.
L	Hydraulic inductance.
m	Mass flow.
M	Mass.
$\mathcal{M}$	Model set, model structure.
$\boldsymbol{M}$	Fisher's information matrix.
n	Exponent or length of a shift register.
np	Dimension of parameter vector $\underline{\theta}$.
nu	Dimension of input vector $\underline{U}$.
nx	Dimension of state variable vector $\underline{X}$.
ny	Dimension of output vector $\underline{Y}$.
ν	Kinematic viscosity.
N	Number of data points.
$\mathcal{N}$	Approximation order.
p	Pressure.
ψ	Heat flux.

P	Probability measure.
$\boldsymbol{P}$	Variance matrix for one step prediction.
Φ	Power.
q	Volumetric flow.
r	Radius.
ρ	Density.
R	Hydraulic or thermal resistance.
$\mathbf{R}$	Euclidean Space.
$\boldsymbol{R}$	Conditional variance matrix.
$\mathcal{R}$	Overall thermal resistance.
Re	Reynolds number.
s	Spatial coordinate.
σ	Standard deviation.
$\boldsymbol{\Sigma}$	Covariance matrix.
t	Time.
τ	Time constant.
θ	Angle.
$\underline{\theta}$	Parameter vector.
T	Temperature or fundamental period of a PRBS-signals.
T_s	Sampling time.
u	Reference signal or input signal.
$\underline{U}$	Vector of inputs.
V	Volume.
w	Fluid velocity.
w	Mean fluid velocity.
$\underline{W}$	Vector of standard Wiener processes.
x	Spatial coordinate.
X	Relative temperature.
$\underline{X}$	Vector of state variables.
y	Model output or spatial coordinate.
$\underline{Y}$	Vector of outputs.
z	Spatial coordinate.
$\mathcal{Z}$	Thermal zone.
ω	Probability space variable or angular frequency.
Ω	Sample space of possible outcomes.

Chapter 1

Introduction

The first section of this chapter provides the background for the present thesis. A short presentation of water based central heating systems is given in the second section. State of the art considerations are provided in the third section. Some industrial aspects are reviewed in the fourth section, while the fifth section is devoted to an outline of the thesis.

1.1 Background

The project was initialized by Grundfos A/S due to the wish to improve the pump system in water based central heating systems, such that the total efficiency of the system, in which the pump is placed, is optimized in benefit for resources, environment and economy. The natural basis for an advanced pump control is a dynamic model of the central heating system.

The presented work is a part of a larger project containing the projects: EF440, EF441, EF451, and EF528. The total project has been financially supported by the Danish Academy of Technical Sciences (ATV, Akademiet for Tekniske Videnskaber) and Grundfos A/S.

It is natural to concentrate the work on circulating pumps and other central heating components, as a big part of the pump market of Grundfos is directed towards heating of single family houses.

The central heating system can be divided into standard components, such as pipes, valves, radiators, pumps, thermostatic valves, boilers and/or heat exchangers, buildings etc. A building is in some sense also a component of the heating system, since it forms the surroundings/environment, in which the central heating system is placed. The heating system, that is addressed in this thesis, is further described in Section 1.2.

The purpose of this work is to get an improved knowledge of the dynamic properties of the individual components and the dynamic interactions between the components. This demands a profound understanding of the dynamics of each single component acting together with the pump. One potential use of the developed dynamic models is of course to investigate how to control the water based central heating system in a more optimal way. Another potential use is the ability to simulate the behaviour of a single component or a complete system.

The dynamic modelling and identification of the central heating system and of its components will be based on the Grey Box modelling method. This modelling method has a number of advantages compared to the conventional methods (White Box and Black Box methods). For the Grey Box modelling method, the model class consists of stochastic differential equations and therefore nonlinear system structures are directly modelled. Moreover, it is possible to use prior knowledge in the model formulation. Examples of prior knowledge are handbook data on physical properties and knowledge about the experimental conditions. As illustrated in Figure 1.1, the "greyness" of model is a tradeoff between the use of prior knowledge and the information in measurement data applied during the identification of the model. The two modelling extremes, white or black, are achieved, when the weight is put completely on prior knowledge or on measurement data, respectively. The Grey Box modelling method is described in Chapter 2.

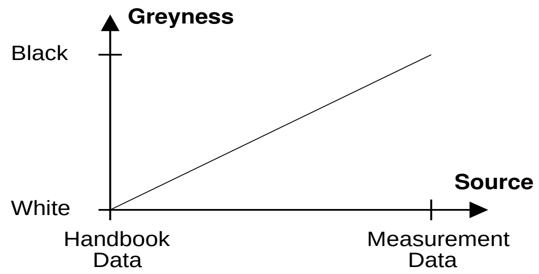

Figure 1.1. *Interpretation of the "greyness" of a model.*

A couple of experimental setups constitutes the basis for the generation of measurement data for the dynamic modelling of water based central heating systems. These setups for pipes, central heating installation and house heating form suitable simplifications for a "real" central heating system, as described in Chapter 4.

1.2 Water based Central Heating Systems

The term "water based central heating system" is quite ambiguous. It covers a set of different heating systems, where water is used to distribute the heat. This section is devoted to a short description of the considered type of central heating system.

A sketch of a water based central heating system for a single family house is shown in Figure 1.2. The purpose of this figure is to give an impression of a typical central heating system in a single family house. Although the sketch only shows one of many possible realizations, it illustrates the essential structure for this type of heating system. The heating system sketched in the figure consists of a heating unit, heat distribution network, hot water tank, circulating pump and a expansion tank.

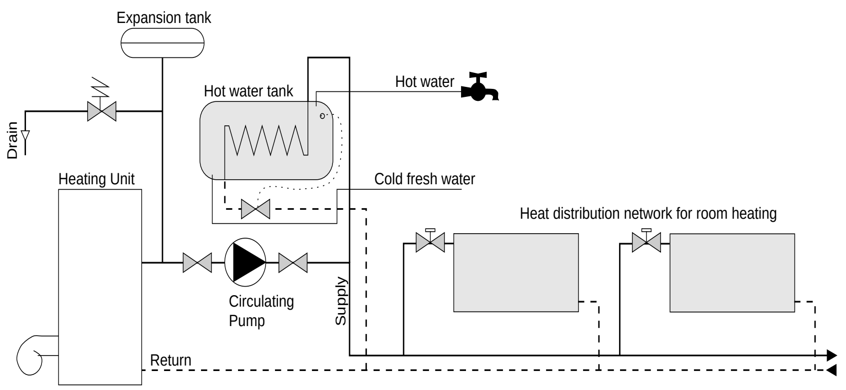

Figure 1.2. *Sketch of a typical water based central heating system.*

The considered heating unit in Figure 1.2 is an oil-fired (or gas, straw, wood) furnace. Another possible heat source is district heating. In this case the heating unit is replaced by a heat exchanger.

The considered heat distribution network is a *two* string connected network with direct return. The heat distribution network can also be build as a *one* string connected network. Both types are commonly used. The one string connected distribution network is cheaper in pipe materials, whereas the dimensioning of the two string connected distribution network is easier to perform. The heat distribution network consists of pipes, radiators and thermostatic valves. When hot water is passed through a radiator, some of the heat in the hot water is transfered to the air, since the air temperature usually is lower than the water temperature. The objective of the thermostatic valves is to maintain a certain air temperature. Thus, the thermostatic valve is sensoring the air temperature and it controls the flow of hot water through the radiator. In this way, the heat supply is controlled.

The hot water tank serves as domestic hot water supply (storage heating). If the temperature in the hot water tank goes below a defined temperature level, a valve opens and hot water from the central heating system heats the water in the hot water tank (through the heat exchanger unit inside of the water tank), until the hot water tank temperature reaches a temperature level above the set point. A modern version of the hot water tank is direct heating. A heat exchanger is connected to the central heating system (instead of the hot water tank). Cold fresh water is directly heated, when passed through a heat exchanger.

Most frequently, the circulating pump is placed together with the heat source in a boiler room. The purpose of the circulating pump is to establish a certain hydraulic pressure in the heating system, in order to provide an operating pressure for the thermostatic valves and to ensure thermal comfort. By the introduction of a circulating pump, the water is forced to circulate (as long as a heat demand is present).

The water based central heating system typically operates at 1 Bar overpressure, hence an expansion tank is needed. The purpose of the expansion tank is to stabilize the pressure in the system, to avoid cavitation and to interact pressure variations, due to temperature dependent water volumetric variations. If the expansion tank cannot manage a certain pressure, the pressure will be unloaded through a spring loaded valve into a drain.

Larger networks may also contain string valves. The purpose of these valves is to maintain a certain pressure in the network (as the thermostatic valves demand a certain operating pressure), or to limit the water flow to a certain level.

1.3 State of the Art

Models of the individual components in the water based central heating system are available today. However, a complete model of the dynamic performance of this system, which supports optimal design of the incorporated controllers, is not yet available. In this section, some references for existing models are reviewed and the contributions of the present work are pointed out. These references are further discussed in the respective chapters.

A dynamic model of a boiler is presented in *(Lawaetz and Bøhm, 1985)*, while dynamic models of heat exchangers can be found in e.g. *(Jonsson, 1990)*, *(Andersson, 1993)* and *(Wollerstrand, 1993)*. The modelling of circulating pumps is considered in e.g. *(Pfleiderer, 1961)*. These components are not modelled in the present thesis.

(Aggerholm, 1983) is concerned with a modelling approach of heat distribution networks based on one-dimensional stationary incompressible water flow and stationary heat dynamics. Compressible flow in pipes is the issue in *(Chaudhry, 1987)*.

Static radiator models are the subject of *(Weber, 1970)* and *(Johansen et al., 1979)*, while a dynamic model radiator model used for simulation is presented in *(Paulsen and Gundtoft, 1985)*.

The thermostatic valve is described in *(Gammelby, 1974)*, *(Frederiksen, 1977)* and *(Svensson, 1978)*, while a dynamic model for simulation is considered in *(Kariž et al., 1989)*.

Dynamic models of the heat transfer in buildings and house heating are presented in *(Sonderegger, 1978)*, *(Madsen et al., 1990)* and *(Bloem, 1994)*.

The main contribution of the present thesis to the modelling of the water based central heating system is on the area of identification and verification of dynamic models. The one-dimensional stationary incompressible water flow considerations in *(Aggerholm, 1983)* is extended with a dynamic model for one-dimensional incompressible water flow in pipes. The applicability of a dynamic radiator model derived from a partial differential equation for the cooling process of a one-dimensional water flow suggested in *(Paulsen and Gundtoft, 1985)* is investigated. A new dynamic model for the thermostatic valve is established. The modelling principles of *(Sonderegger, 1978)* are

applied to a house with a water based central heating system as heating installation.

1.4 Industrial Aspects

The main area of Grundfos is development and production of pumps, motors and pump systems. Grundfos has developed advanced pump control units and established a technologically basis in the areas of power electronics, control algorithms, IC-design, system analysis and power hybrid technology. This knowledge, combined with the experience from the pump business, opens the possibility of using more advanced methods to control the central heating system.

In 1990 Grundfos had developed the frequency converter module X99. With this module it became possible to optimize the pump and the pump system performance. The X99 module has been further developed, and today Grundfos is producing pumps with built-in control units, that can realize a proportional relation between the flow and the pump pressure. An idealized pump characteristic (for three pump speeds) and the proportional control are illustrated in Figure 1.3.

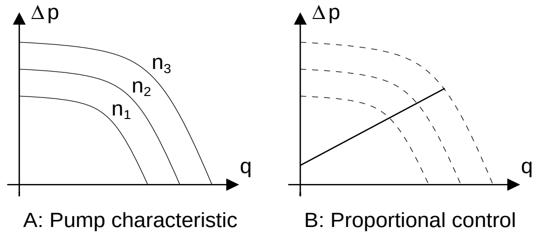

Figure 1.3. *Natural pump characteristic versus proportional control.*

In principle the pump control can be performed after any prescribed relation. Thus, an important question emerges: if it is possible, how should this relation be shaped to achieve an optimal performance of the central heating system?

The main vision of Grundfos for the future pump concept is an intelligent pump, which extracts as much information from the central heating system as possible. This information provides a possible optimization of the central heating system with respect to energy consumption as well as to thermal comfort. A dynamic model of the central heating system is of course an important prerequisite in the development of future pump systems.

Not only Grundfos can benefit from this work. As it is today, every component in the central heating system is individually optimized – even though, this is not necessarily globally optimal. Based on a dynamic model of the central heating system, the properties of a single component and its interaction with its surroundings, can be optimized in such a way that, not only the efficiency of the particular component is optimized, but also the overall efficiency of the central heating system is considered.

1.5 Outline of the Thesis

The main issue of this thesis is dynamic modelling in continuous time of the following central heating system components: pipe, radiator, thermostatic valve and house, and the interactions between these components. Since the central heating system by nature is a nonlinear dynamic system, a Grey Box modelling technique is used. The modelling of the components are based on lumped parameter descriptions in order to keep the models simple. Another attractive feature of the Grey Box modelling methods is that, the parameters in the dynamic models can be estimated directly in continuous time.

Chapter 2 (Grey Box Modelling). This chapter gives a survey of the Grey Box modelling techniques based on stochastic differential equations. The estimation method, which is a maximum likelihood method, is described. Finally a collection of validation methods for the parameter estimates and the performance of model performance are presented.

Chapter 3 (Experimental Design). This chapter deals with basic ideas in experimental design for dynamic systems, i.e. how to design an experiment (e.g. input signals) which gives as much information as possible about the system. Also the problem of identifiability is addressed, together with some considerations on sampling, filtering and subsampling.

Chapter 4 (Experimental Setups). In this chapter three experimental setups considered in this study are described. The purpose of these setups are to form a basis for the system identification of the central heating system components. The first experimental setup is a pipe construction, which is used in connection with the pipe modelling. The second experimental setup is a small mobile water based central heating system, while the third experimental setup is a low energy test house with the experimental setup of the central heating system as heating installation.

The chapters 5, 6, 7 and 8 describe the modelling of the central heating components: pipe, radiator, thermostatic valve and house, respectively. The structure of these chapters follow the general concept of the Grey Box modelling method. The established models are gathered in Model Summaries throughout these chapters.

Chapter 5 (Pipe Modelling). This chapter deals with the dynamic modelling of a straight circular water pipe. Based on physical properties as incompressible flow and conservation of mass and momentum, a nonlinear model for the pipe flow is established. The experimental setup and a set of measurement data are analyzed. The parameters of the model are estimated and the model is verified for turbulent flow.

Chapter 6 (Radiator Modelling). In this chapter radiator modelling is considered. Two radiator dynamic models are presented and a third model is described. The lumped parameter model of the radiator, selected for identification, is derived from a partial differential equation for the cooling of a one-dimensional water flow. It is shown that the selected radiator model has a well known static radiator model as special case.

Chapter 7 (Thermostatic Valve Modelling). In this chapter the modelling of the thermostatic valve is presented. It is shown that a model based on the second law of Newton leads to a model with many parameters. From a structural identifiability point of view, this model is too complex. Therefore a macroscopic modelling approach is applied. The interaction between this macroscopic thermostatic valve model and static water flow is analyzed.

Chapter 8 (House Modelling). This chapter is concerned with the dynamic modelling of the heat transfer in the low energy test house. The experimental setup of the water based heating system is used as heating installation. The house model consist of a two room model, where symmetry considerations are used to reduce the number of model parameters. Moreover, three models of the heat transfer from the radiators to the ambient are considered. One of these models is used for estimation.

Chapter 9 (Central Heating System Simulation). In this chapter some considerations on simulation of central heating systems are presented. The selected simulation tool is Simulink. A solution to a particular simulation problem in Simulink is presented.

Chapter 2

Grey Box Modelling

Recently, a new modelling method has been developed, namely the Grey Box modelling method, which combines and uses the best properties of the conventional methods. Since the Grey Box modelling approach is used throughout the thesis, this chapter offers a short introduction to the basic ideas of this modelling method.

The first section reviews some aspect of system identification and the procedure of the Grey Box modelling method is presented. The second section deals with the applied model class, which consists of stochastic differential equations, while the third section is concerned with the evaluation of these stochastic differential equations. The applied estimation method is based on the maximum likelihood method, as presented in the fourth section, while the Kalman filter, which is an important tool for the applied estimation method, is described in the fifth section. A couple of model validation methods for verification of parameter estimates and model performance are described in the sixth section.

2.1 Modelling and System Identification

Modelling/system identification can be characterized as the methodology of mathematical modelling of a system, based on experimental data. The modelling method is an iterative process consisting of three steps:

1. Identification – specification of the model structure etc.
2. Estimation – of the parameters of the model.
3. Model validation – does the model perform adequate, if "no" goto 1.

Unfortunately, two slightly different interpretations of the term "system identification" exist, one is related to statistics, time series analysis and signal analysis, while the other is related to control engineering. The modelling method presented above is called system identification in the control engineering society. Meanwhile, the other societies are using system identification for the first step in the modelling method. In this context the latter interpretation is considered.

Depending on the use of prior knowledge about the system, the modelling approach can be classified in two extremes, as illustrated in Figure 1.1:

- White Box modelling. The model structure is known and defined by physical knowledge about the system and the parameters are deterministic.
- Black Box modelling. The model structure is unknown and prior knowledge is very humble. The optimal parameters and the optimal model structure are usually found as the combination of parameters and model structure, which offers the best input-output description, i.e. measured by statistical methods on the residuals etc. The advantage of Black Box modelling is that it does not require prior knowledge. The disadvantage is the lack of physical interpretation of the identified model structure and the estimated parameters.

For further reading on Black Box modelling refer to *(Box and Jenkins, 1976)*, *(Ljung, 1987)* or *(Söderström and Stoica, 1989)*.

The modelling procedure of the Grey Box modelling method is sketch in Figure 2.1. The "purpose" of the modelling influences all the modelling procedure. Examples of different purposes are: prediction, simulation, fault detection and system control. The model structure characterization is equivalent to the (system) identification. Experimental design is related to the determination of the interesting parameters and to the intended use of the model. The rest of the figure is self explaining.

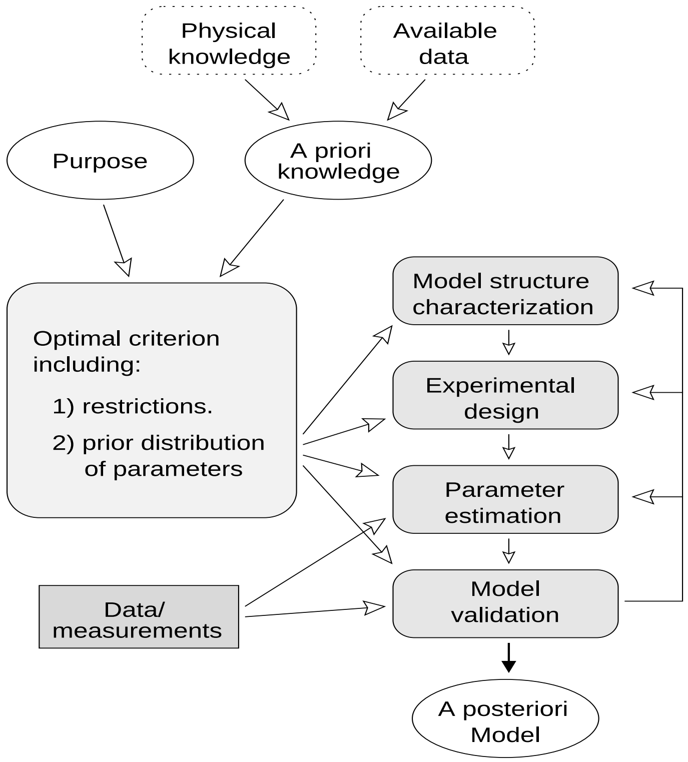

Figure 2.1. *Grey Box modelling method (Adapted from (Melgaard, 1994)).*

The program package CTLSM is an estimation tool based on the maximum likelihood method (as estimation method) and on stochastic differential equations (as model class) *(Melgaard and Madsen, 1993; Melgaard, 1994)*). Additionally, a number validation methods are included in this tool.

Since CTLSM is applied as estimation tool throughout the thesis, the basic principles of this tool are presented in the following sections.

2.2 Stochastic Differential Equations

A conventional way to model a physical system is to express the prior knowledge in a set of differential equations, based on e.g. mass and momentum conservation. The modelling usually leads to (i.e. it can be formulated as) a set of ordinary differential equations:

$$d\underline{X}(t) = \mathrm{F}(\underline{X}(t), \underline{U}(t), t)\, dt, \qquad \underline{X}(0) = \underline{X}_0 \tag{2.1}$$

where $\underline{X}$ denotes a vector of system states (the state variables) and $\underline{U}$ the input vector (e.g. control inputs). F is a function, which describes the evolution of the physical system states. The initial state of the physical system is defined by $\underline{X}_0$.

The basic idea of the Grey Box modelling approach is to exploit both prior knowledge about the system and properties of the measurement data in the formulation of the model for the system. Thus, adding a stochastic term to (2.1), a set of stochastic differential equations is obtained. The class of stochastic differential equations, which is relevant for the modelling of the central heating system, is of the general form:

$$d\underline{X}(t) = \mathrm{F}(\underline{X}(t), \underline{U}(t), \underline{\theta}, t)\, dt \;+\; \mathrm{G}(\underline{U}(t), \underline{\theta}, t)\, d\underline{W}(t), \;\; \underline{X}(0) = \underline{X}_0 \tag{2.2}$$

where $\underline{X} \in \mathbf{R}^{nx}$ is the state variable vector, $\underline{U} \in \mathbf{R}^{nu}$ denotes the input vector, $\underline{\theta} \in \mathbf{R}^{np}$ the parameter vector and $\underline{W}$ is a nx-dimensional Wiener

process with independent increments, zero mean and incremental covariance matrix $\mathbf{\Sigma}_W$. Function F still describes the evolution of the state variables $\underline{X}$, while function G describes how the variation generated by the Wiener process $\underline{W}$ enters the system.

By the introduction of the stochastic term $\underline{W}$ in (2.1), the set of ordinary differential equations is turned into the set of stochastic differential equations (2.2). But also the state variable $\underline{X}$ is affected and it is turned into a set of stochastic processes.

In order to characterize a stochastic process $\{\underline{X}(t)\}$, consider the probability space $(\Omega, \mathcal{F}, P)$, which consists of a sample space Ω of possible outcomes, a σ-algebra $\mathcal{F}$ of subsets of Ω called events and a probability measure P, as described *(Madsen, 1995; Øksendal, 1995)*. The probability measure P assigns a probability $P(\mathcal{F}_j)$ to each event $\mathcal{F}_j$ in $\mathcal{F}$. Thus, a stochastic process $\{\underline{X}(t)\}$ is a collection:

$$\underline{X}(t, \omega), \qquad \omega \in \Omega, \qquad t \in J \tag{2.3}$$

of random variables, which is called a stochastic process with time set J and state space $\mathbf{R}^{nx}$. For a fixed time, $\underline{X}(t, \cdot)$ corresponds to a stochastic variable, while for fixed $\omega \in \Omega$, $\underline{X}(\cdot, \omega)$ corresponds to a realization of the process. $\underline{X}(\cdot, \omega)$ is also called the sample path or the trajectory.

The Wiener process is an example of a stochastic process. The mathematical properties of a nx-dimensional Wiener process $\{\underline{W}(t), t \geq 0\}$ are:

1. $\underline{W}(0) \equiv \underline{0}$.
2. $\underline{W}(t) \in N(\underline{0}, t\, \mathbf{\Sigma}_W)$ for any $t \geq 0$, i.e. the increment $\underline{W}(t_2) - \underline{W}(t_1)$ for any $0 \leq t_1 \leq t_2$ is normally distributed with mean:

$$\mathrm{E}[\underline{W}(t_2) - \underline{W}(t_1)] = \underline{0} \tag{2.4}$$

and variance:

$$\mathrm{Var}[\underline{W}(t_2) - \underline{W}(t_1)] = (t_2 - t_1)\mathbf{\Sigma}_W \tag{2.5}$$

3. $\underline{W}_t$ has independent increments, i.e. for any $0 \leq t_1 \leq t_2 \leq t_3$:

$$\text{Cov}[\underline{W}(t_3) - \underline{W}(t_2), \underline{W}(t_2) - \underline{W}(t_1)] = \mathbf{0} \tag{2.6}$$

Further details can be found e.g. *(Kloeden et al., 1991; Melgaard, 1994)*.

As described in *(Madsen and Melgaard, 1991)*, there are several reasons for the introduction of the noise term:

- Modelling approximations – e.g. due to simplifications, linearization or unmodelled system properties.
- Unrecognized or unmodelled inputs.
- Noise corrupted measurements of the inputs. In this case, the measured inputs are regarded as the actual input to the system, while the deviations from the "true" input are described by $\underline{W}$.

The model formulation in (2.2) is applicable for a range of physical systems. If function G is extended with a dependency of the state variable, also financial systems can be modelled *(Nielsen et al., 1997)*.

2.3 Stochastic Integrals

The price to pay for the good modelling properties of the Grey Box modelling method is a rather complex statistical and mathematical treatment of the model and the data. One of the issues is how to perform a stochastic integration.

As described in *(Kloeden et al., 1991)*, the sample paths of a Wiener process are continuous, but they are not differential in t for any $t \geq 0$ with probability 1. Hence, in order to handle the stochastic differential equations, it is necessary to use other integral concepts than that defined by the standard

Riemann integral. An appropriate stochastic calculus is defined by the Itô stochastic integral.

Consider the one-dimensional stochastic differential equation:

$$dX(t) = \mathsf{a}(t, X(t))\, dt \;+\; \mathsf{b}(t, X(t))\, dW(t) \tag{2.7}$$

where a is a drift coefficient and b is a diffusion coefficient. The stochastic differential equation (2.7) can also be written as the following integral equation:

$$\begin{aligned} X(t,\omega) \;&=\; X(0,\omega) + \int_0^t \mathsf{a}(s, X(s,\omega))\, ds \\ &\quad + \int_0^t \mathsf{b}(s, X(s,\omega))\, dW(s,\omega) \end{aligned} \tag{2.8}$$

where the first integral is a standard Riemann integral for each $\omega \in \Omega$ and the second integral is an Itô stochastic integral.

The Itô stochastic integral is defined as the mean-square limit of the left-hand rectangular approximation:

$$\sum_{j=0}^{N-1} \mathsf{b}(t_j, W(t_j,\omega))(W(t_{j+1},\omega) - W(t_j,\omega)) \tag{2.9}$$

for all partitions $0 \leq t_0 \leq t_1 \leq \cdots \leq t_N = t$ as the maximum step size $\max_j(t_{j+1} - t_j) \to 0$.

More details on the numerical methods for stochastic differential equations can be found in *(Kloeden and Platen, 1989)* or *(Kloeden et al., 1991)*.

2.4 Estimation Method

In Section 2.2, the following nonlinear model structure was introduced:

$$d\underline{X}(t) = \mathrm{F}(\underline{X}(t), \underline{U}(t), \underline{\theta}, t)\, dt + \mathrm{G}(\underline{U}(t), \underline{\theta}, t)\, d\underline{W}(t), \quad \underline{X}(0) = \underline{X}_0 \tag{2.10}$$

where $\underline{X}$ is a vector of state variables, etc. The observations from this model are described by:

$$\underline{Y}(k) = \mathrm{H}(\underline{X}(k), \underline{U}(k), \underline{\theta}, k) + \underline{e}(k) \tag{2.11}$$

where H is a function describing the output relations, k denotes the sample number and $\underline{e}$ the measurement noise, which is assumed to be normally distributed noise with mean $\underline{0}$ and covariance $\mathbf{\Sigma}_e(k)$. In the case of equidistant sampling with sampling time T_s, the time t and the the sample number k are related as $t = kT_s$.

In the identification framework of *(Ljung, 1987)* a model structure is denoted by $\mathcal{M}$ and a particular model by $\mathcal{M}(\underline{\theta})$, which is parametrized by the parameter vector $\underline{\theta} \in \mathcal{D}_{\mathcal{M}} \subset \mathbf{R}^{np}$. The task of the estimation method is to find the optimal parameter estimate $\widehat{\underline{\theta}}$ among the set of models:

$$\mathcal{M}^* = \{\mathcal{M}(\underline{\theta}) | \underline{\theta} \in \mathcal{D}_{\mathcal{M}}\} \tag{2.12}$$

where $\mathcal{D}_{\mathcal{M}}$ denotes a closed subset of values over which the parameter vector $\underline{\theta}$ ranges in the model structure $\mathcal{M}$.

As stressed in *(Ljung, 1987)*, the essence of a model is its prediction ability. Thus, a good model is good at predicting, when it produces small prediction errors:

$$\underline{\varepsilon}(k, \underline{\theta}) = \underline{Y}(k) - \widehat{\underline{Y}}(k|\underline{\theta}) \tag{2.13}$$

where $\underline{Y}$ denotes an observation, $\widehat{\underline{Y}}$ the prediction from a particular model $\mathcal{M}(\underline{\theta})$ and k the actual sample number.

For notational reasons, let $\boldsymbol{U}^N$ and $\boldsymbol{Y}^N$ – denote the matrices of the available inputs and outputs – be defined as:

$$\begin{aligned} \boldsymbol{U}^N &= [\underline{U}(0),\ \underline{U}(1),\ \cdots,\ \underline{U}(N-1),\ \underline{U}(N)] \\ \boldsymbol{Y}^N &= [\underline{Y}(0),\ \underline{Y}(1),\ \cdots,\ \underline{Y}(N-1),\ \underline{Y}(N)] \end{aligned} \tag{2.14}$$

where N denotes the number of samples.

One way to qualify the term "small" (related to the prediction errors) is to use the following norm:

$$\mathcal{V}_N(\underline{\theta}, \boldsymbol{Y}^N, \boldsymbol{U}^N) = \frac{1}{N} \sum_{k=0}^{N} \ell(\underline{\varepsilon}(k, \underline{\theta})) \tag{2.15}$$

where $\ell(\cdot)$ denotes some form of scalar valued criterion function. An often used criterion function is the quadratic norm:

$$\ell(\underline{\varepsilon}(k, \underline{\theta})) = \underline{\varepsilon}(k, \underline{\theta})^\top \underline{\varepsilon}(k, \underline{\theta}) \tag{2.16}$$

In order to put some extra restrictions on the prediction errors, the prediction errors $\underline{\varepsilon}$ can be filtered through a stable linear filter $\Lambda(B)$:

$$\underline{\varepsilon}_\Lambda(k, \underline{\theta}) = \Lambda(B)\, \underline{\varepsilon}(k, \underline{\theta}), \qquad 0 \le k \le N \tag{2.17}$$

where B denotes the backward shift operator. An obvious use of Λ is to remove high frequency disturbances (not essential for the physical model) in the data. Refer to *(Wahlberg and Ljung, 1986)* or *(Ljung, 1987)* for further discussion of the use and effects of the filter Λ.

2.4.1 Maximum Likelihood Method

The maximum likelihood method is an estimation method, which can be applied – provided that the measurement data belong to a predefined distribution. Thus, given a set of observations $\boldsymbol{Y}^N$, as defined in (2.14), the basic idea is to maximize the probability of the observed events, i.e. the parameter vector $\underline{\theta}$ is selected such that the observed measurements become as likely as possible. It is noted that the observations are considered as realizations of a stochastic variable.

The likelihood function $\mathcal{L}$ is based on the joint probability density function of the observations:

$$p(\underline{\theta};\underline{Y}(0),\underline{Y}(2),\cdots,\underline{Y}(N)) = p(\underline{\theta};\boldsymbol{Y}^N) \tag{2.18}$$

Assuming that all the observation $\boldsymbol{Y}^N$ are known, the likelihood function $\mathcal{L}$ of the joint probability density is given as:

$$\begin{aligned}
\mathcal{L}(\underline{\theta};\boldsymbol{Y}^N) &= p(\boldsymbol{Y}^N|\underline{\theta}) &(2.19)\\
&= p(\underline{Y}(N)|\boldsymbol{Y}^{N-1},\underline{\theta})\,p(\boldsymbol{Y}^{N-1},\underline{\theta}) &(2.20)\\
&= \left(\prod_{k=1}^{N} p(\underline{Y}(k)|\boldsymbol{Y}^{k-1},\underline{\theta})\right)\,p(\underline{Y}(0),\underline{\theta}) &(2.21)
\end{aligned}$$

where the rule $p(A\cap B) = p(A|B)p(B)$ (Bayes rule) has been used. $\underline{Y}(0)$ denotes the initial observation. Elaborating further on the likelihood function (2.21), it is observed that:

$$\log(\mathcal{L}(\underline{\theta};\boldsymbol{Y}^N)) = \sum_{k=1}^{N}\log(p(\underline{Y}(k)|\boldsymbol{Y}^{k-1},\underline{\theta})) + \log(p(\underline{Y}(0),\underline{\theta})) \tag{2.22}$$

and from this equation the conditional likelihood function can be defined as:

$$\log(\mathcal{L}(\underline{\theta};\boldsymbol{Y}^N|\underline{Y}(0))) = \sum_{k=1}^{N}\log(p(\underline{Y}(k)|\boldsymbol{Y}^{k-1},\underline{\theta})) \tag{2.23}$$

The task is now to find the parameter vector $\underline{\theta}$, which maximizes the likelihood function (2.21) given the initial observation $\underline{Y}(0)$. Maximizing (2.23) is equivalent to minimizing $-\log(\mathcal{L}(\underline{\theta};\boldsymbol{Y}^N))$, thus the conditional maximum likelihood estimator is found as:

$$\widehat{\underline{\theta}}_{ml} = \arg\min_{\underline{\theta}\in\mathcal{D}_{\mathcal{M}}} -\sum_{k=0}^{N}\log(\mathcal{L}(\underline{\theta};\boldsymbol{Y}^N|\underline{Y}(0))) \tag{2.24}$$

i.e. given the initial observation $\underline{Y}(0)$.

Since $\underline{e}$ and the increment of $\underline{W}$ are normally distributed, also the conditional density of the output is normally distributed. The normal distribution is completely described by the mean and variance. According to *(Madsen et al., 1990)* or *(Nielsen et al., 1997)* the conditional mean and variance can be parameterized as (one step prediction):

$$\begin{aligned}
\widehat{\underline{Y}}(k|k-1) &= \mathrm{E}[\underline{Y}(k)|\underline{Y}(k-1),\underline{\theta}] &(2.25)\\
\boldsymbol{R}(k|k-1) &= \mathrm{Var}[\underline{Y}(k)|\underline{Y}(k-1),\underline{\theta}] &(2.26)
\end{aligned}$$

respectively, implying that the conditional likelihood function can be written as:

$$\begin{aligned}
\log(\mathcal{L}(\underline{\theta};\boldsymbol{Y}^N|\underline{Y}(0))) = -\frac{1}{2}\Big(&ny\log(2\pi) + \sum_{k=1}^{N}\log(\det\boldsymbol{R}(k|k-1))\\
&+\underline{\varepsilon}(k|k-1)^\top\boldsymbol{R}(k|k-1)\underline{\varepsilon}(k|k-1)\Big) \qquad (2.27)
\end{aligned}$$

where ny denotes the dimension of $\underline{Y}$ and the prediction error (2.13) is now based on the one step prediction error:

$$\underline{\varepsilon}(k|k-1) = \underline{Y}(k) - \widehat{\underline{Y}}(k|k-1) \tag{2.28}$$

with zero mean and covariance $\boldsymbol{R}(k|k-1)$.

Due to the fact (see e.g. *(Goodwin and Payne, 1977)*) that the maximum likelihood estimator (2.24) is asymptotically normally distributed with mean $\underline{\theta}$ and covariance:

$$\mathrm{Cov}[\,\hat{\underline{\theta}}\,] \;\approx\; \boldsymbol{H}^{-1} \tag{2.29}$$

where $\boldsymbol{H}$ is the mean Hessian matrix of (2.27), the variance of the parameter estimates can be assessed. The elements of $\boldsymbol{H}$ are estimated as:

$$H_{ij} \;\approx\; -\left(\frac{\partial^2}{\partial\theta_i\partial\theta_j}\,\log(\mathcal{L}(\underline{\theta};\boldsymbol{Y}^N|\underline{Y}(0))\right)\Bigg|_{\underline{\theta}=\hat{\underline{\theta}}} \tag{2.30}$$

The conditional mean and variance are calculated recursively by the Kalman filter technique, as described in the next section. In general, it is not possible to find an analytical solution to (2.27), hence a numerical method has to be applied, see e.g. *(Madsen and Melgaard, 1991)* or *(Melgaard, 1994)*.

If the assumption on the normally distributed measurement data fails, the maximum likelihood is "reduced" to a *Prediction Error Method*. Given a criterion function ℓ, a filter Λ and a model structure $\mathcal{M}$, the task of finding the optimal parameter estimate is equivalent to minimize:

$$\widehat{\underline{\theta}}_N = \;\arg \min_{\underline{\theta}\in\mathcal{D}_\mathcal{M}} \mathcal{V}(\underline{\theta},\boldsymbol{Y}^N,\boldsymbol{U}^N) \tag{2.31}$$

where the optimal parameter estimate $\widehat{\underline{\theta}}_N$ is the argument of the criterion function $\mathcal{V}$, for which the norm (2.31) is minimized, see e.g. *(Ljung, 1987)*.

2.5 Kalman Filter

The Kalman filter can be characterized as a state filtering technique. The purpose of the Kalman filter is to reconstruct the state variables based on the measurements and a given model, as formed by e.g. (2.10) and (2.11).

Thus, the state variables, which presumably are significant for the dynamic evolution of the system, are gathered in $\underline{X}$. However, only partial knowledge of $\underline{X}$ is represented in the measurement $\underline{Y}$. This problem is solved by the use of a state filtering technique. According to e.g. *(Melgaard, 1994)*, the exact solution to the state filtering problem for linear dynamic models is given by the Kalman filter. Loosely speaking, the Kalman filter reconstructs the state variables in $\underline{X}$ from data, i.e. it performs the optimal (minimum variance) linear updating and prediction of $\underline{X}$. Furthermore, the Kalman filter provides calculation of the conditional mean and variance, (2.25) and (2.26) respectively, which are used by the maximum likelihood method.

The linear case

Consider a linear model:

$$\begin{aligned} d\underline{X}(t) &= \boldsymbol{A}\,\underline{X}(t)\,dt \,+\, \boldsymbol{B}\,\underline{U}(t)\,dt \,+\, \boldsymbol{G}\,d\underline{W}(t) \\ \underline{Y}(k) &= \boldsymbol{C}\,\underline{X}(k) \,+\, \boldsymbol{D}\,\underline{U}(k) \,+\, \underline{e}(k) \end{aligned} \tag{2.32}$$

where $\boldsymbol{A}$ denotes the system matrix, $\boldsymbol{B}$ input matrix, $\boldsymbol{G}$ system noise input matrix, $\boldsymbol{C}$ output matrix and $\boldsymbol{D}$ direct output matrix. $\underline{W}$ is a Wiener process with zero mean and incremental covariance $\boldsymbol{\Sigma}_W$ and $\underline{e}$ is Gaussian white noise with zero mean and covariance $\boldsymbol{\Sigma}_e$. $\underline{W}$ and $\underline{e}$ are mutually uncorrelated.

Referring to *(Nielsen et al., 1997)*, the "predicting" part of the continuous-discrete Kalman filter is given as:

$$\frac{d\underline{\widehat{X}}(t|k)}{dt} = \boldsymbol{A}\,\underline{\widehat{X}}(t|k) + \boldsymbol{B}\,\underline{U}(t) \tag{2.33}$$
$$\frac{d\boldsymbol{P}(t|k)}{dt} = \boldsymbol{A}\,\boldsymbol{P}(t|k) + \boldsymbol{P}(t|k)\,\boldsymbol{A}^\top + \boldsymbol{G}\,\boldsymbol{\Sigma}_W\,\boldsymbol{G}^\top \tag{2.34}$$
$$\underline{\widehat{Y}}(k+1|k) = \boldsymbol{C}\,\underline{\widehat{X}}(k+1|k) + \boldsymbol{D}\,\underline{U}(k+1) \tag{2.35}$$
$$\boldsymbol{R}(k+1|k) = \boldsymbol{C}\,\boldsymbol{P}(k+1|k)\,\boldsymbol{C}^\top + \boldsymbol{\Sigma}_e \tag{2.36}$$

where $t \in [kT_s, (k+1)T_s]$ and $\boldsymbol{P}$ is the variance of the one-step ahead prediction, while the "updating" part is given as:

$$\underline{\widehat{X}}(k|k) = \underline{\widehat{X}}(k|k-1) + \boldsymbol{K}(k)\,(\underline{Y}(k) - \underline{\widehat{Y}}(k|k-1)) \tag{2.37}$$
$$\boldsymbol{P}(k|k) = \boldsymbol{P}(k|k-1) - \boldsymbol{K}(k)\,\boldsymbol{R}(k|k-1)\,\boldsymbol{K}^\top(k) \tag{2.38}$$
$$\boldsymbol{K}(k) = \boldsymbol{P}(k|k-1)\,\boldsymbol{C}^\top\,\boldsymbol{R}(k|k-1)^{-1} \tag{2.39}$$

The initial conditions are $\underline{\widehat{X}}(1|0) = \underline{X}_0$ and $\boldsymbol{P}(1|0) = \boldsymbol{\Sigma}_0$. It is noted that the predictions for the conditional mean and variance (2.35) and (2.36) respectively, are evaluated when $t=(k+1)T_s$.

The nonlinear case

Considered the nonlinear model described by (2.10) and (2.11). In order to be able to use the Kalman filter, the nonlinear model has to be linearized in each sample point k. Thus, the system matrix $\boldsymbol{A}$ and the output matrix $\boldsymbol{C}$ are computed as:

$$\boldsymbol{A}(k) = \left.\frac{\partial \mathrm{F}(\underline{X}(t),\, \underline{U}(t),\, \underline{\theta},\, t)}{\partial \underline{X}(t)}\right|_{\substack{\underline{X}(t) = \underline{\widehat{X}}(t|k-1) \\ \underline{U}(t) = \underline{U}(kT_s)}}, \qquad t = kT_s \tag{2.40}$$

and

$$\boldsymbol{C}(k) = \left.\frac{\partial \mathrm{H}(\underline{X}(t),\, \underline{U}(t),\, \underline{\theta},\, t)}{\partial \underline{X}(t)}\right|_{\substack{\underline{X}(t) = \underline{\widehat{X}}(t|k-1) \\ \underline{U}(t) = \underline{U}(kT_s)}}, \qquad t = kT_s \tag{2.41}$$

The idea is now to use (2.40) and (2.41) in the linear case instead of $\boldsymbol{A}$ and $\boldsymbol{C}$, respectively. Moreover, (2.33) and (2.35) are substituted by the deterministic part of (2.10) and (2.11), respectively. For further issues refer to *(Melgaard, 1994)* or *(Madsen and Holst, 1996)*.

2.6 Validation Methods

Model validation is an important part of the modelling process, as illustrated in Figure 2.1. The purpose of the validation is to assess the performance of a suggested model and the parameter estimates, i.e. to judge whether or not an estimated model satisfies a number of posed criteria.

The validation methods for the Grey Box modelling approach are closely related to the techniques used for Black Box modelling. However, one advantage of the Grey Box models is the prior knowledge about the model structure and valid ranges of the parameters.

A number of test methods for validation are presented in this section. For further reading refer to *(Holst et al., 1992)*, which provides a survey of validation methods.

2.6.1 Likelihood based Tests

One of the nice properties of the maximum likelihood method is that the maximum likelihood estimator is consistent. Furthermore, the maximum likelihood estimator is asymptotically normally distributed, as mentioned in Section 2.4.1. This fact is exploited in the following tests.

Parameter Confidence Interval

One test is to check whether or not a parameter is significant, i.e. if zero is included in the confidence interval for the considered parameter estimate. The hypothesis is:

$$H_0:\ \theta_j = 0 \qquad \text{against} \qquad H_1:\ \theta_j \neq 0 \tag{2.42}$$

The test value is given as:

$$\frac{\widehat{\theta}_j}{\widehat{\sigma}_{jj}} \ \in\ t(N-1-np) \tag{2.43}$$

where np is the number of estimated parameters ($\underline{\theta} \in \mathcal{D}_{\mathcal{M}}$).

Parameter Correlation

The maximum likelihood estimator has the asymptotic covariance matrix presented in (2.29). Based on this matrix, the corresponding correlation matrix can be computed. If any correlation between two parameters is 1 (or -1) or close to 1 (or -1), this would be an indication of over-parameterization.

Model Order

Consider the loss function J for a given model structure $\mathcal{M}$ with the parameter vector $\underline{\theta}$. Let $\underline{\theta}_1 \in \mathcal{D}_{\mathcal{M}_1} \subset \mathbf{R}^{n_1}$ denote a parameter estimate from $\mathcal{M}_1$ with the corresponding loss function J_1 value:

$$J_1 = J(\underline{\varepsilon}(k,\underline{\theta}_1)) = \sum_{k=1}^{N} \underline{\varepsilon}(k,\underline{\theta}_1)^\top\, \underline{\varepsilon}(k,\underline{\theta}_1) \tag{2.44}$$

Consider also the parameter vector $\underline{\theta}_2 \in \mathcal{D}_{\mathcal{M}_2} \subset \mathbf{R}^{n_2}$ from the model structure $\mathcal{M}_2$ with $J_2 = J(\underline{\varepsilon}(k,\underline{\theta}_2))$, where $n_2 \geq n_1+1$ and $\mathcal{M}_1 \subset \mathcal{M}_2$. It is possible

to test whether the smaller model (with n_1 parameters) describes the data as well as the larger model (with n_2 parameters). The hypothesis is:

$$H_0:\ \underline{\theta} \in \mathcal{D}_{\mathcal{M}_1} \qquad \text{against} \qquad H_1:\ \underline{\theta} \in \mathcal{D}_{\mathcal{M}_2} \tag{2.45}$$

The test value is given as:

$$\frac{(J_1 - J_2)/(n_2 - n_1)}{J_2/(N - n_2)} \in \mathrm{F}(n_2 - n_1, N - n_2) \tag{2.46}$$

See e.g. *(Madsen, 1995)*.

2.6.2 Residual Analysis

Residual analysis on the prediction errors can be used to check, if any obtained information contradicts the assumptions upon which the models are build. In this section the following residual methods are presented: performance, autocorrelation, crosscorrelation and cumulated periodogram. There are a number of statistical tests available for these methods. If one of the methods indicates a contradiction, the test result might point out in which direction to develop/extend the model.

Visual Performance

According to *(Holst et al., 1992)*, it is important to plot the residuals of the prediction errors and visually judge the graph for trend and non-constancy of the variance. The mean should be zero and the variance (of each element in $\underline{\varepsilon}$) should be constant.

Autocovariance and Autocorrelation Functions

In the scalar case, the autocovariance function C_ε (see *(Madsen, 1995)*) can be estimated as:

$$\widehat{C}_\varepsilon(k, \underline{\widehat{\theta}}) = \frac{1}{N} \sum_{j=1}^{N-|k|} (\varepsilon(j, \underline{\widehat{\theta}}) - \varepsilon_\mu)(\varepsilon(j+|k|, \underline{\widehat{\theta}}) - \varepsilon_\mu) \tag{2.47}$$

where $|k| \in [0, 1, \cdots, N-1]$ and $\varepsilon_\mu = \frac{1}{N}\sum_{k=1}^{N} \varepsilon(k, \underline{\widehat{\theta}})$. From (2.47) the variance of the prediction error can be estimated as $\widehat{\sigma}_\varepsilon^2 = C_\varepsilon(0, \underline{\widehat{\theta}})$. Furthermore, the autocorrelation function can be calculated as:

$$\widehat{\rho}_\varepsilon(k, \underline{\widehat{\theta}}) = \widehat{C}_\varepsilon(k, \underline{\widehat{\theta}}) / \widehat{\sigma}_\varepsilon^2 \tag{2.48}$$

The estimated autocorrelation function will be asymptotically normally distributed with zero mean and variance $1/N$, provided that the prediction errors are white noise. Hence, the following hypothesis can be tested:

$$H_0: \ \widehat{\rho}_\varepsilon(k, \underline{\widehat{\theta}}) = 0 \qquad \text{against} \qquad H_1: \ \widehat{\rho}_\varepsilon(k, \underline{\widehat{\theta}}) \neq 0 \tag{2.49}$$

for $|k| \geq 1$. The critical test value is given as:

$$\widehat{\rho}_\varepsilon(k, \underline{\widehat{\theta}}) \geq N(0, 1/N)_{1-\alpha} \tag{2.50}$$

where α denotes the confidence level. The 95 % significance level is approximately $2\sigma = 2/\sqrt{N}$, while the 99 % significance level is $3\sigma = 3/\sqrt{N}$. The easiest way to perform the test is to plot both the estimated autocorrelation function and the selected significance level. If the autocorrelation test contradicts the white noise assumption (normally distributed), the graph of the autocorrelation function might indicate how to extend the model, see *(Madsen, 1995)*.

Crosscovariance and Crosscorrelation Functions

In the scalar case, the crosscovariance function $C_{u\varepsilon}$ (see *(Madsen, 1995)*) between input u and the prediction error ε can be estimated as:

$$\widehat{C}_{u\varepsilon}(k, \underline{\widehat{\theta}}) = \frac{1}{N} \sum_{j=1}^{N-k} (u(j) - u_\mu)(\varepsilon(j+k, \underline{\widehat{\theta}}) - \varepsilon_\mu) \tag{2.51}$$

$$\widehat{C}_{u\varepsilon}(-k, \underline{\widehat{\theta}}) = \frac{1}{N} \sum_{j=1}^{N-k} (u(j+k) - u_\mu)(\varepsilon(j, \underline{\widehat{\theta}}) - \varepsilon_\mu) \tag{2.52}$$

where $k \in [0, 1, \cdots, N-1]$, $u_\mu = \frac{1}{N}\sum_{k=1}^{N} u(k)$ and $\varepsilon_\mu = \frac{1}{N}\sum_{k=1}^{N} \varepsilon(k, \underline{\widehat{\theta}})$.

Similarly to (2.48), the crosscorrelation function can be calculated as:

$$\widehat{\rho}_{u\varepsilon}(k, \underline{\widehat{\theta}}) = \frac{\widehat{C}_{u\varepsilon}(k, \underline{\widehat{\theta}})}{\widehat{\sigma}_u \, \widehat{\sigma}_\varepsilon} \tag{2.53}$$

The estimated crosscorrelation function will be asymptotically normally distributed with zero mean and variance $1/N$, provided that the prediction errors are white noise. Hence, a significance test equivalent to the one described for autocorrelation function can be performed. If the crosscorrelation test contradicts the white noise assumption (normally distributed), the graph of the autocorrelation function might indicate how to extend the model, see *(Madsen, 1995)*.

Cumulated Periodogram

The cumulated periodogram is a frequency domain method. The basic idea is to measure the information of the prediction errors at the fundamental frequencies $f_j = j/N$ for $j \in [0, 1, \cdots, N/2]$. As the prediction errors are assumed to be white noise, the information should be uniformly distributed over the fundamental frequencies f_j.

The periodogram is defined as:

$$\hat{I}(f_j) = \frac{1}{2\pi N}\left(\left(\sum_{k=1}^{N}\varepsilon(k,\underline{\widehat{\theta}})\cos(2\pi k T_s)\right)^2 + \left(\sum_{k=1}^{N}\varepsilon(k,\underline{\widehat{\theta}})\sin(2\pi k T_s)\right)^2\right) \tag{2.54}$$

and the cumulated periodogram as:

$$\hat{\mathcal{I}}(f_j) = \sum_{i=1}^{j}\hat{I}(f_i)/\sum_{i=1}^{N/2}\hat{I}(f_i) \tag{2.55}$$

Since the periodogram for white noise is uniformly distributed, the cumulated periodogram is a linear function of f_j on the interval $[0,1]$. Hence, a test based on the Kolmogorov-Smirnov test for testing the equality between an assumed distribution $\mathcal{I}_0$ and an empirical distribution $\mathcal{I}$ can be performed. The hypothesis is:

$$H_0:\ \mathcal{I} = \mathcal{I}_0 \qquad \text{against} \qquad H_1:\ \mathcal{I} \neq \mathcal{I}_0 \tag{2.56}$$

The test value is:

$$D_n = \sup_{f_j}|\mathcal{I}_0(f_j) - \mathcal{I}(f_j)| \tag{2.57}$$

where n is the number of frequencies. According to *(Conradsen, 1984)*, the 95 % significance level can be approximated as $1.36/\sqrt{n}$ and the 99 % significance level as $1.63/\sqrt{n}$, provided that $n > 50$.

2.6.3 Cross Validation

Several cross validation methods are available. In this section only two of these are presented. Common for the methods is to compare the model

performance based on e.g. the prediction error, simulation error, criterion value.

Validation of a Parameter Estimate

As mentioned in Section 2.4, the estimation problem is solved as an optimization problem. If the optimization problem satisfies a number of criteria (e.g. convex criterion function), the optimal solution is unique. However if not all conditions are satisfied, the solution is not unique.

This cross validation procedure is a method to investigate/test the generalization properties of a parameter estimate $\underline{\widehat{\theta}}$ given the model structure $\mathcal{M}$. The method is based on two sets of data $\mathcal{D}_1$ and $\mathcal{D}_2$ from the same system. The procedure is to perform an estimation on $\mathcal{D}_1$, from which the parameter estimate $\underline{\widehat{\theta}}(\mathcal{D}_1)$ is achieved. Next step is to perform a simulation based on $\mathcal{D}_2$ and $\underline{\widehat{\theta}}(\mathcal{D}_1)$. The variance of the prediction errors for the estimation and for the simulation may then be compared. If these variances are of equal size, the estimated parameters $\underline{\widehat{\theta}}(\mathcal{D}_1)$ is presumably equal to the optimal parameters. Meanwhile, if the variances are of different size, either the achieved parameter estimate $\underline{\widehat{\theta}}(\mathcal{D}_1)$ corresponds to a local minimum or the model is not adequate. A formal hypothesis and test for this type of cross validation are described in *(Melgaard, 1994)*.

Validation of two Models

Consider two models, $\mathcal{M}_1(\underline{\theta}_1)$ and $\mathcal{M}_2(\underline{\theta}_2)$, obtained on data from a physical system. These models may then be evaluated on a "fresh" data set from the particular physical system. Comparing their performances, the model with the better performance is then favorable.

2.7 Summary

In this chapter, the general concept of the Grey Box modelling method has been presented. Some consideration on system identification was the issue of the first section. As presented in Section 2.2, the model class was based on stochastic differential equations and the model description was in general considered nonlinear. How to handle these equations mathematically was the issue of Section 2.3.

As described in Section 2.4 the applied estimation method was based on the maximum likelihood method. Since only a subset of the state variables were measured in general, it was necessary to apply a state filtering technique, as the Kalman filter in Section 2.5, in order to reconstruct the state variables. One of the attractive features of this estimation approach is that the continuous time parameters are estimated directly.

Several validation methods like the likelihood based tests, residual analysis and cross validation have been presented as tools to assess parameter estimates and model performance, as described in Section 2.6.

The maximum likelihood method, the linear/nonlinear Kalman filter and some of the validation methods have been implemented in the estimation tool CTLSM. This tool will be used for the estimations throughout the thesis. It should be noted that the current implementation is limited to smooth functions, i.e. functions for which the first derivative is continuous.

Chapter 3

Experimental Design

The basic idea of experimental design is to design the experimental conditions in such a way that the experiment is maximally informative. Experimental design for dynamic systems includes choice of sampling time, test signals, control signals, presampling filters, etc.

As stressed in *(Goodwin and Payne, 1977)*, any experimental design must take into account the constraints on the allowable experimental conditions. Typical examples of constraints are amplitude and/or power constraints on the input signal, total time available for the experiment, maximum sampling rate, measuring range of transducers etc. Thus, the purpose of experimental design is in a way, to maximize the information content in data within the limits imposed by the given constraints.

This chapter presents some of the most important issues of experimental design. The first section deals with the identifiability problem, while the second section highlights some issues on sampling. The third section contains a discussion on filters and subsampling of the measured data. In the fourth section, some of the basic ideas in optimal input design are presented.

3.1 Identifiability

A fundamental problem of the system identification is whether or not a model is structural identifiable, i.e. whether or not all the parameters of the model can be uniquely identified from a specified experiment.

The identifiability problem can be divided in two aspects. The first aspect is on the information in the measured data, while the second is on the structure of the model.

3.1.1 Informative Data

The first aspect on the identifiability problem is related to the experimental conditions. For a stable system it is evident that, if the input signals are constant, the system will be in a stationary operating point. Hence in this situation, the parameters related to the dynamics of the system would not be identifiable from data.

In order to achieve informative data, the input signals must be persistently exciting. The persistence of excitation concept is illustrated in the following example.

Example 3.1 *Consider an open loop experiment on a linear single-input, single-output system and the discrete model set:*

$$\mathcal{M}^* = \{\mathcal{G}(B,\underline{\theta}), \mathcal{H}(B,\underline{\theta}) \mid \underline{\theta} \in \mathcal{D}_{\mathcal{M}}\} \tag{3.1}$$

where $\mathcal{G}$ and $\mathcal{H}$ denote the transfer functions from the input u to the output y and from the noise e to the output y, respectively.

Assume that $\underline{\theta}_1$ and $\underline{\theta}_2$ correspond to different models in $\mathcal{M}^*$. For notational convenience, let $\varepsilon_j(t) = \varepsilon(t,\underline{\theta}_j)$, $\mathcal{G}_j(B) = \mathcal{G}(B,\underline{\theta}_j)$, $\Delta\mathcal{G}(B) = \mathcal{G}_1(B) -$

$\mathcal{G}_2(B)$ and analogously for $\mathcal{H}_j(B)$. Furthermore, let $\Delta\varepsilon$ denote the difference between the prediction errors of the two models:

$$\Delta\varepsilon = \varepsilon_1(t) - \varepsilon_2(t) = \frac{-1}{\mathcal{H}_1(B)}\left(\Delta\mathcal{G}(B)\, u(t) + \Delta\mathcal{H}(B)\, \varepsilon_2(t)\right) \tag{3.2}$$

where:

$$\varepsilon_2(t) = \frac{1}{\mathcal{H}_2(B)}\left((\mathcal{G}_0(B) - \mathcal{G}_2(B))\, u(t) + \mathcal{H}_0(B)\, e_0(t)\right) \tag{3.3}$$

where $\mathcal{G}_0$ and $\mathcal{H}_0$ denote the true transfer functions.

Suppose now that the data are not informative, i.e.:

$$\lim_{N\to\infty} \frac{1}{N}\sum_{t=1}^{N} E[\Delta\varepsilon(t)^2] = 0 \tag{3.4}$$

As described in (Ljung, 1987), condition (3.4) would imply that both:

$$\Delta\mathcal{H}(e^{i\omega}) \equiv 0 \qquad \textit{and} \qquad |\Delta\mathcal{G}(e^{i\omega})|^2\Phi_u(\omega) \equiv 0 \tag{3.5}$$

If $\Phi_u(\omega) > 0$, this implies that $\Delta\mathcal{G}(e^{i\omega}) \equiv 0$, i.e. the two models are equal.

Thus, for an open loop experiment, an input signal $\{u(t)\}$ with $\Phi_u(\omega) > 0$ implies that the data are informative enough to discriminate between two different models in $\mathcal{M}^*$. The signal $\{u(t)\}$ with $\Phi_u(\omega) > 0$ is said to be *persistently exciting*.

According to *(Ljung, 1987)*, a closed loop experiment with proportional feedback is not informative, even though the spectrum of the input signal satisfies $\Phi_u(\omega) > 0$. Thus in the case of modelling of closed loop systems, the identifiability becomes more complicated. *(Söderström and Stoica, 1989)* suggests three different approaches for linear systems:

- Direct identification, i.e. to use the input output data as in the open loop case (consequently neglecting possible existence of feedbacks).
- Indirect identification, i.e. first identify the closed loop system and then determine the open loop part assuming the feedback is known.
- Joint input-output identification, i.e. input and output are regarded as a multi-variable time series.

3.1.2 Structural Identifiability

The second aspect of the identifiability problem is related to the structure of the model, i.e. whether different parameterizations give equal models. There are mainly two reasons to consider the structural identifiability. One reason is related to the interpretation/significance of the parameters, as illustrated in the example below. Another reason is that a structural unidentifiable set of parameters may not be uniquely determined from data, which further can imply problems in the estimation. Thus, if the Hessian matrix (see (2.29)) becomes singular, this is a clear sign of identifiability problems.

Example 3.2 *The structural identifiability problem can be illustrated by the electric circuit in Figure 3.1.*

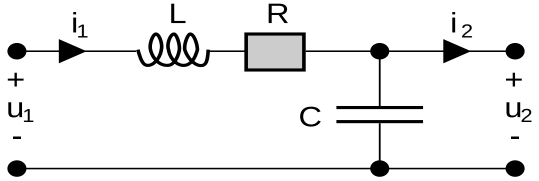

Figure 3.1. Electric circuit.

From Figure 3.1, the following equations are derived:

$$L\,\frac{di_1(t)}{dt} = u_1(t) - u_2(t) - R\,i_1(t) \tag{3.6}$$

$$C\,\frac{du_2(t)}{dt} = i_1(t) - i_2(t) \tag{3.7}$$

where u_j denotes a voltage and i_j a current. L denotes an inductance, R a resistance, while C denotes a capacitance. Using Laplace transformation, the following transfer functions are achieved:

$$\frac{i_1(s)}{i_2(s)} = \frac{1}{LCs^2 + RCs + 1} \tag{3.8}$$

$$\frac{i_1(s)}{u_1(s)} = \frac{Cs}{LCs^2 + RCs + 1} \tag{3.9}$$

These transfer functions must be compared with the observable structure:

$$G(s) = \frac{b_1 s + b_0}{a_2 s^2 + a_1 s + 1} \tag{3.10}$$

Suppose that only i_1 and i_2 are measured, hence only transfer function i_1/i_2 is of interest. Comparing (3.8) with (3.10), the following set of algebraic equation are established:

$$b_0 = 1, \quad a_2 = LC \quad \text{and} \quad a_1 = RC \tag{3.11}$$

This set of equations cannot be solved with respect to L, R and C. Thus, the parameters in (3.8) are not structural identifiable.

Suppose now that i_1 and u_1 are measured, then the same procedure performed for (3.9) yields:

$$b_1 = C, \quad a_2 = LC \quad \text{and} \quad a_1 = RC \tag{3.12}$$

For this set of algebraic equations, the solution with respect to L, R, and C is:

$$C = b_1, \quad L = \frac{a_2}{b_1} \quad \textit{and} \quad R = \frac{a_1}{b1} \tag{3.13}$$

The solution is unique, hence the parameters in (3.9) are structural identifiable.

The example above illustrates the basic idea of the structural identifiability problem, i.e. b_1, a_1 and a_2 are the observable/direct identifiable parameters, while L, R and C are the parameters, which have physical interpretation. The example clearly shows the importance of a correct selection of input and output signals.

The situation is more complicated in the case of nonlinear system model. An explicit algorithm for testing global identifiability for arbitrary model parameterizations is presented in *(Ljung and Glad, 1994)*. The algorithm is based on polynomial expansion in the state variables. The identifiability of parameters related to the noise terms of the stochastic differential equations is described in *(Melgaard, 1994)*.

3.2 Sampling

The choice of sampling frequency f_s is very important. It is related to the bandwidth f_b of the system. If the sampling frequency is selected too small, i.e. as $f_s < 2f_b$, the original signal is corrupted by the high frequency part of the spectrum (of the signal) being *folded* to the low frequency part of the spectrum. This phenomenon is called *aliasing*, see e.g. *(Ljung, 1987)*. To avoid aliasing, the sampling frequency f_s must be two times larger than the bandwidth f_b. Meanwhile, if the sampling frequency is selected much higher than the bandwidth of the system, i.e. $f_s \gg f_b$, this would be waste of disc space.

If the bandwidth of a system has to be based on prior knowledge, e.g. based on some simplified calculations, it would be wise to oversample the expected bandwidth by e.g. a factor 10. The measured data can be subsampled to a more appropriate representation, provided that no risk of aliasing is present. This risk can be minimized by the use of an anti-aliasing filter. The anti-aliasing filter is applied during the data acquisition and it is typically a low-pass filter, with a bandwidth higher than the bandwidth of the system. The sampling frequency should then be selected two times higher than the bandwidth of anti-aliasing filter.

3.3 Filtering

The spectrum of a typically physical system has the shape of a low-pass filter and it can be characterized by the bandwidth frequency f_b. In the case of oversampling (when $f_s \gg f_b$), it is necessary to subsample the data to a more adequate sampling frequency, such that $f_s \geq 2f_b$ is not violated. Since the estimation method uses the one step ahead prediction, it is important that the sampling frequency f_s is close to $2f_b$. The one step prediction is related to the sample frequency as $\Delta t = T_s = 1/f_s$. Thus, a high sampling frequency implies small time steps, which further increase the risk of high frequency noise producing bias in the parameter estimates.

As described in Section 2.4, the prediction errors can be filtered by a stable filter $\Lambda(B)$. According to *(Wahlberg and Ljung, 1986)*, filtering of prediction errors with $\Lambda(B)$ is equivalent to filtering the input and the output data with $\Lambda(B)$, before they are used in the estimation. This is called *prefiltering*.

3.4 Optimal Inputs Design

For an open loop experiment, the data will be informative if the input signals are persistently exciting ($\Phi_u(\omega) > 0$), as discussed in Section 3.1. Meanwhile, an input with $\Phi_u(\omega) > 0, \ \forall \omega$, is not physically possible, as the power of such a signal is infinite.

A method for design of physically possible input signal is called optimal input design. In this section, the design criteria and two approaches are presented.

3.4.1 Design Criteria

As described in *(Goodwin and Payne, 1977)*, a natural approach is to choose a measure (for the goodness of an experiment) related to the expected accuracy of the parameter estimates, which are obtained from the experimental data.

The accuracy of the parameters can be expressed by the Hessian matrix for the maximum likelihood criterion, as in (2.29). It turns out that the Hessian matrix is equivalent, in this case, to Fisher's information matrix given by:

$$\boldsymbol{M} = \mathrm{E}\left[\left(\frac{\partial \log(\mathcal{L}(\underline{\theta}; \boldsymbol{Y}^N | \underline{Y}(0)))}{\partial \underline{\theta}}\right)^\top \left(\frac{\partial \log(\mathcal{L}(\underline{\theta}; \boldsymbol{Y}^N | \underline{Y}(0)))}{\partial \underline{\theta}}\right) \middle| \, \underline{\hat{\theta}}\right] \quad (3.14)$$

In *(Goodwin and Payne, 1977)*, two criteria are suggested as measures of the "goodness". The first criterion is:

$$J_I \;=\; \mathrm{E}_{\underline{\theta}}\left[\, \mathrm{E}[\, \ell(\underline{\theta}, \underline{\widehat{\theta}}) | \underline{\theta}\,]\,\right] \quad (3.15)$$

where $\mathrm{E}_{\underline{\theta}}[\cdot]$ denotes the mean value with respect to $\underline{\theta}$ and ℓ is a scalar valued function of the true parameter vector $\underline{\theta}$ and of the estimated parameter vector $\underline{\widehat{\theta}}$. Using suitable simplified assumptions, (3.15) can be written as:

$$J_I \;=\; \mathrm{E}_{\underline{\theta}}\left[\, \ell(\underline{\theta}, \underline{\theta}) \;+\; \frac{1}{2}\,\mathrm{trace}\left(\frac{\partial^2 \ell}{\partial \underline{\widehat{\theta}}^2}\right) \boldsymbol{M}^{-1}\right] \quad (3.16)$$

A reasonable criterion function is $\ell(\underline{\theta}, \underline{\widehat{\theta}}) = (\underline{\theta} - \underline{\widehat{\theta}})^\top (\underline{\theta} - \underline{\widehat{\theta}})$. Optimization of J_I is equivalent to optimization of:

$$\mathrm{E}_{\underline{\theta}}\left[\mathrm{trace}\left(\frac{\partial^2 \ell}{\partial \underline{\widehat{\theta}}^2}\right) \boldsymbol{M}^{-1}\right] \quad (3.17)$$

The second suggested criterion is:

$$J_{II} \;=\; -\log(\det \boldsymbol{M}) \quad (3.18)$$

which is related to the volume of the highest probability density region for the parameters. Other possible criteria are described in *(Madsen and Holst, 1996)*.

3.4.2 Time Domain Design

Consider now the input design for the linear single-input single-output system:

$$y(t) \;=\; \mathcal{G}(B)\, u(t) \;+\; \mathcal{H}(B)\, e(t) \quad (3.19)$$

where $\mathcal{G}$ and $\mathcal{H}$ are transfer functions, while e is white noise with variance σ_e^2.

The classical example for a time domain design is to consider a moving average model of order n (MA(n) - process), where:

$$\mathcal{G}(B) \;=\; b_1\, B \;+\; b_2\, B^2 \;+\; \cdots \;+\; b_n\, B^n \quad (3.20)$$

$$\mathcal{H}(B) \quad = \quad 1 \tag{3.21}$$

Thus, the parameter vector $\underline{\theta}$ is:

$$\underline{\theta} = \left[\begin{array}{cccc} b_1, & b_2, & \cdots, & b_n \end{array} \right]^\top \tag{3.22}$$

According to *(Goodwin and Payne, 1977)*, Fisher's information matrix can be expressed as:

$$\boldsymbol{M} = \begin{bmatrix} \boldsymbol{X}^\top \boldsymbol{X}/\sigma_e & 0 \\ & \\ 0 & N/2\,\sigma_e^2 \end{bmatrix} \tag{3.23}$$

where N denotes the number of data points and:

$$\boldsymbol{X} = \begin{bmatrix} u(0) & u(-1) & \cdots & u(1-n) \\ u(1) & u(0) & & u(2-n) \\ \vdots & \vdots & & \vdots \\ u(N-1) & u(N-2) & \cdots & u(N-n) \end{bmatrix} \tag{3.24}$$

From (3.23) an average information matrix can be defined as:

$$\overline{\boldsymbol{M}} = \boldsymbol{M}/N = \begin{bmatrix} \boldsymbol{X}^\top \boldsymbol{X}/N\sigma_e & 0 \\ & \\ 0 & 1/2\,\sigma_e^2 \end{bmatrix} \tag{3.25}$$

Applying criterion J_{II} from (3.18), the optimization problem becomes:

$$-\log(\det \overline{\boldsymbol{M}}) \;=\; -\log(\det \boldsymbol{X}^\top \boldsymbol{X}/N\sigma_e^2\,) \;+\; \log(\det 2\,\sigma_e^{n+2}\,) \tag{3.26}$$

As mentioned in *(Goodwin and Payne, 1977)*, the input power must be constrained as follows:

$$\frac{1}{N}\sum_{k=1}^{N} u(k-j)^2 = 1, \qquad j \in \left[\, 1, \quad 2, \quad \cdots, \quad n \,\right] \tag{3.27}$$

The solution to (3.26) subject to the power constraint (3.27) is $\boldsymbol{X}^\top \boldsymbol{X}/N = \boldsymbol{I}$, which is equivalent to the demand:

$$\frac{1}{N}\sum_{k=1}^{N} u(k-i)u(k-j) = \begin{cases} 1, & i = j \\ 0, & i \neq j \end{cases} \tag{3.28}$$

for $i, j \in [1, n]$.

The above presentation is the basic idea behind the pseudo random binary sequence (abbreviated as PRBS), since it nearly satisfies (3.28). Further discussion of the PRBS signals can be found in *(Godfrey, 1980)*. A PRBS signal can be characterized by the following properties:

- The PRBS signal has two levels and it may only switch from one level to another, at time $t = 0,\ T_0,\ 2T_0,\ \cdots$, where T_0 denotes the fundamental time period. The frequency $f_0 = \frac{1}{T_0}$ of the fundamental time period is called the event frequency.
- A PRBS signal is periodic with period 2^n–1, where n is an integer. The PRBS signal may be generated using an n-stage shift back register.
- Since the PRBS signal is periodic, the shift between levels is predetermined and in any period the number of high and low levels are equal.
- The PRBS signal is autocorrelated at lags $2^n - 1,\ 2(2^n - 1),\ \cdots$.

(Godfrey, 1980) suggests to select the fundamental time period T_0 larger than the settling time of the system. The settling time is defined as the time from a perturbing impulse occurs until the system output is within 2 % or 5 % from the start level. The settling time can be approximated by 3 to 5 times the dominating constant of the system.

As a generalization of the PRBS signal, the following pseudo random uniformly distributed sequence (abbreviated by PRUS) is introduced. The

PRUS signal follows the outline of the PRBS signal, except for the binary levels. Instead of the binary levels, the PRUS signal alternates between the levels in a particular interval, prescribed by an uniform distribution. Besides adequate excitation in the frequency domain, as for the PRBS signal, the idea of the PRUS signal is also to perform an excitation in the amplitude. Thus, the switching pattern of the PRUS signal is periodic with period 2^n-1, but it should be stressed that the PRUS signal is not periodic as the PRBS signal.

A PRBS and a PRUS signal, with fundamental time period $T_0 = 1$ and length of shift register $n=4$, are plotted in Figure 3.2. The signals are in phase. It is evident that the PRBS signal is periodic. In the terminology of *(Ljung, 1987)*, the PRBS signal is said to be persistently exciting of order $n=4$.

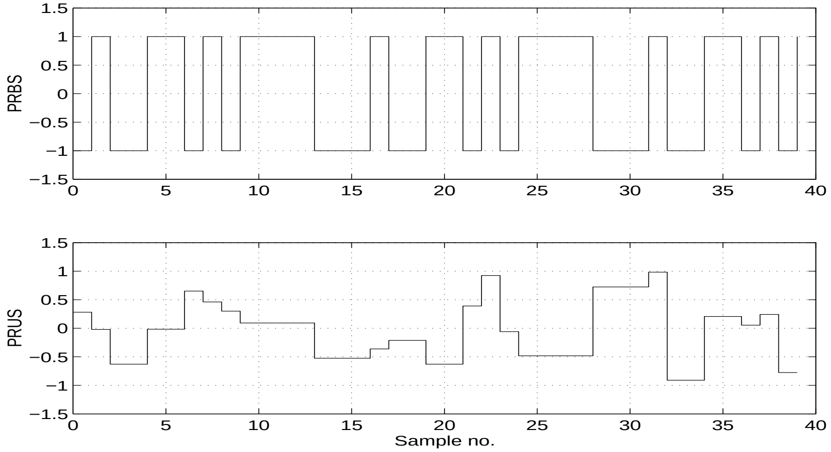

Figure 3.2. *Exemplification of a PRBS signal and a PRUS signal for $n=4$.*

3.4.3 Frequency Domain Design

The frequency domain design is naturally based on the same ideas as the time domain design. Instead of using PRBS signals, the frequency domain design is using sinusoidal signals.

A case study of an optimal input design in the frequency domain is introduced in Section 8.3.3. The case study is based on the experimental setup of the low energy test house presented in Section 4.3.

Refer to *(Goodwin and Payne, 1977)*, *(Madsen and Holst, 1996)* or *(Sadegh, 1996)* for further discussion of the optimal input design.

3.5 Summary

In this chapter some of the important issues of experimental design have been reviewed. The problem of identifiability and the optimal input design were closely related. If the experimental conditions were not taken seriously, the parameter estimation would be affected in a negative direction.

The input design is based on the time domain design (i.e. PRBS signals) throughout the presented experiments in the present thesis, since this design only demands knowledge about the time constants.

Chapter 4

Experimental Setups

The design of experiments for identification of dynamic models of physical systems usually includes selection of: input and output signals, sample rate etc. Sometimes the design of experiments even involves the design of experimental setups e.g. in order to get well-known experimental conditions or to accommodate some desirable simplification terms with respect to the modelling.

In this chapter, a couple of experimental setups are presented. The main purposes of these setups are 1) to define the experimental conditions, 2) to provide the modelling in the succeeding chapters with prior system knowledge and 3) to support the model estimation with measurement data. The system design of the setups is aimed at reflecting as much as possible of normal system conditions.

The first section describes an experimental setup of a pipe, where the attention is focused on the hydraulic dynamics of the water in the pipe. In the second section, an experimental setup of a central heating system is designed. The focus in this setup is mainly on the thermal dynamics. The third section is dedicated to the description of an experimental setup, based on a low energy house with the central heating system as heating installation *(Hansen, 1996)*.

4.1 A Pipe System

This section is concerned with the experimental setup of a pipe system. The purpose of the setup is to conform a simple system description adequate for identification of a dynamic model of flow in pipes and for estimation of the model parameters. The modelling of the pipe will be described in Chapter 5. The interesting pipe parameters in this connection are the hydraulic resistance of the pipe and the time constant of the pipe flow.

The main components of the experimental setup are a water tank, an expansion tank, an experimental circulating pump driven by a DC-motor and a 22 m long pipe system, as illustrated in Figure 4.1. The water tank forms a water reservoir for the circulating pump. The dimensions of the water tank are: diameter 0.25 m and height 1.20 m. In order to avoid cavitation the system has one Bar overpressure. Hence, the purpose of the expansion tank is to stabilize the pressure in the system. The diameter of the pipe is $d = 15$ mm, the length is $l = 22$ m and the pipe material is galvanized steel. For practical reasons, the pipe system is based on four parallel pipes, as sketched in Figure 4.1. The speed of the circulating pump is controlled through a reference signal u from the data acquisition equipment.

The basic idea of the pipe experiment is to measure the pressure drop over the pipe $\Delta p = p_2 - p_r$ and the flow in the pipe q in order to identify a dynamic model of the pipe. In Figure 4.1 the measured quantities are:

p_1 : pressure just before the pump.

p_2 : pressure just after the pump.

p_r : pressure at the end of the pipe system.

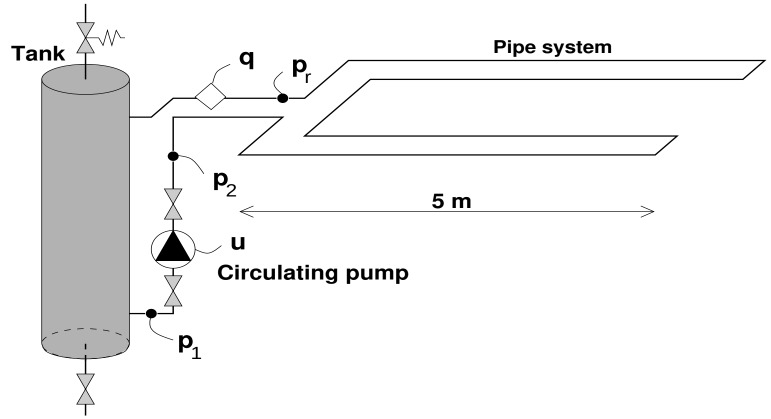

Figure 4.1. *Layout of the experimental setup for identification of a dynamic model of the pipe flow.*

q : flow at the end of the pipe system.

and the controlled quantity is:

u : reference signal to the speed controller of the circulating pump.

The difference between p_2 and p_1 represents the pump pressure, while the difference between p_2 and p_r represents the pressure drop over the pipe. The temperature of the water is assumed to be equal to the room temperature, i.e. about 22 °C. As mentioned earlier, the speed of the pump is controlled by the data acquisition equipment. A sudden variation of the pump speed will change the pump pressure and by that also the pipe pressure. As a result, the flow performs a dynamic response and adjusts to the new pressure.

The experimental setup is equipped with three pressure sensors (MBS 33, Danfoss) and one flow meter (Speedmag, EH-Flowtec). The measuring ranges are:

- Pressure: 0–25 mWc.
- Flow: 1–100 % full scale, where full scale is a preprogrammable flow between 6 l/h and 135 l/h.

The maximal pump pressure is 6 mWc. The pressure drop over a galvanized water pipe, with diameter $d = 15$ mm is 0.092 mWc per meter at 2.1 m^3/h, see *(Grundfos, 1991)*, and a 90° pipe bend is approximately 0.01 mWc. As the length of the pipe part is 22 m and contains 11 pipe bends, the expected pressure drop over the pipe system (at 100 l/h) is approximately $\frac{0.092}{2.1^2} \cdot 0.1^2 \cdot 22 + 11 \cdot 0.01 \approx 0.15$ mWc. This value must be compared with the resolution level of the data acquisition equipment, which is $\frac{25-0}{2^{11}} \approx$ 0.012 mWc (12-bit AD converter, one bit used for sign). Hence, due to the resolution the noise to signal ratio is $0.012/0.16 \approx 0.08$ at 100 l/h, which is applicable. The noise to signal ratio could of course be improved by using a pipe with a smaller diameter, a longer pipe or a pipe with a larger roughness. The selected pipe diameter is a common size.

4.2 A Central Heating System

The motivation for the experimental setup of a central heating system was initiated by the desire to make a full scale experiment in a house equipped with a proper central heating system. In this context, the term "proper" covers a central heating system equipped with a data acquisition system, which measures *the important* pressures, flows and temperatures in the system. The selected house will be described in the next section.

This section is concerned with the design of the setup of a water based central heating system, see also *(Hansen, 1996)*. The design was governed by the following demands:

- The heat distribution network should be configured as a 2-string network.

- It should be possible to use the experimental setup as stand alone system.
- All important pressures, flows and temperatures must be measured.
- It should fit the heat consumption of the house.

The result of these demands is sketched in Figure 4.2. The setup of the central heating system consists of a heating unit and two radiator terminals, as illustrated in the figure. The radiator terminals are denoted as Box 1 and Box 2. The heating unit and the boxes are interconnected by insulated plastic tubes with diameter 15 mm and length 5 m. These tubes are illustrated by "loops" in Figure 4.2.

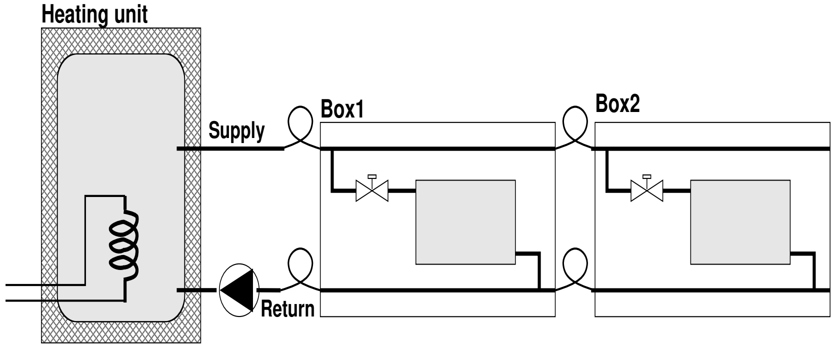

Figure 4.2. *Sketch of the experimental setup of a central heating system.*

The design and the functionality of this setup are described in the following subsections.

4.2.1 Heating Unit

The main purpose of the heating unit is to serve as a hot water supply (i.e. heat supply) for the heat distribution network. The designed heating unit has the capacity of 80 liters. The water tank is placed inside a movable box unit. The space between the water tank and the walls of the box unit is insulated, as sketched in Figure 4.3. The width of the heating unit is 0.65 m and the height is less than 2 m.

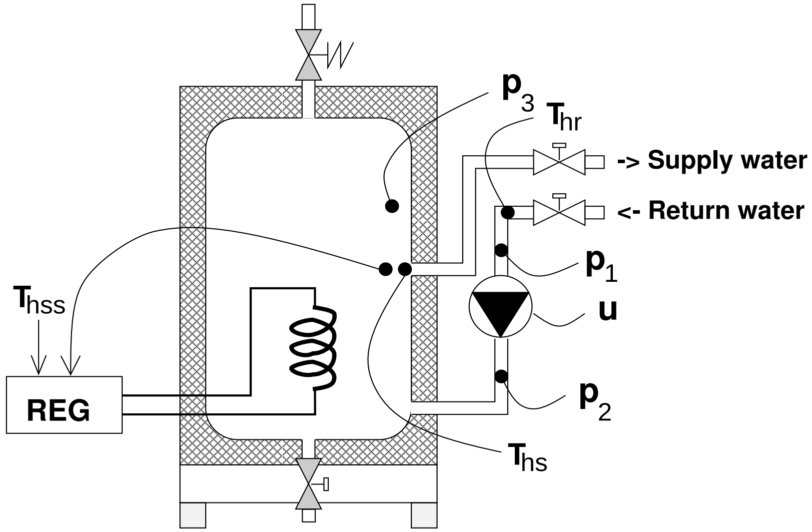

Figure 4.3. *Sketch of the heating unit.*

In Figure 4.3 the measured quantities are:

p_1 : inlet pressure of the pump.

p_2 : outlet pressure of the pump.

p_3 : pressure in the water tank next to the tank outlet.

T_{hs} : temperature of the supply water.

T_{hr} : temperature of the return water.

and the controlled quantities are:

u : reference signal to the speed control of the circulating pump.

T_{hss} : reference signal to the water temperature control of the heating unit (i.e. set point for the water supply temperature).

As for the experimental setup for the pipe system, the difference between p_2 and p_1 represents the pump pressure. It should be noted that the flow is indirectly measured by the flow measurement in the two radiator terminals.

The heating unit is equipped with three pressure sensors (MBS 33, Danfoss) and two temperature sensors (pt-100). The measuring ranges are:

- Pressure: 0–25 mWc.
- Temperature: 0–100 °C.

As mentioned above, the heating unit has two controllable inputs:

- The set point of the water supply temperature is 0–100 °C.
- The reference signal to the circulating pump is 0–5 V, which depending on the flow yields a pump pressure between 0.1–6 mWc.

The heat source is a 2.5 kW electric heat element, which is on/off controlled by an E5AJ controller (Omron). The set point temperature T_{hss} for the water supply temperature T_{hs} can be set to a value between 0 °C and 100 °C, either on a local display or remote by the data acquisition system. The water temperature is measured next to the outlet of the tank (alias the supply temperature). An experimental version of circulating pump UPE 25-60 180 (Grundfos) is placed in the return pipe from the heat distribution network. The speed control of this pump is slightly modified, which makes it possible to remote control the speed from the data acquisition system by the 0–5 V signal. Thereby, the pump pressure can be changed from 0.1 to 6.0 mWc (depending on the flow). The heating unit is also equipped with an expansion tank. As mentioned in Section 1.2, the purpose of the expansion tank is to stabilize the pressure at approximately 10 mWc overpressure.

4.2.2 Radiator Terminals

Two radiator terminals together with insulated tubes form the heat distribution network in the experimental setup, as sketched in Figure 4.2. The design demands, listed in Section 4.2, have been satisfied by the introduction of a thermal box concept. The idea of this concept is to build an insulated box around the radiator. Hence, the radiator is placed in a small room, i.e. inside a box as shown in Figure 4.4. It is noted that:

- The 2-string network can directly be implemented in the box structure.
- It supports the stand alone demand, as the radiator is separated from the surroundings by the insulated box walls. In order to be able to use the radiator as a "normal" radiator (heat supply), three of the box walls are removable, i.e. top, bottom and front wall.
- The relevant pressure, flow and temperature measurements can be directly implemented in the box structure.

The final demand is related with the heat consumption of the house. In Section 4.3.3 it will be explained, how the size of the radiator has been calculated to 400 W.

The two thermal boxes are built identically. The used radiator is a 395 W panel radiator (Thor) with an additional convector on its backside. The physical dimensions are: height 30 cm, length 60 cm and volume 5 liters. A thermostatic valve, RA-FN 15 (Danfoss), is placed in the inlet pipe of the radiator. The frame of thermal box is based on non-massive iron uprights. The box walls are sandwich constructions consisting of three layers: 3 mm iron plate (outer layer), 75 mm of mineral wool (middle layer) and 1 mm lattice (with approximately 40% perforation) aluminium plate (inner layer). The volume of the closed box is approximately 500 liters and the dimensions of the thermal box are shown in Figure 4.4. Top and front wall are equipped with cooling element, which can be applied, when the thermal box is used as stand alone (i.e. the box is closed). 395 W as heat supply for a "room"

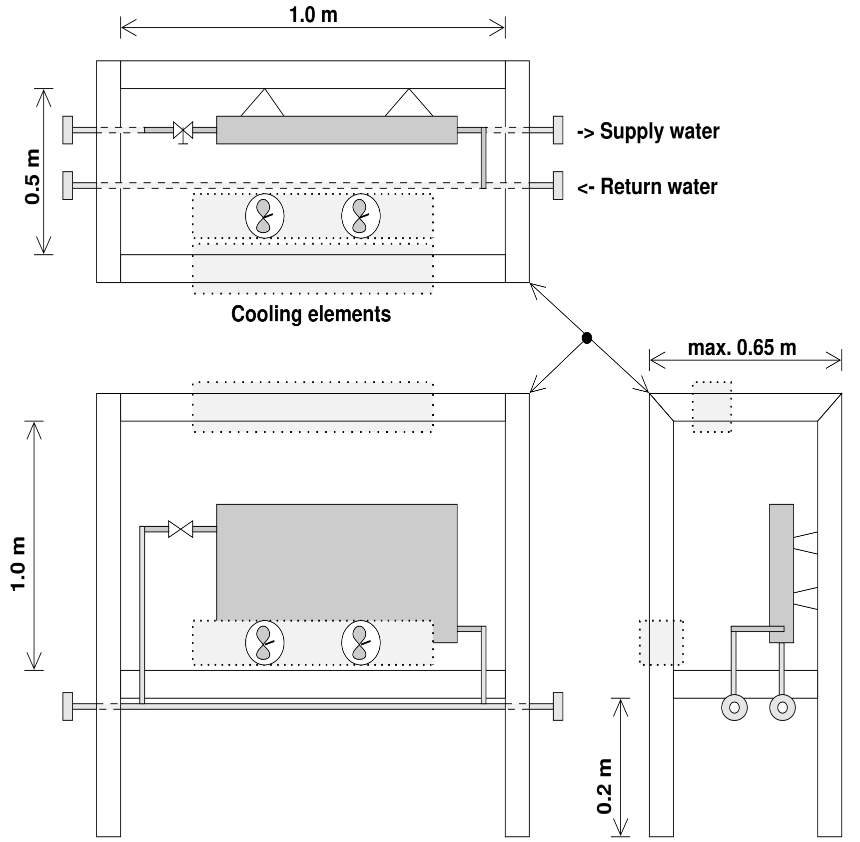

Figure 4.4. *Sketch of the radiator box unit, seen from the top, the front and the right hand side. The top, front and bottom walls can be removed. Moreover, top and front wall each contain cooling elements.*

of 500 liters is indeed more than enough. Hence, the purpose of the cooling elements is to transport heat from the inside of the box to the outside of the box in a relatively controlled way. The cooling elements are based on peltier elements (AA 181-24-22-00-00, Supercool), i.e. electric devices. Thus the cooling power can be measured by measuring the voltage and current of the peltier elements. Each peltier element has a cooling power of 181 W at 0 K temperature difference over the element. The cooling power decreases linearly as function of the temperature difference.

As sketched in Figure 4.5, the thermal box is equipped with three pressure sensors (MBS 33, Danfoss), one flow meter (Speedmag, EH-Flowtec) and four temperature sensors (pt-100) – two for water measurements and two for air measurements. The measuring ranges are:

- Pressure: 0–25 mWc.
- Flow: 1–100 % full scale, where full scale is a preprogrammable flow between 6 l/h and 135 l/h.
- Temperature: 0–100 °C.

The thermostatic valve, which is placed at the inlet of the radiator, has a temperature selector:

S_i : selector for the set point temperature of the thermostatic valve. Indicator levels 1–5 denote reference temperatures from 14–26 °C.

The measured quantities are:

p_{vj} : pressure just in front of the thermostatic valve.

p_{rj} : pressure between the valve and the radiator.

p_{oj} : pressure after the outlet of the radiator.

q_j : flow through the thermostatic valve and radiator.

T_{ij} : water temperature at the radiator inlet.

T_{oj} : water temperature at the radiator outlet.

T_{bj} : air temperature next to the sensor of thermostatic valve.

T_{aj} : air temperature near the thermal box at the upper right corner.

Index j is in this context related to either Box 1 or Box 2. The difference between p_{vj} and p_{rj} describes the pressure drop over the thermostatic valve, while the difference $p_{rj} - p_{oj}$ forms the pressure drop over the radiator. In Figure 4.5, P_{c1j} and P_{c2j} respectively, refer to the cooling power of the two peltier elements.

The thermal box can be operated in two modes, either as stand alone or as heat supply. When the box is used as stand alone (the box is closed), the heat loss of the box can be influenced by the cooling elements. When the removable walls are removed, the "thermal box" can serve as a "normal" radiator (i.e. as heat supply) in a house.

4.2.3 Data Acquisition System

The previous sections refer to a data acquisition system. The purpose of this system is to sample acquire data, store the measurements and to control the controllable input at a predefined sample rate.

The heart of the data acquisition system is a 75 MHz Pentium computer with 16 Mbyte memory and 1 Gbyte disc space. The data acquisition is based on a DT 3003 board (Data Translation). The DT 3003 board contains 32 differential or 64 single ended input channels (AD – analog to digital), two output channels (DA – digital to analog), 8 digital input/output lines and one counter/timer unit. The resolution of both input and output signals is 12 bit (unsigned). A sketch of the data acquisition system is shown in Figure 4.6. In order to protect the DT 3003 board from shortcuts, high

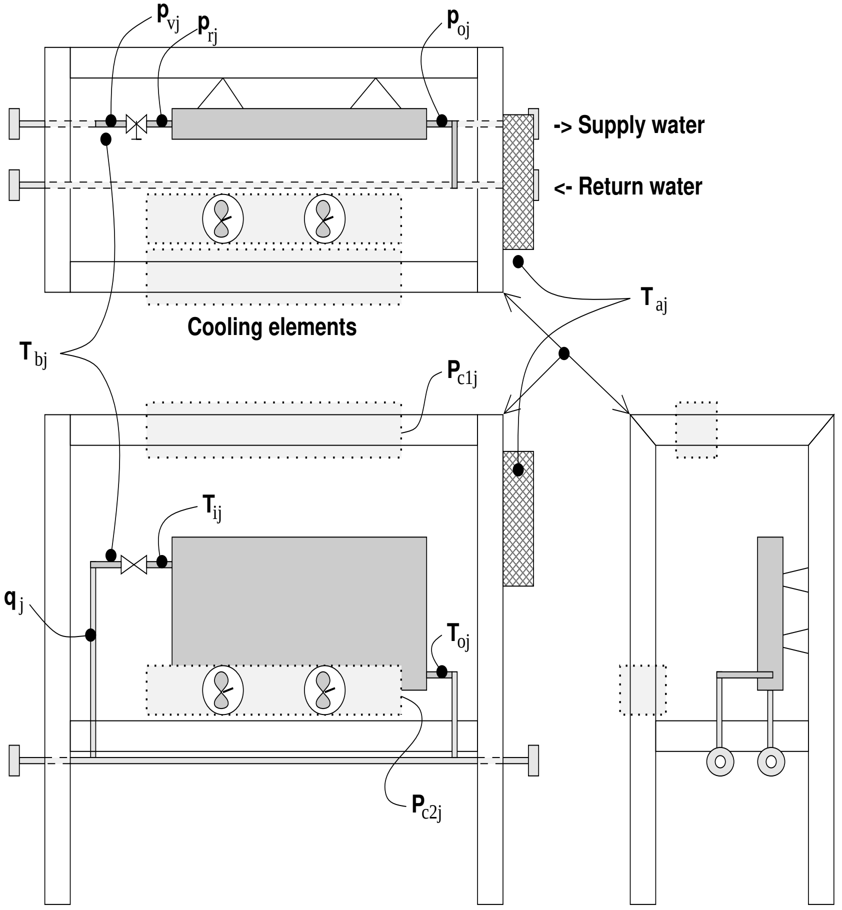

Figure 4.5. *Quantities measured in the radiator box. Index j refers to either Box 1 or Box 2.*

voltages etc., a galvanicly separated interface has been designed. Wires from the sensor are directly mounted to this interface.

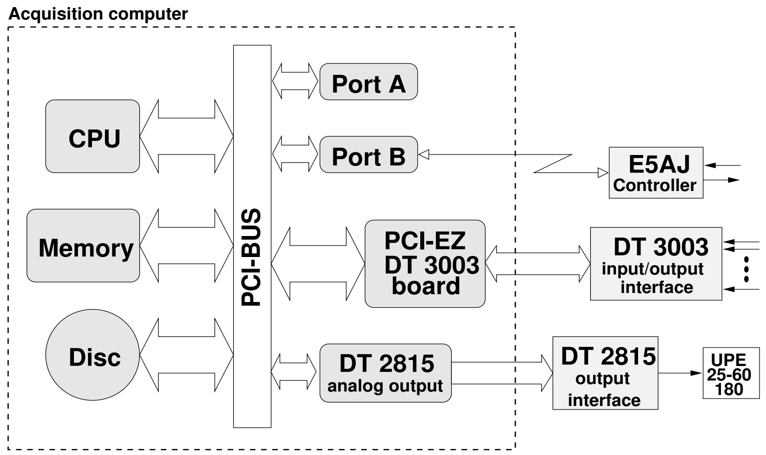

Figure 4.6. *Configuration of the data acquisition system.*

As indicated in Figure 4.6, the data acquisition system also contains a DT 2815 board (Data Translation). The DT 2815 board has 8 (12 bit) DA channels. One of the channels is used to generate the pump speed reference signal u, see Section 4.2.1. This board is also protected by a galvanicly separated interface. The set point T_{hss} of the water supply temperature is communicated to the E5AJ controller through serial communication on port B. The E5AJ controller also supports other services, as for instance an indication of how large a proportion time the heating is active.

The data acquisition system is based on the software product HP VEE (Data Translation). It runs both under Window 3.1 and Windows 95. HP VEE is a visual object oriented programming software tool for data acquisition, see *(Data Translation, 1995)*. Hence, the programming of a data acquisition program consists in putting standard objects together in more complex structures – structures which reflect the actual system. A number of data acquisition setups have been customized to fit the needs of the experimental setup, described in the previous section. These setups acquire, convert and store the 21 measured quantities and control the pump speed and the water supply temperature at a sample rate of 10 seconds.

4.3 A Test House

The idea with the test house is to make a full scale house heating experiment with a water based central heating system as heating installation. The purpose of the full scale experiment is to identify dynamic models for the heat transfer from the central heating system to the house and from the house to the surrounding environment. For example the interaction between house and heating installation, the influence of the solar radiation on the system and the observability of the system can be investigated based on the identified models.

A low energy test house on the campus area of DTU turned out to be an adequate test house (see Section 4.2). The low energy test house (Building 121 A) belongs to the Department of Buildings and Energy (IBE). It was built around 1980. The term *low energy* refers to the nominal heat consumption of the house, which is only 2.5 kW at standard conditions, i.e. -12 °C outside and 20 °C inside. This test house is adequate, in the sense that it accommodates a number of desirable simplifications: unoccupied, simple design, well-known structure and still it constitute a real house.

The following subsections describe the test house, the data acquisition system and some considerations on the energy consumption of the test house.

4.3.1 Low Energy Test House

This description of the selected test house is based on prior knowledge, i.e. available physical knowledge and results obtained by previous experiments, see e.g. *(Rasmussen and Saxhof, 1982)*, *(Hansen, 1985)* and *(Madsen et al., 1990)*.

The low energy test house is a single-storey building with a non-ventilated crawl space and a roof space used as office. The ground floor of the test house forms a test area of 120 m^2. As sketched in Figure 4.7, the ground floor is divided into two equal sized rooms (each of 60 m^2) by a wall insulated with 95 mm mineral wool. The west room is denoted by “B”, and the east room by “A”. Furthermore, each room is partly separated into four smaller rooms by a cross wall in the middle of the room (see Figure 4.7). The room height is 2.4 m. The total window area in room A is 7.5 m^2, where 4.8 m^2 are facing south and 2.7 m^2 north. The windows in room B are identical to those in room A, except that the windows in room B are covered up. The outer wall and the ceiling of the ground floor are light sandwich constructions, based on a masonite beam insulated with 300 mm mineral wool. All windows are triple glassed. The test house is extremely tight. The two cross walls in the center of each room form the load-bearing walls, as the load-bearing capacity of the outer wall is small due to its construction.

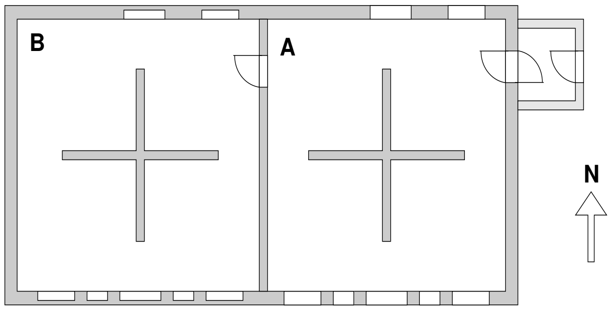

Figure 4.7. *A sketch of the ground plan of the low energy test house. Each room is 60 m^2.*

The floors in room A and B are layer constructions. From the bottom and upwards, the floor in room A consists of: 22 mm plywood, 300 mm mineral wool, 22 mm plywood, and 75 mm concrete, while the floor in room B consists of: 22 mm plywood, 300 mm mineral wool, 22 mm plywood, 50 mm polystyrene, and 22 mm chipboard. This makes room A thermally more heavy than room B. However, the floor in room B is (almost) covered with a double layer of concrete flags, each flag with area 0.16 m^2 and thickness 50 mm. Thus, the thermal heat capacity of room B should be about the same as the thermal heat capacity of room A.

In order to get well defined experimental conditions, the test house is divided into two zones:

- Room A is considered as the thermal test zone (measurement area).
- Room B is considered as the control zone (to be used for auxiliaries).

Room A is divided into a northern and a southern oriented test room (indicated in Figure 4.8 by the cross pattern in the walls) in order to separate the two radiator terminals of the experimental setup of a central heating system described in Section 4.2. Referring to Figure 4.8, the follow notation is introduced:

Room An: northern test room containing Box 2.
Room As: southern test room containing Box 1.
Room B : control room containing the heating unit and data acquisition system, denoted by "HU" and "PC", respectively.

The sensor configuration in the test house is sketched in Figure 4.8. The test house is equipped with 8 air temperature sensors (thermocouples, type T) and three sensors for solar radiation. The measuring ranges are:

- Temperature: -50–100 °C.
- Solar radiation: 0–600 W/m^2.

The measured quantities are:

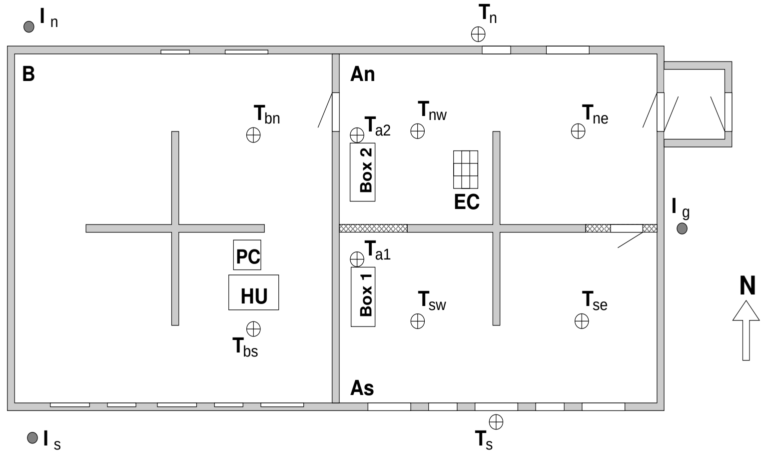

Figure 4.8. *Sensor configuration in the test house.*

T_{bn} : air temperature in north-east part of room B.

T_{bs} : air temperature in south-east part of room B.

T_{nw} : air temperature in north-west part of room An.

T_{ne} : air temperature in north-east part of room An.

T_{sw} : air temperature in south-west part of room As.

T_{se} : air temperature in south-east part of room As.

T_n : northern ambient air temperature.

T_s : southern ambient air temperature.

I_n : horizontal solar radiation (direct and diffuse) from north.

I_s : horizontal solar radiation (direct and diffuse) from south.

I_g : vertical solar radiation (direct and diffuse) on top of the roof.

Besides the measured quantities listed above, also all the quantities described in Section 4.2.1 and 4.2.2 are measured. The thermal boxes are used in the heat supply configuration (i.e. the top, front and bottom walls are removed). As indicated in Figure 4.8, by T_{a1} and T_{a2} (compare with Figure 4.5), the front sides of the thermal boxes are oriented towards the center of the test rooms. For simplicity, the insulated tubes connecting the heating unit with Box 1 and Box 1 with Box 2 are not shown Figure 4.8.

The windows in room B are covered up, as illustrated in Figure 4.8. Meanwhile the windows in the two test rooms are not modified. The purpose of this arrangement is to avoid correlation phenomena in the measurements due to the heat input from the solar radiation entering all the rooms. The windows in the two test rooms are not modified. To avoid the correlation between room An and room As, an additional heat input is placed in room An (denoted by "EC" in Figure 4.8). The idea of the additional heat input is to simulate e.g. an electric cooker (abbreviated as EC) or another heat producing device in a normal house. Hence, the EC must satisfy the following demands:

- Have a work schedule uncorrelated with the daily rhythm of the sun.
- Submit a significant heat input into room An.

The EC is realized as a shielded bulb. The radiation from the bulb is converted to convective heat by the shield. The EC is remote controlled from the data acquisition system, i.e. the data acquisition system controls a switch yielding an on/off heat input from the EC. The size of the significant heat input will be discussed in Section 4.3.3.

4.3.2 Extended Data Acquisition System

The data acquisition system in Section 4.2.3 has to be extended in order to be able to handle the new measurements described in the previous section. The 8 thermocouple signals are converted to Celsius by 8 modules of

type 6B11 (Analog Devices). These modules are gathered on a 4B board (Analog Devices). The converted data are accessed through a serial communication between port A in the data acquisition system and the 4B board, see Figure 4.9.

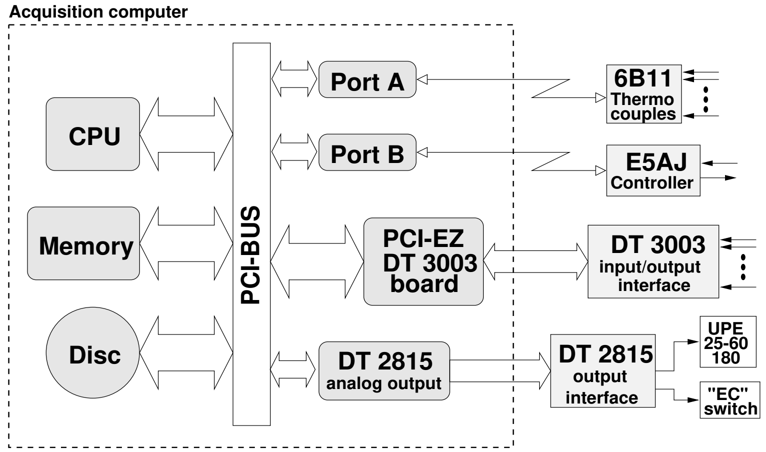

Figure 4.9. *Configuration of the extended data acquisition system.*

As shown in Figure 4.9, the control signal to the EC is generated from the DT 2815 board. The solar radiation signals are connected to the interface of the DT 3003 board.

4.3.3 On Energy Consumption

The nominal energy consumption of the low energy test house is 2.5 kW. This yields a nominal heat loss of 78 W/°C at standard conditions and the nominal heat consumption of one test room becomes 625 W.

Ambient temperatures around and below -12 °C are not frequent in the Copenhagen area. Hence, during winter time, the actual energy consumption of one test room is smaller than 625 W.

The nominal radiator power is set to 400 W and the heat input of EC is set to 150 W. These settings are compromised by:

- The energy consumption of one test room is smaller than 625 W.
- The energy contributions to room An consist of: heat loss from the tubes (connecting Box 2 to Box 1), nominally 400 W from the radiator, heat input from indirect solar radiation and 150 W from the EC.
- The energy contributions to room As consist of: heat loss from the tubes, nominally 400 W from the radiator and heat input from direct and indirect solar radiation.

The nominal energy consumption of room B is 12.5 kW. As room B serves as control zone, the temperature can be smaller than 20 °C. The energy contribution to room B comes from the two test rooms, heat loss from the heating unit and from the data acquisition system (consumption heat). The sizes of these heat contributions are not important, as room B is considered to be a control zone and not a test zone.

4.4 Summary

In this chapter three experimental setups have been presented. The first experimental setup was designed for identification of a dynamic model for a pipe. The second experimental setup was of a water based central heating system. The purpose of this setup was to be used for identification of dynamic models of the heat transfer processes from the central heating installation to the ambient air. The setup was designed to fulfill two tasks, to serve as heating installation in a full scale house heating experiment and to be used as a stand alone system.

The third experimental setup was a low energy test house with the central heating system applied as heating installation. The purpose of this setup

was the identification of the heat transfer processes, from the central heating installation, through the house, to the ambient air.

A lot of experiences on the central heating system has been achieved through the modelling presented in the following chapters. The basic idea of the thermal boxes was good. However, a number of changes for the experimental of the central heating system can be recommended:

1. From a thermal point of view, the radiator terminal constructions contain several thermal bridges. Thus, if the two radiator boxes are to be used as thermal boxes, the inner walls have to be exchanged by some kind of rigid insulation material, in order to 1) protect the mineral wool and 2) minimize the existence of thermal bridges.
2. The flow meter should be move to the outside of the box, as the energy consumption of the flow meter is converted to heat. Thus, the flow meter acts as a small heat source, when the box is closed.
3. The cooling elements must be equipped with power measurement, in order to get more precise knowledge on the cooling power, when the thermal boxes are used as stand alone.
4. The temperature measurement of the “last section” in the radiator has to be improved.
5. Thermostatic valves with smaller capacity should be implemented in the boxes.
6. The experimental setup of the central heating system is exposed to corrosion from the water. This implies “sludge production”, which tends to influence the hydraulic resistance in the flow meters (due to their small diameter).

Some of these recommendation will be more understandable, when the rest of thesis is read.

Chapter 5

Pipe Modelling

This chapter deals with modelling of incompressible flow in pipes. The modelling is focussed on pipes used in the heat distribution network of the central heating system. The purpose of the pipe modelling is to identify and estimate the parameters of a dynamic model of the flow in a pipe.

Flow is usually characterized by the following terms:

- Viscous versus inviscid.
- Incompressible versus compressible.
- Laminar versus turbulent.
- Steady versus unsteady.

An abundance of literature exists on flow modelling. *(Fox and McDonald, 1985)* and *(Larsen, 1984)* serve as background for the deterministic part of the modelling phase of this chapter.

The first section gives a short introduction to the basic theory of flow in pipe systems. In the second section, a dynamic model of the flow in a straight circular pipe is derived based on the assumption of having one-dimensional incompressible flow. The third section presents pipe measurements, which are measured on the pipe system described in Section 4.1, while estimations with these measurement data are performed and described in the succeeding section.

5.1 Flow in Pipe Systems

The basic theory of flow in pipes is based on the assumption of steady incompressible flow. This concept will be further elaborated below. A detailed modelling approach of central heating systems based on steady incompressible flow is described in *(Aggerholm, 1983)*.

The components of a pipe system can be divided into straight pipes and non straight pipes. This partitioning makes the modelling of pipes more convenient.

5.1.1 Straight Pipes

A steady incompressible flow without friction losses is described by the Bernoulli equation:

$$E_V = p_s + \frac{1}{2}\rho w^2 + \rho g h = \text{constant} \tag{5.1}$$

where p_s denotes the static pressure, ρ and w the density and the velocity of the fluid, respectively, g denotes the acceleration of gravity and h the vertical distance to an arbitrary reference level. The basic concept of the Bernoulli equation is the conservation of energy. The presented Bernoulli equation (5.1) has been normalized with respect to volume.

As flow in a water based central heating systems is subjected to friction losses, (5.1) can be reformulated as:

$$(p_{s1} - p_{s1}) + \frac{1}{2}(\rho w_1^2 - \rho w_2^2) + \rho g(h_1 - h_2) = \Delta E_V \tag{5.2}$$

where the indices refer to two different cross sections and ΔE_V denotes the volume specific energy loss due to friction. This version of the Bernoulli equation is often used in calculations of the layout of the pipe system, when the heat distribution network for a central heating system is designed.

Using (5.2) for a pipe with constant cross section area A_p and length l, the work due to friction is related to the friction force F_f as follows:

$$\Delta E_V \; A_p \, l = F_f \; l \tag{5.3}$$

Thus, the friction force F_f can be expressed in terms of the pressure drop Δp_f due to friction (alias the energy loss ΔE_V):

$$F_f = \Delta p_f \; A_p \tag{5.4}$$

The flow in pipes is classified by the flow being laminar or turbulent. In this context, the term “flow” is used as an abbreviation for volumetric flow. The flow type is distinguished by the actual velocity field profile, since the one-dimensional velocity field profile of laminar flow in a circular pipe is parabolicly shaped (with the highest velocity in the center), while the one-dimensional velocity field profile of turbulent flow has “a flat plateau”, as illustrated in Figure 5.1. The more turbulent the flow is – the wider the “plateau” is. Both profiles are symmetric around the center axis of the pipe.

Fluid velocity in a pipe is often characterized by the mean fluid velocity. The mean fluid velocity w of a one-dimensional flow in a circular pipe is

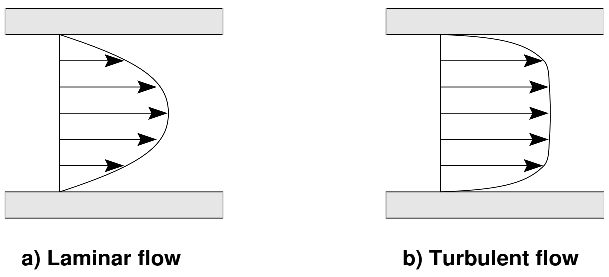

Figure 5.1. *Fluid velocity field profiles for one-dimensional flow in a pipe.*

in principle easily found using polar coordinates (due to the center axis symmetric):

$$w = \frac{1}{A_p} \int_0^{\frac{d}{2}} \int_0^{2\pi} w(r,\theta)\, d\theta dr = \frac{2\pi}{A_p} \int_0^{\frac{d}{2}} w(r)\, dr \tag{5.5}$$

where r and θ are polar coordinates and A_p denotes the cross section area of the pipe. For example, the velocity field profile of laminar flow in a circular pipe is:

$$w(r,\theta) = w(r) = \left(\frac{d}{2} - r\right)^2 w_{max} \tag{5.6}$$

where w_{max} denotes the largest fluid velocity. A description of the fluid velocity profile of turbulent flow is found in *(Zoebl and Kruschik, 1978)*.

It is well-known that the flow type can be distinguished by the Reynolds number:

$$\begin{aligned} \text{Re} &= \frac{w\, d}{\nu} && (5.7) \\ &= \frac{d}{\nu\, A_p}\, q && (5.8) \end{aligned}$$

where d denotes the diameter of the pipe, ν the kinematic viscosity of the fluid, while q denotes the flow. The Reynolds number describes the ratio of inertia to the viscous forces. The flow classification is as follows:

- Re $<$ 2300 implies laminar flow.
- Re $>$ 3000 implies turbulent flow.
- 2300 $\leq$ Re $\leq$ 3000 implies that either laminar or turbulent flow is possible – also denoted as the transient region.

It can be observed in Table A.1, that the kinematic viscosity ν is temperature dependent. The influence of this dependency on the flow in a circular pipe with diameter $d = 15$ mm can be assessed as presented in Table 5.1; using the upper laminar flow limit Re=2300, expression (5.8) and data for the kinematic viscosity ν in Table A.1. From Table 5.1, it can be concluded that the upper limit of laminar flow decreases, when the water temperature increases.

Table 5.1. *Upper limit of laminar flow (at Re=2300) for a straight circular pipe with diameter d=15 mm, as function of the water temperature.*

Water temperature	10	30	50	70	90	°C
Laminar flow limit	127	79	54	40	32	l/h

Using dimensional analysis, as described in *(Fox and McDonald, 1985)*, the pipe pressure drop Δp_f (alias the volume specific energy loss ΔE_V) due to friction can be modelled as:

$$\begin{aligned} \Delta p_f &= \lambda\, \frac{\rho\, l}{d}\, \frac{w^2}{2} && (5.9) \\ &= \lambda\, \frac{\rho\, l}{2\, d\, A_p^2}\, q^2 && (5.10) \end{aligned}$$

where λ denotes the friction factor and w the mean velocity of the fluid. Equation (5.9) is also known as the Darcy-Weisbach equation. It is observed that the pipe pressure drop Δp_f is a function of the friction factor λ and the flow q. The friction factor λ depends on the actual flow type. This dependency is investigated below.

Laminar Flow

In laminar flow the friction factor is defined as:

$$\lambda = \frac{64}{\mathrm{Re}} \tag{5.11}$$

This result can be substituted into (5.10) as follows:

$$\Delta p_f = \frac{64}{\mathrm{Re}} \frac{\rho l}{d} \frac{w^2}{2} = 32 \frac{\rho\, l \nu}{d^2\, A_p} q \tag{5.12}$$

Hence, it is observed that in laminar flow the relation between pressure drop due to friction Δp_f and flow q is linear.

Turbulent Flow

In turbulent flow the friction factor λ is approximated by the implicit Colebrook equation*(Fox and McDonald, 1985)*:

$$\frac{1}{\sqrt{\lambda}} = -2 \log_{10} \left(\frac{2.51}{\mathrm{Re}\,\sqrt{\lambda}} + \frac{e}{3.71\, d} \right) \tag{5.13}$$

where e denotes the pipe roughness.

Values of the roughness e for different pipe materials are presented in Table 5.2. From the Colebrook equation (5.13), it is observed that the friction

factor in turbulent flow depends on the Reynolds number, the pipe diameter and the pipe roughness. This implicit dependency can be sketched in a chart form as in Figure 5.2, i.e. the friction factor λ is depicted as function of the Reynolds number Re and the ratio between pipe roughness and pipe diameter e/d.

Table 5.2. *Roughness for different pipe materials.*

Material	Pipe state	Roughness e
Copper, glass, plastic and light-alloy metal	New	0.001–0.005
Galvanized steel	New	0.1–0.3
	Lime layered	0.5–2.0
Cast iron	New	0.2–0.6
	Rusty	0.5–1.5
	Very rusty	2–5
Unit		mm

Data compiled from *(Thøgersen, 1992)*.

The turbulent region in Figure 5.2 can be divided into smaller regions *(ASHRAE, 1989)*. For example, when the Reynolds number is less than $1{\cdot}10^5$ and the pipe is smooth (i.e. e is small), the friction factor λ can be described by the Blasius equation *(Fox and McDonald, 1985)*:

$$\lambda = \frac{0.316}{\mathrm{Re}^{0.25}} \tag{5.14}$$

The evaluation of (5.8) with Reynolds number Re$=1{\cdot}10^5$, pipe diameter d =10 mm and kinematic viscosity $\nu = 0.326{\cdot}10^{-6}$ m^2/s (i.e. at water temperature 90 °C, see Table A.1), yields a pipe flow of approximately $q = 0.9$ m^3/h – a quite large flow for radiators used in single family houses. Hence, it can be argued that the Reynolds number *always* is less than $1{\cdot}10^5$,

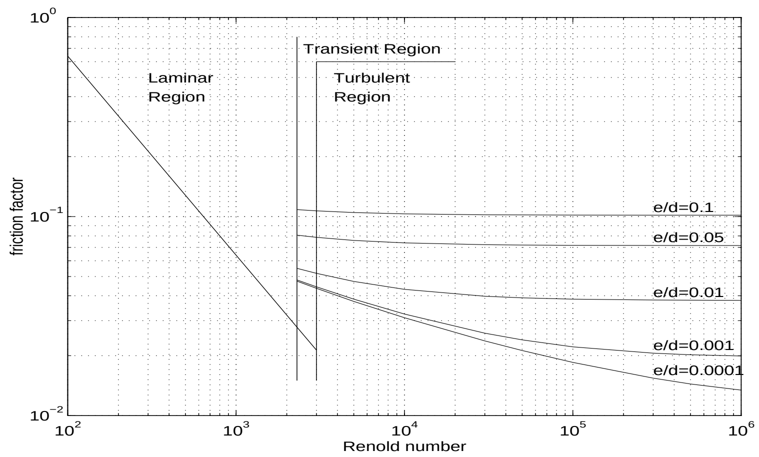

Figure 5.2. *Relation between friction factor, Reynolds number and the ratio e/d between pipe roughness and pipe diameter.*

which implies that the general Colebrook equation (5.13), can be substituted by the Blasius equation (5.14), if the applied pipe is smooth. Using (5.14) and (5.8) together with (5.10), the relation between pressure drop due to friction Δp_f and flow q becomes:

$$\Delta p_f = 0.158 \, \frac{\rho \, l \nu^{0.25}}{d^{1.25} \, A_p^{1.75}} \, q^{1.75} \tag{5.15}$$

provided that $3000 \leq \mathrm{Re} \leq 1 \cdot 10^5$ and that the pipe is smooth. Thus, by the use of the Blasius equation it becomes evident that in turbulent flow the relation between pressure drop due to friction Δp_f and flow q is nonlinear.

5.1.2 Non Straight Pipes

Examples of non straight pipes are: pipe bends, pipe fittings, contraction pipes, expansion pipes, T-pipes and valves. The pressure drop Δp_f (energy loss) caused by fluid friction in this type of pipes, will be briefly described in the following.

The basic model for the pressure drop across a non straight pipe is:

$$\Delta p_f = K \, \frac{w^2}{2} \tag{5.16}$$

where K denotes a loss coefficient. Instead of using a loss coefficient in (5.16), the "loss coefficient" is sometimes expressed in terms of the friction factor λ, an equivalent pipe length l_e and the diameter d, i.e. as:

$$K = \lambda \, \frac{\rho \, l_e}{d} \tag{5.17}$$

It is noted that substitution of (5.17) into (5.16) yields the Darcy-Weisbach equation (5.9). The flow in a non straight pipe is usually turbulent.

As described in *(Aggerholm, 1983)*, loss coefficients are often determined experimentally. A comprehensive collection of loss coefficients can be found in *(ASHRAE, 1989)*.

5.2 Dynamic Flow Model

In the previous section some basic terms of flow theory were presented. In this section a dynamic pipe flow model will be derived based on the fundamental principles of conservation of mass and momentum.

These fundamental principles will be applied on a straight circular pipe. Moreover, the dynamic pipe flow model will be based on the assumptions of incompressible, one-dimensional and fully developed flow in horizontal pipes. The temperature dependency of kinematic viscosity and density of the water are neglected.

5.2.1 Conservation of Mass

In order to examine the conservation of mass a *control volume* is usually defined. The idea is to keep account of the mass flow through the surface of the control volume. The mass flow in (or out) of a control volume with respect to a transition area $\mathcal{A}$ can in general be calculated as:

$$\frac{dm}{dt} = \int_{\mathcal{A}} \rho(x,y,z,t)\, w(x,y,z,t)\, dA \tag{5.18}$$

where ρ denotes the density of the fluid and w the velocity of the fluid in a given point (x,y,z) at time t. This principle can be applied to e.g. a straight pipe with constant cross section area A_p, as illustrated in Figure 5.3. The mass flow is only in the x-direction, i.e. it is one-dimensional.

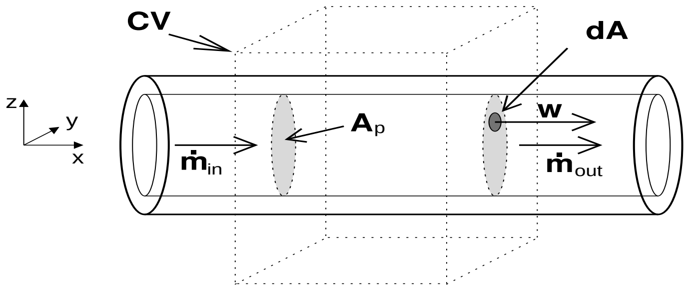

Figure 5.3. *Sketch of a pipe illustrating the mass flow through the control volume CV.*

Let M denotes the total mass of fluid inside the control volume CV. Using the following assumptions:

1. the density of the fluid is uniformly distributed with respect to the sectional area, implying that $\rho(x,y,z,t) = \rho(x,t)$.
2. the profile of the fluid velocity field is one-dimensional, implying that $w(x,y,z,t) = \mathrm{w}(x,t)$.

3. incompressible flow, implying that $\frac{dM(x,y,z,t)}{dt} = 0$ (i.e. constant M).

the mass flow in (or out) of CV, as shown in Figure 5.3, becomes:

$$\frac{dm}{dt} = \int_{A_p} \rho(x,t)\mathrm{w}(x,t)\, dA \tag{5.19}$$

$$= \rho(x,t)\mathrm{w}(x,t)A_p = [\rho(t)\mathrm{w}(t)]_x A_p \tag{5.20}$$

where the notation $[\cdot]_x$ is introduced as a convenient abbreviation of the spatial dependency.

In case of an in-stationary process, the mass conservation equation can be written as:

$$\frac{dM(x,y,z,t)}{dt} = \sum_{in} \left[\frac{dm}{dt}\right]_{in} - \sum_{out} \left[\frac{dm}{dt}\right]_{out} \tag{5.21}$$

It may be noted that for a control volume CV, which is fixed in space, $\frac{dM(x,y,z,t)}{dt}$ is reduced to $\frac{dM(t)}{dt}$. Thus, the conservation of mass for the control volume CV shown in Figure 5.3 can be described as:

$$\frac{dM(t)}{dt} = \dot{m}_{in} - \dot{m}_{out} \tag{5.22}$$

$$= [\rho(t)\mathrm{w}(t)]_{in} A_p - [\rho(t)\mathrm{w}(t)]_{out} A_p \tag{5.23}$$

The assumption of incompressible flow implies two things: 1) the mass inside the control volume is constant, i.e. $\frac{dM(t)}{dt} = 0$ and 2) the density of the fluid is constant, i.e. $\rho(x_{in},t) = \rho(x_{out},t) = \rho(t)$. Therefore, (5.23) is reduced to:

$$[\mathrm{w}(t)]_{in} A_p = [\mathrm{w}(t)]_{out} A_p \;\Leftrightarrow\; [q(t)]_{in} = [q(t)]_{out} = q(t) \tag{5.24}$$

Thus, the restrictions of one-dimensional flow, uniform density at a given cross section and incompressible flow applied on a straight pipe, imply that the flow entering a pipe must be equal to the flow out of the pipe.

5.2.2 Conservation of Momentum

As in the previous section, a control volume will be used – this time to examine the conservation of momentum. The momentum equation for a non-accelerating control volume containing the mass M can in general be written as *(Larsen, 1984)*:

$$\frac{d}{dt}\left(M(t)\,w(x,y,z,t)\right) = F_{ex}(x,y,z,t) + \dot{P}_{flow}(x,y,z,t) \tag{5.25}$$

where F_{ex} denotes the sum of external forces (surface and body forces) acting on the control volume and $\dot{P}_{flow}$ denotes the rate of efflux of momentum through the surface of the control volume.

This fundamental principle will now be applied to a straight circular pipe with constant cross section area A_p shown in Figure 5.4. Moreover, the assumptions on page 78 are extended with:

4. uniform pressure distribution at a given cross section, implying that $p(x,y,z,t) = p(x,t)$, where p denotes the cross section pressure.

in order to justify one-dimensional flow.

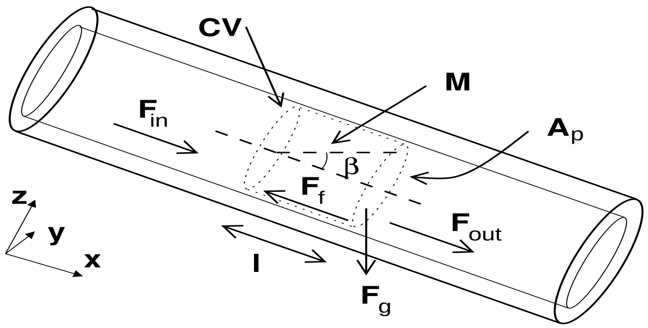

Figure 5.4. *Sketch of the forces acting on the control volume CV in a pipe.*

It follows from assumption 2 and 3 that:

$$\frac{d}{dt}\left(M(t)\,w(x,y,z,t)\right) = M\frac{dw(t)}{dt} \tag{5.26}$$

Another consequence of the incompressibility assumption is the conservation of mass (5.24), which implies that $\dot{P}_{flow}(x,t) = 0$. Thus, the momentum equation (5.25) is reduced to (alias Newton's second law):

$$M\frac{dw(t)}{dt} = F_{in} - F_{out} + F_g - F_f \tag{5.27}$$

where F_{in} and F_{out} denote the cross section pressure forces at the "inlet and outlet" of CV, respectively, F_g the force of gravitation and F_f the friction force.

The assumption of uniform cross section pressure yields:

$$F_{in} - F_{out} = [p(t)A_p]_{in} - [p(t)A_p]_{out} = \Delta p(t)\,A_p \tag{5.28}$$

Moreover, the influence of the force of gravitation can be expressed:

$$F_g = M\,g\,\sin(\beta) \tag{5.29}$$

where g denotes the acceleration of gravity and β the pipe inclination. In case of a horizontal pipe $\beta = 0$. The gravitational force both contributes to the flow in a central heating system and counteracts it. Consequently, as the central heating system is a recirculating system and as the temperature dependency of the density is neglected, the influence of the gravitational force can be neglected, i.e. $\beta = 0$ in general.

Applying the considerations above, imply that (5.27) is reduced to:

$$M\frac{dw(t)}{dt} = \Delta p(t)\,A_p - \Delta p_f\,A_p \tag{5.30}$$

where $\Delta p = p_{in} - p_{out}$. Expressed in terms of flow, (5.30) becomes:

$$\rho\, l\, \frac{dq(t)}{dt} = \Delta p(t)\, A_p - \Delta p_f A_p \tag{5.31}$$

using that $M = \rho\, l\, A_p$ and $q = A_p w$.

Hence, applying the restrictions of one-dimensional flow, uniform density at a given cross section, incompressible flow, uniform pressure distribution at a given cross section and horizontal pipes on a straight pipe, the conservation of momentum is reduced to a first order differential equation.

5.2.3 General Dynamic Pipe Flow Model

Based on conservation of mass and momentum, a dynamic model for incompressible flow in a straight pipe has been derived. As described in Section 5.1.1, the friction force F_f depends on the pressure drop Δp_f due to friction and the cross section area A_p. Moreover, the pressure drop Δp_f depends on the flow type.

For laminar flow – i.e. using (5.12) – the dynamic model of incompressible pipe flow (5.31) becomes:

$$L\, \frac{dq(t)}{dt} = \Delta p(t) - R_l q(t) \tag{5.32}$$

where $L = \frac{\rho\, l}{A_p}$ and $R_l = 32\, \frac{\rho\, l\, \nu}{d^2\, A_p}$. The two parameters, L and R_l, are interpreted as the hydraulic inductance and the hydraulic resistance, respectively.

For turbulent flow – i.e. using (5.10) – the dynamic model of incompressible pipe flow (5.31) becomes:

$$L\, \frac{dq(t)}{dt} = \Delta p(t) - R_t(\lambda)\, q(t)^2 \tag{5.33}$$

where $L = \frac{\rho\, l}{A_p}$, $R_t(\lambda) = \lambda\, \frac{\rho\, l}{2\, d\, A_p^2}$. It is noted that the hydraulic resistance R_t is a function of the friction factor λ, which is determined by the implicit Colebrook equation (5.13).

As argued in Section 5.1.1, the Colebrook equation can be approximated by the Blasius equation (5.14) for Reynolds numbers that are valid for the current setup. In this case, the dynamic model of incompressible pipe flow (5.31) is reduced to:

$$L\, \frac{dq(t)}{dt} = \Delta p(t) - R_{tb}\, q(t)^{1.75} \tag{5.34}$$

where $L = \frac{\rho\, l}{A_p}$ and $R_{tb} = 0.158\, \frac{\rho\, l\, \nu^{0.25}}{d^{1.25}\, A_p^{1.75}}$, provided that the Reynolds number satisfies the inequalities $3000 \leq \mathrm{Re} \leq 1 \cdot 10^5$ and that the pipe is smooth. It is noted that the hydraulic resistance R_{tb} is an explicit parameter.

An electrical equivalent for the dynamic model of laminar flow is shown in Figure 5.5. Similarly to laminar flow, an electrical equivalent for the dynamic model of turbulent flow can be established, when the model is linearized.

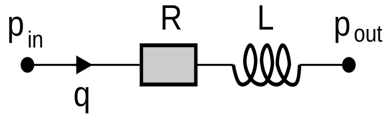

Figure 5.5. *Electrical equivalent of the flow in a straight pipe. L denotes the hydraulic inductance and R the hydraulic resistance, which generally depends on the friction factor λ.*

Two dynamic models describing incompressible flow in a straight circular pipe have now been established – one model for laminar flow (5.32) and one model for turbulent flow (5.33) or (5.34). The two dynamic models can be gathered as follows:

Model Summary 5.1 (General Dynamic Model of Flow in a Pipe) *Given a straight circular pipe with length l, diameter d and roughness e, the dynamic model of one-dimensional incompressible flow q, driven by the pressure Δp across the pipe, can be expressed as:*

$$L\,\frac{dq(t)}{dt} = \Delta p(t) - R_\kappa\, q(t)^\kappa \tag{5.35}$$

where L denotes the hydraulic inductance of the pipe, R_κ the hydraulic resistance of the pipe and κ is a parameter used to determine the flow type and the interpretation of parameter R_κ. The hydraulic parameters are defined as:

$$L = \frac{\rho\, l}{A_p} \tag{5.36}$$

$$R_1 = R_l = 32\,\frac{\rho\, l\, \nu}{d^2\, A_p} \tag{5.37}$$

$$R_2 = R_t(\lambda) = \lambda\,\frac{\rho\, l}{2\, d\, A_p^2} \tag{5.38}$$

where ρ and ν denote the density and the kinematic viscosity of the fluid, respectively, λ the friction factor and $A_p = \frac{\pi}{4} d^2$ the cross section area of the pipe. R_1 denotes the hydraulic resistance in laminar flow and R_2 the hydraulic resistance in turbulent flow.

What about the transition between these models of laminar and turbulent pipe flow? Would it be right to claim that $R_l\, q \equiv R_t(\lambda)\, q^2$ in the moment of transition? As sketched in Figure 5.2, there is a transient area between laminar and turbulent flow. The transition between the flow types is quite casual, when the flow is in the transient zone. It will probably include a lot of time and effort to obtain a good model for this transition. As described in the next section, the problem can be avoided by performing measurements under either laminar or turbulent flow conditions.

5.3 Experiments

The experimental setup was described in Section 4.1. The idea is now to perform a series of experiments in order to estimate the hydraulic inductance and the hydraulic resistances presented in Model Summary 5.1.

5.3.1 Analysis and Input Design

In this section prior knowledge will be compared with measurements on the experimental setup, in order to evaluate the modelling with respect to the flow type and the bandwidth of the flow. The achieved knowledge can then be used for input design.

Analysis of the Flow Type

The first step is to calculate the flows q at the two boundaries of the transition region, i.e. at Reynolds numbers, Re=2300 and Re=3000. Calculated flows for two diameters – one matching the pipe d_{pipe} and one matching the flow meter d_{fm} – are based on data for the experimental setup in Section 4.1 and the result is presented in Table 5.3.

Table 5.3. *Boundary flows of the transient flow region between laminar and turbulent at a water temperature of 25 °C. The pipe diameter is $d_{pipe} =$ 15 mm, while the diameter of the flow meter is $d_{fm} = 2$ mm.*

	Lower limit	Upper Limit	Unit
Re	2300	3000	–
q_{pipe}	86	112	l/h
q_{fm}	11	15	l/h

Inspired by the pipe flows in Table 5.3, a measurement has been performed with a *zigzag*-signal as reference to the circulating pump. The amplitude of the zigzag-signal is tuned in a way, which assures flow measurements "around" the transient region. The measurements are shown in Figure 5.6. In the first subplot of Figure 5.6, the dynamic pressure over the pump p_2-p_1 and over the tank p_r-p_1 are plotted. The second subplot contains the dynamic pressure drop over the pipe Δp, while the third subplot shows the pipe flow q. It is observed that the pipe flow q contains a "sudden shift" in the range of 50 l/h. This strange flow behaviour is not due to the applied reference signal.

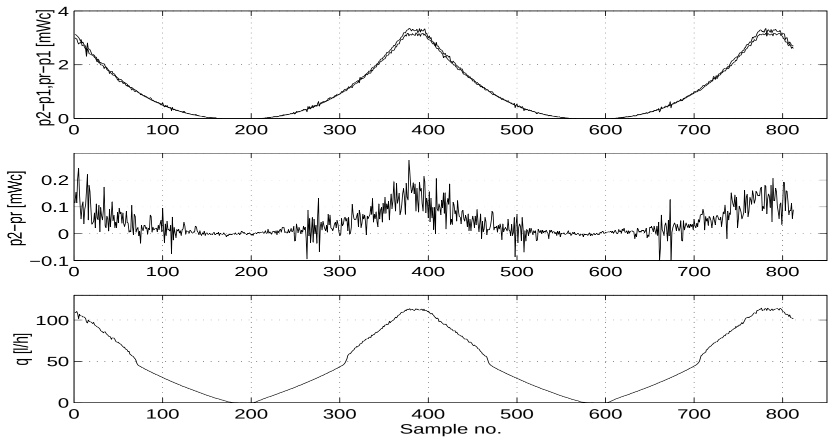

Figure 5.6. *Low-pass filtered measurement data of the pressures p_2-p_1, p_r-p_1, p_2-p_r and flow q from the experimental setup. Sample frequency of plotted data is 2 Hz.*

Could the transient flow region between laminar and turbulent flow for the pipe setup be in the range from 40 l/h to 60 l/h? Comparing this range with the expected transition flow regions presented in Table 5.3, there is a mismatch. Meanwhile, the computation of transient flow regions in Table 5.3 are based on one long straight pipe. This is not quite the case in the experimental setup, as it contains 11 pipe bends in the pipe system.

Due to these pipe bends, the flow in the pipe system will become turbulent at a lower flow compared to a straight pipe of equivalent length. Hence, the strange behaviour observed in the range of 50 l/h, probably is the transient flow region of the pipe system after all.

From Figure 5.6, it is further observed that the dynamic pressure drop over the pipe Δp has a high noise/signal ratio. Moreover, the noise level on the pressure seems to be affected by the size of the flow. For pipe flows less than 25 l/h (approximately), the equivalent pressure drop over the pipe system disappears in the AD quantization. Hence, laminar flow cannot be measured properly in the present pipe system setup. Meanwhile, for pipe flows larger than 65-70 l/h, the equivalent pressure drop over the pipe system is measurable. Thus, turbulent flow can be measured properly, i.e. assuming that the transition flow region is in the approximate range of 40 l/h to 60 l/h.

As described in Section 4.1, the applied flow meter supports flow measurement until 135 l/h. Therefore, the input design is constrained to provide flows in range of 70 l/h to 130 l/h.

Analysis of the Bandwidth

The next step in the analysis is to investigate the bandwidth of the dynamic flow model. The idea is to take a look at the transfer function between the pressure drop over the pipe Δp and the flow q. The transfer function can be achieved as a first order Taylor expansion of the general dynamic flow model (5.35):

$$L\frac{dq}{dt} = (\Delta p_0 - R_\kappa q_0^\kappa) + (\Delta p - \Delta p_0) - \kappa R_\kappa q_0^{\kappa-1}(q - q_0) \tag{5.39}$$

where $(\Delta p_0, q_0)$ denotes the operation point. It is noted that the dependency of the friction factor λ in parameter R_κ (when $\kappa = 2$) has been neglected in (5.39) in order to keep the modelling simple.

In a stationary operation point $(\Delta p_0, q_0)$, the Taylor expansion (5.39) is reduced to:

$$L\frac{d\overline{q}}{dt} = \overline{\Delta p} - \kappa R_\kappa q_0^{\kappa-1}\,\overline{q} \tag{5.40}$$

where $\overline{\Delta p} = \Delta p - \Delta p_0$ and $\overline{q} = q - q_0$ denote the deviation from the stationary operation point. Hence, the transfer function of the linearized pipe flow model is:

$$\frac{\overline{q}(s)}{\overline{\Delta p}(s)} = \frac{G}{\tau s + 1} \tag{5.41}$$

where s denotes the Laplace operator, G the gain and τ the time constant of the pipe flow defined as:

$$G = \frac{1}{\kappa R_\kappa q_0^{\kappa-1}} \quad \text{and} \quad \tau = \frac{L}{\kappa R_\kappa q_0^{\kappa-1}} \tag{5.42}$$

For laminar flow, the parameters of the transfer function are reduced to:

$$G = \frac{1}{R_l} \quad \text{and} \quad \tau = \frac{L}{R_l} \tag{5.43}$$

A set of time constants based on the transfer function for the linearized flow model (5.41) are presented in Table 5.4. The first column ($\kappa = 1$) contains data for the laminar case and the two other columns ($\kappa = 1.75$ alias the Blasius approximation and $\kappa = 2$ alias the Colebrook approximation) contain data for the turbulent cases at operating flow $q_0 = 100$ l/h. As known from Section 4.1, the pipe material is cast iron. The roughness of a new and slightly rusty pipe is about $e = 0.5$ mm, see Table 5.2. In principle this out rules the use of the Blasius equation (5.14), as $e = 0.5$ mm is related to non smooth pipes. Nevertheless, calculations based on the Blasius approximation are presented in Table 5.4. Hence, the difference between a smooth and non smooth pipe can be assessed.

Table 5.4. *Theoretical time constants and 3 dB bandwidth based on the transfer function for the linearized flow model (5.41) at a water temperature of 25 °C.*

	Laminar	Turbulent		Unit
κ	1	1.75	2	–
$L = \frac{\rho\, l}{A_p}$		1.13		10^8 kg/m^4
$R = \kappa R_\kappa q_0^{\kappa-1}$	1.42	4.56	8.11	10^7 kg/(m^{4}sec)
τ	7.95	2.48	1.40	sec.
f_{3dB}	0.02	0.06	0.11	Hz

Pipe roughness: $e = 0.5$ mm and pipe diameter $d = 15$ mm.
Turbulent operating flow: $q_0 = 100$ l/h.

The time constants presented in Table 5.4 indicate that the bandwidth of turbulent flow is larger than the bandwidth of laminar flow. The bandwidth of a smooth pipe ($\kappa = 1.75$) is between the bandwidth of laminar flow and the bandwidth of the non smooth pipe ($\kappa = 2$). Moreover, the time constant of laminar flow can be expressed as:

$$\tau = \frac{L}{R_l} = \frac{d^2}{32\nu} \tag{5.44}$$

i.e. only dependent of the pipe diameter d and the water temperature, since ν depends on the water temperature, while the time constant of turbulent flow ($\kappa = 2$):

$$\tau = \frac{L}{2\,R_t\,q_0} = \frac{\pi d^3}{4\,\lambda\,q_0} \tag{5.45}$$

depends on the diameter d, the operating flow q_0 and the friction factor λ, which is determined by the Colebrook equation (5.13). It is noted that the friction factor λ depends on the Reynolds number Re, which again is related to the flow as in (5.8). Thus, time constant of turbulent flow actually depends on the diameter d, the operating flow q_0 and the water temperature (through the kinematic viscosity ν).

The *real* bandwidth of the experimental pipe setup can be extracted using sinusoidal input signals as reference signal to the circulating pump. The idea is to “measure” the magnitude amplification and the phase shift at different frequencies around the expected 3 dB bandwidth, i.e. to plot the frequency response of the transfer function from the pressure difference over the pipe stretch Δp and the flow q.

The frequency response shown in Figure 5.7 is based on three sets of sweep signals with linear sweep frequency going from:

- 0.5 mHz to 10 mHz.
- 5.0 mHz to 100 mHz.
- 50 mHz to 1.0 Hz.

using $f_s = 25$ Hz as sample frequency. The amplitude and the offset of the input signals has been tuned to produce flows in the range of 70 l/h to 130 l/h.

The frequency response depicts a nonlinear transfer between Δp and q. Meanwhile, comparing the frequency response in Figure 5.7 with the characteristics of a linear first order transfer function, it can be observed that:

- The magnitude amplification seems to decrease with approximately 20 dB/decade.
- The phase shift at “high“ frequencies does not stabilize at -90 degrees.
- The bandwidth measured at the 3 dB magnitude drop and at the 45 degrees phase shift occurs approximately at 0.12 Hz

Thus, the measured frequency response of the transfer function between the pipe pressure Δp and the pipe flow q has a shape, which to some extend

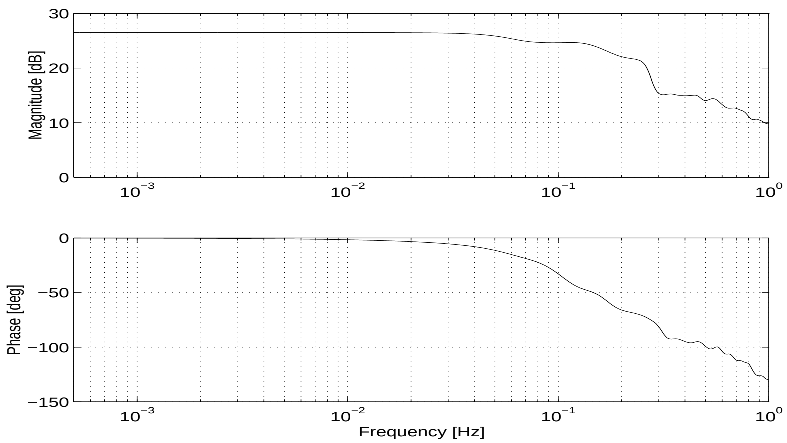

Figure 5.7. *Frequency response of the transfer function from the pressure difference over the pipe stretch Δp to the flow q, based on frequency sweep measurements.*

reminds of the shape of a linear first order transfer function, i.e. when neglecting the fact that the phase decreases more than -90 degrees. Moreover, the measured 3 dB bandwidth is approximately equal to the theoretical bandwidth of the turbulent model for $\kappa = 2$, presented in Table 5.4.

Input Design

The achieved system knowledge can now be used to design proper input signal with respect to the succeeding estimation of Grey Box models. The input design is based on the PRBS and PRUS signals described in Section 3.4.2.

The following set of parameters are used as design parameters for both PRBS and PRUS design:

n : length of the shift register is chosen as $n = 8$ in order to get both short constant periods and longer constant periods.

T_0 : fundamental time period is chosen as $T_0 = 1.6$ seconds.

The event frequency $\frac{1}{T_0}$ of both the PRBS and of PRUS design is approximately five times larger than the expected 3 dB bandwidth of the pipe flow. The two input signals will be denoted as $\mathcal{D}_{PRBS}$ and $\mathcal{D}_{PRUS}$, respectively.

5.3.2 Measurement Data

The experimental setup of the pipe system has been exposed to the two input signals designed above, at a sample frequency of $f_s = 50$ Hz. The sample frequency f_s was selected much higher than the bandwidth of the flow for two reasons:

1. to get many samples describing the level shifts.

2. to be able to lowpass filter the pressure measurement due to the high noise level.

The measurements are shown in Figure 5.8 and 5.9, respectively. The amplitude and the mean value of the two input signals have been tuned to produce a mean flow of 100 l/h with 70 l/h and 130 l/h as minimum and maximum flows, respectively, in order to satisfy the flow restrictions described in the previous section. The measured pipe pressures are in general quite noisy. However, they contain significant peaks indicating level shifts in the input signal to the pump.

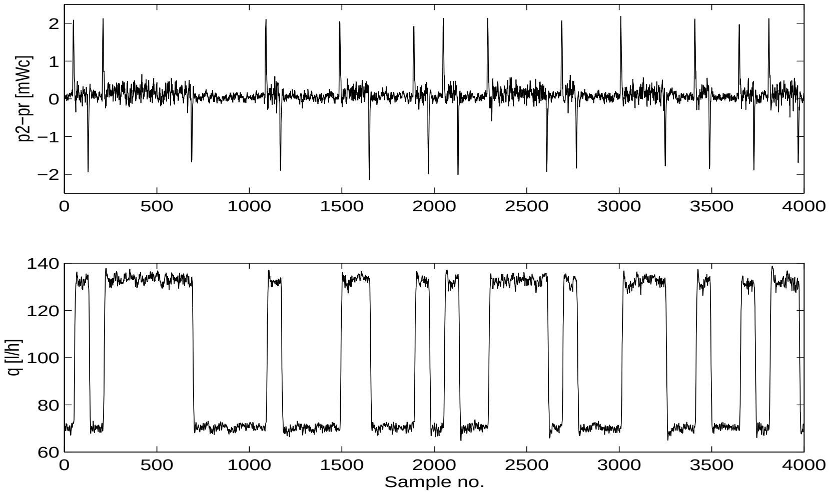

Figure 5.8. *Measured pressure Δp over the pipe and pipe flow q using $\mathcal{D}_{PRBS}$ as reference signal to the pump.*

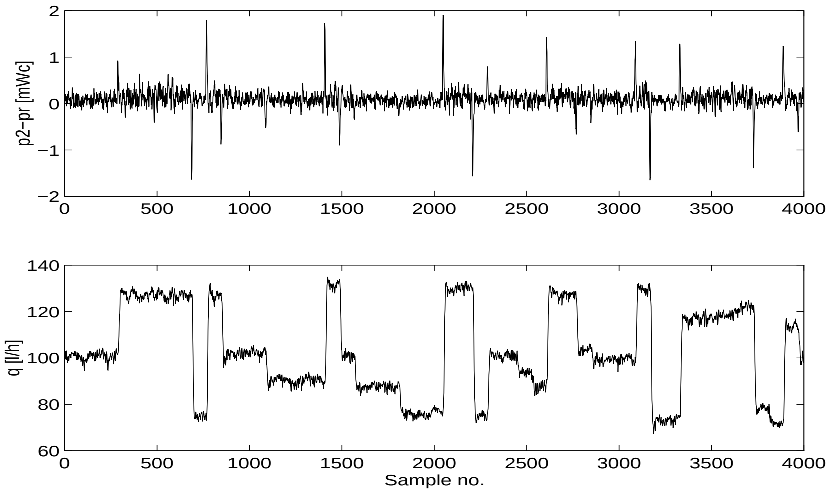

Figure 5.9. *Measured pressure Δp over the pipe and pipe flow q using $\mathcal{D}_{PRUS}$ as reference signal to the pump.*

5.4 Estimation of Grey Box Models

Prior knowledge has in Section 5.2 been used to derive a dynamic model of the flow in a straight circular pipe. In Section 5.3 measurement restrictions have been discussed and two sets of measurements have been presented. Hence, the idea is now to estimate the parameters of the dynamic pipe flow model in Model Summary 5.1.

5.4.1 Identifiability

Before any estimation is performed, the identifiability of the parameters in the dynamic pipe flow model should be investigated. The general dynamic pipe flow model in Model Summary 5.1:

$$L\,\frac{dq(t)}{dt} = \Delta p(t) - R_\kappa\, q(t)^\kappa \tag{5.46}$$

contains the parameters L (hydraulic impedance), R_κ (hydraulic resistance) and κ the power of the flow, where $\kappa = 1.75$ and $\kappa = 2$ indicate turbulent flow in a smooth pipe and in a non smooth pipe, respectively.

The question is now whether or not all three parameters are identifiable? Unfortunately, a clear answer to this question has not been found. It is not possible to test the identifiability of (5.46) using the method described in *(Ljung and Glad, 1994)*, as this method is limited to models, where the state can be expressed in a polynomial form. Nevertheless it can be argued that the answer is *no*. The hydraulic inductance L is independent of the flow type, whereas the hydraulic resistance R_κ and the power κ of the flow depend on the flow type. For a certain value of κ (either 1, 1.75 or 2) R_κ has a certain interpretation (either R_l, R_{tb} or R_t, see Section 5.2.3) and vice versa. Hence, some correlation seems to exist between these two parameters, which further implies that both R_κ and κ cannot be estimated

at the same time. This fact has been confirmed through estimation. R_κ and κ are getting 100 % correlated.

In case of a linear first order model only two parameters can be identified, e.g. the gain G and the time constant τ in (5.41). Thus, based on the discussion above, it may be concluded that L and either R_κ or κ are identifiable.

5.4.2 Turbulent Flow Model

Measurement data are limited to turbulent flow and as the pipe is non smooth, the power of the flow κ is selected as $\kappa = 2$. The Grey Box model of the turbulent flow in Model Summary 5.1 can be expressed as:

$$\begin{aligned} dq(t) &= \frac{1}{L}\left(\Delta p(t) - R_2\, q(t)^2\right)\, dt + \frac{1}{L}\, dW(t) \\ y(k) &= q(k) + e(k) \end{aligned} \tag{5.47}$$

where W is assumed to be a Wiener process with zero mean and incremental variance σ_W^2, y denotes the measured flow and e denotes the measurement noise, which is assumed to be white noise with zero mean and variance σ_e^2. Furthermore, W and e are assumed to be mutually uncorrelated. The hydraulic resistance R_2 is assumed to be constant in order to keep the modelling simple, i.e. $R_2 = R_t(\lambda_0)$ (see (5.38)) where λ_0 corresponds to the operating flow $q_0 = 100$ l/h.

The estimation method minimizes the one step prediction error. The sample frequency of the measured data is 50 Hz and the expected bandwidth of the flow in the experimental setup is 0.1 Hz. Hence, the measurement data must be subsampled in order to avoid high frequency noise to bias the estimated parameters. In Figure 5.10, the Fourier transformations for the measurements with the $\mathcal{D}_{PRUS}$ as input signal are shown. The event frequency $\frac{1}{T_0} = 0.625$ Hz can be recognized in the spectra for both the pipe pressure Δp and the flow q. Moreover, the bandwidth of the subsampled data should not be less than 1.25 Hz, which implies 20 as reasonable subsampling factor.

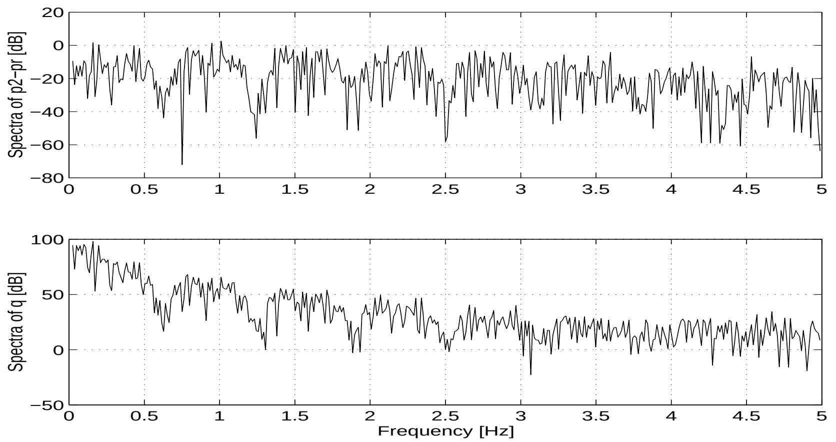

Figure 5.10. *Spectra of pipe pressure Δp and pipe flow q for the measurements with $\mathcal{D}_{PRUS}$ as reference signal.*

The subsampled measurement data have been used as estimation data. The estimated parameters for the two input signals are presented in Table 5.5. All the estimated parameters are significant and there are no significant correlations between the estimates.

The autocorrelation function for the prediction error, the crosscorrelation function between the input Δp and the prediction error and the cumulated periodogram for the prediction error are shown in Figure 5.11 and Figure 5.12 for the measurement data $\mathcal{D}_{PRBS}$ and $\mathcal{D}_{PRUS}$, respectively. The 95 % and 99 % significance intervals are indicated by line type "$-\cdot$" and "$--$", respectively. The two autocorrelation functions are almost enclosed by the 99 % significance interval. The crosscorrelation function shows a significant crosscorrelation at lag zero and at lag 4, indicating that there is still some information in the input signal Δp, which is not described by the model.

Table 5.5. *Estimated parameters of the turbulent flow model (5.47).*

	Input	$\mathcal{D}_{PRBS}$		$\mathcal{D}_{PRUS}$	
Param.	Unit	Est.	Std	Est.	Std
L	mWc h sec/l	$4.84\cdot10^{-3}$	$1.30\cdot10^{-4}$	$5.35\cdot10^{-3}$	$1.82\cdot10^{-4}$
R_2	mWc $(\mathrm{h/l})^2$	$1.01\cdot10^{-5}$	$5.05\cdot10^{-7}$	$9.82\cdot10^{-6}$	$4.25\cdot10^{-7}$
$q(0)$	l/h	70.6	5.39	101	3.98
σ_W^2	$(\mathrm{mWc})^2$	$4.40\cdot10^{-1}$	$4.62\cdot10^{-2}$	$2.37\cdot10^{-1}$	$1.29\cdot10^{-1}$
σ_e^2	$(\mathrm{l/h})^2$	$3.35\cdot10^{-4}$	$1.27\cdot10^{-4}$	$1.04\cdot10^{-3}$	$1.01\cdot10^{-4}$
$-\log\mathcal{L}$	–	641		570	
Mean(PE)	l/h	0.446		0.190	
Var(PE)	$(\mathrm{l/h})^2$	32.4		15.3	

The cumulated periodogram is also enclosed by the 99 % significance interval; an aspect which suggests that the prediction error is white noise. Furthermore, the event frequency 0.625 Hz of the input signals can be recognized in both cumulated periodograms.

The conclusion is that due to the significant crosscorrelation, the turbulent flow model (5.47) is not sufficient.

To support the statistical tests above the performance of the estimated models are visualized in Figure 5.13 and Figure 5.14. The first subplot contains the measured pipe flow and the one step predicted pipe flow. The second subplot contains the prediction error, while the third subplot contains the measured pipe flow and the simulated pipe flow given the estimated parameters and the pipe pressure Δp. Both plots of the prediction error clearly show peaks at every level change in the same direction as the peaks in the input signal Δp – compare e.g. Figure 5.13 and Figure 5.8.

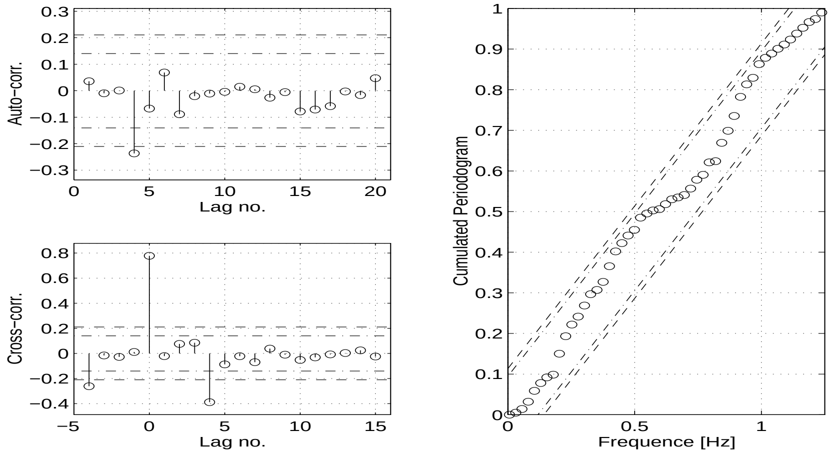

Figure 5.11. *Autocorrelation function for the prediction error, crosscorrelation function between input Δp and prediction error and cumulated periodogram for the prediction error for the estimation with $\mathcal{D}_{PRBS}$.*

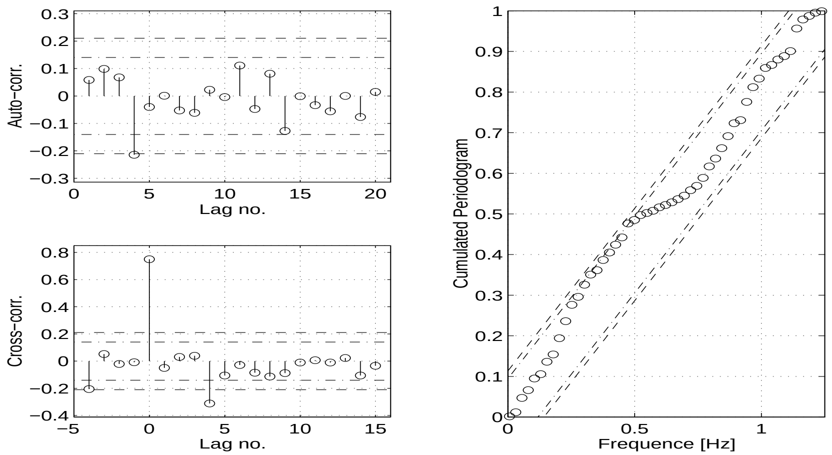

Figure 5.12. *Autocorrelation function for the prediction error, crosscorrelation function between input Δp and prediction error and cumulated periodogram for the prediction error for the estimation with $\mathcal{D}_{PRUS}$.*

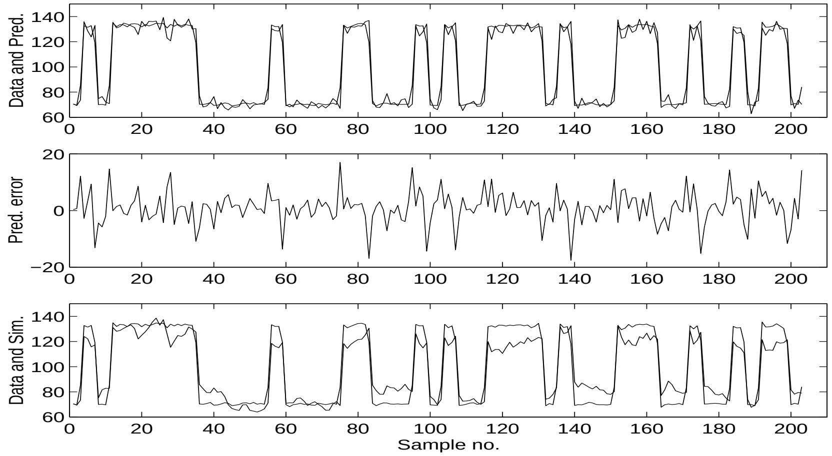

Figure 5.13. *Model performance of the turbulent flow model with $\mathcal{D}_{PRBS}$ as reference signal.*

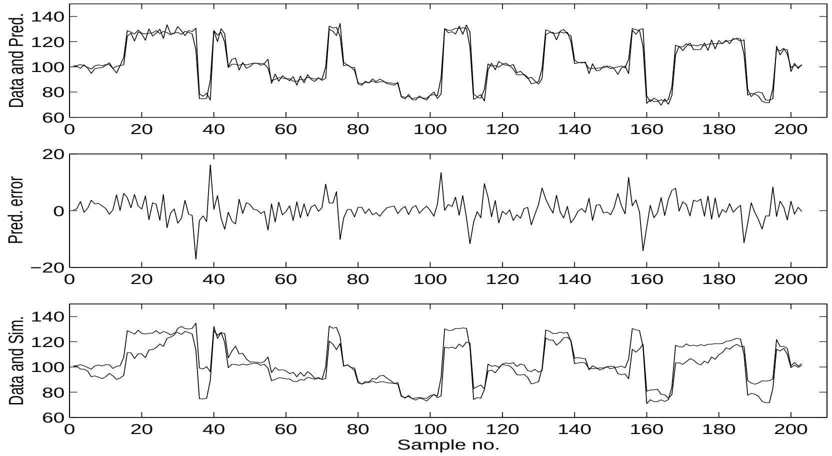

Figure 5.14. *Model performance of the turbulent flow model with $\mathcal{D}_{PRUS}$ as reference signal.*

5.4.3 Extended Turbulent Flow Model

The turbulent flow model (5.47) has to be extended. The large crosscorrelation at lag zero suggests the introduction of a direct term between the output (measured flow $y(t)$) and input (the pipe pressure Δp). Thus, the extended Grey Box model of the previous turbulent flow model can be written as:

$$\begin{aligned} dq_d(t) &= \frac{1}{L}\left(\Delta p(t) - R_2\, q_d(t)^2\right) dt + \frac{1}{L}\, dW(t) \\ q_i(t) &= K_{\Delta p}\, \Delta p(t) \\ y(k) &= q_d(k) + q_i(k) + e(k) \end{aligned} \tag{5.48}$$

where W is assumed to be a Wiener process with zero mean and incremental variance σ_W^2, y denotes the measured flow and e denotes the measurement noise, which is assumed to be white noise with zero mean and variance σ_e^2. Furthermore, W and e are assumed to be mutually uncorrelated. The measured flow y in this extended flow model consists of two flows: the dynamic flow q_d and the instantaneous flow q_i. The parameter $K_{\Delta p}$ describes the connection between the instantaneous flow q_i and the input Δp. In some sense, $K_{\Delta p}$ measures how much of the flow variation is directly caused by the pipe pressure. The hydraulic resistance R_2 is still assumed to be constant, i.e. $R_2 = R_t(\lambda_0)$, where λ_0 corresponds to the operating flow $q_0 = 100$ l/h.

Again the measurement data are subsampled by the factor 20 and then used as estimation data for the model (5.48). The estimated parameters are presented in Table 5.6. All the estimated parameters are significant, except the estimated variance of the measurement noise σ_e^2. There are no significant correlations between the estimates. This time, both the autocorrelation function and the crosscorrelation function are enclosed by the 99 % significance interval – for both data sets, as shown in Figure 5.15 and Figure 5.16, respectively. The 95 % and the 99 % significance intervals are indicated by line type "−·" and "−−". In case of $\mathcal{D}_{PRBS}$, the cumulated periodogram is entirely enclosed in the 99 % significance interval, while in the case of $\mathcal{D}_{PRUS}$, some frequencies around 0.3-0.4 Hz are significant. The event frequency 0.625 Hz of the input signals is not "visible" anymore in the cumulated periodograms. However some frequencies around 0.35 Hz have become significant.

Table 5.6. *Estimated parameters of the extended turbulent flow model (5.48).*

	Input	$\mathcal{D}_{PRBS}$		$\mathcal{D}_{PRUS}$	
Param.	Unit	Est.	Std	Est.	Std
L	mWc h sec/l	$3.87\cdot10^{-3}$	$6.76\cdot10^{-5}$	$3.92\cdot10^{-3}$	$9.04\cdot10^{-5}$
R_2	mWc h^2/l^2	$9.70\cdot10^{-6}$	$2.90\cdot10^{-7}$	$9.99\cdot10^{-6}$	$2.27\cdot10^{-7}$
K_d	l/(mWc h)	20.1	1.13	25.0	1.47
$q(0)$	l/h	69.9	6.14	98.3	2.57
σ_W^2	(mWc)^2	$1.46\cdot10^{-1}$	$1.54\cdot10^{-2}$	$8.28\cdot10^{-2}$	$8.39\cdot10^{-3}$
σ_e^2	(l/h)^2	$1.22\cdot10^{-3}$	$2.05\cdot10^{-3}$	$1.19\cdot10^{-3}$	$4.14\cdot10^{-3}$
$-\log\mathcal{L}$	–	550		485	
Mean(PE)	l/h	-0.244		-0.617	
Var(PE)	(l/h)^2	13.2		6.96	

In Figure 5.17 and Figure 5.18 the performance of the estimated model are visualized. The first subplot contains the measured flow and the one step predicted flow. The second subplot contains the prediction error, while the third subplot contains the measured flow and the simulated flow given the estimated parameters and the pipe pressure Δp. Comparing the predictions errors in Figure 5.17 and Figure 5.18 with those in Figure 5.13 and Figure 5.14, it is clear that the systematic peaks around the level changes have vanished.

The conclusion is that model (5.48) is verified, since the estimated autocorrelation and crosscorrelation fulfills the validation demands described in Section 2.6.2.

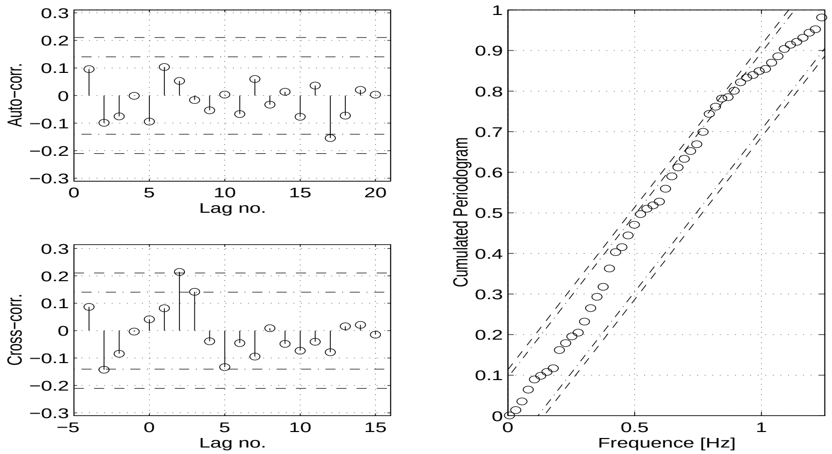

Figure 5.15. *Autocorrelation function for the prediction error, crosscorrelation function between input Δp and prediction error and cumulated periodogram for the prediction error for the estimation with $\mathcal{D}_{PRBS}$.*

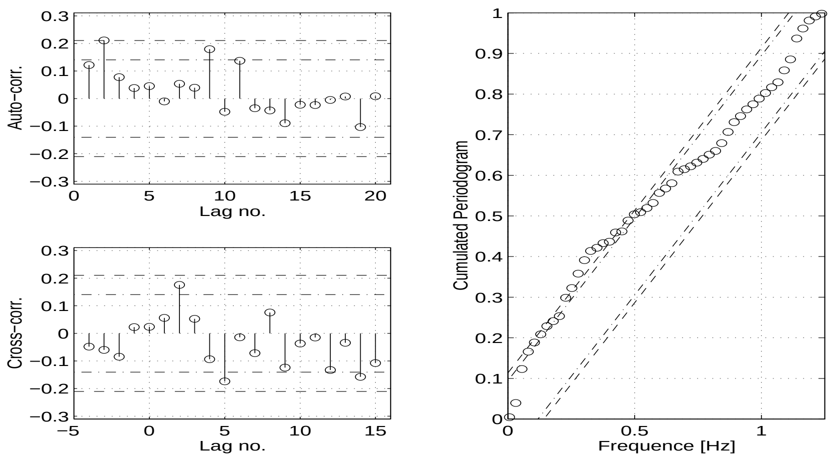

Figure 5.16. *Autocorrelation function for the prediction error, crosscorrelation function between input Δp and prediction error and cumulated periodogram for the prediction error for the estimation with $\mathcal{D}_{PRUS}$.*

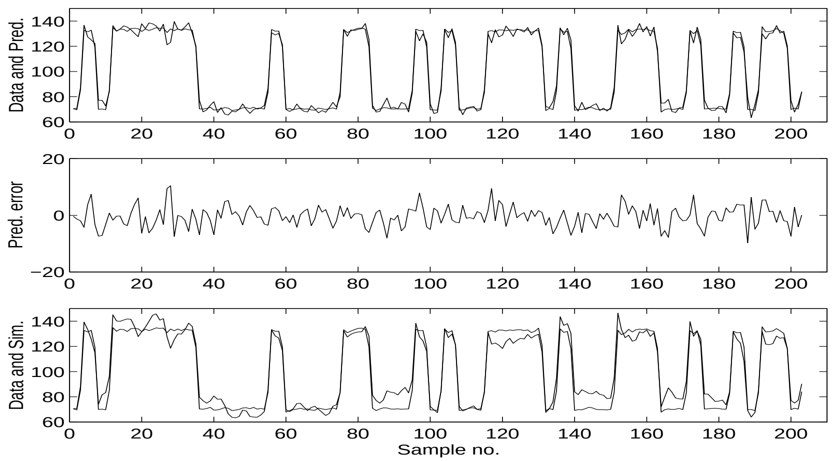

Figure 5.17. *Model performance of the extended turbulent flow model with $\mathcal{D}_{PRBS}$ as reference signal.*

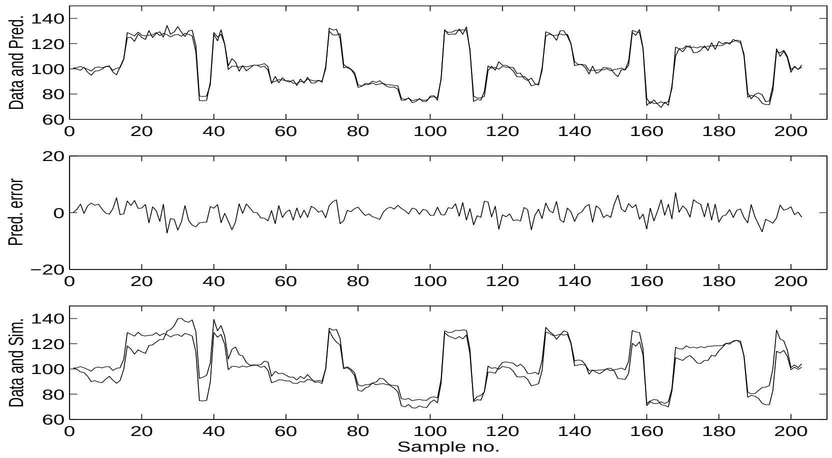

Figure 5.18. *Model performance of the extended turbulent flow model with $\mathcal{D}_{PRUS}$ as reference signal.*

The introduction of the instantaneous flow $q_i(t) = K_{\Delta p}\Delta p(t)$ in the output equation of (5.48) was enough to satisfy the validation criteria of the residual analysis. What is the physical interpretation of the instantaneous flow q_i?

Two arbitrary selected level switches of the measurement data in Figure 5.8 – a positive and a negative step – are replotted in Figure 5.19. The presented data in Figure 5.19 for p_2, p_r and q (defined in Figure 4.1) have been scaled into the range between -1 and 1. These scaled data are identified as: p_2 by "$\circ$", p_r by "$\times$" and q by "$+$". Furthermore the pressure over the pipe Δp is plotted as a full line based on the difference between the scaled versions of p_2 and p_r. It is observed that the "time delay" from p_2 to p_r is about 5 or 6 samples. Since the sample frequency is 50 Hz, the velocity of an assumed waterhammer wave would be about 200 m/sec. As described in e.g. *(Chaudhry, 1987)*, the velocity of a waterhammer wave depends on the quantity of undissolved gases in the fluid and on the rigidity of the pipe. The assumption of waterhammer wave dynamics in the experimental setup of the pipe can be rejected, as the 200 m/sec. is smaller than the velocity of sound in air $\sim$ 340 m/sec. (at 15 °C). In addition, the assumption of incompressible flow is justified.

It is further observed that the "time delay" from p_2 (and Δp) to q is about 6 or 7 samples. From a discrete time modelling point of view, the measurement data should not be subsampled by more than a factor 6 or 7. As the measurement data are subsampled by a factor 20 – which is necessary – the instantaneous flow q_i sort of describes the flow at the first sample of a step (level switch) in the pipe pressure Δp.

As the model (5.48) has been accepted, the parameter estimates can be assessed. First of all the time constant can be evaluated using (5.42). For $\mathcal{D}_{PRBS}$ the time constant at 100 l/h becomes $\tau = 1.99$ seconds, while for $\mathcal{D}_{PRUS}$ signal it becomes $\tau = 1.96$ seconds. These two time constants may be compared with the theoretical time constant $\tau = 1.40$ seconds in Table 5.4 (for $\kappa = 2$). It should be noted that the theoretical time constant is calculated on slightly arbitrary selection of the pipe roughness e.

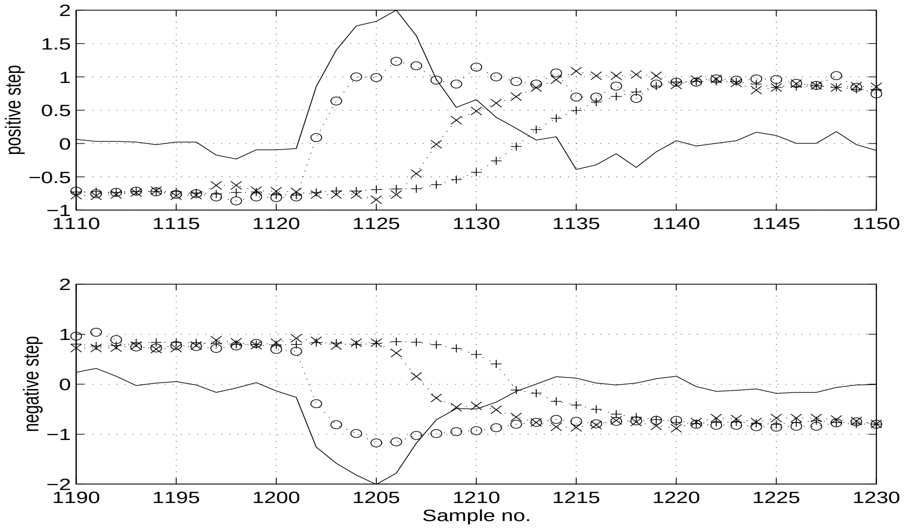

Figure 5.19. *Zoom of Figure 5.8 showing scaled signals of a positive and a negative pressure step. The scaled signals are identified as: p_2 by "$\circ$", p_r by "$\times$" and q by "$+$". The scaled version of Δp is sketched as a full line.*

The estimates of the hydraulic parameters $\widehat{L}$ and $\widehat{R}_t$ can be transformed into SI-units. The transformation is given as:

$$L_{SI} = 3.6 \cdot 10^{10}\widehat{L} \quad \text{and} \quad R_{st} = 10^4(3.6 \cdot 10^6)^2\widehat{R}_t \tag{5.49}$$

The hydraulic impedance becomes $L_{SI} = (1.39 \pm 0.073) \cdot 10^8$ kg/m^4 for the $\mathcal{D}_{PRBS}$ signal, while it is $L_{SI} = (1.41 \pm 0.098) \cdot 10^8$ kg/m^4 for the $\mathcal{D}_{PRUS}$ signal. These hydraulic impedances may be compared to the theoretical value $L = 1.13 \cdot 10^8$ kg/m^4 in Table 5.4. Again the resemblance between the estimated and the theoretical value is acceptable. Assume that the pipe diameter is $d = 0.015$ m and that the density of the water is $\rho = 1000$ kg/m^3. With a hydraulic impedance $L = 1.4 \cdot 10^8$ kg/m^4, the equivalent length of the pipe would be $l = 24.7$ m, which is quite close to the real length $l = 22$ m.

The same proceeding may be performed for the hydraulic resistance. From Table 5.4 it is known that $2R_t q_0 = 8.11 \cdot 10^7$ kg/(m^{4}sec), implying that $R_t = 1.46 \cdot 10^{12}$ kg/m^7. For $\mathcal{D}_{PRBS}$ the hydraulic resistance becomes $1.25 \cdot 10^{12}$kg/m^7, while for $\mathcal{D}_{PRUS}$ it becomes $1.29 \cdot 10^{12}$ kg/m^7. Assume that the pipe diameter $d = 0.015$ m, the length $l = 24.7$ m and the density $\rho = 1000$ kg/m^3. With a hydraulic resistance $R_t = 1.3 \cdot 10^{12}$ kg/m^7, the equivalent friction factor would be $\lambda = 4.93 \cdot 10^{-2}$, implying a pipe roughness in the neighborhood of $e = 0.5$ mm, as suggested in Table 5.4.

The deviations between reality and estimate can be caused by a number of reasons:

- The model does not contain the 11 pipe bends in the experimental setup.
- The noise to signal ratio of the pipe pressure is quite large.
- Insecure prior knowledge on the physical parameters.

Finally, it should be noted that the variance of the Wiener process σ_W^2 has a lower bound due to quantization noise due to the AD-conversion. The range of the pressure sensor: 0-25 mWc, is AD-converted by 12-bit with sign, which yields the lower noise bound: $\sigma^2 = (25/2^{11})^2/12 = 1.24 \cdot 10^{-5}$ (mWc)^2. The estimated variance is ~ 0.1 (mWc)^2.

5.4.4 Cross Validation

Revering to Table 5.6, the $-\log \mathcal{L}$ value for $\mathcal{D}_{PRUS}$ is more negative than for $\mathcal{D}_{PRBS}$. The variance of prediction error for $\mathcal{D}_{PRUS}$ is approximately half the variance of the prediction error for $\mathcal{D}_{PRBS}$. Hence, the model performance for $\mathcal{D}_{PRUS}$ is slightly better than for $\mathcal{D}_{PRBS}$.

The considerations above can be assessed through a cross validation. For the extended turbulent flow model the estimates of $\mathcal{D}_{PRBS}$ have been used in a simulation with the $\mathcal{D}_{PRUS}$ data and vice versa. The prediction errors of these cross validations are presented in Table 5.7.

Table 5.7. *Cross validation based on the variance of the prediction errors for the extended turbulent flow model ($\kappa = 2$).*

Evaluation data	$\mathcal{D}_{PRBS}$	$\mathcal{D}_{PRUS}$
Estimates of $\mathcal{D}_{PRBS}$	13.2	11.9
Estimates of $\mathcal{D}_{PRUS}$	7.37	6.96
Unit	(l/h)^2	

Looking at the cross validation results in Table 5.7, it can be observed that the variances are in the same range. Thus, it can be concluded that the extended turbulent flow model provides a general description of the measured data. From Table 5.7, it can also be observed that the model performance for $\mathcal{D}_{PRUS}$ is better than for $\mathcal{D}_{PRBS}$. Hence, the amplitude excitation of the PRUS signal has proven to be useful.

5.5 Summary

In this chapter the dynamic modelling of a straight circular pipe has been described. In the first section basic theory of flow in pipes was reviewed, while prior knowledge was used to derive a lumped parameter model for the flow in a pipe in the second section, i.e. a model composed of dynamic models for laminar and turbulent flow. The modelling was based on conservation of mass and momentum, and the most important assumption for the modelling was the assumption of incompressible flow.

In Section 5.3 the measurements/modelling were restricted to cover turbulent flow. Analysis of measurement data revealed that only measurements for turbulent flow were reliable. Simplification for the dynamic model of turbulent flow by the Blasius equation was ruled out, due to the non smooth pipe material. This was further confirmed by an analysis of the bandwidth based on measurements from the considered experimental setup of a pipe system.

In Section 5.4 the dynamic model of turbulent flow was reformulated in terms of a stochastic first order differential equation. The estimation results showed that the turbulent flow model could not be accepted. The model had to be extended. Based on the statistical tests, the turbulent flow model was extended with a direct term between input and output. The estimation results showed that the extended turbulent flow model could be accepted. Interpretation of the estimates of the extended turbulent flow showed a nice agreement between model and reality. Moreover, an analysis showed that the assumption of incompressible flow was reasonable. A cross validation performed on the presented measurement confirmed the good modelling properties of the extended turbulent flow model. Furthermore, the model performance for $\mathcal{D}_{PRUS}$ turned out to be the best.

In order to get a more significant pressure drop over the pipe, a pipe with smaller diameter, a longer pipe or a larger pipe roughness should be applied. In this way also laminar flow can be analyzed. Of course the case of laminar flow has to be verified equivalent to the turbulent flow, i.e. subjected to estimation and validation. Meanwhile, comparing the case of laminar flow with the case of turbulent flow, the validation of the laminar flow model should be a formality. Thus, the challenging part of the future pipe modelling is to find a proper model concept for the transition between the two types of flow.

Chapter 6

Radiator Modelling

The present chapter deals with the modelling of a (panel) radiator. The modelling is focused on the thermodynamic properties of the radiator and the purpose of the radiator modelling is to identify and estimate the parameters of the dynamic radiator model. The goal of the dynamic radiator model is to describe the heat transport from the hot supply water to the ambient air temperature.

It should be noted that the radiator modelling is concentrated on one particular type and size of radiator, which has been applied in the experimental setup of the central heating system. Nevertheless, it should be possible to apply the basic ideas of the dynamic models on other radiator designs.

The first section gives a short introduction to the basic concept of thermal dynamics. Two static standard radiator models are also presented. In the second section, the hydraulic modelling of the radiator is discussed. The third section is dedicated for thermal models of the radiator and three dynamic modelling approaches are presented. The fourth section presents measurements for the radiator, while estimation with these measurements are performed in the fifth section.

6.1 Radiator Models

In Section 4.2.2, the two radiator terminals were described. The implemented radiator is of type Thor Riffel 300-11-600. According to the data sheet on this radiator, see *(Thor Eura, 1990)*, the nominal power is 395 W. The length is 0.6 m, the height 0.3 m, the total weight 5.20 kg (8.66 kg/m), the contents of water 1.07 l (1.78 l/m) and the two radiator exponents are $n_1 = n_2 = 1.25$. The radiator material is steel and the width of the steel plate is 1.25 mm. The radiator has one convector layer on its backside, as illustrated in Figure 6.1. The idea of the convector is to increase the surface of the radiator in order to increase the amount of convective heat from the radiator.

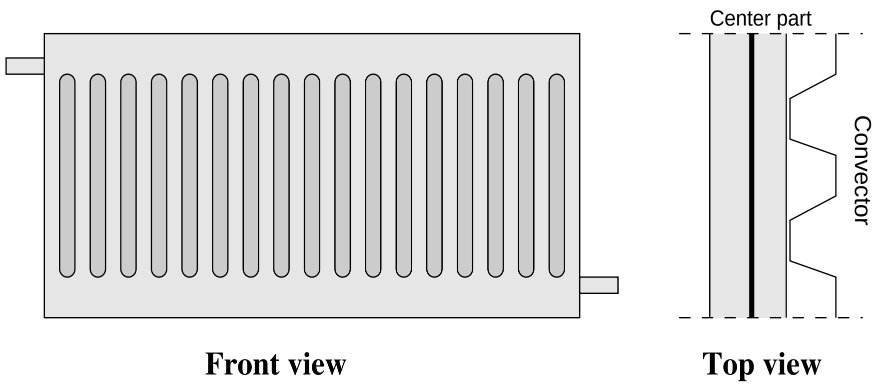

Figure 6.1. *Front and top view of the applied radiator.*

The radiator conforms the "heat bridge" between the central heating system and its ambient surroundings (i.e. a building). Hot supply water enters the radiator while less hot water leaves the radiator. The drop in water energy

is first converted into conductive heat in the radiator material. Afterwards the conductive heat is converted into convective and radiant heat.

The nominal power Φ_0 of the radiator is defined at standard conditions, which refer to the following temperatures: water supply temperature $T_{i,0} = 90$ °C, return water temperature $T_{o,0} = 70$ °C and ambient air temperature $T_{a,0} = 20$ °C (alias the room temperature). It should be noted that the definitions recently have been redefined to lower values with respect to the water temperatures. The standard conditions also involve a standard water flow q_0, which is given as:

$$\Phi_0 = c_{p,w}\, \rho_w\, q_0\, \Delta T_{w,0} \quad \Rightarrow \quad q_0 = \frac{\Phi_0}{c_{p,w}\, \rho_w\, \Delta T_{w,0}} \tag{6.1}$$

where $\Delta T_{w,0} = (T_{i,0} - T_{o,0}) = 20$ K denotes the nominal cooling of the water, while $c_{p,w}$ and ρ_w denote the heat capacity and the density of the water, respectively. Hence, the nominal flow of the applied radiator is $q_0 = 17$ l/h.

For convenience, the two following mean temperature differences are introduced. The first, the *arithmetic* mean temperature difference, is defined as:

$$\Delta T_{ma} = \frac{T_i + T_o}{2} - T_a \tag{6.2}$$

and the second, the *logarithmic* mean temperature difference, is defined as:

$$\Delta T_{ml} = \frac{T_i - T_o}{\log_e(\frac{T_i - T_a}{T_o - T_a})} \tag{6.3}$$

where $\log_e$ is the natural logarithm. These mean temperature differences provide a measure of the static temperature difference between the mean temperature of the radiator and the room temperature. At standard conditions $\Delta T_{ma,0} = 60$ °C and $\Delta T_{ml,0} = 59.4$ °C.

The two most common thermal radiator models in the technical literature are the one exponent formula and the two exponent formula. The *one exponent formula* is given as (see e.g. *(Weber, 1970; Becher, 1972)*):

$$\Phi = \Phi_0 \left(\frac{\Delta T_m}{\Delta T_{m,0}} \right)^{n_1} \tag{6.4}$$

where ΔT_m is one of the mean temperature differences, i.e. (6.2) or (6.3) at the actual set of temperature $T_i/T_o/T_a$ and $\Delta T_{m,0}$ is ΔT_m at the standard conditions. The exponent n_1 is usually around 1.3.

As described in *(Johansen et al., 1979)*, the performance of the one exponent formula (6.4) at larger values $\Delta T_w > 20$ K (i.e. at larger cooling of the water) is not satisfactory. Hence, in *(Johansen et al., 1979)*, the *two exponent formula* is introduced as an alternative to the one exponent formula:

$$\Phi = \Phi_0 \left(\frac{\Delta T_{ml,1}}{\Delta T_{ml,0}} \right)^{n_1} \left(\frac{\Delta T_{ml,2}}{\Delta T_{ml,1}} \right)^{n_2} \tag{6.5}$$

$$= \Phi_0 \left(\frac{\Delta T_{ml,1}}{\Delta T_{ml,0}} \right)^{n_1 - n_2} \left(\frac{\Delta T_{ml,2}}{\Delta T_{ml,0}} \right)^{n_2} \tag{6.6}$$

where the logarithmic mean temperature differences with respect to the indices are defined as:

$ml,0$: standard conditions $(T_{i,0}/T_{o,0}/T_{a,0})$.

$ml,1$: actual water supply temperature T_i and at standard water flow q_0 (i.e. the nominal flow).

$ml,2$: actual set of temperatures (T_i and T_o).

and the two exponents are related to:

n_1 : changes in the mean temperature difference, when the water supply temperature is changed at constant water flow.

n_2 : changes in the mean temperature difference, when the water flow is changed at constant water supply temperature.

The two exponents are in the ranges: $1.2 < n_1 < 1.4$ and $1.2 < n_2 < 2.1$, see *(Johansen et al., 1979)* or *(Hallgreen and Paulsen, 1982)*. The two exponent formula (6.6) includes the dependency of the water flow through the rather complex definition of $\Delta T_{ml,1}$. It is noted that in (6.6) the ambient temperature is set to 20 °C, irrespective of the actual ambient temperature. The definition of $\Delta T_{ml,1}$ should be interpreted as:

$ml,1$: at the actual water supply temperature T_i and at the return water temperature $T_{o,1}$, which would set in as a result of the actual water supply temperature T_i and the standard flow q_0.

As described in *(Lawaetz, 1984)*, the return water temperature $T_{o,1}$ has to be found iteratively using (6.6) together with:

$$\frac{\Phi}{\Phi_0} = \frac{c_{p,w}\, \rho_w\, q_0\, (T_i - T_{o,1})}{c_{p,w}\, \rho_w\, q_0\, (T_{i,0} - T_{o,0})} \quad \Rightarrow \quad T_{o,1} = T_i - 20\, \frac{\Phi}{\Phi_0} \tag{6.7}$$

until $T_{o,1}$ has converged to a value with some predefined precision. In *(Hallgreen and Paulsen, 1982)* an efficiency factor ϵ_j is defined as:

$$\epsilon_j = \frac{T_{i,j} - T_{o,j}}{T_{i,j} - T_{a,j}} \tag{6.8}$$

where index j is defined as in (6.6). *(Lawaetz, 1984)* provides a simplified efficiency factor as following:

$$\epsilon = \frac{T_i - T_o}{T_i - 20} \tag{6.9}$$

and states that (6.6) can be approximated by:

$$\frac{\Phi}{\Phi_0} = \left(\frac{T_i - 20}{70} \right)^{n_1} \left(\frac{1.08 - \epsilon}{0.8} \right)^{n_2/2} \tag{6.10}$$

as long as the efficiency factor ϵ is between 0.1 and 0.9.

As presented above, the exponent values for the applied radiators are $n_1 = n_2 = 1.25$. Thus for this particular radiator, (6.6) is reduced to:

$$\frac{\Phi}{\Phi_0} = \left(\frac{\Delta T_{ml,2}}{\Delta T_{ml,0}}\right)^{n_2} = \frac{c_{p,w}\,\rho_w\,q\,(T_i - T_o)}{c_{p,w}\,\rho_w\,q_0\,(T_{i,0} - T_{o,0})} \tag{6.11}$$

A graphical illustration of (6.11) is shown in Figure 6.2, where the normalized power Φ/Φ_0 is plotted as function of the normalized flow q/q_0, where $\Phi_0 = 395$ W and $q_0 = 17$ l/h.

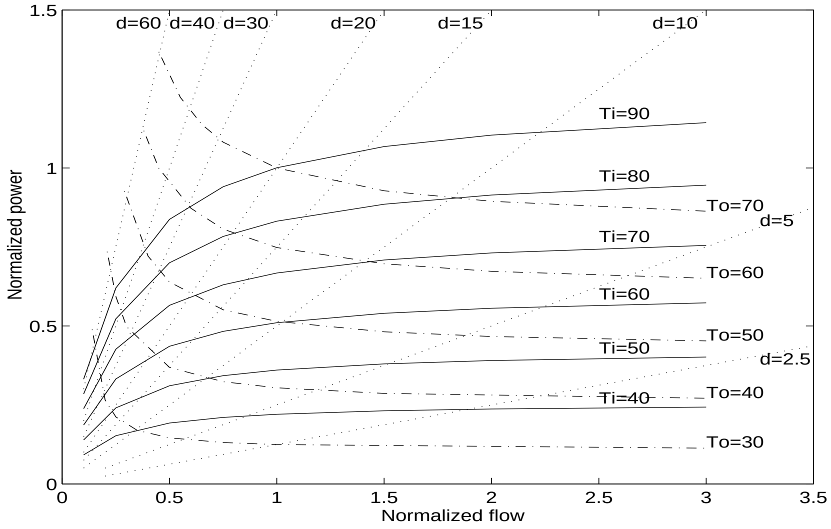

Figure 6.2. *Radiator diagram. The stationary normalized power Φ/Φ_0 versus the normalized q/q_0 at different water supply temperatures T_i and return water temperatures T_o. $\Phi_0 = 395$ W, $q_0 = 17$ l/h and $d = T_i - T_o$.*

The radiator contains both hydraulic and thermal dynamics. Moreover, the thermal dynamic consists of different kinds of thermal processes, i.e. both heat conduction, convection and radiant heat. This fact is reflected in the structure of the following sections on the dynamic modelling of the radiator.

6.2 Dynamic Hydraulic Model

From a hydraulic point of view, the radiator can be viewed as just a special type of pipe, i.e. a pipe with e.g. a rectangular cross section area. A non circular area can be represented by an equivalent circular area using an equivalent hydraulic diameter (see e.g. *(Fox and McDonald, 1985)*) defined as:

$$d_h = \frac{4A_h}{P_h} \tag{6.12}$$

where A_h denotes the cross section area and P_h the perimeter of the cross section area of A_h. It should be noted that other definitions of the equivalent hydraulic radius exist. The advantage of (6.12) is that, it has the circle as a special case, i.e.:

$$d_h = \frac{4\,\frac{\pi}{4}\,d^2}{\pi d} = d$$

Hence, by the use of the hydraulic diameter (6.12), the applicability of the dynamic pipe flow model in Chapter 5 becomes possible.

A sketch of the applied radiator was shown in Figure 6.1. The radiator looks nice, i.e. it is symmetric and simple. Nevertheless, the hydraulic resistance of the radiator is not easy to compute. An alternative is to use empirical data. A diagram of the pressure losses for the radiator is presented in *(Thor Eura, 1990)*. The total pressure loss over the radiator consists of two contributions: one due to the friction inside the radiator and one due to the entrance of the water into the radiator, where the latter is dominating. A reading of the diagram yields a pressure loss of 0.1 mWc at 650 l/h, which implies a hydraulic resistance of $2.4 \cdot 10^{-7}$mWc h^2/l^2. This is about 40 times smaller than the estimated resistance of the 22 m long pipe, see Table 5.6. Assuming that the radiator can be approximated by 18 parallel channels of length 0.3 m and hydraulic diameter 1 cm^2, an estimate of the hydraulic inductance becomes $5.9 \cdot 10^{-6}$mWc h sec/l, i.e. almost a factor

1000 smaller compared to the estimated inductances in Table 5.6. Thus, using (5.42) at a flow of 100 l/h, the time constant of the water flow in the radiator becomes 0.12 seconds. Comparing this time constant to the time constants in Table 5.6, it becomes evident that the flow dynamic in the applied radiator is approximately 10 times faster than the 22 m long pipe.

The conclusion is that the applied radiator almost will be “invisible” from a hydraulic point of view.

6.3 Dynamic Thermal Models

The thermal modelling of the radiator is divided into three modelling approaches. The first approach can be viewed as a generalized model of the one exponent formula, thus this approach forms a macroscopic modelling approach. The two other modelling approaches are of more microscopic nature, as the first model considers the heat transfer from the water in the radiator to the radiator surface and the second model deals with the heat transfer from the radiator surface to the ambient air with the underlying heat transfer dynamics in mind.

6.3.1 Dynamic One Exponent Formula

In *(Paulsen and Gundtoft, 1985)* a dynamic model for the radiator is presented. The model is based on the following partial differential equation:

$$C_l \frac{\partial T}{\partial t} = c_{p,w}\, \rho_w\, q\, \frac{\partial T}{\partial x} - h_l (T - T_a) \tag{6.13}$$

where T denotes the water temperature, T_a the ambient air temperature, C_l the heat capacity of water and radiator material (per length), while h_l denotes the heat transmission coefficient between the radiator and the ambient air. It should be noted that h_l depends on the temperature difference

between the water in radiator and the ambient air, i.e. $h_l = h(T - T_a)^{n_1 - 1}$. The basic idea of (6.13) is to describe the heat transfer process from the water to the ambient air as the cooling of a one-dimensional water flow. This model is not concerned with all the types of heat transfer processes involved, as the one exponent expression only is related to convective heat.

In the following a more suitable version of (6.13) will be used:

$$C_l \frac{\partial T}{\partial t} = c_{p,w}\, \rho_w\, q\, \frac{\partial T}{\partial x} - \Phi_{0l} \left(\frac{T - T_a}{\Delta T_{ma,0}} \right)^{n_1} \tag{6.14}$$

where Φ_{0l} denotes the nominal power of the radiator (per length), $\Delta T_{ma,0}$ the arithmetic mean temperature difference at standard conditions (see (6.2)) and n_1 is an exponent in the range of 1.2 to 1.4. The reformulation of (6.13) into (6.14) makes it more clear that (6.14) (and (6.13)) is a generalization of the one exponent formula (6.4).

In order to handle (6.14) numerically, the radiator is divided into a number of sections of equal size (in the vertical sections). Based on the following set of assumptions:

- No heat transfer in the stream direction of the flow, i.e. convective heat transfer in the water is neglected – the mass transport (the water flow) is dominating.
- No mixing of water in the stream direction of the flow. All the water in the j'th section has the temperature T_j.
- No temperature gradient across the flow. This assumptions is connected to the one-dimensional flow.
- No temperature difference between the water and the radiator material, implying that the thermal resistance of the radiator material is neglected and the heat capacity of the water and radiator material are lumped together.

the following model for the j'th section can be derived from (6.14):

$$\frac{C}{\mathcal{N}\,\Delta x}\,\frac{dT_j}{dt} = c_{p,w}\,\rho_w\,q\,\frac{\Delta T_j}{\Delta x} - \frac{\Phi_0}{\mathcal{N}\,\Delta x}\left(\frac{T_j - T_a}{60}\right)^{n_1} \tag{6.15}$$

where C denotes the heat capacity of water and radiator material, Φ_0 the nominal heat of the radiator and $\mathcal{N}$ the number of sections (alias, the approximation order). $\mathcal{N}\Delta x$ is equal to the height of the radiator. Moreover, the temperature difference over the j'th section ΔT_j is given as:

$$\Delta T_j = T^*_{j-1} - T^*_j \tag{6.16}$$

where T^*_{j-1} and T^*_j denote the boundary temperatures between section $j-1$ and j and section j and $j+1$, respectively. The two outer boundary temperatures are of course equal to the water supply temperature $T^*_0 = T_i$ and the return temperature $T^*_{\mathcal{N}} = T_o$.

The radiator model based on the partial differential equation (6.14) has now been lumped into $\mathcal{N}$ ordinary differential equations, where the problem is to find a proper distribution/description for the boundary temperatures $T^*_1, \cdots, T^*_{\mathcal{N}-1}$. A simple model for the j'th boundary temperature based on the section temperatures:

$$T^*_j = (1-\phi)T_j + \phi T_{j+1} \tag{6.17}$$

where ϕ denotes a fractional number between 0 and $\frac{1}{2}$. ϕ can be interpreted as the degree of mixing water between two sections or as a measure of the temperature gradient at the boundary between section j–1 and j. In general ϕ could be related to (or be dependent on) the flow and the cooling of the water in some way. The two extreme values of ϕ are reached, when:

- $\phi = 0$: all the water in a particular section has the same temperature, i.e. no temperature gradient along the flow direction inside of the section.
- $\phi = \frac{1}{2}$: the mixing of water is constant along the flow direction or the water flow is relative large and the cooling of the water is small.

Using the simple model for the j'th boundary temperature (6.17) in (6.16), the temperature difference over the j'th section ΔT_j becomes:

$$\Delta T_j = (1-\phi)T_{j-1} + (2\phi - 1)T_j - \phi T_{j+1} \tag{6.18}$$

A dynamic radiator model based on the partial differential equation of the cooling of a one-dimensional water flow has now been established. The model is formulated as follows:

Model Summary 6.1 (Dynamic One Exponent Formula)
A dynamic model of the one exponent formula is achieved by lumping the partial differential equation of the cooling of a one-dimensional water flow (6.14) into $\mathcal{N}$ sections (using the set of assumptions on page 117):

$$\frac{C}{\mathcal{N}\,\Delta x}\,\frac{dT_j}{dt} = H_q\,q\,\frac{\Delta T_j}{\Delta x} - \frac{\Phi_0}{\mathcal{N}\,\Delta x}\left(\frac{T_j - T_a}{60}\right)^{n_1} \tag{6.19}$$

where C denotes the heat capacity of water and radiator material, Φ_0 the nominal power of the radiator, $H_q = c_{p,w}\,\rho_w$, Δx the section height and $\mathcal{N}$ denotes the approximation order. $\mathcal{N}\Delta x$ is equal to the height of the radiator. The temperature difference over the j'th section ΔT_j is modelled as:

$$\Delta T_j = (1-\phi)T_{j-1} + (2\phi - 1)T_j - \phi T_{j+1} \tag{6.20}$$

using (6.17), where $\phi \in [0, \frac{1}{2}]$. Thus, the first and the j'th section are given as:

$$\frac{C}{\mathcal{N}}\,\frac{dT_1}{dt} = H_q\,q\,(T_i - (1-\phi)T_1 - \phi T_2) - \frac{\Phi_0}{\mathcal{N}}\left(\frac{T_1 - T_a}{60}\right)^{n_1} \tag{6.21}$$

and

$$\frac{C}{\mathcal{N}}\frac{dT_j}{dt} = H_q q((1-\phi)T_{j-1}+(2\phi-1)T_j-\phi T_{j+1})-\frac{\Phi_0}{\mathcal{N}}\left(\frac{T_j-T_a}{60}\right)^{n_1} \quad (6.22)$$

while the last section is given as:

$$\begin{aligned}\frac{C}{\mathcal{N}}\frac{dT_{\mathcal{N}}}{dt} &= H_q q((1-\phi)T_{\mathcal{N}-1}+\phi T_{\mathcal{N}}-T_o)-\frac{\Phi_0}{\mathcal{N}}\left(\frac{T_{\mathcal{N}}-T_a}{60}\right)^{n_1} \\ &\approx H_q\, q\,(T_{\mathcal{N}-1}-T_{\mathcal{N}})-\frac{\Phi_0}{\mathcal{N}}\left(\frac{T_{\mathcal{N}}-T_a}{60}\right)^{n_1} \quad (6.23)\end{aligned}$$

For the $\mathcal{N}$'th section $\phi = 0$ must be applied in order to make the section temperatures T_j observable, thus $T_{\mathcal{N}} \equiv T_o$.

Four remarks on Model Summary 6.1:

R1 The model is in principle only valid, when there is a flow. Nevertheless, it will used to describe the case of zero flow. The problem is that, when the flow is zero, the model is separated into $\mathcal{N}$ independent first order differential equations. Meanwhile the physical conditions in the radiator are tied together through convective heat transport in the water.

R2 The dynamic model is not concerned with all three types of heat transfer processes involved in the cooling of the water flow in the radiator. The advantage of such a description is that, it is simple and based on only two parameters: the nominal power Φ_0 and the radiator exponent n_1. The disadvantage is that, it might be too simple, i.e. not capable of describing the real cooling process in all valid operation points.

R3 The parameter ϕ has some kind of dependency of the flow and the cooling of the water as mentioned above. For simplicity only the two extreme values ($\phi = 0$ and $\phi = \frac{1}{2}$) will be considered.

R4 The product H_q of the specific heat $c_{p,w}$ and the density ρ_w is considered to be independent of the water temperature, see Appendix A.3, and so is the capacity C.

In *(Paulsen and Gundtoft, 1985)*, the case of $\phi = 0$ is used as model for the j'th boundary temperature. Hence, applying $\phi = 0$, (6.22) is reduced to:

$$\frac{C}{\mathcal{N}}\frac{dT_j}{dt} = H_q\, q\,(T_{j-1}-T_j)-\frac{\Phi_0}{\mathcal{N}}\left(\frac{T_j-T_a}{60}\right)^{n_1} \quad (6.24)$$

Note that $T_j = T_i$ for $j = 0$ and $H_q = c_{p,w}\,\rho_w$. According to *(Paulsen and Gundtoft, 1985)*, $\mathcal{N} = 10$ is a fair choice. The dynamic model (6.24) is illustrated by an electrical equivalent in Figure 6.3.

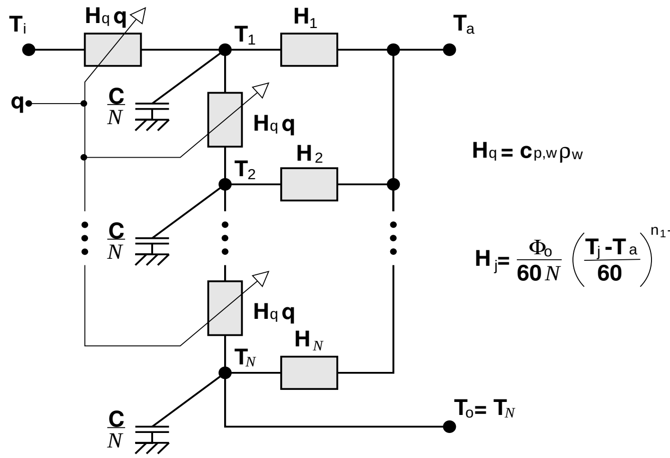

Figure 6.3. *Electric equivalent of the dynamic one exponent formula for the case of $\phi = 0$. The thermal transmittance $H_q\,q$ only submits "connection" in the water flow direction.*

The case of two sections with dynamic section size is considered in *(Andersen, 1997)*.

6.3.2 Water to Radiator Surface

A more detailed view than that in Section 6.3.1 can be applied on the cooling process of the water flow. Assuming the surface temperature of the radiator is known, a model can be formulated describing the heat transport from the water to the surface - or as in the next section, from the surface of the radiator to the ambient air. This more detailed modelling approach is motivated by the desire of getting closer to the underlying heat transport dynamics.

The heat transfer process from the water to the surface of the radiator consists of heat conduction through the radiator material. As in the previous section, a partial differential equation for the cooling of the one-dimensional water flow q can be formulated:

$$C_l \frac{\partial T}{\partial t} = c_{p,w}\, \rho_w\, q\, \frac{\partial T}{\partial x} + H_{f,l}(T_{s,f} - T) + H_{b,l}(T_{s,b} - T) \tag{6.25}$$

where T denotes the water temperature (in the vertical direction), $T_{s,f}, T_{s,f}$ front and backside surface temperatures of the radiator, C_l the heat capacity of water and radiator material (per length) and $H_{f,l}, H_{b,l}$ denote the front and backside heat transmittances (thermal conductivities) of the radiator material (per length).

In the previous section, the radiator was lumped into a number of sections (in the vertical direction) of equal size. This time the size of the sections is selected individual in order to be able to cover the geometry of the radiator. Based on the following set of assumptions:

- No heat transfer in the stream direction of the flow, i.e. convective heat transfer in the water is neglected – the mass transport (the water flow) is dominating.
- No mixing of water in the stream direction of the flow. All the water in the j'th section has the same temperature T_j.

- No temperature gradient across the flow. This assumptions is connected to the one-dimensional flow.
- The heat capacity of the water and radiator material are lumped together. The temperature difference between the water and the surface of the radiator is due to the thermal transmittance of the radiator material.
- The front and backside of the radiator are identical. This assumptions keeps the modelling simple with respect to the surface temperature of the radiator.

the model for the j'th section can be derived as:

$$\frac{C_j}{\Delta x_j} \frac{dT_j}{dt} = H_q\, q\, \frac{\Delta T_j}{\Delta x_j} + 2\, H_{m,j}\, (T_{sj} - T_j) \tag{6.26}$$

where C_j denotes the heat capacity of water and radiator material, $H_{m,j}$ the heat transmittance of the radiator material (per length) and Δx_j the height – all with respect to section j. The surface temperature is denoted by T_{sj} and the water temperature as T_j. Note that $H_q = c_{p,w}\, \rho_w$ is considered to be independent of the water temperature, see Appendix A.3. The sum of Δx_j is equal to the height l_h of the radiator and the sum of C_j is equal to the total heat capacity of the radiator C – ditto for $H_{m,j}$ and the heat transmittance H_m. The temperature difference over the j'th section ΔT_j is as defined in (6.16).

The simple model for the boundary temperature based on the section temperatures is used, see (6.17), thus for this model the temperature difference over the j'th section ΔT_j is also described as in (6.18).

Model Summary 6.2 (Heat Model: Water to Radiator Surface)
A dynamic model of heat transfer from the water in the radiator to the (outer) radiator surface is achieved by lumping the partial differential equation of the cooling of a one-dimensional water flow (6.25) into $\mathcal{N}$ sections

(using the set of assumptions on page 122) of individual size. The j'th section is given as:

$$C_j \frac{dT_j}{dt} = H_q\, q\, \Delta T_j + 2\frac{\Delta x_j}{l_h} H_m (T_{sj} - T_j) \tag{6.27}$$

where C_j denotes the heat capacity of water and radiator material, H_m the heat transmittance (thermal conductivity) of the radiator material, Δx_j the height of section j and l_h the height of the radiator. The sum of C_j is equal to the total heat capacity of the radiator C. T_{sj} denotes the surface temperature and T_j the water temperature. Note that $H_q = c_{p,w}\, \rho_w$. The temperature difference ΔT_j over the first and the j'th section is given as:

$$\Delta T_1 = T_i - (1-\phi)T_1 - \phi T_2 \tag{6.28}$$

and

$$\Delta T_j = (1-\phi)T_{j-1} + (2\phi - 1)T_j - \phi T_{j+1} \tag{6.29}$$

while the temperature difference over the last section is

$$\begin{aligned} \Delta T_{\mathcal{N}} &= (1-\phi)T_{\mathcal{N}-1} + \phi T_{\mathcal{N}} - T_o \\ &\approx T_{\mathcal{N}-1} - T_{\mathcal{N}} \end{aligned} \tag{6.30}$$

where $\phi \in [0, \frac{1}{2}]$ as described in Section 6.3.1 and $\mathcal{N}$ denotes the approximation order. For the $\mathcal{N}$'th section, $\phi=0$ must be applied in order to make the section temperatures T_j observable, thus $T_{\mathcal{N}} \equiv T_o$.

Four remarks on Model Summary 6.2:

R1 In the formulation of (6.27) it is implicit assumed that the thickness of the radiator wall is homogeneous. Thus the cooling of the water is proportional to the height of the section.

R2 The distribution of Δx_j and C_j is dictated by the geometry of the radiator.

R3 The front and backside of the radiator are assumed to be identical. This is of course a rude approximation as the backside is equipped with a convector, but it simplifies the number of surface measurements by a factor two.

R4 In this model the interpretation of ϕ as a temperature gradient in the flow direction makes good sense. A large flow and a small cooling converges towards $\phi = \frac{1}{2}$. On the other hand, boundary layers in a water column is a known phenomenon, which would be equal to the case of $\phi=0$ (under the premise that the sectioning and the boundaries are coincident). Hence, the actual value of ϕ is somewhere between 0 and $\frac{1}{2}$ dependent on flow and cooling conditions. It might even be possible that ϕ has a local performance.

Comparing the two dynamic radiator models presented in Model Summary 6.1 and Model Summary 6.2, the following observations are made:

- The two radiator models have the same limitation, namely the zero flow situation. When the flow is zero both models are separated into $\mathcal{N}$ independent first order models – implying that only the last section is observable. This means that during estimation the Kalman filter has to simulated the heat discharge process for the non observed water temperatures until the flow starts and all the sections become observable again.
- The difference between the two radiator models is the definition of the ambient boundary temperature. The water to surface heat transfer model is in principle a submodel of the dynamic one exponent formula model. Meanwhile, the water to radiator surface model is more complex than the dynamic one exponent formula model, as it comes closer to the underlying physical cooling process (heat conduction) by

including the geometry of the radiator, whereas the cooling process in the dynamic one exponent formula model is lumped into the two parameters: the nominal radiator power and the radiator exponent. Therefore, the water to surface transfer model is also more demanding than the dynamic one exponent formula model with respect to measurements, model approximations etc.

In order to make a visual comparison between the dynamic one exponent formula in Model Summary 6.1 (see Figure 6.3) and the dynamic model of heat transfer from the water to the radiator surface presented in Model Summary 6.2, the water to radiator surface model is illustrated in Figure 6.4.

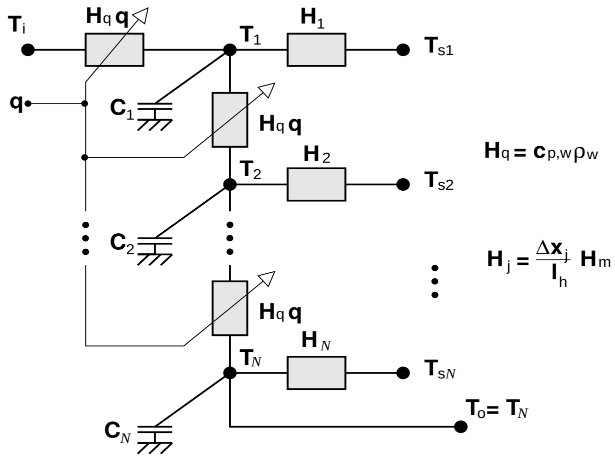

Figure 6.4. *Electric equivalent of the dynamic model of the heat transfer from the water to the surface of the radiator for the case of* $\phi = 0$. *The thermal transmittance* $H_q\,q$ *only submits "connection" in the water flow direction.*

6.3.3 Radiator Surface to Ambient Air

A dynamic model for the heat transfer from the water to the radiator surfaces was presented in the previous section. This section deals with the other half of the heat transfer, i.e. from the surface to the ambient air.

The heat transfer process from the radiator surface to the ambient air consists of convective and radiant heat. In the previous section the front and the backside of the radiator were assumed to be identically. This assumption might be too rude. An equivalent assumption for the air in front of and behind the radiator is not applicable due to the interaction between the backside of the radiator and wall. Figure 6.5 illustrates a thermal model for the heat transfer from the surface to the ambient air in the case when the radiator surface is divided into six sections – three on each side. Radiant heat from the backside of the radiator (indicated in the figure by the "arrow"-symbol) will be converted to convective heat, when the radiant heat hits the wall as sketched in Figure 6.5. Thus, the air on the backside is heated more efficient than the air on the front side.

A set of differential equations can be formulated based on the thermal network in Figure 6.5. But with the present experimental setup (refer to Section 4.2), the heat dynamic from the radiator surface to ambient air is too extensive to be measured properly. Therefore, the modelling considerations described above for heat transfer from radiator surface to the ambient air, are presented as a supplement to Model Summary 6.2 – in order to get the *full picture* of the thermal dynamics of the radiator.

6.4 Experiments

The experimental setup described in Section 4.2 is used to generate measurement data for the radiator. The basic idea is of course to design a good

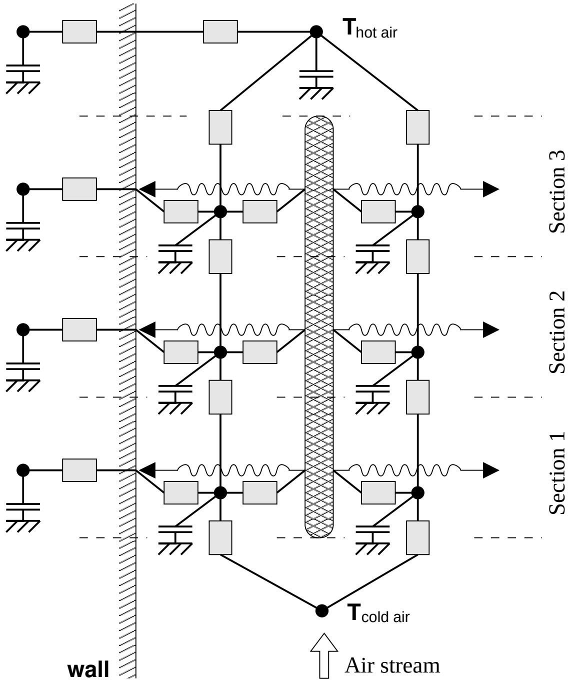

Figure 6.5. *Lumped parameter model of the heat transfer (convective and radiant) from the surface of the radiator to the ambient air.*

experiment in order to estimate the parameters in the dynamic radiator models.

6.4.1 Experimental Setup

Three radiator models have been presented in Section 6.3. The first, the dynamic one exponent formula (6.24), requires the following three input signals: 1) the water temperature T_i at the inlet of the radiator, 2) the ambient temperature T_a and 3) the flow q as defined in Figure 4.5. The

output of this model is the temperature of the water in the last section, which is indirectly measured by the temperature of the water T_o in the outlet pipe. Thus the experimental setup is equipped to cover the measurements in the case of the dynamic one exponent formula.

Besides the already mentioned signals the two other models also require measurements of the surface temperature of the radiator. With only 8 extra temperature signals available, the dynamic "surface to ambient air" model is ruled out due to its complexity. All of these 8 temperature signals are based on thermocouples (type T), which should ensure a sufficient high sensoring dynamic. A layout of the surface temperature measurement in connection with "the water to radiator surface" model (6.26) is shown in Figure 6.6. As sketched in this figure, six signals are used to measure the surface temperatures $T_{s1}, \cdots, T_{s6}$, while the two remaining signals are dedicated to measure the incoming air temperature T_{aa} and the outgoing air temperature T_{ab}. The six thermocouples used in the surface measurements have been taped to the radiator surface with insulation tape.

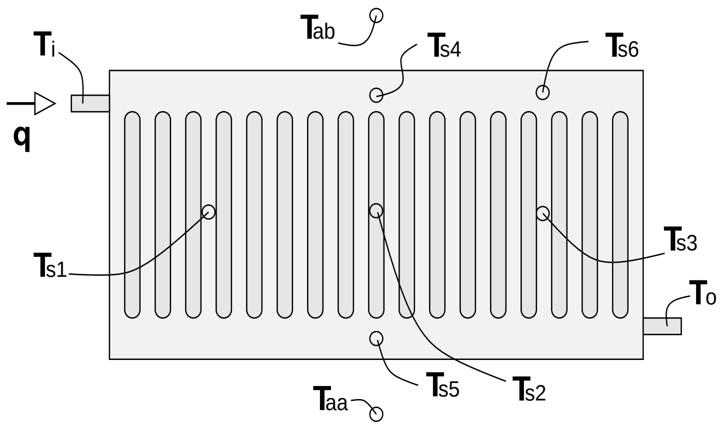

Figure 6.6. *Layout of temperature signals for the radiator surface measurements using six thermocouples and two thermocouples for the air measurements.*

6.4.2 Analysis and Input Design

The analysis is focused on determination of the time constant of the dynamic one exponent formula in Model Summary 6.1, as this model describes the heat transfer process all the way from the water to the ambient air. For simplicity ϕ is set to zero. In order to derive the time constant of the heat dynamic from the water to the ambient air, (6.24) has to be linearized and a first order Taylor expansion yields:

$$\begin{aligned} \frac{C}{\mathcal{N}} \frac{dT_j}{dt} &= H_q\, q_{op}\,(T_{j-1,op} - T_{j,op}) - \frac{\Phi_0}{\mathcal{N}} \left(\frac{T_{j,op} - T_{a,op}}{60}\right)^{n_1} \\ &+ H_q\, q_{op}\,(\overline{T}_{j-1} - \overline{T}_j) + H_q\,(T_{j-1,op} - T_{j,op})\,\overline{q} \\ &- \frac{n_1}{\mathcal{N}} \frac{\Phi_0}{60} \left(\frac{T_{j,op} - T_{a,op}}{60}\right)^{n_1 - 1} (\overline{T}_j - \overline{T}_a) \end{aligned} \tag{6.31}$$

where $H_q = c_{p,w}\,\rho_w$ and index *op* indicates a specific operation point, while the variables with the "bar" sign denote a deviation from the operation point, e.g. $\overline{T}_j = T_j - T_{j,op}$. In a stationary operation point $(T_{j,op}, T_{j-1,op}, q_{op}, T_{a,op})$, (6.31) is reduced and rewritten as:

$$\begin{aligned} \frac{C}{\mathcal{N}} \frac{d\overline{T}_j}{dt} &= -H_q\, q_{op}\,\overline{T}_j - \frac{n_1}{\mathcal{N}} \frac{\Phi_0}{60} \left(\frac{T_{j,op} - T_{a,op}}{60}\right)^{n_1 - 1} \overline{T}_j \\ &+ H_q\, q_{op}\,\overline{T}_{j-1} + H_q\,(T_{j-1,op} - T_{j,op})\,\overline{q} \\ &+ \frac{n_1}{\mathcal{N}} \frac{\Phi_0}{60} \left(\frac{T_{j,op} - T_{a,op}}{60}\right)^{n_1 - 1} \overline{T}_a \end{aligned} \tag{6.32}$$

Moreover, this linearized model of the j'th section can be rewritten by using the Laplace transformation. Thus, the following set of transfer functions are obtained:

$$\frac{\overline{T}_j(s)}{\overline{T}_{j-1}(s)} = \frac{H_q\, q_{op}}{K_{op}} \frac{1}{\tau s + 1} \tag{6.33}$$

$$\frac{\overline{T}_j(s)}{\overline{q}(s)} = \frac{H_q\,(T_{j-1,op} - T_{j,op})}{K_{op}} \frac{1}{\tau s + 1} \tag{6.34}$$

$$\frac{\overline{T}_j(s)}{\overline{T}_a(s)} = \frac{K_{op} - H_q\, q_{op}}{K_{op}} \frac{1}{\tau s + 1} \tag{6.35}$$

where K_{op} and τ are defined as:

$$K_{op} = H_q\, q_{op} + \frac{n_1}{\mathcal{N}} \frac{\Phi_0}{60} \left(\frac{T_{j,op} - T_{a,op}}{60}\right)^{n_1 - 1} \tag{6.36}$$

respectively as:

$$\tau = \frac{C}{\mathcal{N} K_{op}} \tag{6.37}$$

K_{op} denotes a constant, while τ represents the time constant of the thermal radiator dynamic for the dynamic one exponent formula (6.24).

It is noted that (6.31) in principle has two stationary operation points:

$q_{op} = 0$: when the water flow is zero, the previous section does not interact with the present section, see (6.33), hence the water temperatures of each section will seek towards the ambient temperature T_a (discharge heat) as already mentioned in Section 6.3.2. If the exponent $n_1 = 1$, the heat discharge will decrease exponentially.

$q_{op} > 0$: when there is a water flow, the distribution of the stationary temperatures T_j in the radiator is a tradeoff between the water supply temperature T_i and the ambient temperature T_a – for a particular flow q.

It is obvious that if only one of the input variables T_i, T_a or q is changed, the distribution of the water temperatures in the radiator is also changed. Thus, the term "constant" in connection with the time constant does only make sense, when the variations from the operation point are small. Meanwhile (6.37) can be used to compute an upper bound for the time constant, i.e. when $q_{op}=0$ and $T_{j,op}\approx T_{a,op}$:

$$\tau < \frac{C}{\mathcal{N}\,\frac{n_1}{\mathcal{N}}\,\frac{\Phi_0}{60}} = \frac{60\,C}{n_1\,\Phi_0} \tag{6.38}$$

Based on the informations on the radiator presented in Section 6.1, an estimate of the total heat capacity of the radiator can be calculated as:

$$C \approx 7800 \cdot (5.2 - 1.1) + 4200 \cdot 1.1 \approx 36 \text{ kJ/K}$$

Hence, the upper bound on the time constant becomes approximately 73 minutes. A lower bound can also be derived from (6.37). As sketched in Figure 6.2, the difference between the inlet temperature and outlet temperature is decreasing when the relative flow is increasing. Assuming that $T_o=T_i=90°\text{C}$ at say five times q_0, the lower bound on the time constant becomes approximately:

$$\tau > \frac{C}{\mathcal{N}\,H_q\,5\,q_0} \approx 6 \text{ minutes} \tag{6.39}$$

As mentioned before, the input signals for the dynamic one exponent formula consists of the water supply temperature T_i, the water flow q and the ambient temperature T_a. The task is now to design some proper input signals for the estimation. Meanwhile, the placement of the experimental setup of the central heating system in the test house (see 4.3) or in any other building puts restrictions on the input design. An analysis of the input signals yields:

- q : the dynamic of water flow is much faster than the thermal dynamic of the radiator, hence a proper input signal can be designed for the flow.

- T_i : the dynamic of the water supply temperature is slower than the dynamic of the radiator due to the big heat capacity (of the water etc.) in the heating unit. Thus this signal does not support good excitation properties in relation to the radiator experiment. Nevertheless, some water supply temperature excitation is possible, as variations in the water flow will result in variations in the water supply temperature, due to heat loss in the supply pipes. The disadvantage of this excitation is that the water supply temperature T_i becomes correlated with the flow q.
- T_a : the ambient temperature (alias room temperature) is in principle a controlled quantity rather than an input variable, since the thermostatic valve/radiator setup is supposed to heat and control this temperature. Hence, in the present setup the ambient temperature has to viewed as a non controllable input, which is correlated with the heat submission from the radiator – and this is equivalent to be correlated with the water flow and supply temperature.

Thus, it can be concluded that the prospects for excellent estimates and good statistical tests – with the present setup – are not too good.

In order to extract some empirical knowledge from the radiator, a small experiment has been performed. As described above, it is only possible to make a proper input design for the flow. For this experiment the following design has been used:

1. A long period without flow. The radiator is discharging heat to the ambient.
2. A short period with flow. The radiator is refilled with hot supply water.
3. Repeating item 1 and 2 a couple of times.

The result is shown in Figure 6.7 and Figure 6.8 at a sample time of 10 seconds. Referring to Figure 6.6, the first subplot in Figure 6.7 contains the flow q. The flow is about 7 l/h (smaller than the nominal flow of 17 l/h) and the increasing trend in the flow is due to the decreasing trend in the ambient temperature, which forces the thermostatic valve to become more and more open. With a radiator volume of 1.1 l, this implies approximately 9 minutes (or about 50 samples) to exchange the water in the radiator. The second subplot presents the water supply temperature T_i and the output temperature T_o. It is noted that the reference temperature for the supply temperature was set to 68°C. The measured radiator surface temperatures $T_{s1}, \cdots, T_{s6}$ are shown in the first subplot of Figure 6.8, while the air temperatures T_a, T_{aa} and T_{ab} are plotted in the second subplot of Figure 6.8. The ambient temperature T_{ab} shown in Figure 6.8 is (not surprising) correlated with the water supply temperature T_i.

The output temperature T_o presented in Figure 6.7 has a "strange" behaviour for the sample numbers in the ranges [1200,2300] and [2650,3000]. The strange behaviour is probably caused by a small batch of hot water in the insulated return pipe (under the radiator) moving up in the radiator, as a result of the fact that hot water is not as heavy as cold water. Another fact is that the measurement of the output temperature T_o is measured in the outlet pipe and not in the "last section" of the radiator. This could impose another error in the measurement of the output temperature T_o. Therefore, when the flow is zero or very close to zero, the measurement of the output temperature T_o (and also the input temperature T_i) might be corrupted.

Still referring to Figure 6.6, it is noted that the surface temperatures in Figure 6.8 are gathered into 3 groups consisting of:

1. T_{s4}, T_{s6}: the two top temperatures as the hottest part of the radiator.

2. T_{s5}: the bottom temperature as the coldest part of the radiator.

3. T_{s1}, T_{s2}, T_{s3}: the center row of surface temperatures with temperatures significantly below the mean value of the top and bottom temperature.

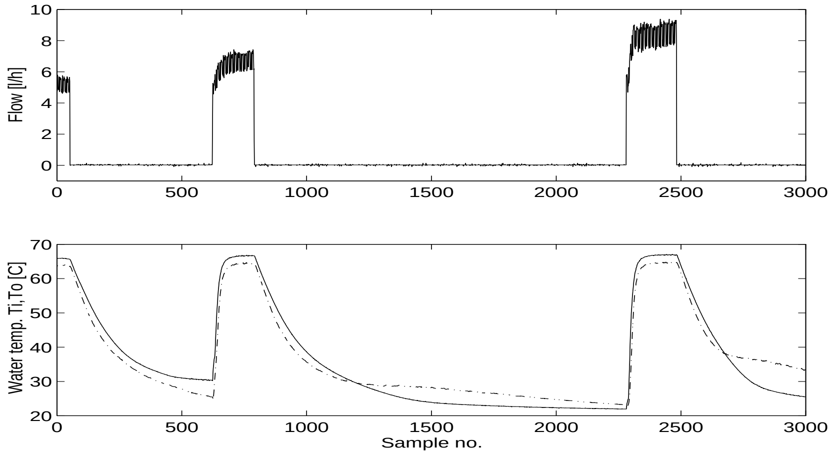

Figure 6.7. *Measured flow q, water supply temperature T_i and return temperature T_o (indicated by "-·").*

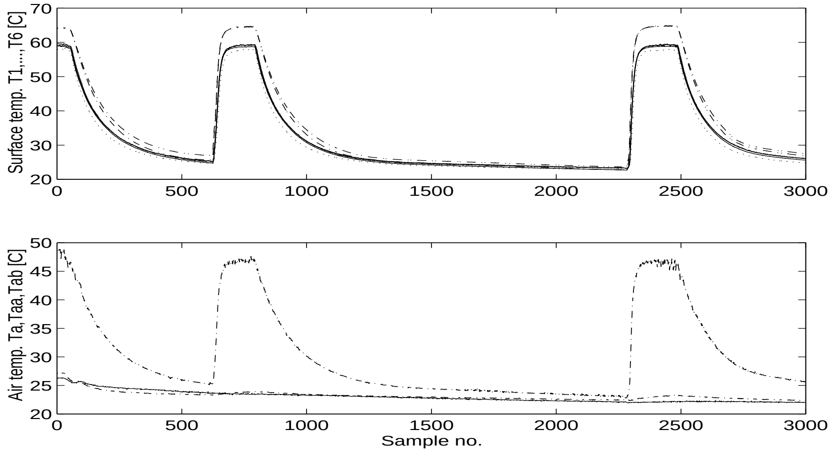

Figure 6.8. *Measured surface temperatures T_{s1}, T_{s2}, T_{s3} (indicated by full line), T_{s4}, T_{s6} (indicated by "-·" line), T_{s5} (indicated by "· · ·" line) and the air temperatures T_{aa}, T_{ab} (both indicated by "-·") and T_a.*

The fact that, the distribution of the surface temperatures can be grouped as isotherms in the horizontal direction, justifies the basic idea of the one-dimensional water flow in the vertical direction as postulated in the partial differential equations in Section 6.3.1 and Section 6.3.2.

The results from the analysis combined with knowledge from the experiment described above, suggest that the input design should avoid situations, where the water flow becomes zero or very small. A PRBS signal with fundamental time period of about $T_0 = 15$ minutes (or more) and the size of the shift register selected as $n=4$, should give sufficient excitation from the flow input. In an attempt to make the flow input and the water supply temperature less correlated, also the some variation of the set point for the water supply temperature should be performed.

A final remark to the analysis. Looking at the approximately stationary input and output temperature, at the end of e.g. the last flow pulse, the temperature difference is about 4 K and the flow about 8 l/h, which implies an instant radiator power of approximately 35 W. This instant power may be compared with radiator diagram in Figure 6.2. Using a supply temperature of 67 °C and a normalized flow of 0.5 (due to 8/17) the normalized power becomes approximately 0.5 (alias 200 W) and the temperature difference over the radiator should be 20 K. Hence, a significant deviation between the measured and the expected power is a fact, as the measured power only forms 20 % of the expected. The radiator diagram is based on an ambient temperature of 20 °C, while the actual temperature at the end of the last flow pulse is 23 °C. Assume that the mean temperature of the radiator is 63 °C – an estimate of the influence of the slightly higher ambient temperature on the theoretical value is a reduction factor of:

$$\frac{(63-23)^{1.25}}{(63-20)^{1.25}} = 0.91$$

or a 9 % lower radiator power (not 80 % lower).

Another possible reason for power reduction is described in *(Becher, 1972)*. If a radiator is located underneath a wide windowsill or in any other way placed in a position, where the free air flow (convection) is inhibited, a reduction in the radiator power will be the result. The radiator is build into the thermal box, but during the experiment the box is used in its open configuration, see 4.2.2, thus a power reduction of 80 % due to “encapsulation” cannot be the case. The radiator in the open configuration is placed as a normal radiator would be placed.

6.4.3 Measurement Data

An experiment based on the input design described above has been performed. Unfortunately the surface temperatures were not measured at this experiment. The measured data $\mathcal{D}_1$ and $\mathcal{D}_2$ are shown in Figure 6.9 and Figure 6.10 at a sample time of 10 seconds, respectively.

Figure 6.9 contains the data $\mathcal{D}_1$ from Box 1 that will be used for estimation with the dynamic one exponent formula model, Model Summary 6.1, while the data $\mathcal{D}_2$ from Box 2 in Figure 6.10 will be used for cross validation. For both figures the flows q_1 and q_2 are plotted in the first subplots. The decreasing trend of the flow in the first part of the data is due to an increasing trend in the ambient temperature and the thermostatic valves. At sample number 383, Box 2 was cutoff by a valve, at 542 the valve was reopened and at sample number 1033 the same valve was used to throttle the flow to Box 2. The second subplot contains the water supply temperature T_i, the return temperature T_o, the ambient temperature T_a and the heating unit supply temperature T_{hs} (see 4.2.1), respectively in both figures. The set point temperature for the supply temperature in the heating unit is 60 °C at the start of the experiment. At sample number 160 this reference has been changed to 70 °C, at 1000 to 90 °C and at 2260 to 70 °C. These changes can be observed in the measurement data. It is observed that the temperature loss from the heating unit to Box 2 is larger than it is to Box 1. This is not strange, as the water flow to Box 1 is q_1+q_2, while the flow from

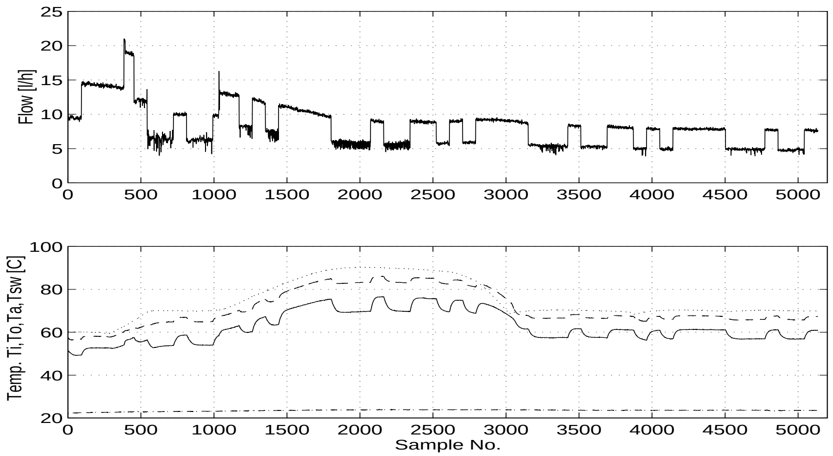

Figure 6.9. $\mathcal{D}_1$: *Measured flow q, water supply temperature T_i (indicated by “--”), return temperature T_o and ambient temperature (indicated by “-·”) and heating unit supply temperature T_{hs} (indicated by “· · ·”).*

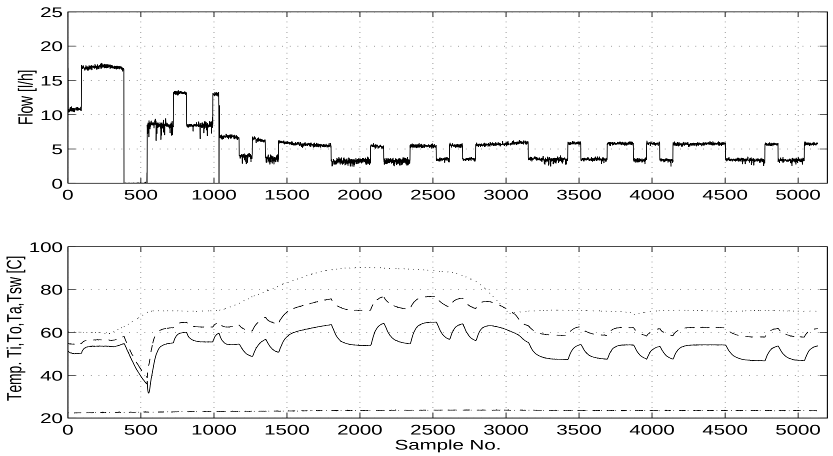

Figure 6.10. $\mathcal{D}_2$: *Measured flow q, water supply temperature T_i (indicated by “--”), return temperature T_o, the ambient temperature (indicated by “-·”) and heating unit supply temperature T_{hs} (indicated by “· · ·”).*

Box 1 to Box 2 only is q_2. At the smaller flow, the water has “more time” to discharge heat through the insulated pipes to the surroundings.

Looking at the instant radiator power at large flows, e.g. at sample number 300, the following data are observed for $\mathcal{D}_1$ and $\mathcal{D}_2$, respectively:

$$q_1 \approx 14 \text{ l/h}, \quad T_i \approx 58°\text{C}, \quad T_o \approx 53°\text{C} \quad \Rightarrow \quad P_{r1} \approx 84 \text{ W}$$

$$q_2 \approx 17 \text{ l/h}, \quad T_i \approx 56.5°\text{C}, \quad T_o \approx 53.5°\text{C} \quad \Rightarrow \quad P_{r2} \approx 61 \text{ W}$$

The instant radiator power at smaller flows, e.g. at sample number 4400, the following data are observed for $\mathcal{D}_1$ and $\mathcal{D}_2$, respectively:

$$q_1 \approx 8 \text{ l/h}, \quad T_i \approx 67.5°\text{C}, \quad T_o \approx 61°\text{C} \quad \Rightarrow \quad P_{r1} \approx 62 \text{ W}$$

$$q_2 \approx 6 \text{ l/h}, \quad T_i \approx 62.5°\text{C}, \quad T_o \approx 54°\text{C} \quad \Rightarrow \quad P_{r2} \approx 61 \text{ W}$$

Comparing these data with the radiator diagram in Figure 6.2, it becomes clear again that the theoretical radiator power (based on the normalized flow q/q_0 and the water supply temperature T_i) is much bigger than the measured radiator power.

6.5 Estimation of Grey Box Models

In Section 6.3 three dynamic models were presented. As no applicable data have been sampled for the two (more complex and demanding) models described in Section 6.3.2 and Section 6.3.3, only the model in Section 6.3.1 is subject for estimation. The measurement $\mathcal{D}_1$ presented in Section 6.4.3 will be used for estimation, while the measurement $\mathcal{D}_2$ is dedicated for cross validation.

6.5.1 Identifiability

The identifiability of the proposed model in Model Summary 6.1 has to be investigated. The model for the j'th section is resumed below:

$$\frac{C}{\mathcal{N}}\frac{dT_j}{dt} = H_q q((1-\phi)T_{j-1}+(2\phi-1)T_j-\phi T_{j+1})-\frac{\Phi_0}{\mathcal{N}}\left(\frac{T_j-T_a}{60}\right)^{n_1} \tag{6.40}$$

where $H_q = c_{p,w}\,\rho_w$ and $\phi \in [0, \frac{1}{2}]$.

As it was the case for the pipe model, neither this radiator model can be analyzed with respect to it identifiability by the algorithm described in *(Ljung and Glad, 1994)*. The problem is again an exponent – this time the radiator exponent n_1. Thus, the identifiability has to be handled the manual way. In the case, when the number of sections is selected as $\mathcal{N}=1$ (implying $\phi=0$), the model is reduced to:

$$C\,\frac{dT}{dt} = H_q\,q\,(T_i - T) - \Phi_0\left(\frac{T-T_a}{60}\right)^{n_1} \tag{6.41}$$

i.e. a non linear first order model with the four parameters: C, H_q, Φ_0 and n_1. It is noted that for $\mathcal{N} \geq 2$, the model gets ϕ as an additional parameter. As it is shown in Appendix B.1, it is only possible to identify two out of these four parameters. Increasing the number of sections $\mathcal{N}$ does not improve the identifiability, but it improves the approximation of the partial differential equation. If the identifiability of the model is to be improved, the number of model outputs must be increased.

6.5.2 Dynamic One Exponent Formula

A Grey Box model of the dynamic one exponent formula model in Model Summary 6.1 can be formulated as:

$$\begin{aligned}
\frac{C}{\mathcal{N}}\,dT_1(t) &= \Big(H_q\,q(t)\,(T_i-(1-\phi)T_1(t)-\phi T_2(t)) \\
&\quad -\frac{\Phi_0}{\mathcal{N}}\left(\frac{T_1(t)-T_a(t)}{60}\right)^{n_1}\Big)\,dt + dW_1(t) && (6.42)\\
\frac{C}{\mathcal{N}}\,T_j(t) &= \Big(H_q q(t)((1-\phi)T_{j-1}(t)+(2\phi-1)T_j(t)-\phi T_{j+1}(t)) \\
&\quad -\frac{\Phi_0}{\mathcal{N}}\left(\frac{T_j(t)-T_a(t)}{60}\right)^{n_1}\Big)\,dt + dW_j(t) && (6.43)\\
\frac{C}{\mathcal{N}}\,T_{\mathcal{N}}(t) &= \Big(H_q\,q\,(T_{\mathcal{N}-1}(t)-T_{\mathcal{N}}(t)) \\
&\quad -\frac{\Phi_0}{\mathcal{N}}\left(\frac{T_{\mathcal{N}}(t)-T_a(t)}{60}\right)^{n_1}\Big)\,dt + dW_{\mathcal{N}}(t) && (6.44)
\end{aligned}$$

with the observation equation:

$$y(k) = T_{\mathcal{N}}(k) + e(k) \tag{6.45}$$

where the system noise $\underline{W} = [W_1, \cdots, W_{\mathcal{N}}]^\top$ is assumed to be a Wiener process with the incremental covariance matrix:

$$\Sigma_W = \begin{bmatrix} \sigma^2_{W,1} & 0 & \cdots & & 0 \\ 0 & \sigma^2_{W,2} & 0 & \cdots & 0 \\ \vdots & \ddots & \ddots & \ddots & \vdots \\ 0 & \cdots & 0 & \sigma^2_{W,\mathcal{N}-1} & 0 \\ 0 & & \cdots & 0 & \sigma^2_{W,\mathcal{N}} \end{bmatrix} \tag{6.46}$$

and e denotes the measurement noise, which is assumed to be white noise with zero mean and variance σ_e^2. Furthermore, $\underline{W}$ and e are assumed to be mutually uncorrelated.

The stochastic version of the dynamic one exponent formula contains five model parameters: the flow gain H_q, the heat capacity of the water and radiator material C, the nominal radiator power Φ_0, the radiator exponent n_1 and the "gradient" approximation parameter ϕ, together with $\mathcal{N}+1$ variance parameters. As described above, it is not possible to estimate all five model parameters at a time. Therefore the radiator exponent is set to 1.25 (according to the data sheet *(Thor Eura, 1990)*), H_q is set to $c_{p,w}\,\rho_w \approx 1.2 \cdot 3.6 \cdot 10^6$ J/m^{3}K (note that q: [l/h]=3.6·10^6[m^3/sec]) and the estimation is divide into two case: $\phi=0$ and $\phi=\frac{1}{2}$.

Estimation with $\phi=0$

Three of the five model parameters has been fixed using prior knowledge. This reduces the optimization problem to estimation of the heat capacity C, the nominal radiator power Φ_0, the system noise variances $\sigma^2_{W,1},\cdots,\sigma^2_{W,\mathcal{N}}$, the measurement noise σ^2_e and $\mathcal{N}$ initial state values $T_1(0),\cdots,T_{\mathcal{N}}(0)$.

Two cases of estimations are presented below, where the following effects on the estimated parameters are to be investigated:

- The influence of approximation order $\mathcal{N} \in [1,\cdots,6]$ on the partial differential equation approximation and on the estimated parameters.
- The influence of a "local" versus a "moving" operating point on the estimated parameters. In order to do so, two cases are considered:
  1. Local operating point: consider the last 1900 samples of the measurement data shown in Figure 6.9. In this part of the measurement data the variations in the flow q, the water supply temperature T_i and the ambient temperature T_a are quite small. Using a time horizon of e.g. 500 samples, it can be observed that the mean values of the inputs are almost constant.
  2. Moving operating point: consider all of the measurement data shown in Figure 6.9. Using a time horizon of 500 samples again, the mean values of the inputs have a significant variation.

  The data sets of these two cases will be referred to as $\mathcal{D}_1^{loc}$ and $\mathcal{D}_1^{all}$.

Data set $\mathcal{D}_1^{loc}$:

In case of $\mathcal{D}_1^{loc}$, the estimated parameters and model performance parameters are presented in Table 6.1. It can be observed that the approximation order $\mathcal{N}=1$ yields the most negative likelihood value, which implies that one section is sufficient in the partial differential equation approximation. The estimated thermal heat capacity of the radiator forms only one fourth of the heat capacity of the water in the radiator, i.e. much smaller than expected. Also the estimated nominal radiator power is smaller than expected, but only one fourth smaller.

Table 6.1. $\mathcal{D}_1^{loc}$: *Estimated model parameters and model performance parameters as function of* $\mathcal{N}$ *for* $\phi=0$, $H_q=1.2/3.6\cdot 10^6$ *J/m*^{3} *K and* $n_1=1.25$.

	C		Φ_0		$-\log\mathcal{L}$	Pred. Error	
$\mathcal{N}$	Est.	Std.	Est.	Std.	Value	Mean	Var.
1	1.09	0.124	111	0.639	-1.15	5.35	52.5
2	1.34	0.856	104	0.725	1.36	6.89	51.7
3	1.46	0.126	102	0.744	3.80	7.33	53.5
4	1.53	0.131	101	0.760	5.08	6.56	56.1
5	1.56	0.065	100	0.721	5.70	4.15	59.7
6	1.60	0.083	100	0.679	5.99	8.00	64.1
Unit	kJ/K		W		–	10^{-3} °C	10^{-3} °C^2

Statistical tests for $\mathcal{N}=1$ are shown in Figure 6.11. The autocorrelation plot for the prediction error shows that none of the autocorrelation are significant on a 99 % level, but on a 95 % level a number of autocorrelation are significant. Looking at the crosscorrelation plots several crosscorrelation are significant even on a 99 % level. Thus the model can not be accepted, but it is quite close to be accepted on a 99 % level. Based on the estimates in Table 6.1, the evaluation of the upper and lower bounds, (6.38) and (6.39), for the time constant τ, yields the range $\frac{1}{2}$ minute $< \tau <$ 10 minutes.

The model performance is presented in Figure 6.12, where the first subplot contains the measured output temperature and the predicted output

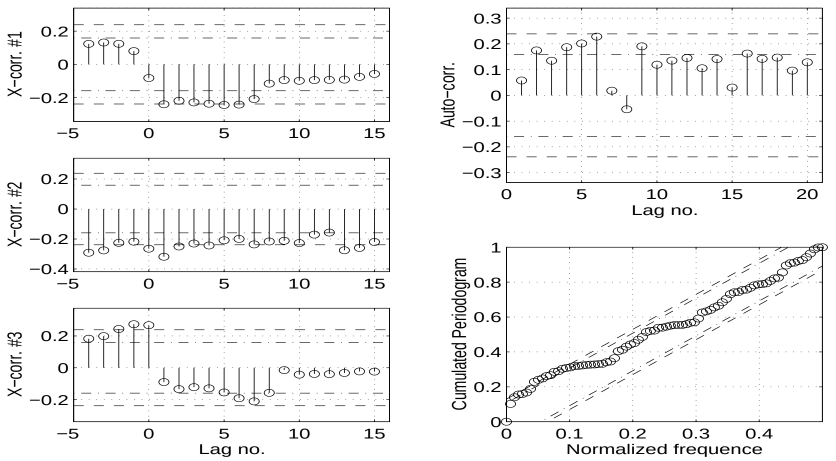

Figure 6.11. $\mathcal{D}_1^{loc}$: *Statistical tests for the prediction error when $\mathcal{N} = 1$; showing the autocorrelation, cumulated periodogram and the crosscorrelations between $\#1 : T_i$, $\#2 : T_a$, $\#3 : q$ and the prediction error.*

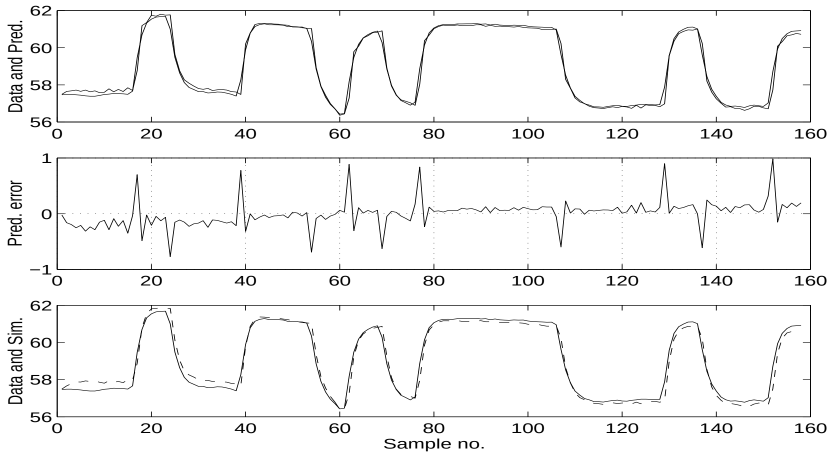

Figure 6.12. $\mathcal{D}_1^{loc}$: *Model performance for $\mathcal{N} = 1$ and $\phi = 0$ (Sample time: two minutes).*

temperature, while the second subplot contains the prediction error. The measured output versus a simulation (the "--"-line), based on the achieved estimates and the given inputs, are shown in the third subplot. It is obvious, that the prediction errors are not white noise due to the peaks, which occur every time the flow level is changed. Moreover an increasing trend in the mean value of prediction errors is also present, i.e. the predictions of the output temperature are too big in the first part and too low in the last part of the data. This is also the case for the simulation in the third subplot. Whether this trend is due to the flow or the supply temperature is difficult to say, as both quantities are decreasing.

Data set $\mathcal{D}_1^{all}$:

In case of $\mathcal{D}_1^{all}$, the estimated parameters and model performance parameters are presented in Table 6.2, while the estimated variances are listed in Table 6.3. From Table 6.2 it can be observed that the approximation order $\mathcal{N}=2$ yields the most negative likelihood value – implying that two sections conform the best approximation to the applied data set. At the same time (i.e. for $\mathcal{N}=2$) the prediction error exhibits its smallest variance.

Table 6.2. $\mathcal{D}_1^{all}$: *Estimated model parameters and model performance parameters as function of $\mathcal{N}$ for $\phi=0$, $H_q=1.2/3.6\cdot10^6$ J/m^3 K and $n_1=1.25$.*

	C		Φ_0		$-\log\mathcal{L}$	Pred. Error	
$\mathcal{N}$	Est.	Std.	Est.	Std.	Value	Mean	Var.
1	4.69	0.204	134	1.44	88	-7.63	68.9
2	3.74	0.111	129	1.53	-175	2.52	34.2
3	3.61	0.866	126	0.52	-141	-0.26	37.4
4	3.90	0.196	125	1.55	-107	-1.21	40.8
5	4.37	0.174	124	1.03	-85	-1.26	42.7
6	4.81	0.210	123	1.63	-70	-1.03	43.8
Unit	kJ/K		W		–	10^{-3} °C	10^{-3} °C^2

Evaluating the estimated model parameters C and Φ_0 it turns out that:

C : the estimated heat capacity – which was assumed to consist of the water and the radiator material – is slightly smaller than the heat capacity of the expected amount of water in the radiator. The expected heat capacity was 36 kJ/K, see Section 6.4.2.

Φ_0 : the nominal radiator power is 395 W, whereas the estimated power is about 130 W, i.e. about one third. A smaller value of the nominal radiator was already expected from the analysis in Section 6.4.2 and Section 6.4.3.

Table 6.3. $\mathcal{D}_1^{all}$: *Estimated variance parameters as function of* $\mathcal{N}$ *for* $\phi=0$, $H_q = 1.2/3.6 \cdot 10^6$ J/m^3 K *and* $n_1 = 1.25$. *The* $(\cdot)$ *denotes the standard deviation of the estimated variance.*

$\mathcal{N}$	$\sigma^2_{W,1}$	$\sigma^2_{W,2}$	$\sigma^2_{W,3}$	$\sigma^2_{W,4}$	$\sigma^2_{W,5}$	$\sigma^2_{W,6}$	σ^2_e
1	1.4 (0.06)						132 (24)
2	12.0 (0.69)	80.1 (28.5)					126 (568)
3	27.5 (0.51)	1.41 (0.66)	452 (29.9)				125 (32)
4	41.5 (4.37)	1.43 (9.76)	2554 (641)	0.339 (0.064)			141 (400)
5	56.8 (4.28)	1.44 (7.39)	1.51 (3.81)	3.44 (0.453)	0.24 (0.05)		114 (45)
6	75.4 (1.82)	2.11 (2.55)	3.36 (1.64)	0.945 (0.056)	3.32 (0.14)	226 (12.1)	132 (409)
Unit	10^{-3}	10^{-6}	10^{-6}	10^{-3}	10^{-3}	10^{-6}	10^{-9}

Looking at Table 6.3 it is observed that the measurement noise σ_e^2 seems to be independent of approximation order $\mathcal{N}$, which is reasonable, but the level is quite small. The largest of the estimated variances is found to be

first system noise variance $\sigma^2_{W,1}$ for all values of $\mathcal{N}$. This larger noise level is probably related to the radiator supply temperature T_i.

Statistical tests for $\mathcal{N}=1$ and $\mathcal{N}=2$, respectively, are shown in Figure 6.13 and Figure 6.14. The autocorrelation in Figure 6.13 reminds of an AR(1)-process. Increasing the approximation order $\mathcal{N}$ by one step, most of this AR(1)-process is grabbed by the model extension, as it can be observed from the autocorrelation plot in Figure 6.14. Also the crosscorrelation between the water supply temperature T_i and the prediction error is improved. Increasing the approximation order further, does not improve nor deteriorate the statistical tests. Thus, based on the statistical tests presented in Figure 6.14, the model described in Model Summary 6.1 with the optimal approximation order $\mathcal{N} = 2$ cannot be accepted. But as pointed out in Section 6.4.2, the performed radiator experiment suffers from insufficient excitation and more or less correlated input signals and a "less ideal" measurement of the output temperature. Thus the statistical tests can hardly become prefect.

The model performance is presented in Figure 6.15, where the first subplot contains the measured output temperature and the predicted output temperature, while the second subplot contains the prediction error. The measured output versus a simulation (the "--"-line), based on the achieved estimates and the given inputs, are shown in the third subplot. It is obvious that the flow and the prediction error are correlated, since every time a change occurs in the output temperature as a result of a change in the flow, it is followed by a peak in the prediction error. It is further observed that the prediction error has an increasing trend in its mean value, which could resemble the increasing trend in the ambient temperature remarkably, but it is more likely that this trend is correlated with the flow or the supply temperature, as it was observed for $\mathcal{D}_1^{loc}$. Looking at the third subplot, it can be observed that the simulated output temperature is too high in the first part of the simulation and too low in the last part, as it also was observed for $\mathcal{D}_1^{loc}$. This general trend in the prediction error is caused by a mismatch

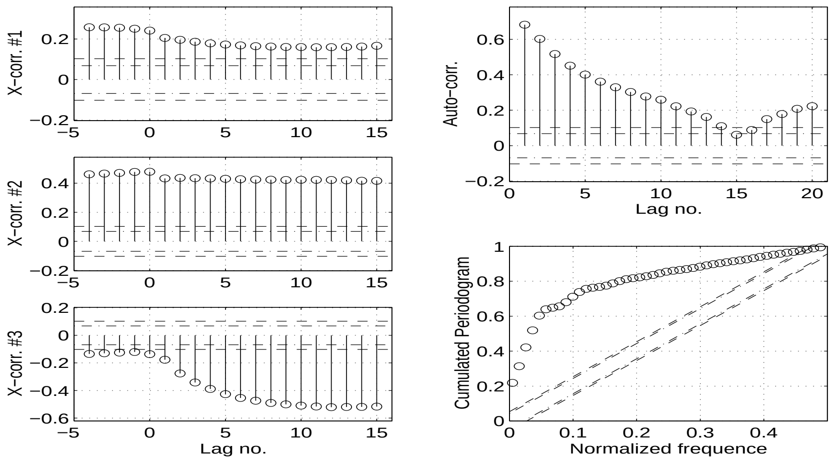

Figure 6.13. $\mathcal{D}_1^{all}$: *Statistical tests for the prediction error when* $\mathcal{N} = 1$; *showing the autocorrelation, cumulated periodogram and the crosscorrelations between* $\#1 : T_i$, $\#2 : T_a$, $\#3 : q$ *and the prediction error.*

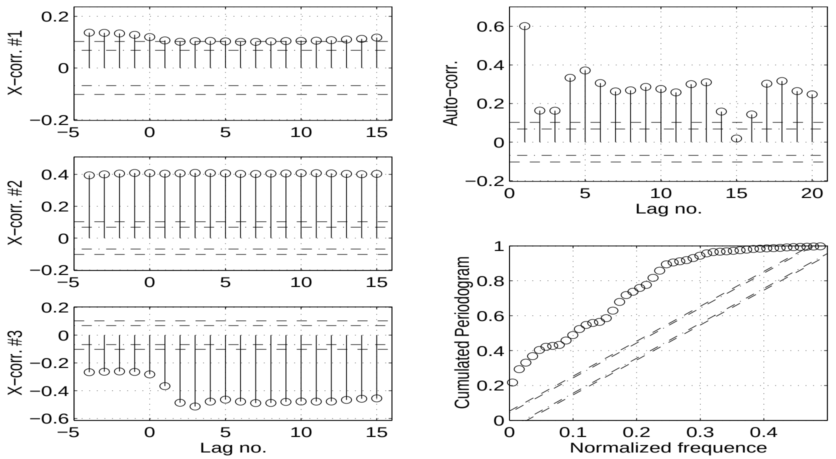

Figure 6.14. $\mathcal{D}_1^{all}$: *Statistical tests for the prediction error when* $\mathcal{N} = 2$; *showing the autocorrelation, cumulated periodogram and the crosscorrelations between* $\#1 : T_i$, $\#2 : T_a$, $\#3 : q$ *and the prediction error.*

between the heat flow in and out of the radiator. Hence, the model description between the radiator temperature and the ambient temperature is too simple.

Comparing the estimates of $\mathcal{D}_1^{loc}$ with the estimates of $\mathcal{D}_1^{all}$, it is noted that the estimates of $\mathcal{D}_1^{all}$ are closer to the expectations. On the other hand, the statistical test for $\mathcal{D}_1^{all}$ are not as good as for $\mathcal{D}_1^{loc}$. Thus, the data set with the moving operating point (alias $\mathcal{D}_1^{all}$) puts higher demands on the accuracy of the model, as the data contain more information about the real system.

An attractive features of the Kalman filter technique is the ability to recreate/predict non measured/measurable (but observable) states. An example for $\mathcal{N} = 4$ is shown in Figure 6.16, where three dashed lines indicate the radiator temperatures T_1, T_2 and T_3 and the input and output temperatures, T_i and T_o respectively, are plotted as full lines. It is noted that the model output T_4 and T_o are supposed to be identical. It is observed from Figure 6.16 that the behaviour of the Kalman states is physical, in the sense that, they stay within the bounds made up by the input and output temperature.

Estimation with $\phi = \frac{1}{2}$

Another series of estimations for the approximation order $\mathcal{N} \in [1, \cdots, 6]$ have been performed on $\mathcal{D}_1^{all}$ in order to evaluate the influence of parameter ϕ on the partial differential equation approximation. It is noted that for the $\mathcal{N}$'th section, ϕ is set to zero as described in Model Summary 6.1. The estimated model parameters with performance parameters are presented in Table 6.4.

Again it turns out that the approximation order $\mathcal{N} = 2$ yields the most negative likelihood value and that the prediction error exhibits its smallest variance – implying that two sections still conform the best approximation to the applied data set. For $\mathcal{N} = 6$ the likelihood value makes a jump, which is due to convergence problems. Thus, this set of estimates is corrupted. The

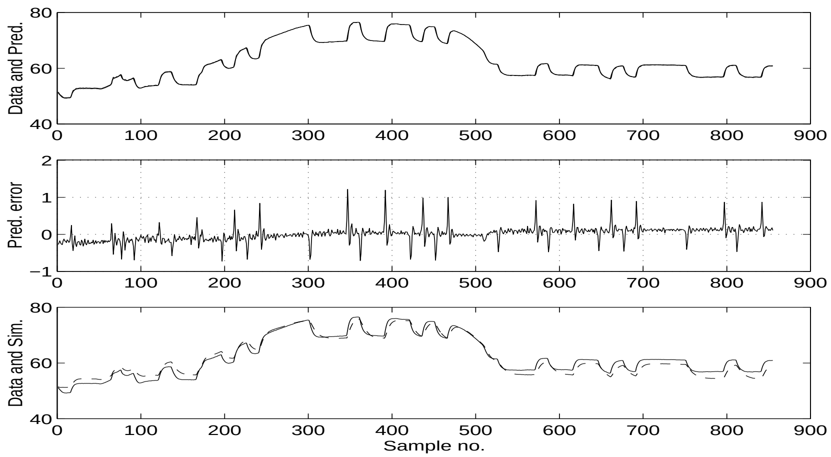

Figure 6.15. $\mathcal{D}_1^{all}$: *Model performance for $\mathcal{N}=2$ and $\phi=0$ (Sample time: one minute).*

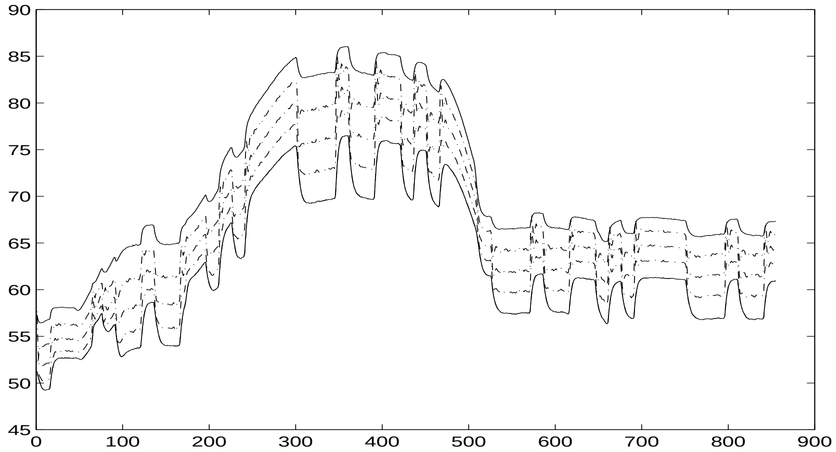

Figure 6.16. $\mathcal{D}_1^{all}$: *Distribution of the radiator temperatures $T_1,\cdots,T_4$, alias the Kalman states (indicated by "-·") for $\mathcal{N}=4$. Note that $T_4 \approx T_o$ and $\phi=0$ (Sample time: one minute).*

Table 6.4. *Estimated parameters and model performance parameters as function of $\mathcal{N}$ for $\phi=\frac{1}{2}$, $H_q=1.2/3.6\cdot 10^6$ J/m^3 K and $n_1=1.25$.*

	C		Φ_0		$-\log \mathcal{L}$	Pred. Error	
$\mathcal{N}$	Est.	Std.	Est.	Std.	Value	Mean	Var.
1	4.69	0.204	134	1.44	88	-7.63	68.9
2	4.27	0.160	165	1.87	-185	2.88	33.8
3	4.02	0.172	146	1.68	-100	-0.30	42.1
4	5.18	0.300	138	1.21	-36	-0.99	47.9
5	6.57	0.122	135	1.75	11	2.70	52.5
6	5.69	0.009	129	3.59	1165	-28.8	866
Unit	kJ/K		W		–	10^{-3} °C	10^{-3} °C^2

estimates of heat capacity and the nominal radiator power are generally of the same size, but slightly bigger, compared to $\phi=0$. Comparing the likelihood value for $\phi=0$ and $\phi=\frac{1}{2}$, it is observed that $\phi=0$ yields the best performance for all values of $\mathcal{N}$, except for $\mathcal{N}=2$. The same observations that were made for Table 6.2, can also be made for Table 6.4. The table corresponding to Table 6.3 is not presented, as also these data for $\phi=0$ and $\phi=\frac{1}{2}$ are approximately the same.

Statistical tests for $\mathcal{N}=2$ and $\mathcal{N}=5$ are shown in Figure 6.17 and Figure 6.18, respectively. Again the tests indicate both autocorrelations and crosscorrelations, hence neither for $\phi=\frac{1}{2}$ can the model described in Model Summary 6.1 with the optimal approximation order $\mathcal{N}=2$ be accepted. The tests in Figure 6.17 of course remind a lot of the tests in Figure 6.14. Comparing Figure 6.17 and Figure 6.18, it can be observed that the statistical tests are improved for the larger value of the approximation order $\mathcal{N}$ – a general tendency which was not the case for $\phi=0$.

The model performance for $\mathcal{N}=2$ is presented in Figure 6.19, where the first subplot contains the measured output temperature and the predicted output temperature etc. Also this figure reminds of its predecessor, Figure 6.15,

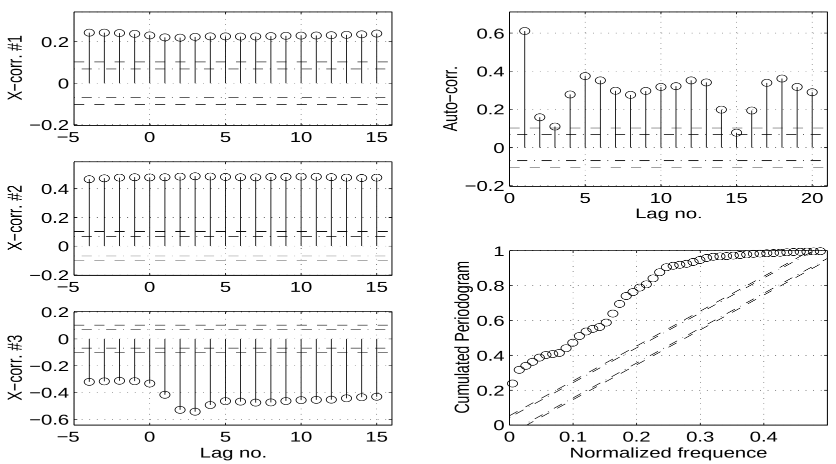

Figure 6.17. $\mathcal{D}_1$: *Statistical tests for the prediction error when* $\mathcal{N}=2$*; showing the autocorrelation, cumulated periodogram and the crosscorrelations between* $\#1 : T_i$, $\#2 : T_a$, $\#3 : q$ *and the prediction error.*

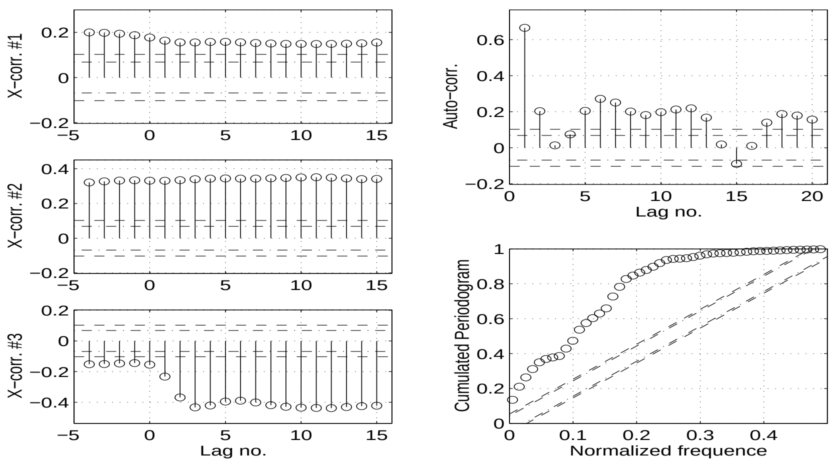

Figure 6.18. $\mathcal{D}_1$: *Statistical tests for the prediction error when* $\mathcal{N}=5$*; showing the autocorrelation, cumulated periodogram and the crosscorrelations between* $\#1 : T_i$, $\#2 : T_a$, $\#3 : q$ *and the prediction error.*

with peaks and trend in the prediction error and offset between data and simulation.

Optimal ϕ

For both cases of ϕ, the optimal approximation order turns out to be $\mathcal{N}=2$. Moreover, the case of $\phi = \frac{1}{2}$ results in a better model performance than $\phi=0$. Hence, it could be interesting to determine whether $\phi=\frac{1}{2}$ or some value of ϕ between 0 and $\frac{1}{2}$ is the optimal value. The result of such an analysis is presented in Table 6.5 and it is clear that $\phi=\frac{1}{2}$ yields the best model performance (when $\mathcal{N}=2$).

6.5.3 Cross Validation

As it has been shown above the case of $\phi = \frac{1}{2}$ results in a better model performance, than $\phi = 0$. Since as $\phi = 0$ in general (for $\mathcal{N} > 2$) has the best model performance, this value will be used in the cross validation. The data $\mathcal{D}_2$, dedicated for cross validation, has been measured on Box 2, refer to Figure 6.10. In a sense the following cross validation is double, i.e. the cross validation is based on estimation data and validation data as usual. Meanwhile, these data have been measured on two – in principle – equivalent radiator setups.

The cross validation is presented for $\phi=0$ and optimal approximation order $\mathcal{N}=2$. The applied cross validation involves computation of the prediction error variance and the variance of the deviation between measured data and simulations. The result is presented in Table 6.6. The model estimated on $\mathcal{D}_1$, actually performs slightly better on the validation data $\mathcal{D}_2$.

The model performance with the validation data is shown in Figure 6.20, where the first subplot contains the measured output temperature and the predicted output temperature (of Box 2), while the second subplot contains

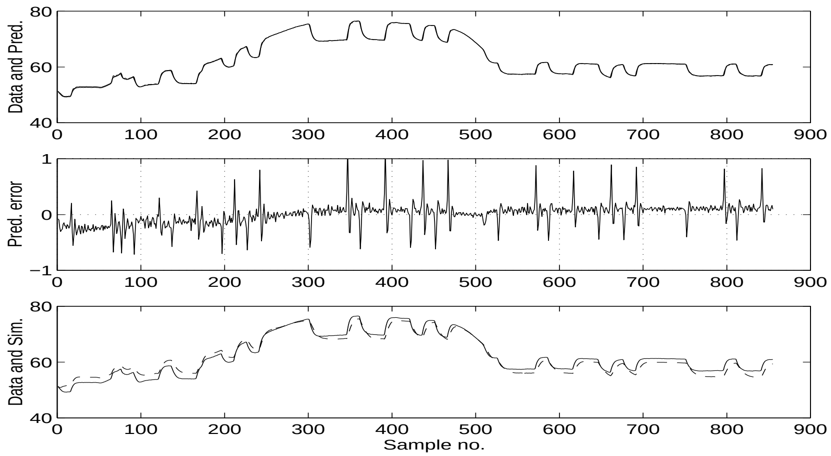

Figure 6.19. $\mathcal{D}_1$: *Model performance for* $\mathcal{N} = 2$ *and* $\phi = \frac{1}{2}$ *(Sample time: one minute).*

Table 6.5. *Estimated parameters and model performance parameters as function of* ϕ *for* $\mathcal{N}=2$, $H_q=1.2/3.6\cdot 10^6$ J/m^3 K *and* $n_1=1.25$.

	C		Φ_0		$-\log\mathcal{L}$	Pred. Error	
ϕ	Est.	Std.	Est.	Std.	Value	Mean	Var.
0.0	3.74	0.111	129	1.53	-175	2.52	34.2
0.1	3.83	0.199	135	1.67	-178	2.63	34.1
0.2	3.93	0.375	141	1.03	-180	2.72	33.9
0.3	4.04	0.131	148	1.56	-182	2.79	33.8
0.4	4.15	0.624	156	4.29	-184	2.84	33.8
0.5	4.27	0.160	165	1.87	-185	2.88	33.8
Unit	kJ/K		W		–	10^{-3} °C	10^{-3} °C^2

Table 6.6. *Cross validation data using the parameter values* $\mathcal{N}=2$, $\phi=0$, $H_q=1.2/3.6\cdot 10^6$ J/m^3 K *and* $n_1=1.25$.

Data	Pred. error	Simul. error
estimation set $\mathcal{D}_1$	34.2	2.57
validation set $\mathcal{D}_2$	32.3	1.87
Unit	10^{-3} °C^2	°C^2

the prediction error. The measured output (of Box 2) versus the simulated output (the "--"-line), based on the achieved estimates (from Box 1) given the inputs from the validation data set (i.e. from Box 2), are shown in the third subplot.

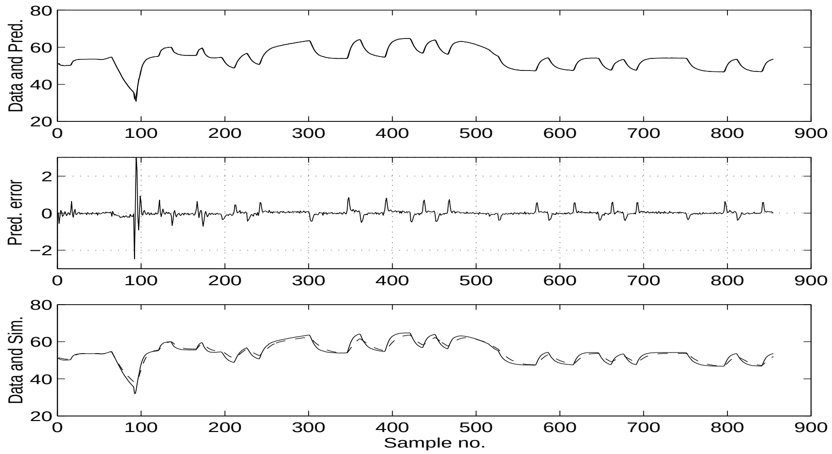

Figure 6.20. $\mathcal{D}_2$: *Model performance for* $\mathcal{N}=2$ *and* $\phi=0$ *using the estimated parameters of* $\mathcal{D}_1$ *(Sample time: one minute).*

Comparing Figure 6.20 with Figure 6.15, it is observed that no increasing trend is present in prediction error in Figure 6.20. Hence, for this data set, there is a good balance between the heat flow in and out of the radiator, except for the central part of the data (i.e. for sample no. 250 to 525), where a small positive deviation is notable. A closer look at the simulation plot (third subplot of Figure 6.20) reveals that the simulation cannot keep up with the dynamic of the measured output temperature.

6.6 Summary

In this chapter the modelling of a panel radiator has been considered. A short description of the applied radiator and a couple of static radiator models were presented in the first section. The hydraulic behaviour of the radiator was discussed in Section 6.2 and the influence of the radiator on the hydraulic system was found to be very small – at least for the applied radiator.

In Section 6.3 three models for the thermal dynamics of the radiator have been presented. The basic idea of the first model, Model Summary 6.1, was a macroscopic modelling approach based on a partial differential equation of the cooling of a one-dimensional water flow. This model was viewed as a generalization of the static one exponent formula. The two other models were based on more microscopic modelling approaches, as the surface temperature, the geometry and the location of the radiator were included, whereas the first model only considered the relation between the water temperature in the radiator and the ambient air temperature. The advantage of the macroscopic modelling approach was of course its simplicity and the small amount of parameters and input variables, while the disadvantage was loss of generality (i.e. not able to describe all the workspace).

The radiator experiment and the experimental conditions were analyzed in Section 6.4, based on the dynamic model of the one exponent formula and a simple experiment. A time constant for the radiator dynamic was extracted from the dynamic model of the one exponent formula, together with estimates of a lower and an upper bound. The prospects for experimental design of the radiator experiment were discussed and the conclusion was that only the flow input could be given a proper design. The measurements presented in Figure 6.9 and Figure 6.10 did support the analysis with the following information:

- The measurement of the output temperature might be corrupted, when the flow was zero or very small.
- The actual power from the radiator was significantly smaller than the theoretical power postulated in the radiator diagram in Figure 6.2.
- The measured surface temperatures supported the one-dimensional flow assumption in connection with the partial differential equations. The measured surface temperatures in the flow direction in the radiator was not linear function of the height. It was observed that the center row of temperatures, T_{s1}, T_{s2}, T_{s3}, were quite close to the bottom temperature.

The last observation did not exclude the dynamic model of the one exponent formula, as this model contained the exponential temperature difference description, characterized by the exponent n_1, which in a way simulated the nonlinear temperature distribution of the surface temperature. But a more adequate modelling approach would be to model the radiator as a heat exchanger, which has been the underlying idea of the presented microscopic modelling approaches.

In Section 6.5 only the dynamic model of the one exponent formula was used for estimations, since no applicable data had been sampled for the two models described in Section 6.3.2 and Section 6.3.3. The identifiability of the dynamic model of the one exponent formula was analyzed and the number of identifiable parameters was two. Furthermore, the influence of different factors was investigated with the following conclusions:

- Boundary temperature. Parameter ϕ was evaluated for $\phi = 0$ and $\phi = \frac{1}{2}$ and the best model performance was in general achieved for $\phi = 0$, except for $\mathcal{N} = 2$ where $\phi = \frac{1}{2}$ had the best performance.
- Approximation order. It turned out that the approximation order $\mathcal{N}$ was influenced by the operation point, as the optimal number of sections was $\mathcal{N} = 1$ for the local operation point and $\mathcal{N} = 2$ for the moving operation point (for $\phi = 0$).
- Local versus moving operation point. The dynamic one exponent model provided a fair description of the radiator dynamic around a local operation point, but the estimated parameters were far from the expected values. In case of the moving operation point, it became clear that the model was too simple. Meanwhile, the estimated parameters were closer to the expectations. According to the data sheet the nominal radiator power was 395 W, but as it was pointed out in Section 6.4.2 the actual radiator power submission was less. Thus the estimated nominal radiator power in the range of 130 W to 160 W seamed reasonable. While the heat capacity of the radiator was expected to consist of both water and radiator material, the estimated values were approximately equal to heat capacity of the water in the radiator.

As long as the model is imperfect, it is difficult to say whether the estimated value or the expectation is wrong. Moreover, it is important to have measurements representing all the workspace, as then heat dynamic of the radiator is nonlinear. For a dynamic system it is also important to have good excitation (informative data) – and this is not quite the case for the applied estimation data. Hence, the described experimental setup of the radiator should be modified, such that (at least) the flow and the radiator supply temperature can be treated as independent input variables.

The dynamic model based the one exponent formula yields an usable description of the thermal radiator dynamic, but the model part describing the heat flow out of the radiator can/should be improved. For example, the

temperature distribution of the measured surface temperature indicates a nonlinear distribution in the vertical direction. On this basis a nonlinear distribution of the temperatures in the radiator could be expected, but this is not reflected in the present model, as visualized by the Kalman temperatures. In order to get on, the microscopic modelling approaches can be further refined and afterwards used to derive a better macroscopic model.

Based on some of the experiences presented in this chapter, alternative radiator model formulations are investigated in *(Andersen, 1997)*.

Chapter 7

Thermostatic Valve Modelling

In this chapter the modelling of a gas based (saturated vapor) thermostatic radiator valve is presented. The modelling deals with the hydraulic and thermodynamic properties of the thermostatic valve. As mentioned in the previous chapters, the purpose of the dynamic modelling is to identify and estimate the parameters of the dynamic model.

The structure of the chapter is as follows: the first section gives an introduction to the basic concept of the thermostatic valve. In the second section, two modelling approaches of the gas based thermostatic valve are presented. The first approach is based on the second law of Newton, while the second approach is a macroscopic approach based on empirical data for the relation between the relative temperature and the valve constant. The third section describes the experimental setup of the thermostatic valve together with performed measurements, while estimation and validation results for the macroscopic thermostatic valve model are presented in the fourth section.

7.1 The Gas based Thermostatic Valve

Today the thermostatic radiator valve is a standard component in water based heating systems. As described in *(Gammelby, 1974)*, different thermostatic valve designs exist and requirements for the gas based thermostatic valve are described in the European standard EN 215-1 (see e.g. *(Dansk Standard, 1988)*). In the following, only the gas based thermostatic valve is considered. This type of thermostatic valve consists of a thermostatic head (the sensor part) and a valve body (the actuator part), as sketched in Figure 7.1.

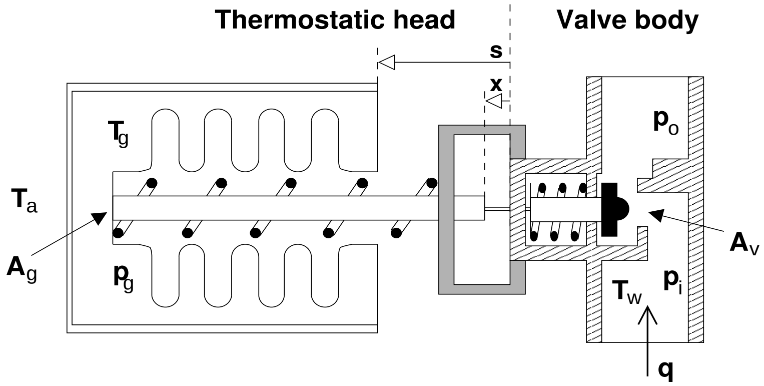

Figure 7.1. *Schematic drawing of a gas based thermostatic radiator valve. Compiled from (Dansk Standard, 1988).*

7.1.1 The Thermostatic Head

As illustrated in Figure 7.1, the thermostatic head is based on a spring/pod arrangement and an encapsulated temperature sensitive gas (saturated vapor). The temperature sensitive gas will expand or contract depending on the air temperature T_a (ambient temperature) around the thermostatic head. For example, if the gas temperature T_g is increased due to an increased T_a, the gas pressure p_g will increase. Hence, the pressure force

of the gas acting on the spring/pod arrangement will also increase, which eventually – depending on the friction force – will produce a displacement of the valve stem. The displacement of the valve stem (and thus the offset of spring/pod arrangement) is denoted by x in Figure 7.1, while s is related to the displacement of the pod offset. By a displacement of the pod offset the balance of the forces is changed and in this way the range of the temperature sensitiveness of the thermostatic head can be changed. This fact is the idea behind the set point temperature T_{set}, hence when the thermostatic head is turned (e.g. clockwise), the displacement of the pod offset is altered and thus also the set point temperature T_{set}.

The position of the valve stem x is determined by the gas pressure force, the forces in the spring/pod arrangement and the water flow force, i.e. the pressure force from the pressure difference over the valve disc. Meanwhile the displacement of the valve stem x has a lower and an upper limit:

- At the lower limit, the valve is closed, i.e. $x = 0$ and the valve disc is standing on the valve seal.
- At the upper limit, the valve is full open, i.e. $x = 100$ %.

The forces in the spring/pod arrangement and the gas pressure force are much bigger than the water flow force, hence the position of the valve stem x can be viewed as a function of the gas temperature T_g and eventually of the surrounding air temperature T_a. Idealized, the relation between the position of the valve stem x and the ambient air temperature T_a is linear as sketched in Figure 7.2, i.e. the thermostatic head can be viewed as a P-controller. According to the specifications for the thermostatic valve, the width of the P-band temperature is 6 K. At point A the valve is full open (upper limit) and at point S the valve is closed (lower limit). A definition of the closing temperature at point S is given in EN 215-1. In addition to the closing temperature, the set point temperature T_{set} (alias point B) is defined 2.0 degrees below point S.

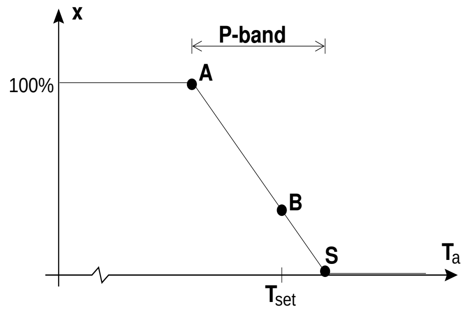

Figure 7.2. *The P-band temperature. Idealized relation between valve stem position x and ambient air temperature T_a.*

A relative temperature X_p is defined as:

$$X_p = T_{set} + 2 - T_a \tag{7.1}$$

i.e. as the difference between the actual P-band temperature (through T_{set}) and the ambient air temperature T_a. Hence, when the ambient temperature T_a is 2 degrees larger than the set point T_{set}, the relative temperature X_p is zero and the valve is closed.

Note that in the literature X_p is usually denoted as the *P-band temperature*, which is correct as long as the "P-band" is referring to P-band of the thermostatic head (sketched in Figure 7.2), but it is misguiding to think of X_p as a "P-band" temperature in connection with the valve flow. Therefore, in order to avoid any misunderstanding X_p is denoted as the *relative temperature*.

7.1.2 The Valve Body

The other half of the thermostatic valve, the valve body, is a seat valve (conical valve), which contains a mitre shaped valve disc, as sketched in

Figure 7.1. In Section 5.1.2, the basic model for pressure drop Δp and the flow q in connection with a non straight pipe was presented. Therefore, let the relation between the pressure drop Δp_v across the valve body (valve seat) and the valve flow q be defined as:

$$\Delta p_v = R_v q^2 \tag{7.2}$$

where R_v denotes the hydraulic resistance of the valve or as:

$$q = K_v \sqrt{\Delta p_v} \tag{7.3}$$

where $K_v = \frac{1}{R_v^2}$ denotes the valve constant. It should be noted that the flow q in (7.2) and (7.3) implicit is turbulent flow and that both R_v and K_v depend on the position of the valve disc. The little spring arrangement in the valve body (see Figure 7.1) assures that the valve is full open, if no thermostatic head is attached.

7.1.3 Thermostatic Valve

The connection between the thermostatic head and the valve body is a thin dowel connecting the valve stem of the thermostatic sensor with the stem of the valve body, see Figure 7.1. When a displacement of the valve stem (of the thermostatic sensor) occurs, this displacement is directly transfered to the stem of the valve body, i.e. the valve constant K_v (ditto the hydraulic resistance R_v) depends on x. Hence, in this way the valve constant K_v is controlled by the surrounding air temperature T_a, through the relative temperature X_p.

The relation between the relative temperature X_p and the valve flow q is usually listed in the data sheet of a thermostatic valve. Data for the considered thermostatic valve are presented in Table 7.1. All the presented flows are related to a pressure drop of 1 Bar over the valve, thus the K_v-values are easily calculated by (7.3). According to the specifications for the thermostatic valve, K_v must be zero when X_p is zero.

Table 7.1. *Thermostatic radiator valve data for type RA-FN 15 data. Compiled from (Danfoss, 1988).*

Quantity	Unit	$\Delta p_v = 1$ Bar				
X_p	K	0.5	1.0	1.5	2.0	6.0
q	m^3/h	0.22	0.40	0.55	0.65	0.85
K_v	$m^3/h/Bar^{0.5}$	0.22	0.40	0.55	0.65	0.85

7.1.4 On the Control

The purpose of a thermostatic valve is to control the water flow q through a radiator in order to maintain a certain room temperature T_r. This is illustrated in Figure 7.3, where Φ denotes the heat flow from the radiator. As described above, the thermostatic valve operates as a P-controller on

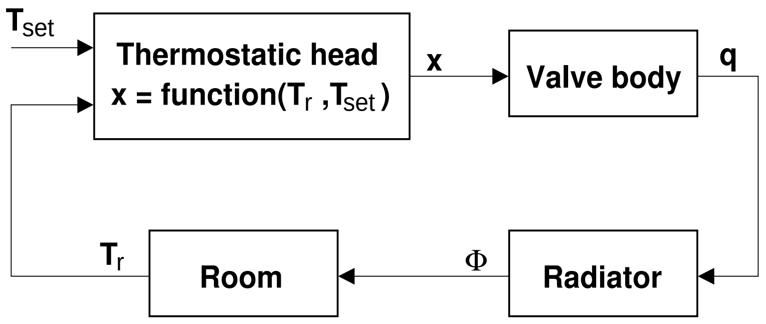

Figure 7.3. *Block diagram of the thermostatic valve control loop.*

the valve constant with respect to the ambient temperature. The control

property of the closed loop system in Figure 7.3 is usually assessed by the *valve authority* concept, as defined in e.g. *(Frederiksen, 1977)* by the fraction:

$$\frac{K_{vl}}{K_{vs}} \tag{7.4}$$

where K_{vs} refers to the value of the valve constant K_v at full open valve and K_{vl} to the value of the valve constant K_v at 100 % load, which is defined as:

$$K_{vl} = \frac{q_0}{\sqrt{\Delta p_{vl}}} \tag{7.5}$$

where q_0 denotes nominal water flow of radiator and Δp_{vl} denotes the available pressure over the thermostatic valve at 100 % load.

It should be noted that alternative definitions of the valve authority exists, e.g. *(Håkansson, 1988)*:

$$\frac{\Delta p_{vs}}{\Delta p_s} \tag{7.6}$$

where Δp_{vs} denotes the pressure across the full open thermostatic valve and Δp_s the total pressure difference in the particular part of the hydraulic system, where the thermostatic valve affects the flow. Which one of the valve authority definitions is the best, is probably a personal matter. In the following (7.4) will be used.

When the heat loss of a room is estimated, a suitable radiator can be selected and the nominal water flow q_0 can be calculated. Based on a desirable pressure drop across the valve body and on the nominal flow, the "theoretical" K_{vl} value is computed and a corresponding thermostatic valve can be selected, i.e. a thermostatic valve, which has approximately the desired K_{vl} value at e.g. the set point temperature (i.e. at $X_p = 2\ K$). According to *(Frederiksen, 1977)* the following criteria should be fulfilled:

- The computed K_{vl} value is within the K_v interval defined by $X_p = 1$ and $X_p = 3$ of the selected thermostatic valve.

- The valve authority is larger than 0.3.

in order to get good control properties. A relative temperature of $X_p = 2$ K is often used, as it forms an appropriate compromise between thermal comfort and stability in the central heating system.

As stated in (7.3), the flow q is a result of the valve constant K_v and the pressure drop Δp_v over the valve body. Hence, the thermostatic valve shares the control of flow with the pressure in the hydraulic system, as the valve pressure Δp_v depends on the pressure generated by the circulating pump and on the actual distribution of the hydraulic resistance in the heat network (pipes, radiators, valves etc.). When the thermostatic valve is in its P-band (i.e. in control of the flow), the hydraulic resistance of the thermostatic valve is dominating the rest of the hydraulic system resistances. Thus in this case, both valve flow q and valve pressure Δp_v depend on valve stem position, which further implies that the room temperature (alias ambient temperature) is in control of flow to the radiator, as it was sketched Figure 7.3.

7.2 Dynamic Models of the Thermostatic Valve

In this section the modelling approaches of the thermostatic valve will be presented, where the first approach is a "microscopic" approach based on the second law of Newton, while the second is a "macroscopic" approach based on empirical data for the thermostatic valve.

7.2.1 On the Physical Properties

(Gammelby, 1974) describes 4 types of thermostatic valves and reports of different general thermostatic valve properties. In *(Svensson, 1978)* additional thermostatic valve properties are described and measured values for the properties together with some experiences are reported. *(Dansk Standard, 1988)* describes the same properties as *(Gammelby, 1974)* and a set of requirements for the gas based thermostatic valve is defined.

Summarizing the properties of thermostatic valve:

- Time delay between ambient air temperature and flow response.

- Time constant between ambient air temperature and flow response. As the relation between the ambient air temperature and the valve flow is nonlinear, a response time has been defined in *(Dansk Standard, 1988)*.

- Hysteresis, i.e. when the ambient air temperature is increased (enough to close the valve) and afterwards decreased (enough to open the valve), the two temperatures, where the valve was closing and opening, are not equal. The hysteresis is mainly caused by friction.

- Sensitive to the water supply temperature, i.e. the flow is more or less influenced by variations in the water supply temperature to the radiator. According to the requirements in *(Dansk Standard, 1988)*, the effect of a step in the water temperature of 30 K, may not influence the sensor gas temperature by more the 1.5 K.

- Elasticity, i.e. elasticity with respect to the closing point. As described in Section 7.1.1, the force from the water flow is small compared to the other forces, but it is big enough influence the set point temperature. Thus, changes in the system pressure imply different flows at the same setpoint. This little problem has the largest impact around the closing point.

It is concluded in *(Gammelby, 1974)* that, the gas based thermostatic valve is the most advantageous type of thermostatic valve, due to its relative small time constant, a very small hysteresis band and its small dependency of the water supply temperature.

With the considerations above in mind, a dynamic model for the thermostatic valve will now be derived.

7.2.2 Second Law of Newton

The following "microscopic" modelling approach is based on the second law of Newton. As the thermostatic valve forms a mechanical system, it must obey the second law of Newton, which expresses the conservation of momentum. In order to simplify the modelling, the following assumptions will be applied:

- The temperature sensitive gas behaves as an ideal gas, thus:

  $$\frac{p_g V_g}{T_g} = K_g \tag{7.7}$$

  where K_g denotes the gas constant and V_g the volume of the gas.

- No hysteresis, i.e. no friction forces.

- The springs in the spring arrangement, both in the thermostatic head and in the valve body, can be modelled as one spring with the spring constant k_s, while the spring constant of the pod in the thermostatic head is denoted as k_p.

Referring to Figure 7.1, the volume of the temperature sensitive gas in the thermostatic head can be modelled as:

$$V_g = V_0 - A_g(x - s + s_{max}) \tag{7.8}$$

where A_g denotes the "central" cross section area of the pod and V_0 the largest possible gas volume, i.e. when the valve is closed (alias $x = 0$) and the set point temperature T_{set} is in the position $s = s_{max}$ (referring to the offset of the pod).

The forces acting on the valve stem are sketched on Figure 7.4, where F_g denotes the pressure force of the gas, F_s the joint force of the springs, F_p the force of the pod and F_w the force from the water flow. These forces must satisfy the second law of Newton:

$$\begin{aligned}
M_s \frac{d^2x}{dt^2} &= -F_g + F_s + F_p + F_w && (7.9)\\
&= -p_g A_g - k_s(x - x_0) - k_p(x - s - s_0) + \Delta p_v A_v && (7.10)\\
&= \frac{-K_g A_g}{V_0 - A_g(x - s + s_{max})} T_g - k_s(x - x_0) \\
&\quad -k_p(x - s - s_0) + \Delta p_v A_v && (7.11)
\end{aligned}$$

where A_v denotes the cross section area of the pipe connection between input and output chamber of the valve body, M_s the mass of the valve stem and x_0, s_0 refer to the zero offsets of the springs and pod, respectively. Moreover, $x < x_0$ and $x - s < s_0$.

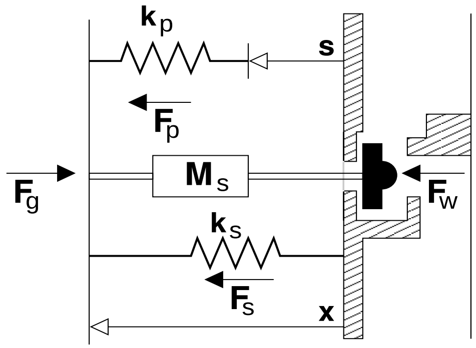

Figure 7.4. *Sketch of the forces acting on the valve stem of the thermostatic valve.*

The model for the valve stem, (7.11), is achieved by the use of (7.7) and (7.8) and it is a second order differential equation containing 10 parameters of which some might be difficult to evaluate/determine. Moreover, (7.11) only describes the relation between the gas temperature T_g and the valve stem position x. The relation between the ambient temperature of the thermostatic head T_a and the gas temperature T_g will involve a first order differential equation (see next section), while the relation between the valve stem position x and the valve constant K_v demands profound knowledge of the valve body's geometry. Taking all these considerations into account, the final model becomes a complex model with many parameters – i.e. too many parameters with respect to the structural identifiability point of view.

Therefore, in order to simplify the model, two assumptions are introduced:

1. $V_0 \gg A_g(x - s - s_{max})$, the volume of the gas is much bigger than volume changes due to the valve stem displacement.

2. $M_s \frac{d^2x}{dt^2} \approx 0$, the dynamic of the valve stem is neglected, which is fair compared to the thermal dynamic of the sensor gas.

and when applied on (7.11), the model for the valve stem is reduced to:

$$\frac{K_g A_g}{V_0} T_g = -k_s(x - x_0) - k_p(x - s - s_0) + \Delta p_v A_v \tag{7.12}$$

It is noted that this simplified valve stem model is only a part of the total thermostatic valve model. From the structural identifiability point of view, this simplified model still contains too many parameters.

A similar modelling approach is described in *(Kariž et al., 1989)*, where the achieved thermostatic valve model is used for simulation with a heater. Also this model contains many parameters.

7.2.3 Macroscopic Model Approach

As described above the microscopic modelling approach of the thermostatic valve gets comprehensive (too ambiguous). Therefore, a macroscopic modelling approach has to be applied. The inspiration for a more simple model is based on the empirical data in Table 7.1, which provides data for the static relation between the relative temperature X_p and the valve constant K_v.

Assuming turbulent flow in the valve body and that hysteresis and elasticity can be neglected, an adequate continuous description of the relation between the relative temperature X_p and the valve constant K_v is suggested as:

$$\mathrm{K}_v(X_p) = \begin{cases} a \tanh(bX_p), & X_p > 0 \\ 0 & \text{otherwise} \end{cases} \tag{7.13}$$

where a and b are two parameters, which characterize a particular thermostatic valve type. It is noted that, if X_p becomes less than zero, K_v is defined to be zero. A negative valve constant does not make sense. It is further noted that the first derivative of (7.13) is discontinuous for $X_p = 0$.

Using the suggested model of the valve constant $\mathrm{K}_v(X_p)$, the hydraulic valve resistance R_v can be expressed as:

$$\mathrm{R}_v(X_p) = \frac{1}{\mathrm{K}_v^2(X_p)} = \frac{1}{(a \tanh(bX_p))^2}, \qquad X_p > 0 \tag{7.14}$$

It is noted that, (7.14) only is valid for $X_p > 0$. For $X_p \leq 0$ there is a problem of numerical nature – also in relation to (7.2), as e.g. when $X_p = 0$ (the valve is closed) Δp_v is equal to the system pressure, the hydraulic valve resistance R_v is infinite and the flow q is zero. In other words, when the valve is closed, it is no longer (7.2) that defines the pressure across the thermostatic valve. It is the conditions in the surrounding hydraulic system. Hence in principle, the model for the pressure across the thermostatic valve has to be exchanged every time the relative temperature X_p passes zero. The problem can be handled in one of two ways:

1. Use discrete event handling, which is a special numerical technique, see *(Enright et al., 1988)*.

2. Avoid the situation of $X_p \leq 0$.

Of course the latter is the easiest solution, it just puts an extra demand to the experimental design. Thus, in the following the relative temperature X_p is assumed positive.

An analysis of (7.13) and (7.14) yields:

$$X_p \to 0_+ \quad \text{implies that} \quad \begin{cases} \mathrm{K}_v \to 0 & \text{and} \quad \frac{d\mathrm{K}_v}{dX_p} \to ab \\ \mathrm{R}_v \to \infty & \text{and} \quad \frac{d\mathrm{R}_v}{dX_p} \to \infty \end{cases} \tag{7.15}$$

$$X_p \to \infty \quad \text{implies that} \quad \begin{cases} \mathrm{K}_v \to a & \text{and} \quad \frac{d\mathrm{K}_v}{dX_p} \to 0 \\ \mathrm{R}_v \to \frac{1}{a^2} & \text{and} \quad \frac{d\mathrm{R}_v}{dX_p} \to 0 \end{cases} \tag{7.16}$$

The characteristic parameters, a and b, of the applied thermostatic valve are estimated by a nonlinear least squares estimation, based on (7.13) and the data in Table 7.1 combined with the requirement, $X_p = 0$ implying $\mathrm{K}_v = 0$. The obtained estimates of a and b together with the standard deviation σ_F of the residuals are presented in Table 7.2.

Table 7.2. *Estimates for the characteristic parameters, a and b, of the applied thermostatic valve.*

Parameter	a	b	σ_F
Estimate	0.85	0.51	$4.23 \cdot 10^{-3}$
Unit	$\mathrm{m^3/h/Bar^{0.5}}$	1/K	$\mathrm{m^3/h/Bar^{0.5}}$

The advantage of (7.13) compared to the modelling approach in Section 7.2.2 is that the relation between the gas temperature T_g and the valve constant has been modelled by a model with only two parameters. What is left to

model, is the relation between the gas temperature T_g and the ambient temperature T_a.

As described in Section 7.2.1, the thermostatic valve contains a time constant and it is influenced by the temperature of the water supply. The influences from the ambient temperature T_a and the water supply temperature T_w on the gas temperature T_g, can – from a thermal point of view – be modelled as:

$$\frac{dT_g}{dt} = \frac{1}{\tau_a}(T_a - T_g) + \frac{1}{\tau_w}(T_w - T_g) \tag{7.17}$$

where the heat transfer dynamics have been lumped into the two time constants τ_a and τ_w, which denote the time constant from the ambient to the gas and from the water to the gas, respectively. The time constant τ_a can be interpreted as the product of the thermal capacity of the gas and the thermal resistance of the cylindric wall of the thermostatic head, while τ_w is the product of the thermal capacity of the gas and the thermal resistance between the gas and the water.

In Section 7.1 the relative temperature X_p was defined as:

$$X_p = T_{set} + 2 - T_a \tag{7.18}$$

based on static conditions. In the dynamic case, the relative temperature X_p should of course be related to the gas temperature as:

$$X_p = T_{set} + 2 - T_g \tag{7.19}$$

A dynamic model of the thermostatic valve based on empirical knowledge has now been established. The model is formulated as follows:

Model Summary 7.1 (Dynamic Model of a Thermostatic Valve)
Flow performance data, supplied by data sheets on thermostatic valves, are

used to calibrate the static nonlinear relation between the valve constant K_v and the relative temperature X_p:

$$\mathrm{K}_v(X_p) = \begin{cases} a\tanh(bX_p), & X_p > 0 \\ 0 & \text{otherwise} \end{cases} \tag{7.20}$$

where the two parameters, a and b, characterize the applied thermostatic valve type. Equation (7.20) implicit includes the three assumptions:

1. *Turbulent flow.*
2. *No hysteresis.*
3. *No elasticity.*

The dynamic model of the gas based thermostatic valve, relating the ambient air temperature T_a to the valve constant K_v, consists of the static nonlinear relation in (7.20) and the following first order differential equation for the temperature T_g of the gas in the thermostatic head:

$$\frac{dT_g}{dt} = \frac{1}{\tau_a}(T_a - T_g) + \frac{1}{\tau_w}(T_w - T_g) \tag{7.21}$$

where T_a denotes the ambient temperature and T_w the temperature of the water supply. The two time constants τ_a and τ_w denote the time constants from the ambient to the gas and from the water supply to the gas, respectively. The relative temperature X_p and the gas temperature T_g are related as in (7.19).

Three remarks on Model Summary 7.1:

R1 The output description of the thermostatic valve model (7.20) is not differentiable for $X_p = 0$, as it was mentioned in (7.13). Referring to

Section 2.7, this implies a violation of the model class implemented in the estimation tool. The violation problem is avoided, if $X_p > 0$ is put as a demand in the experimental design.

R2 The output of the thermostatic valve model is $K_v(X_p)$ is not directly measurable. It has to be generated based on measurements of the pressure across the valve Δp_v and the flow q, i.e. as:

$$\mathrm{K}_v(X_p) \sim \frac{q}{\sqrt{\Delta p_v}} \tag{7.22}$$

R3 Would it be easier to use (7.3) as output description, i.e.:

$$q(X_p) = \mathrm{K}_v(X_p)\sqrt{\Delta p_v} \tag{7.23}$$

where K_v is generated by the model (i.e. (7.20)) and Δp_v is supplied e.g. by measurements?
The answer is no. Looking at the derivative of (7.23) with respect to the relative temperature X_p:

$$\frac{dq(X_p)}{dX_p} = \frac{d\mathrm{K}_v(X_p)}{dX_p}\sqrt{\Delta p_v} + \mathrm{K}_v(X_p)\frac{1}{2\sqrt{\Delta p_v}}\frac{d\Delta p_v}{dX_p} \tag{7.24}$$

it becomes evident that (7.23) cannot be used, since the derivative $\frac{d\Delta p_v}{dX_p}$ is unknown under the given circumstances, implying that a numerical approximation would have to be used. Hence, the output of the thermostatic valve model K_v has to be measurement as in (7.22).

7.2.4 Extended Model View

Applying a wider view, the interaction between the hydraulic system and the dynamic model of the thermostatic valve can be analyzed. An electrical equivalent diagram of the central heating system, presented in Section 4.2, is shown in Figure 7.5. It is assumed that all the hydraulic inductances can be gathered in L_s and all the hydraulic resistances can be gathered in

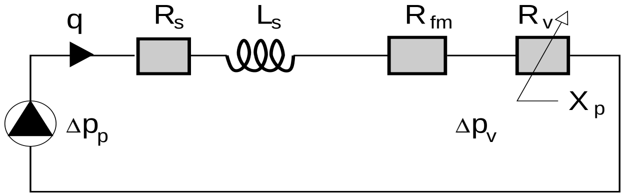

Figure 7.5. *Electric equivalent of the hydraulic components in the central heating system presented in Section 4.2.*

R_s, except the hydraulic resistance of the flow meter R_{fm} and of the valve $\mathrm{R}_v(X_p)$.

Assuming turbulent flow (not only in the thermostatic valve), a model of the hydraulic system in Figure 7.5 can be written as (for $X_p > 0$):

$$L_s \frac{dq}{dt} = \Delta p_p - (R_s + R_{fm} + \mathrm{R}_v(X_p))\, q^2 \tag{7.25}$$

Comparing the expected time constant of (7.25) with the expected time constants of (7.21) (i.e. hydraulic dynamic versus thermal), the latter is dominating and as Δp_p usually is kept constant, it seems reasonable to assume a static relation between Δp_p and q. The small diameter in the flow meter implies that $R_{fm} \gg R_s$. Thus (7.25) is reduced to:

$$q(X_p) = \frac{\sqrt{\Delta p_p}}{\sqrt{R_{fm} + \mathrm{R}_v(X_p)}} = \frac{\mathrm{K}_v(X_p)}{\sqrt{R_{fm}\mathrm{K}_v^2(X_p) + 1}} \sqrt{\Delta p_p} \tag{7.26}$$

and it follows:

$$\frac{dq(X_p)}{dX_p} = \frac{ab(1 - \tanh^2(bX_p))}{(R_{fm}a^2 \tanh^2(bX_p) + 1)^{3/2}} \sqrt{\Delta p_p} \tag{7.27}$$

Based on this "wider view", it has become possible to express the derivative $\frac{dq}{dX_p}$, see (7.24), by known quantities. An expression for the pressure across

the thermostatic valve can also be derived from Figure 7.5 using the same simplification as above:

$$\Delta p_v(X_p) = \frac{\mathrm{R}_v(X_p)}{R_{fm} + \mathrm{R}_v(X_p)} \Delta p_p = \frac{1}{R_{fm}\mathrm{K}_v^2(X_p) + 1} \Delta p_p \tag{7.28}$$

This model for the pressure across the thermostatic valve does not have "the problem" encountered for (7.2) – referring to the discussion in connection with (7.14) – as the case of $X_p = 0$ implies that $\Delta p_v = \Delta p_p$, as it should be.

An analysis of (7.26) and (7.28) (equivalent to page 174) shows:

$$X_p \to 0_+ \quad \text{implies} \quad \begin{cases} q \to 0 & \text{and} \quad \frac{dq}{dX_p} \to ab\sqrt{\Delta p_p} \\ \Delta p_v \to \Delta p_p & \text{and} \quad \frac{d\Delta p_v}{dX_p} \to 0 \end{cases} \tag{7.29}$$

$$X_p \to \infty \quad \text{implies} \quad \begin{cases} q \to \sqrt{\frac{a^2}{R_{fm}a^2+1}}\sqrt{\Delta p_p} & \text{and} \quad \frac{dq}{dX_p} \to 0 \\ \Delta p_v \to \frac{1}{R_{fm}a^2+1}\sqrt{\Delta p_p} & \text{and} \quad \frac{d\Delta p_v}{dX_p} \to 0 \end{cases} \tag{7.30}$$

that (7.28) is differentiable for $X_p = 0$, while (7.26) is not.

The "extended" thermostatic valve models, (7.26) and (7.28), are useful in the assessment of the influence/dominance of the thermostatic valve on the hydraulic system. In Figure 7.6, the flow in (7.26) and valve pressure in (7.28) are sketched as function of X_p for four different values of R_{fm}:

1. $R_{fm} = 0.1/a^2$ indicated by '···'.
2. $R_{fm} = 1/a^2$ indicated by '—'.
3. $R_{fm} = 10/a^2$ indicated by '– –'.
4. $R_{fm} = 100/a^2$ indicated by '–·'.

based on the parameter estimates for a and b in Table 7.2 and the pump pressure Δp_p set to 4 mWc.

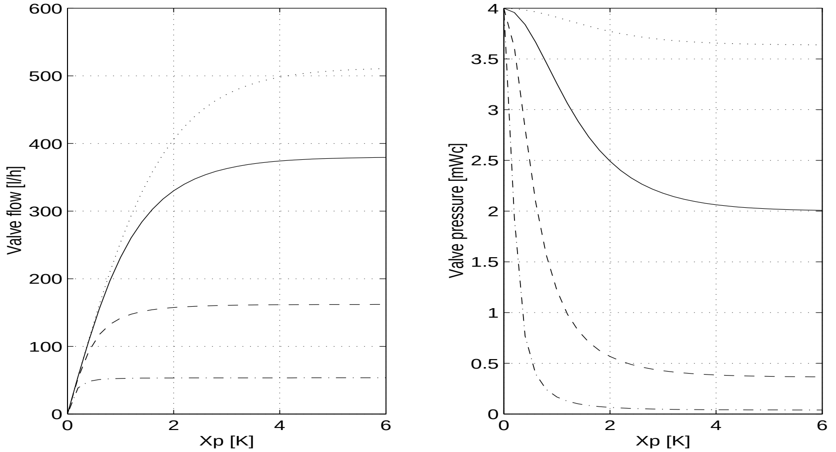

Figure 7.6. *The valve flow q and the valve pressure across the valve Δp_v as function of the relative temperature X_p, for the following four values of* $R_{fm} \in [0.1, 1.0, 10, 100]/a^2$ Bar h^2/m^6.

In Figure 7.6, it is observed that R_{fm} has a considerable influence on the control property of the thermostatic valve. As a measure for the linearity of the thermostatic valve control, the following definition is introduced:

Definition 7.1 (P-band Temperature) *Let the P-band temperature for thermostatic valve control of the flow be defined as the temperature interval of the relative temperature X_p, for which the relative temperature X_p and the valve flow q can be considered proportional. A level of 10 % is accepted as the maximal deviation from proportionality.*

This definition of P-band temperature for thermostatic valve control of the flow is motivated by the final paragraph in Section 7.1.1.

In the definition of the P-band temperature, a maximal deviation of 10 % from proportionality is suggested as an acceptable deviation level. Using this measure for the of the P-band temperature, it follows that:

$$\frac{ab\sqrt{\Delta p_p}\, X_p - q(X_p)}{ab\sqrt{\Delta p_p}\, X_p} \leq 0.1 \tag{7.31}$$

where the largest value of the relative temperature X_p satisfying the inequality is equal to the P-band temperature (alias the width). A graphical evaluation of (7.31) in the case of (7.26) is shown in Figure 7.7, where the nomenclature corresponds to the one used in Figure 7.6. For example in the case of $R_{fm} = 0.1/a^2$, the P-band temperature is approximately 1.05 K. Inserting (7.26) into (7.31), it can be observed that the P-band temperature is independent of the actual pump pressure Δp_p, while the influence of R_{fm} is considerable.

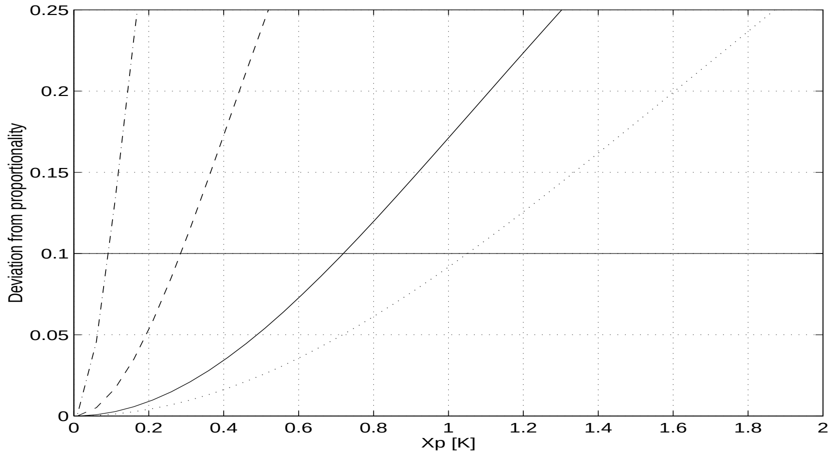

Figure 7.7. *Graphical evaluation of (7.31), where the intersection with 10 % deviation level defines the P-band temperature of thermostatic valve control.*

Figure 7.6 illustrates the importance of using the "prober" size of thermostatic valve from a hydraulic point of view. A too dominating thermostatic valve (alias $1/a^2 \gg R_{fm}$) yields a relative large flow control range and a big pressure loss in the thermostatic valve at all temperatures. If the nominal flow of the radiator is small compared to the maximal valve flow, this would probably lead to on/off control. Meanwhile, a dominating hydraulic system (alias $1/a^2 \ll R_{fm}$) yields a relative small flow and a relative small pressure loss in the thermostatic valve (as long as it is open). If the nominal radiator flow is equal to the maximal valve flow, the room heating will seem slow. Moreover, there is risk of insufficient heat supply.

As described in Section 7.1.4 the valve authority concept is used to assess the the control property of the thermostatic valve. Thus, using (7.5) on the simplified system in Figure 7.5, it follows:

$$K_{vl} = \frac{q_0}{\sqrt{\Delta \mathrm{p}_v(X_p)}} = \frac{q_0}{\sqrt{\Delta p_p}}\sqrt{R_{fm}a^2\tanh^2(bX_p)+1} \tag{7.32}$$

and from the valve authority (7.4) and the lower valve authority limit of 0.3, it further follows:

$$\frac{K_{vl}}{K_{vs}} = \frac{q_0}{\sqrt{\Delta p_p}}\frac{\sqrt{R_{fm}a^2\tanh^2(bX_{p0})+1}}{a} > 0.3 \tag{7.33}$$

where X_{p0} denotes the a design temperature between 1 K and 3 K. This inequality can be used either as an assessment tool or as a design tool for the system in Figure 7.5.

The interaction between the thermostatic valve and the hydraulic system has been studied above. Thus, an extended thermostatic valve model can be formulated as:

Model Summary 7.2 (Extended Thermostatic Valve Model)
Referring to the dynamic model of the thermostatic valve in Model Summary 7.1 and to the to heat system defined in Figure 7.8, where Δp_s denotes the branch pressure, q the branch flow and R_s the total hydraulic resistance of the branch, excluding the hydraulic resistance of the thermostatic valve R_v.

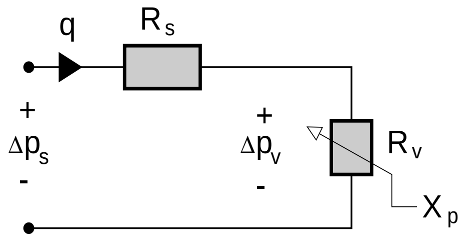

Figure 7.8. Electric equivalent of a branch in a central heating system, where R_v denotes the hydraulic resistance of the thermostatic valve and R_s the hydraulic resistance of the rest.

Assume the branch pressure Δp_s is known and that the relation between the branch pressure Δp_s and the branch flow q is static. The model for the branch flow q can then be written as:

$$q(X_p) = \frac{K_v(X_p)}{\sqrt{R_s K_v^2(X_p)+1}}\sqrt{\Delta p_s} \tag{7.34}$$

and the pressure Δp_v across the thermostatic valve as:

$$\Delta p_v(X_p) = \frac{1}{R_s K_v^2(X_p)+1}\Delta p_s \tag{7.35}$$

where K_v denotes the valve constant and X_p the relative temperature, as described in Model Summary 7.1.

Two remarks on Model Summary 7.2:

R1 During the analysis, the hydraulic dynamic between the branch pressure and the branch flow was neglected, since the time constant of the thermostatic valve under normal conditions will be dominating. Due to this assumption, all the constant hydraulic resistances can be gathered in R_s.

R2 The first derivative of the model for the branch flow q in (7.34) is discontinuous for $X_p = 0$, as the model for the valve constant (7.20) is discontinuous for $X_p = 0$. Thus, when this flow model is used for estimation, $X_p > 0$ will still be a demand in the experimental design.

The basic idea of Model Summary 7.2 is to describe the interaction between the hydraulic system and the thermostatic valve. Due to the dynamic model for the thermostatic valve it is now possible to analyze how an ambient temperature influences the hydraulic conditions in the central heating system.

7.3 Experiments

An experimental setup of the thermostatic valve is described below. The idea is now to perform a series of experiments in order to estimate the time constants τ_a and τ_w, the set point temperature T_{set} and the two characteristic parameters a and b of the considered thermostatic valve and also R_s in the extended model.

7.3.1 Experimental Setup

The basic idea of the experiment on the thermostatic valve is to manipulate the air temperature T_a around the thermostatic head. In order to perform experiment on the thermostatic valve in a "normal" environment, a slight extended version of the experimental setup described in Section 4.2 is used. The extension consists of a heat blower arrangement, see Figure 7.9. While the heat blower continuously blows air up towards the thermostatic valve, the heating element of the heat blower is on/off controlled by the data

acquisition system, as sketched in Figure 7.9. In this way, the ambient air temperature T_a is manipulated.

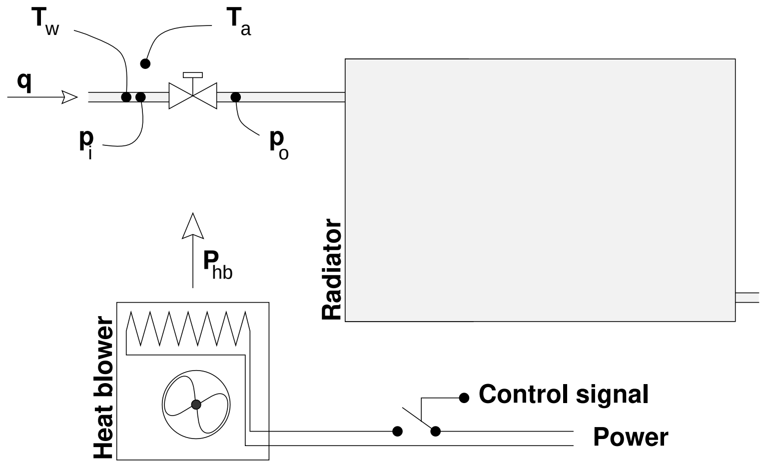

Figure 7.9. *Sketch of the experimental thermostatic valve setup. The thermostatic valve is manipulated through on/off control of the heat blower heat element.*

The power of the heat element is 500 W (the smallest possible power of this heat blower). The measured signals are: p_i, p_o, T_w, T_a and q, see Figure 7.9, and they follow the outlines of Section 4.2, as they are identical to p_{vj}, p_{rj}, T_{ij}, T_{aj} and q_j in Figure 4.5, respectively. Moreover the pump pressures p_1 and p_2 are measured as in Figure 4.3, while the pressure across the thermostatic valve is generated as $\Delta p_v = p_i - p_o$. Both Δp_p and Δp_v represent dynamic pressures (the static pressures are removed).

7.3.2 Input Design

Much of the analysis on the thermostatic valve has all ready been presented in the previous section. Thus, the analysis presented in this section is focused on extracting informations, that are of interest in the input design with respect to PRBS signals.

The input signals of the thermostatic valve model in Model Summary 7.1 consist of the ambient air temperature T_a and the water temperature T_w, as sketched in Figure 7.9, while the output is measured as the flow divided by the square root of the pressure across the thermostatic valve. Looking at Model Summary 7.2, it is clear that also the branch Δp_s (system pressure) is input to the model.

If the branch pressure (alias the pressure of the circulating pump) is kept constant, all the variation in q is due to the variation in the valve constant K_v, as it can be observed in (7.34). Hence, a constant circulating pump pressure is a good design. As mentioned in Section 6.4.2, the water temperature T_w (alias water supply temperature T_i) does not support good excitation properties, as input signal to the radiator model. Neither is it the case for the thermostatic valve model. Therefore, the water supply temperature is designed to be 30 °C. This design has three advantages:

1. The water supply temperature T_w is approximately 5 degrees higher than the expected mean value of the gas temperature T_g. When the thermostatic valve is heated by the air stream from the heat blower, see Figure 7.9, interactions with the water temperature is almost avoided, as the water temperature T_w is higher than the mean temperature of the air stream T_a.

2. The water supply temperature is relative close to the mean value of the gas temperature, hence the influence of the water supply temperature T_w on the gas temperature T_g can be neglected. This implies that thermal model (7.21) is reduced to:

$$\frac{dT_g}{dt} = \frac{1}{\tau_a}(T_a - T_g) \tag{7.36}$$

Hence, if any significant influence from the water temperature exists, it will be small and constant (not correlated with the air stream temperature).

3. The control loop of the thermostatic valve, sketched in Figure 7.3, is changed to an open loop system, since the radiator power is very small due to the low water supply temperature T_w.

The disadvantage of this design is that the time constant τ_w from the water supply temperature to the gas temperature cannot be estimated. Nevertheless, a lower bound for this time constant can be derived from (7.21). The requirement to the thermostatic valve is, that a temperature jump in the water temperature of $\Delta T_w = 30$ K may not influence the gas temperature by more than $\Delta T_g \leq 1.5$ K. Thus, using (7.21), this requirement can be expressed as:

$$\begin{aligned} \tfrac{1}{\tau_a}(T_a - T_{g1}) + \tfrac{1}{\tau_w}(T_{w1} - T_{g1}) &= 0 \\ \tfrac{1}{\tau_a}(T_a - T_{g2}) + \tfrac{1}{\tau_w}(T_{w2} - T_{g2}) &= 0 \end{aligned} \tag{7.37}$$

where indices 1 and 2 refer to before and after the jump in the water supply temperature, respectively. From (7.37) it follows:

$$T_{g2} - T_{g1} \geq \frac{\tau_a}{\tau_a + \tau_w}(T_{w2} - T_{w1}) \quad \Rightarrow \quad \tau_w \geq \left(\frac{30}{1.5} - 1\right)\tau_a \tag{7.38}$$

Based on (7.21) and (7.38), it is concluded that τ_w must be at least 19 times larger than τ_a in order to fulfill the requirement for the thermostatic valve.

The remaining input signal, which will be designed now, is the air temperature T_a. *(Svensson, 1978)* reports time constants from 13 minutes up to 60 minutes, while the requirement in *(Dansk Standard, 1988)* defines 40 minutes as the upper bound for the response time. From these considerations, two input sequences have been designed based on PRBS signals:

S1: The length of the shift register is chosen as $n_{s1} = 3$ and the fundamental time period as $T_{s1} = 50$ seconds.

S2: The length of the shift register is chosen as as $n_{s2} = 5$ and the fundamental time period as $T_{s2} = 20$ seconds.

The fundamental time periods of S1 and S2 might seem short compared to the expected time constant. They form a "controllable" (but not optimal) compromise between the 500 W heat input and the demand of $X_p > 0$ (i.e. the valve is open all the time). During the experiment, the heat input from the heat blower has to be supervised in order to assure $X_p > 0$, which becomes quite a task (for the considered experimental setup) – if the fundamental time periods are increased more than suggested above.

7.3.3 Measurement Data

The two sets of measurement data $\mathcal{D}_{S1}$ and $\mathcal{D}_{S2}$, presented in Figure 7.10 and 7.11, are based on the input design, described above. The sample time is 10 seconds and the set point temperature T_{set} is set to mark "4".

The measurement data $\mathcal{D}_{S1}$ shown in Figure 7.10 are performed with design S1. The first subplot contains the ambient temperature T_a and the water supply temperature T_w (indicated by "$-\cdot$"). The second subplot contains the pressure across the thermostatic valve Δp_v and the pressure over the circulating pump Δp_p (indicated by "$-\cdot$"), while the flow q is shown in the third subplot. The valve constant K_v, measured as (7.22), is plotted in the fourth subplot. The input design S1 is clearly identified in the ambient temperature T_a. The increasing trend in the mean value of T_a is due

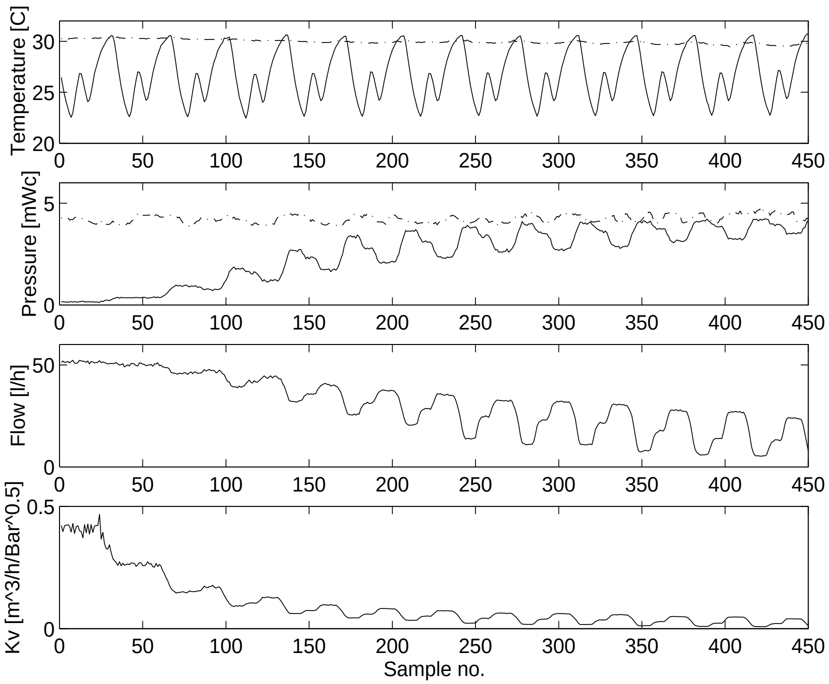

Figure 7.10. *$\mathcal{D}_{S1}$: Measurement data based on input sequence S1.*

to the 500 W heat blower power, which increases the temperature in the room. Thus, the input signal T_a contains both a high and a low frequency excitation.

The measurement data $\mathcal{D}_{S2}$ shown in Figure 7.11 follow the outlines of Figure 7.10. The input design S2 can by identified in the ambient temperature T_a, together with a slow variation in the mean value of T_a. The increasing part of the mean value of T_a is due to the 500 W heat blower power, while its decreasing part is due to a mild ventilation of the room. Hence, also this time, T_a contains a high and low frequency excitation.

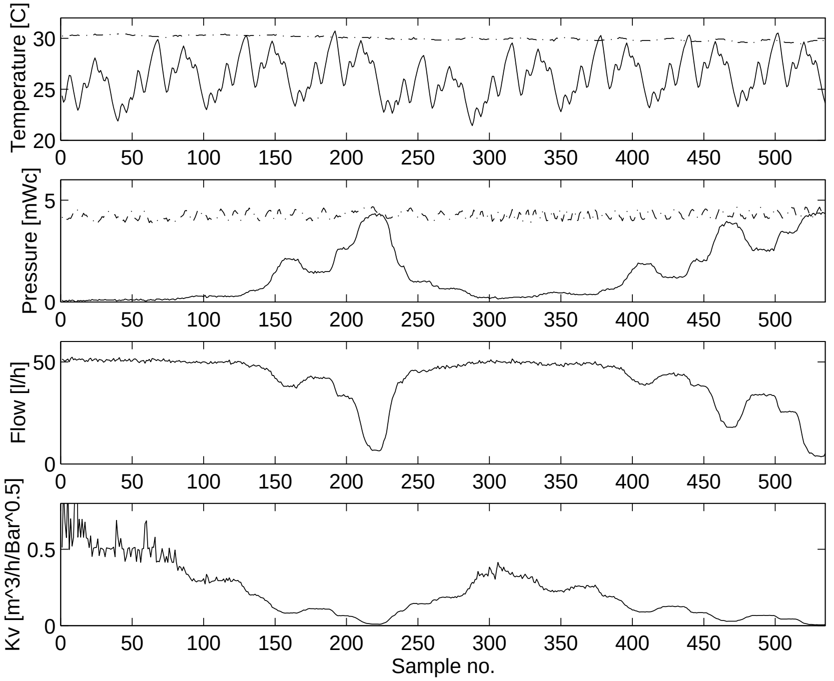

Figure 7.11. $\mathcal{D}_{S2}$: *Measurement data based on input sequence S2.*

Common for the two sets of measurement data is that the ambient temperature T_a is lower than the set point temperature T_{set} at the beginning of the experiments. This fact can be observed as the low pressure across the thermostatic valve. The pressure is close to zero, hence the valve is almost full open, an aspect which implies that the hydraulic resistance R_s of the flow meter, pipes etc. is dominating the hydraulic resistance of the thermostatic valve R_v. Using (7.34) in the case when the thermostatic valve is full open, the hydraulic resistance can be computed as:

$$R_s = \frac{\Delta p_s}{q^2} - \frac{1}{a^2} = \frac{0.42}{0.05^2} - \frac{1}{0.85^2} \approx 167 \, \frac{\text{Bar}}{\text{m}^6/\text{h}^2} \tag{7.39}$$

The resistance has a big value, which mainly is due to the flow meter. Thus, the actual flow control in the experimental setup is approximately equal to the flow indicated by "$-\cdot$" in Figure 7.6. As the nominal flow of the radiator is 17 l/h, the thermostatic valve can supply the radiator with a sufficient flow. Meanwhile, a thermostatic valve with a smaller flow capacity would have been preferable for these thermostatic valve experiments, as the smaller flow capacity implies a more dominating thermostatic valve. This would imply more information about the thermostatic valve in the measurement data.

7.4 Estimation of Grey Box Models

In Section 7.3, two sets of measurements have been presented and analyzed. These data will now be used to estimate the parameters of the thermostatic valve models described in Model Summary 7.1 and Model Summary 7.2. As a result of the input design, the influence from the water supply temperature T_w is neglected. Moreover, this implies a reduction in the thermal part of the thermostatic valve model, i.e. (7.21) is reduced to (7.36).

7.4.1 Identifiability

As in the previous chapters, the identifiability of the proposed model should be investigated. It is noted that in relation with the identifiability of the thermostatic valve model, the simplification in (7.36) is not important.

The model in Model Summary 7.1 of the thermostatic valve contains five parameters: τ_a, τ_w, a, b and T_{set}, together with two inputs and one output. As shown in Appendix B.2, the characteristic thermostatic valve parameter a and b are not structural identifiable. Therefore only 4 parameters can be estimated.

The model in Model Summary 7.2 contains six parameters: τ_a, τ_w, a, b, T_{set} and R_s, together with three inputs and one output. For this model five parameters are structural identifiable as described in Appendix B.2. Again, parameter a and b are structural unidentifiable.

Estimation results support the identifiability considerations presented in Appendix B.2, as a and b are getting correlated with correlation 1. As a consequence the characteristic parameter a must be kept constant during the estimation in the thermostatic valve model.

7.4.2 The Thermostatic Valve Model

Due to the input design, the thermostatic valve model in Model Summary 7.1 is simplified as described in (7.36). Hence, a Grey Box model of the remaining thermostatic valve can be expressed as:

$$dT_g(t) = \frac{1}{\tau_a}\left(T_a(t) - T_g(t)\right) dt + dW(t) \tag{7.40}$$

$$X_p(t) = T_{set} + 2 - T_g(t) \tag{7.41}$$

$$y(k) = a \tanh(bX_p(k)) + e(k) \tag{7.42}$$

where the system noise W is assumed to be a Wiener process with zero mean and incremental variance σ_W^2, y denotes the "measured" valve constant (see R2 of Model Summary 7.1) and e denotes the measurement noise, which is assumed to be white noise with zero mean and variance σ_e^2. Furthermore, W and e are assumed to be mutually uncorrelated.

The assumption of white noise for the measurement noise in (7.42) can be discussed, as the measurement of the valve constant is generated by (7.22), i.e. by two virtual measured signals with presumable zero means and some given variances. For large values of the valve constant the noise is bigger than for small values, which can be observed in Figure 7.10 and Figure 7.11. Nevertheless, for simplicity the resulting distribution of (7.22) is approximated as white noise with zero mean and variance σ_e^2.

Table 7.3. *Estimated model parameters and model performance parameters for* $a = 0.85\ \mathrm{m^3/h/Bar^{0.5}}$.

Measurement data		$\mathcal{D}_{S1}$		$\mathcal{D}_{S2}$	
Parameter	Unit	Est.	Std.	Est.	Std.
τ_a	sec.	614	16.8	729	71.7
b	10^{-3}/K	103	6.88	185	11.7
T_{set}	°C	25.1	0.040	24.9	0.230
$T_g(0)$	°C	21.7	0.363	21.5	0.315
σ_W^2	10^{-3}(°C/sec.)^2	6.35	3.51	198	0.701
σ_e^2	10^{-6}(°C)^2	100	0.971	600	95.4
$-\log\mathcal{L}$		-241		-191	
Mean(Pred.Error)		$2.50{\cdot}10^{-4}$		$2.52{\cdot}10^{-3}$	
Var(Pred.Error)		$1.00{\cdot}10^{-4}$		$6.00{\cdot}10^{-4}$	

The estimated parameters of the Grey Box model and the model performance parameters are presented in Table 7.3. It can be observed, that the time constant τ_a is in the range of 10-12 minutes, i.e. a little bit smaller than that reported in *(Svensson, 1978)*. The characteristic thermostatic valve parameter b is estimated to a set of values, 3 to 5 times smaller than the expected b-value, refer to Table 7.2. The estimates for the set point temperature T_{set} are approximately 2 degrees higher, than expected with the temperature selector in step "4", alias 23 °C. $\mathcal{D}_{S1}$ and $\mathcal{D}_{S2}$ contain 450 and 535 samples, respectively. Comparing the likelihood value per sample and the prediction error for both set of data, it is observed that the model performs best on $\mathcal{D}_{S1}$.

Statistical tests for $\mathcal{D}_{S1}$ are presented in Figure 7.12. The autocorrelation is significant at lag 6 and 12. The same pattern is observed in the cross-correlation for lag 0, 6 and 12. Looking at the cumulated periodogram, an explanation for this lag pattern is found. The grouping of data in levels is due to the small value of the fundamental time period of S1. As mentioned in Section 7.3.2, the selected fundamental time period T_{s1} forms a compromise rather than the fundamental time period of the optimal PRBS signal. The fundamental time periods were deliberately selected too small as stressed in 7.3.2.

In Figure 7.13, the model performance of $\mathcal{D}_{S1}$ is plotted. The first subplot contains measured and predicted valve constant, while the second subplot provides the prediction error for $\mathcal{D}_{S1}$. The third subplot shows the measured valve constant versus the simulated valve constant. The prediction of the valve constant is more influenced by the ambient air temperature than the measured valve constant. The oscillation in the prediction error is clearly correlated with the ambient air temperature. This difference between model output and measurement could be due to the hysteresis in the thermostatic valve.

Corresponding to $\mathcal{D}_{S1}$, statistical tests and model performance for $\mathcal{D}_{S2}$ are presented in Figure 7.14 and Figure 7.15, respectively. All the estimated autocorrelations and crosscorrelations are included in the 99 % significance interval, see Figure 7.14. Thus, the thermostatic valve model provides a sufficient description of $\mathcal{D}_{S2}$. Also the model performance in Figure 7.15 yields a good impression. The large prediction errors in the beginning of $\mathcal{D}_{S2}$ is related with measurement noise rather than model mismatch. A little deviation between the measurement data and the simulation of the valve constant can be observed.

The estimated behaviour (the Kalman state) of the gas temperature in the thermostatic head is plotted together with the ambient temperature in Figure 7.16 and Figure 7.17, respectively for the two data sets. It can be observed that the gas temperature forms a nice low-passed version of the ambient temperature.

7.4.3 Extended Model

Due to the input design, the thermostatic valve model combined with the hydraulic system, as described in Model Summary 7.2, is also simplified

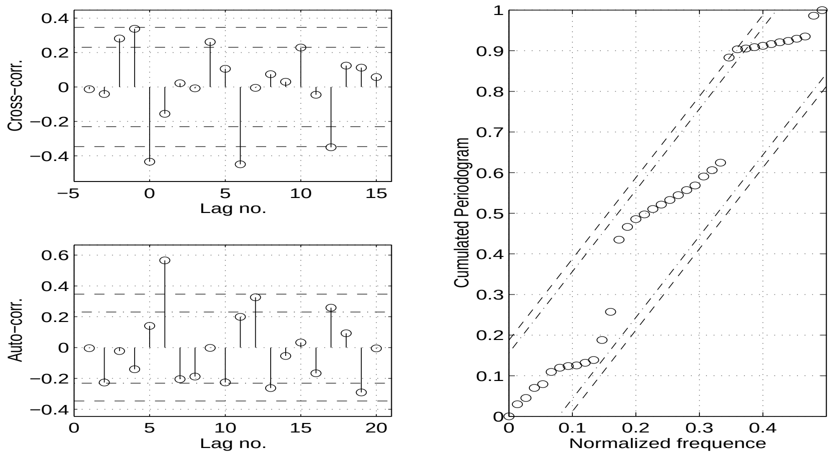

Figure 7.12. *$\mathcal{D}_{S1}$: Statistical tests for the prediction error on the valve constant K_v, showing the autocorrelation, cumulated periodogram and the crosscorrelations between T_a and the prediction error.*

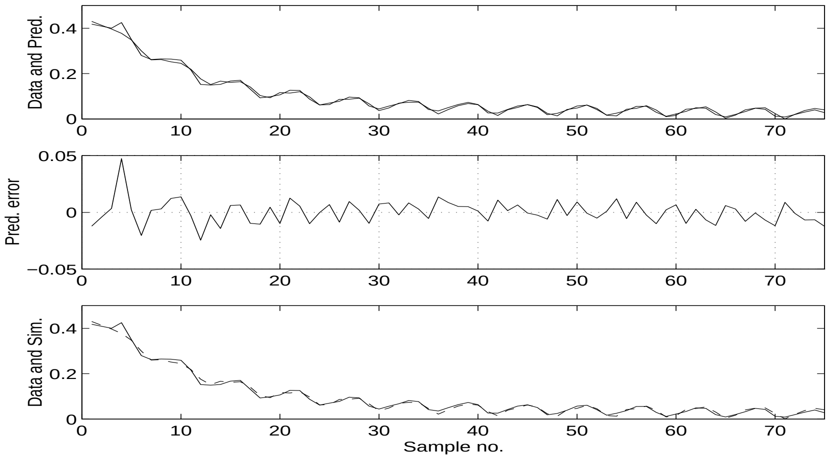

Figure 7.13. *$\mathcal{D}_{S1}$: Model performance for the thermostatic valve model (Sample time: one minute).*

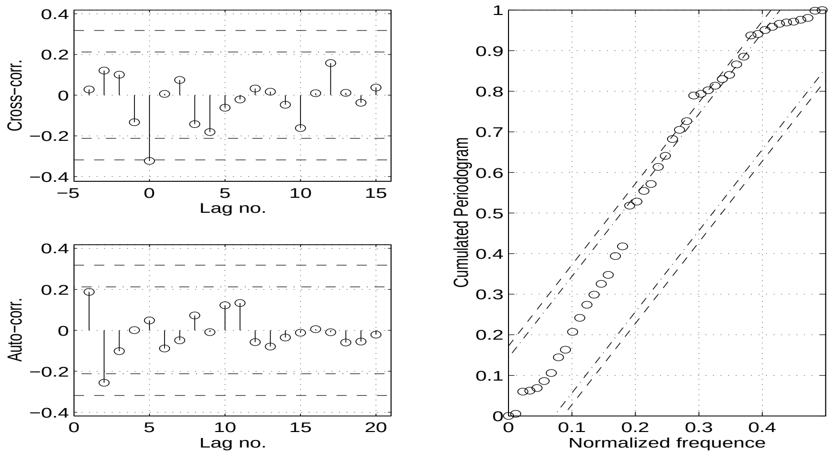

Figure 7.14. *$\mathcal{D}_{S2}$: Statistical tests for the prediction error on the valve constant K_v, showing the autocorrelation, cumulated periodogram and the crosscorrelations between T_a and the prediction error.*

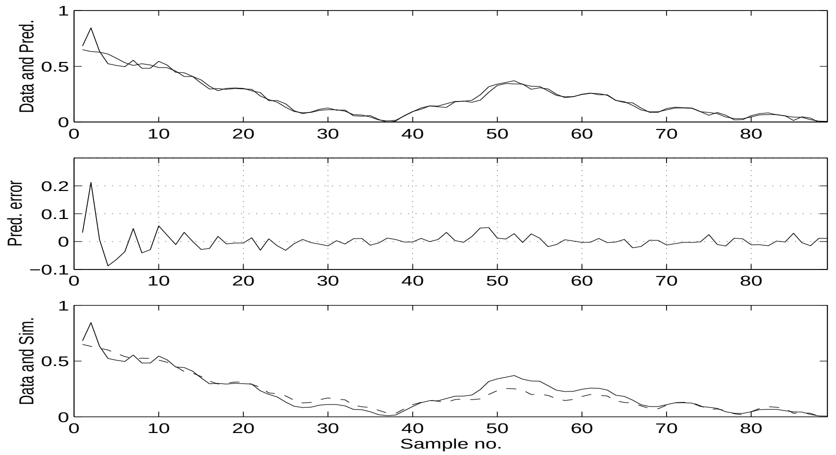

Figure 7.15. *$\mathcal{D}_{S2}$: Model performance for the thermostatic valve model (Sample time: one minute).*

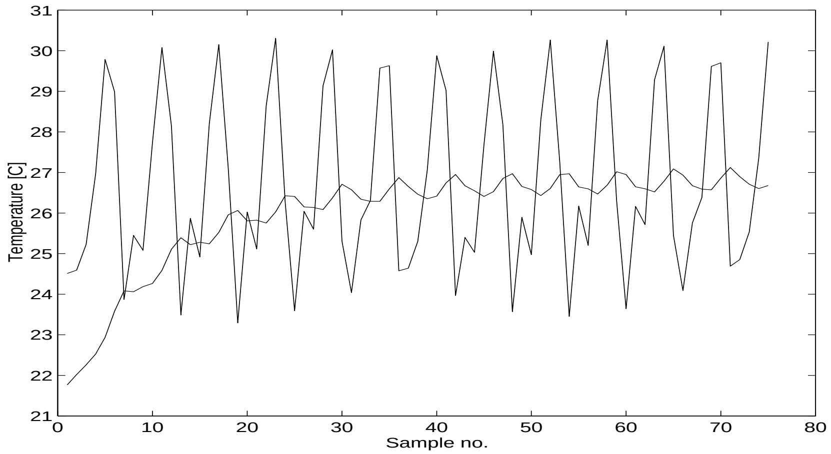

Figure 7.16. *$\mathcal{D}_{S1}$: Ambient air temperature T_a and estimated gas temperature T_g for the thermostatic valve model (Sample time: one minute).*

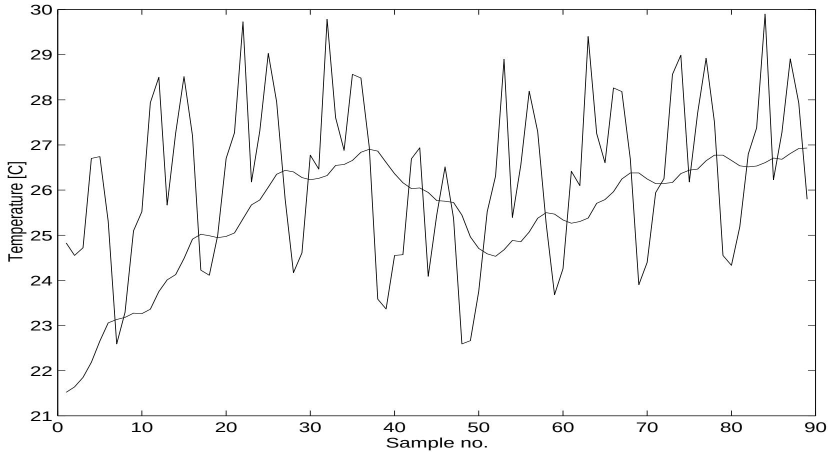

Figure 7.17. *$\mathcal{D}_{S2}$: Ambient air temperature T_a and estimated gas temperature T_g for the thermostatic valve model (Sample time: one minute).*

as in (7.36). Thus the Grey Box model of the remaining model can be expressed as:

$$dT_g(t) = \frac{1}{\tau_a}\left(T_a(t) - T_g(t)\right)dt + dW(t) \tag{7.43}$$

$$X_p(t) = T_{set} + 2 - T_g(t) \tag{7.44}$$

$$y(k) = \frac{a\tanh(bX_p(t))}{\sqrt{R_s a^2 \tanh^2(bX_p(t)) + 1}}\sqrt{\Delta p_s(k)} + e(k) \tag{7.45}$$

where the system noise W is assumed to be a Wiener process with zero mean and incremental variance σ_W^2, y denotes the measured flow, while e represents the measurement noise, which is assumed to be white noise with zero mean and variance σ_e^2. As usual, W and e are assumed to be mutually uncorrelated. It is noted that the white noise assumption on the measurement noise is more reasonable for (7.45) than for (7.42).

The estimated parameters and the model performance parameters for the extended thermostatic valve model are presented in Table 7.4. It can be observed that the estimates for the time constant τ_a are in the range of 15-16 minutes, i.e. a couple of minutes larger compared to the estimates in Table 7.3. The estimates for parameter b and for the set point temperature T_{set} are approximately the same as in Table 7.3. The estimates for the initial gas temperature are bigger compared to the estimates in Table 7.3, a fact which is due to the larger time constant. The estimates of the hydraulic resistance of the system R_s are almost identical. Comparing the estimates of R_s with the calculated value in (7.39), the calculated value is larger. Meanwhile, for the calculation of (7.39), the thermostatic valve was assumed to be full open. Thus, the estimates of R_s in Table 7.4 constitute more realistic estimates than (7.39) does. Looking at the model performance parameters for the extended model, it can be observed that this model performs better on $\mathcal{D}_{S2}$, with respect both to the likelihood value per sample and to the variance of the prediction error.

Table 7.4. *Estimated model parameters and model performance parameters for* a = 0.85 m^3/h/Bar$^{0.5}$.

Measurement data		$\mathcal{D}_{S1}$		$\mathcal{D}_{S2}$	
Parameter	Unit	Est.	Std.	Est.	Std.
τ_a	sec.	963	25.6	923	12.3
b	10^{-3}/K	121	6.32	186	6.10
R_s	Bar/(m^3/h)^2	131	3.77	137	1.36
T_{set}	°C	25.0	0.0196	24.9	0.0136
$T_g(0)$	°C	24.8	0.112	25.5	0.0645
σ_W^2	10^{-6}(°C/sec.)^2	34.8	14.5	27.8	4.31
σ_e^2	(l/h)^2	6.44	1.01	5.73	1.00
$-\log\mathcal{L}$		176		205	
Mean(Pred.Error)		$2.44\cdot10^{-2}$		$2.44\cdot10^{-3}$	
Var(Pred.Error)		6.44		5.73	

Statistical tests for $\mathcal{D}_{S1}$ are presented in Figure 7.18. The autocorrelation and the crosscorrelation with respect to the ambient temperature T_a have a lag pattern equivalent to the pattern in Figure 7.12. Hence, the extended model has a performance equivalent to non extended model.

Looking at the model performance in Figure 7.19, it can be observed that the variance of the prediction error is increasing, when the flow is decreasing. This could be an effect of the hysteresis in the thermostatic valve, as it was also mentioned in connection with Figure 7.13.

The statistical tests for $\mathcal{D}_{S2}$ are presented in Figure 7.20. It can be observed that a couple of lags are significant in the autocorrelation and crosscorrelation plots. Furthermore, the cumulated periodogram indicates that the high frequency part of the prediction error is not described as well as the rest. This can also be observed in the model performance plot in Figure 7.21. It is noted that the variance of the prediction error increases when the flow

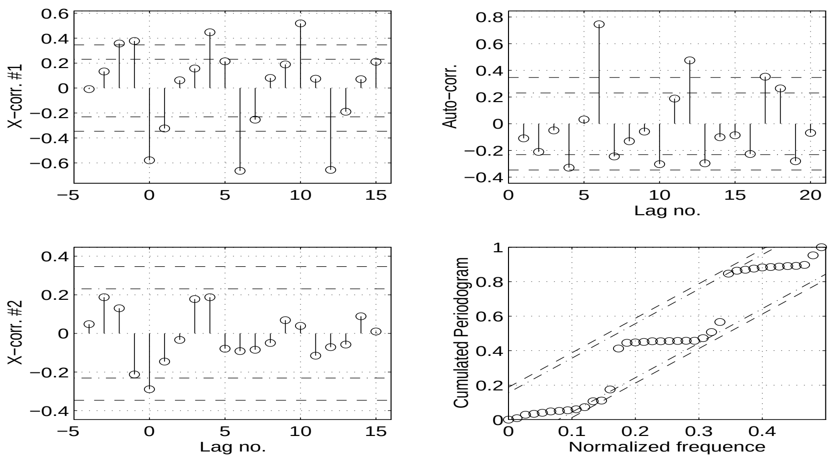

Figure 7.18. *$\mathcal{D}_{S1}$: Statistical tests for the prediction error on the valve q, showing the autocorrelation, cumulated periodogram and the crosscorrelations between $\#1 : T_a$, $\#2 : \Delta p_s$ and the prediction error.*

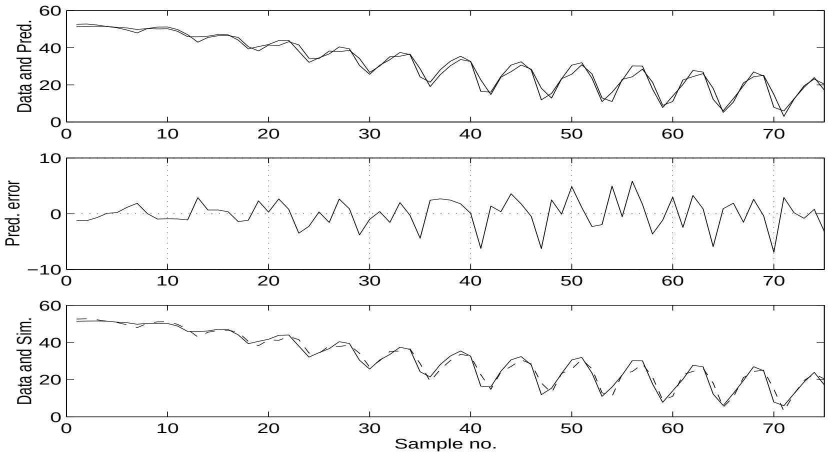

Figure 7.19. *$\mathcal{D}_{S1}$: Model performance for the thermostatic valve model with extension (Sample time: one minute).*

decreases. On the other hand, the simulation of the flow is quite good, which is also the case in Figure 7.19.

The estimated behaviour (the Kalman state) of the gas temperature in the thermostatic head for the extended model is illustrated in Figure 7.22 and Figure 7.23, respectively for the two data sets. Neither this time, does the gas temperature performance conflict with a physical expectation.

7.4.4 Cross Validation

Until now the estimates related to the two data sets have been assessed by simple comparison. A more systematic comparison can be performed by a cross validation.

In this section only the prediction error is used in the cross validation. The basic idea is to use the estimates e.g. of $\mathcal{D}_{S1}$ in a simulation with $\mathcal{D}_{S2}$. The initial value of the gas temperature depends on the actual set of estimates. This implies that an appropriate value for the initial gas temperature has to be calculated before the simulation is performed. In case of the thermostatic valve model, the initial gas temperature is estimated as:

$$\widehat{T}_g(0) = \widehat{T}_{set} + 2 - \frac{1}{\widehat{b}} \operatorname{arctanh}\Big(\frac{1}{\widehat{a}} K_v(0)\Big) \tag{7.46}$$

where the parameters with the hat symbol denote estimates, while $K_v(0)$ is the initial valve constant from the validation data. Corresponding in case of the extended model, the initial gas temperature is estimated as:

$$\widehat{T}_g(0) = \widehat{T}_{set} + 2 - \frac{1}{\widehat{b}} \operatorname{arctanh}\left(\frac{1}{\widehat{a}} \frac{\frac{q(0)}{\sqrt{\Delta p_s(0)}}}{\sqrt{1 - \frac{q^2(0)}{\Delta p_s(0)} \widehat{R}_s}} \right) \tag{7.47}$$

The results of the cross validation are shown in Table 7.5, where all the presented variances are computed as *empirical* variances.

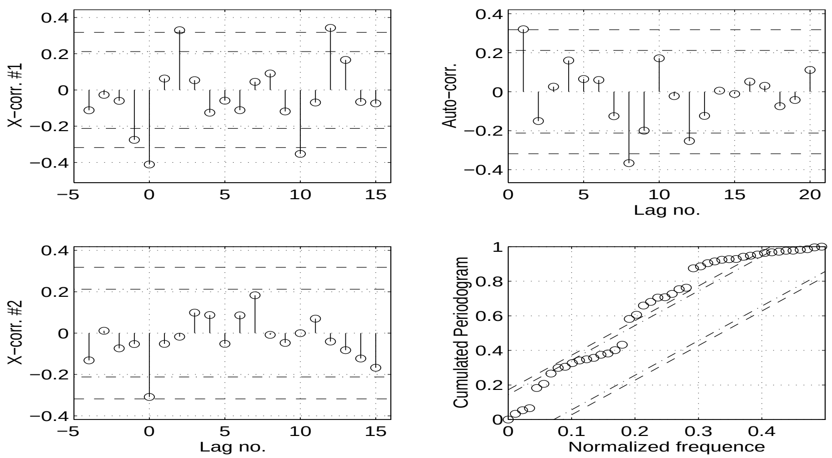

Figure 7.20. *$\mathcal{D}_{S2}$: Statistical tests for the prediction error on the valve q, showing the autocorrelation, cumulated periodogram and the crosscorrelations between $\#1 : T_a$, $\#2 : \Delta p_s$ and the prediction error.*

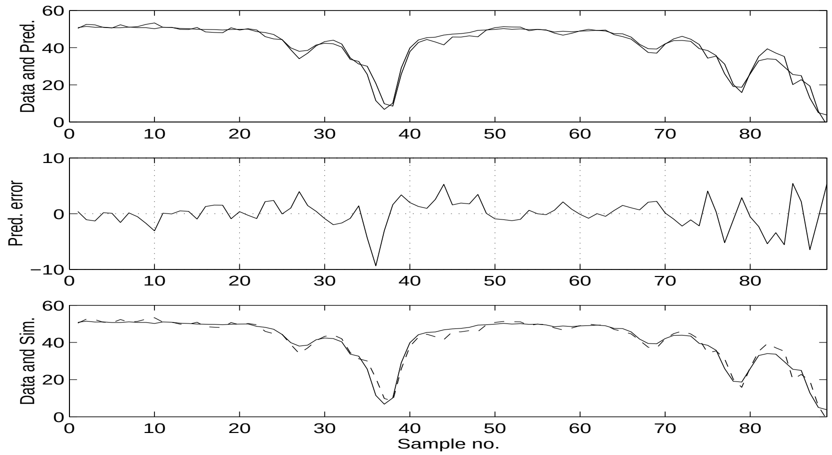

Figure 7.21. *$\mathcal{D}_{S2}$: Model performance for the thermostatic valve model with extension (Sample time: one minute).*

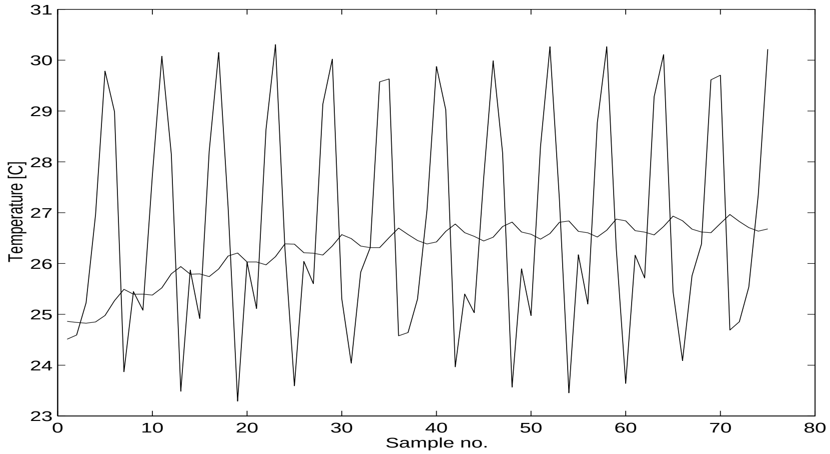

Figure 7.22. *$\mathcal{D}_{S1}$: Ambient air temperature T_a and estimated gas temperature T_g for the thermostatic valve model with extension (Sample time: one minute).*

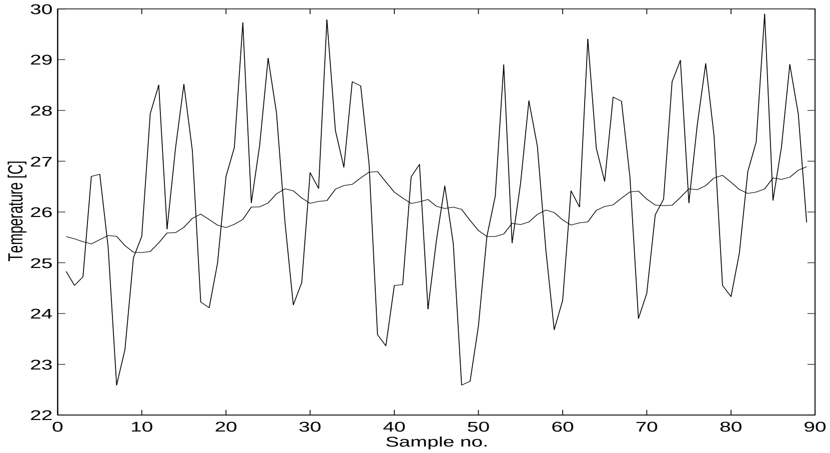

Figure 7.23. *$\mathcal{D}_{S2}$: Ambient air temperature T_a and estimated gas temperature T_g for the thermostatic valve model with extension (Sample time: one minute).*

Table 7.5. *Cross validation results based on the variance of the prediction errors for* $a = 0.85$ m^3/h/Bar$^{0.5}$.

	Thermostatic valve		Extended model	
Evaluation data	$\mathcal{D}_{S1}$	$\mathcal{D}_{S2}$	$\mathcal{D}_{S1}$	$\mathcal{D}_{S2}$
Estimates of $\mathcal{D}_{S1}$	$9.92{\cdot}10^{-5}$	$3.16{\cdot}10^{-3}$	6.53	16.5
Estimates of $\mathcal{D}_{S2}$	$2.58{\cdot}10^{-4}$	$9.90{\cdot}10^{-4}$	18.9	6.03
Unit	(m^3/h/Bar$^{0.5}$)^2		(l/h)^2	

Looking at the results for the thermostatic valve model, it is noted that the estimates of $\mathcal{D}_{S1}$ evaluated on $\mathcal{D}_{S2}$ yields a large prediction error variance compared to the variance of prediction error of $\mathcal{D}_{S1}$, while the estimates of $\mathcal{D}_{S2}$ evaluated on $\mathcal{D}_{S1}$ yields a variance of the same range compared to the variance of prediction error of $\mathcal{D}_{S2}$. Hence, the estimates of $\mathcal{D}_{S2}$ constitute a better set of estimates than the estimates of $\mathcal{D}_{S1}$.

In case of the extended model, there is approximately a factor 2.5 between the variance of estimation data and the variance of validation data – for both sets of data. For this model, the estimates of $\mathcal{D}_{S1}$ constitute a better set of estimates than the estimates of $\mathcal{D}_{S2}$.

Comparing the results of the cross validation for two models, the extended model performs better than non extended model.

7.5 Summary

The dynamic modelling of the gas based thermostatic valve has been considered. In the first section, the thermostatic valve was described together with some considerations on the thermostatic valve control.

In Section 7.2, the physical properties were presented and two modelling approaches were described, i.e. a microscopic modelling approach based on

the second law of Newton and a macroscopic modelling approach, which was based on empirical data for the thermostatic valve. The microscopic model resulted in many parameters – too many from an identifiability point of view. The macroscopic modelling approach led to two model formulations, one for the thermostatic valve and one considering the thermostatic valve and its interaction with the hydraulic system. The advantage of the macroscopic models were the low model order and the small number of parameters. A disadvantage of the suggested thermostatic valve models was encountered in relation to the applied estimation tool – as the first derivative of the thermostatic valve model had a discontinuity for $X_p = 0$. Thus, the input design was obliged to fulfill the requirement of $X_p > 0$.

The experimental setup of the thermostatic valve, the experimental design and the performed experiments were described in Section 7.3. From the analysis of the input signals, it was concluded that the excitation properties of the water supply temperature were insufficient, thus in order to get a good experimental design the water supply temperature was design to be constant and close to the ambient temperature. Based on this design the influence of the water supply temperature could be neglected. A strategy for excitation of the thermostatic valve through the ambient air was established, which could fulfill the demand of $X_p > 0$. The applied PRBS signal for the ambient air temperature was deliberately designed too fast, i.e. compared to the expected size of the time constant τ_a, in order to be able to supervice the demand $X_p > 0$.

In Section 7.4 the suggest dynamic model of the thermostatic valve and the extended model were used for estimation. The conclusion of the identifiability analysis of the thermostatic valve model was, that the characteristic parameters, a and b, of the thermostatic valve were not structural identifiable. Therefore, a was set to 0.85 m^3/h/Bar$^{0.5}$. The estimation results showed that the time constant τ_a of the thermostatic valve (from the ambient air to the gas in the thermostatic head) was in the range of 12-16 minutes. The estimates for the characteristic parameter b of the thermostatic valve were 3 to 5 times lower than the expected value of b. The set point temperature T_{set} was estimated to 25 °C, i.e. approximately 2 degrees higher than expected. The statistical tests indicated good, but not perfect modelling properties, both for the thermostatic valve model and for the extended model. So did the model performance plots. Finally, cross validation tests showed that the extended model provided a better generalization properties than non extended model.

It can be concluded that the suggested macroscopic modelling approach for the thermostatic valve results in a good dynamic model – despite the fact that the effects of hysteresis and elasticity are not covered by the model. Moreover, the extended model constitutes a good model for the interaction between the thermostatic valve and the hydraulics of the central heating system.

Chapter 8

House Modelling

The house modelling presented in this chapter is focused on thermal properties of the low energy test house, described in Section 4.3. The purposes of the house modelling are: 1) to investigate the interaction between room temperatures, solar radiation and the thermal behaviour of the experimental setup of the central heating system and 2) to identify and estimate the parameters of the dynamic house model. The goal of the modelling is to establish low order models for the room temperatures in the house.

The first section gives a short introduction to the basic concepts of the applied house modelling approach. The dynamic model of the low energy test house is described in the second section. The modelling is based on the thermal network approximation. Due to the closed loop formed by the thermostatic valve, radiator and room, three dynamic models are suggested. The input design and the performed test house experiment are presented in the third section, while estimation and validation results for the first test house model are discussed in the fourth section.

The test house data described in Section 8.3 are further investigated in *(Andersen, 1997)*.

8.1 On Thermal House Models

A lot of work on thermal house modelling has already been performed. Two different approaches can be applied in the modelling of a house depending on the purpose, which is either simulation or estimation. The two approaches are characterized as follows:

Simulation : This approach is usually based on a finite element method for distributed parameter models. In the modelling, empirical knowledge about building materials is used and the resulting model is of high order. DOE, ESP-r and TRANSYS are implementation examples for this approach.

Estimation : This approach is usually based on a lumped parameter description and it is further divided into a thermal network approximation technique (see e.g. *(Rabl, 1994)*) and a frequency domain technique (see e.g. *(Lindfors, 1994)*). In the modelling, the lumped parameters are estimated and the model is of low order. CTLSM, Matlab, MRQT are examples of applied tools for this approach.

The finite element method in the simulation approach is in principle equivalent to the thermal network approximation for the estimation approach. Therefore, the applied models for conductive, convective and radiant heat transfer are also equivalent. The main difference is the number of applied model states and in some sense the purpose of the modelling.

In the present modelling of the test house, the estimation approach is considered. Since the applied estimation method is based on the maximum likelihood method for time domain models, the thermal network approximation technique is used.

8.1.1 Thermal Network Approximation

As described in *(Sonderegger, 1978)*, the heat conduction across any slab of building material can be regarded one-dimensional, under the assumption that corner effects, thermal bridges and other inhomogeneities are neglected. This implies the use of the following one-dimensional heat conduction equation (alias the Fourier equation):

$$\frac{\partial T(x,t)}{\partial t} = \alpha \frac{\partial^2 T(x,t)}{\partial x^2} \tag{8.1}$$

where $T(x,t)$ denotes the spatial temperature distribution across the slab, α the heat diffusivity, x the position in the slab and t the time. The heat diffusivity is defined as:

$$\alpha = \frac{\lambda}{c\rho} \tag{8.2}$$

where λ denotes the heat conductivity, c the mass specific heat capacity and ρ the density, all with respect to the slab material. Analytical solutions are available for (8.1), in the case of steady periodic temperatures in a homogeneous slab with constant thermal diffusivity. Using the Laplace transformation on (8.1), the general solution can be written as in *(Sonderegger, 1978; Melgaard, 1994)*:

$$T(x,s) = \mathrm{F}_1(s)\sinh(x\sqrt{s/\alpha}) + \mathrm{F}_2(s)\cosh(x\sqrt{s/\alpha}) \tag{8.3}$$

where s denotes the Laplace operator. The two functions F_1 and F_2 are found by matching (8.3) to a given set of boundary conditions for a particular slab. An compact matrix formulation can further be derived from (8.3):

$$\begin{pmatrix} T(x_1,s) \\ \psi(x_1,s) \end{pmatrix} = \boldsymbol{N}(s) \begin{pmatrix} T(x_2,s) \\ \psi(x_2,s) \end{pmatrix} \tag{8.4}$$

where ψ denotes the heat flux and indices "1" and "2" are related to the surfaces of the slab, as illustrated in Figure 8.1. $\boldsymbol{N}$ denotes the transmission matrix and it is defined as:

$$\boldsymbol{N}(s) = \begin{bmatrix} \cosh(d\sqrt{s/\alpha}) & \frac{\sinh(d\sqrt{s/\alpha})}{\lambda\sqrt{s/\alpha}} \\ \lambda\sqrt{s/\alpha}\sinh(d\sqrt{s/\alpha}) & \cosh(d\sqrt{s/\alpha}) \end{bmatrix} \tag{8.5}$$

where $d = x_2 - x_1$ denotes the thickness of the slab. The elegance of (8.4) becomes evident in the case of a multilayer slab.

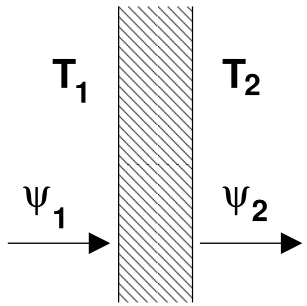

Figure 8.1. *Profile of a slab (or a wall).*

The introduction of $\mathcal{R} = d/\lambda$, the overall thermal resistance [Km^2/W] and of $\mathcal{C} = dc\rho$, the overall thermal capacity per unit area [J/Km^2] of a slab, makes possible to rewrite (8.5) as:

$$\boldsymbol{N}(s) = \begin{bmatrix} \cosh(\sqrt{s\mathcal{RC}}) & \frac{\mathcal{R}}{\sqrt{s\mathcal{RC}}}\sinh(\sqrt{s\mathcal{RC}}) \\ \frac{\sqrt{s\mathcal{RC}}}{\mathcal{R}}\sinh(\sqrt{s\mathcal{RC}}) & \cosh(\sqrt{s\mathcal{RC}}) \end{bmatrix} \tag{8.6}$$

which is a more convenient parametrization. Both a thin, thermal light and conductive slab or a slow time variability, imply that the argument $|s\mathcal{RC}| \ll 1$. In this case (8.6) is reduced to:

$$\boldsymbol{N}(s) = \begin{bmatrix} 1 & \mathcal{R} \\ 0 & 1 \end{bmatrix} \tag{8.7}$$

which leads to the well-known static heat balance expression:

$$\psi(x_1,s) = \psi(x_2,s) = \frac{T(x_1,s) - T(x_2,s)}{\mathcal{R}} \tag{8.8}$$

Consider now that index "1" refers to the inside of the wall (slab), while index "2" refers to the outside of the wall. As described in *(Sonderegger, 1978)*, the interesting part of (8.4) is the relation between the inside heat flux ψ_{in} and the inside and outside temperatures, T_{in} and T_{out}:

$$T_{in}(s) = \frac{\mathcal{R}}{\sqrt{s\mathcal{RC}}}\frac{\sinh(\sqrt{s\mathcal{RC}})}{\cosh(\sqrt{s\mathcal{RC}})}\psi_{in}(s) + \frac{1}{\cosh(\sqrt{s\mathcal{RC}})}T_{out}(s) \tag{8.9}$$

This transfer function is adequate for the frequency domain technique. Meanwhile, the basic idea in the thermal network technique is to substitute the two transfer functions in (8.9) by their Taylor expansions or by their infinite product expansions, see *(Sonderegger, 1978; Melgaard, 1994)*, where also assessments of these approximations are presented.

The considerations above should be seen as justification for using the $\mathcal{RC}$ approximation to the one-dimensional heat conduction equation (8.1), i.e a justification for the thermal network technique.

8.1.2 Conductive and Convective Heat Transfer

In the following, heat transfer due to the radiation is neglected for simplicity. Furthermore, the air change of rooms (ventilation) is assumed to be zero. Moreover, the thermal resistance R [K/W^2] and the thermal capacity C [J/K] are introduced.

A conductive heat transport through a wall is caused by a temperature difference. As illustrated in Figure 8.2, the heat transport from the internal temperature T_{in} to the external temperature T_{out} consists of both convective and conductive heat transport.

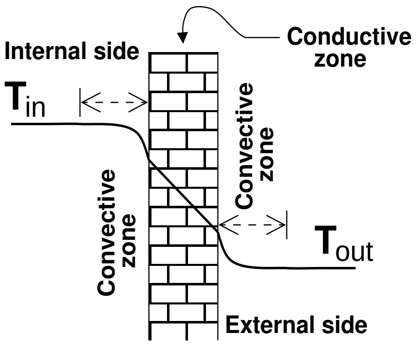

Figure 8.2. *Stationary temperature profile across a wall with convective zones.*

Conductive heat transfer through a wall is usually expressed as:

$$\Phi = \frac{\lambda}{s} A \Delta T \tag{8.10}$$

where s and A denote the depth and the surface area of the wall, respectively, λ the heat conductivity and ΔT the difference between the two wall surface temperatures. Convective heat transfer next to a wall is often expressed as:

$$\Phi = h_c A \Delta T \tag{8.11}$$

where h_c denotes the convective coefficient and ΔT the difference between the surface temperature and the ambient air temperature, which is measured in a proper distance from the surface of the wall as sketched in Figure 8.2.

According to *(ASHRAE, 1989)*, the convective coefficient h_c for a vertical plate in the case of natural convection is given as:

$$h_c = \begin{cases} 0.29 \left(\frac{\Delta T}{l_h}\right)^{0.25} & \text{for small plates, laminar air flow} \\ 0.19 \, (\Delta T)^{0.33} & \text{for large plates, turbulent air flow} \end{cases} \tag{8.12}$$

where l_h denotes the height of the plate. A thermal resistance between the surface temperature and the ambient air temperature can be defined as:

$$R = \frac{\Delta T}{\Phi} = \frac{1}{h_c A} \tag{8.13}$$

It should be noted that by the application of (8.12) in (8.13), the thermal resistance for convection R turns out to be a nonlinear function of the temperature difference ΔT.

As final remark note that substitution of (8.12) into (8.11) implies an equation similar to the one exponent formula, i.e. of the form

$$\Phi = K \Delta T^{n_1} = \Phi_0 \left(\frac{\Delta T}{\Delta T_0}\right)^{n_1} \tag{8.14}$$

where the constant K can be expressed as:

$$K = \left\{ \begin{array}{l} 0.29 \left(\frac{\Delta T}{l_h}\right)^{0.25} A \\ \\ 0.19 \, (\Delta T)^{0.33} A \end{array} \right\} \sim \Phi_0 \frac{1}{\Delta T_0^{n_1}} \tag{8.15}$$

The modelling principles presented so far are sufficient for the test house, since the considered test house is quite simple seen from a thermal point of view. If the test house had been e.g. inhabited, the modelling would have been more complex.

8.2 Dynamic Test House Model

In this section, the dynamic model of the low energy test house will be presented. The modelling is based on the thermal network technique introduced in the previous section. Hence, the first task is to define the temperature zones of the test house.

8.2.1 Uniform Temperature Zones

In order to keep the modelling simple, the house is divided into temperature zones, where the temperature reasonably can be considered uniform in each zone. The thermal mass of the j'th zone is lumped into the thermal capacity C_j, while the thermal resistance R_{ji} represents the connection between zone j and the adjacent zone i. It is not easy to formulate general rules on how to distribute the zones in a house or a building, as the "zoning" depends on the size, shape, adjacency and on the contents of the rooms (furnitures, etc.). This issue is further discussed in *(Sonderegger, 1978)*.

The structural properties of the test house have already been described in Section 4.3, in connection with the measurement layout. As the walls of

the test house are constructed of thermal light materials, they are regarded as thermal resistances only. If the test house walls had been constructed of more thermal heavy materials, it would also have been necessary to define temperature zones for the walls. Thus, based on these considerations and on the structure of the test house, sketched in Figure 4.8, the following set of main temperature zones are defined:

$\mathcal{Z}_{an}$: the air and the radiator terminal in room An.

$\mathcal{Z}_{as}$: the air and the radiator terminal in room As.

$\mathcal{Z}_{fn}$: the floor in room An.

$\mathcal{Z}_{fs}$: the floor in room As.

In order to get a well defined surroundings for the main temperature zones, the following set of auxiliary zones are defined:

$\bar{\mathcal{Z}}_{b}$: the air in room B.

$\bar{\mathcal{Z}}_{en}$: the air north of the test house.

$\bar{\mathcal{Z}}_{es}$: the air south of the test house and the solar radiation.

The bar sign indicates that the zone is an auxiliary zone. It is noted that the heat capacity of a auxiliary zone is without interest. A sketch of the spatial adjacency of the temperature zones is presented in Figure 8.3.

Temperature zone $\mathcal{Z}_{an}$ (or $\mathcal{Z}_{as}$) could be further divided into two zones, a zone containing the air in room An and a zone containing the radiator terminal. Whether or not this extra "sub-zoning" is necessary, can only be answered by estimation of the models.

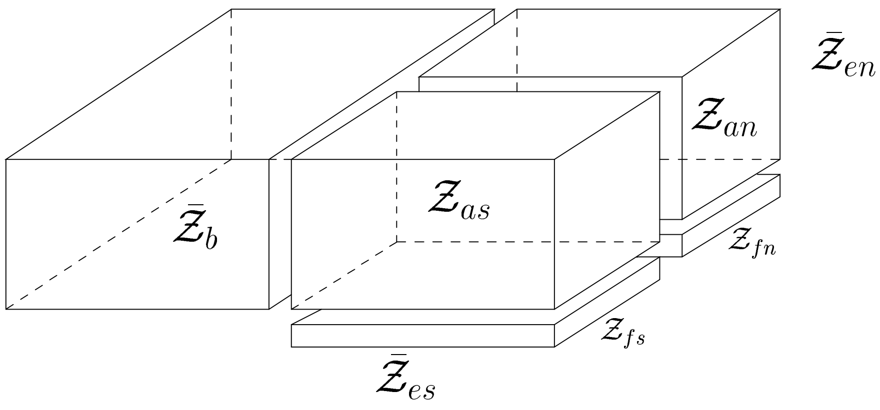

Figure 8.3. *Sketch of the spatial adjacency of the test house temperature zone layout.*

8.2.2 Model of Room An

As mentioned above, room An contains the two temperature zones $\mathcal{Z}_{an}$ and $\mathcal{Z}_{fn}$. The thermal network model for room An is illustrated in Figure 8.4.

The thermal resistances in Figure 8.4 form the connections between a main temperature zones and the auxiliary zones or between the main zones mutually. In principle, each of these thermal resistances consists of a convective resistance, a conductive resistance and again a convective resistance, except the thermal resistance R_{fn}, which only consists of a convective resistance.

To obtain the model in Figure 8.4, the following assumptions are applied:

- The temperature T_{an} of the air and of the floor T_{fn} in room An are uniform, implying two temperature zones.
- No heat transfer through the ceiling. This assumption can be justified by two facts: 1) the ceiling is well insulated and 2) the temperature

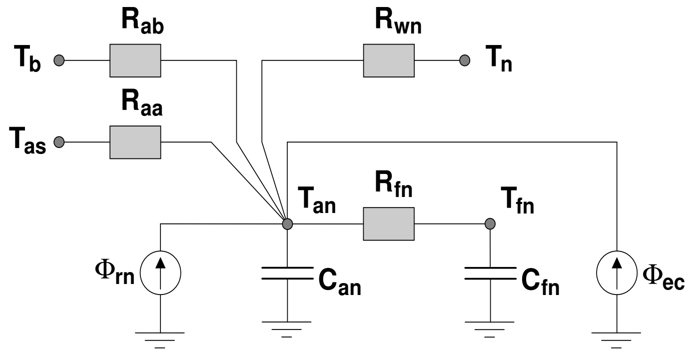

Figure 8.4. *Thermal RC network for room An, including the main temperature zones $\mathcal{Z}_{an}$ and $\mathcal{Z}_{fn}$.*

level in the roof-storey (the office space) is approximately the same as in room An.

- No influence from windy or rainy weather on the thermal resistance R_{wn} of the outer wall.
- Radiative heat transfer is negligible.
- No influence from solar radiation through the window area of room An, see *(Andersen, 1997)*.
- No ventilation and no influence from the humidity of the air.

Based on Figure 8.4, the following second order model can be formulated for the dynamic heat transfer in room An:

$$C_{an}\frac{dT_{an}}{dt} = \frac{1}{R_{fn}}(T_{fn}-T_{an}) + \frac{1}{R_{aa}}(T_{as}-T_{an}) + \Phi_{ec} + \frac{1}{R_{ab}}(T_b - T_{an}) + \frac{1}{R_{wn}}(T_n - T_{an}) + \Phi_{rn} \quad (8.16)$$

$$C_{fn}\frac{dT_{fn}}{dt} = \frac{1}{R_{fn}}(T_{an}-T_{fn}) \quad (8.17)$$

where Φ_{ec} denotes the heat input from the electric cooker (see Section 4.3) and Φ_{rn} the power supply from the radiator (Box 2). The power input from the electric cooker will be designed in Section 8.3, while the modelling of the radiator power Φ_{rn} will be further elaborated in Section 8.2.4.

8.2.3 Model of Room As

Room As contains the two temperature zones $\mathcal{Z}_{as}$ and $\mathcal{Z}_{fs}$. The thermal network for this room is illustrated in Figure 8.5.

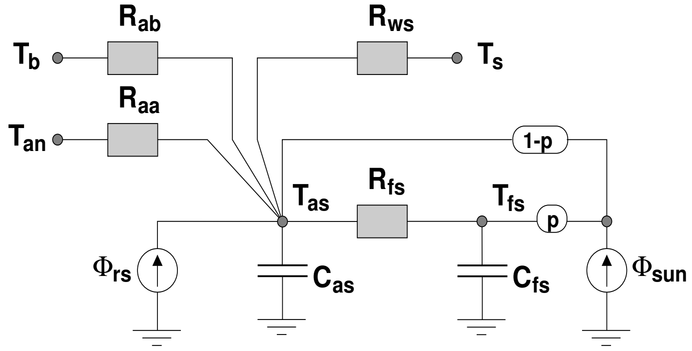

Figure 8.5. *Thermal RC network for room As, including the main temperature zones $\mathcal{Z}_{as}$ and $\mathcal{Z}_{fs}$.*

The thermal resistances in Figure 8.5 follow the outlines in the previous section. The heat input from the electric cooker Φ_{ec} has been exchanged by the heat input from solar radiation Φ_{sun}, which consists of both direct and diffuse radiation. The measurement of the solar radiation on the south side of the test house is denoted as I_s (see Section 4.3). The heat input from solar radiation Φ_{sun} depends on the efficient window area A_w facing south, i.e. $\Phi_{sun} = A_w I_s$. The efficient window area A_w is the physical window area corrected for shade effects, absorption and reflection by the glazed windows. In Figure 8.5, parameter p is a fraction, which describes the amount of the heat from the solar radiation that heats the floor in room As, while $1-p$

heats the air in room As. In *(Madsen et al., 1990)*, p is reported to be close to zero.

To obtain the model in Figure 8.5, the following assumptions are applied:

- The temperature T_{as} of the air and of the floor T_{fs} in room As are uniform, implying two temperature zones.
- No heat transfer through the ceiling.
- No influence from windy and rainy weather on the thermal resistance R_{ws} of the outer wall.
- Radiative heat transfer is negligible, except the solar radiation.
- No ventilation and no influence from the humidity of the air.

Based on Figure 8.5, a second order model can be formulated for the dynamic heat transfer in room As:

$$C_{as}\,\frac{dT_{as}}{dt} = \frac{1}{R_{fs}}\,(T_{fs}-T_{as}) + \frac{1}{R_{aa}}\,(T_{an}-T_{as}) + (1-p)\Phi_{sun} + \frac{1}{R_{ab}}\,(T_b-T_{as}) + \frac{1}{R_{ws}}\,(T_s-T_{as}) + \Phi_{rs} \tag{8.18}$$

$$C_{fs}\,\frac{dT_{fs}}{dt} = \frac{1}{R_{fs}}\,(T_{as}-T_{fs}) + p\,\Phi_{sun} \tag{8.19}$$

where Φ_{rs} denotes the power supply from the radiator (Box 1).

8.2.4 On the Radiator Power

The radiators, the electric cooker (see Section 6.4.2) and the heat input from the solar radiation are regarded as the main heat sources. The inevitable heat loss from the pipes is in reality a minor heat source. For simplicity, this heat loss is assumed to be zero and the assumption is more or less justified by the fact that the pipes are insulated.

In *(Madsen et al., 1990)* the time constant for the air was estimated to 26 minutes, while the time constant of the floor was 154 hours. It is noted that the experiment in *(Madsen et al., 1990)* was conducted under different conditions compared to the present setup. For example, the thermal capacity of the floor was increased by placing two layers of concrete flags on the floor. Nevertheless, the 26 minutes for time constant of the air will be used as a guideline.

A couple of modelling approaches for the radiator has been described in Chapter 6. The value of the time constant of the radiator model in Model Summary 6.1 was in Section 6.4.2 found to be in the range of 6-73 minutes based on prior knowledge and suitable assumptions. Meanwhile, based on the parameter estimates presented in Table 6.1 the range was calculated to be in the 0.5-10 minutes – which is considered to be more realistic.

Thus, the question emerges whether or not the dynamic of the radiator is faster than the time constant of the air. To handle this aspect two modelling approaches are considered:

1. Static radiator model. The thermal dynamic in the radiator is much faster than the time constant of the air in the test room. Thus, the heat inputs from the radiator, e.g. in room An, can be described by the one exponent formula:

$$\Phi_{rn} = \Phi_0 \left(\frac{T_{rn} - T_{an}}{60} \right)^{n_1} \tag{8.20}$$

   where T_{rn} denotes the mean temperature of the radiator, Φ_0 the nominal radiator power and n_1 the radiator exponent.

2. Dynamic radiator model. The model presented in Model Summary 6.1 will be used as radiator model with an approximation order of $\mathcal{N} = 2$ and $\phi = 0$, which for e.g. room An becomes:

$$\frac{1}{2}\, C_r\, \frac{dT_{rn1}}{dt} = H_q\, q_2\, (T_{i2} - T_{rn1}) - \frac{\Phi_0}{2} \left(\frac{T_{rn1} - T_{an}}{60} \right)^{n_1} \tag{8.21}$$

$$\frac{1}{2}\, C_r\, \frac{dT_{rn2}}{dt} = H_q\, q_2\, (T_{rn1} - T_{rn2}) - \frac{\Phi_0}{2} \left(\frac{T_{rn2} - T_{an}}{60} \right)^{n_1} \tag{8.22}$$

   where T_{rn1} and T_{rn2} denote the temperatures of the water in the radiator of Box 2, T_{i2} the water supply temperature and q_2 the water flow in Box 2 (corresponding to Figure 4.5). The power supply from the radiator Φ_{rn} can be expressed as:

$$\Phi_{rn} = \frac{\Phi_0}{2} \left(\left(\frac{T_{rn1} - T_{an}}{60} \right)^{n_1} + \left(\frac{T_{rn2} - T_{an}}{60} \right)^{n_1} \right) \tag{8.23}$$

   With this radiator model, the total model order of the dynamic heat transfer in room An becomes of fourth order.

In Section 7.4 the estimates for the time constant of the thermostatic sensor (of the thermostatic valve) were estimated to be in the range of 10-15 minutes. Hence, the dynamic of the valve is faster than the dynamic of the air. This seems reasonable, since the thermostatic valve is supposed to control the air temperature.

As stressed in Section 3.1.1, system identification in closed loop systems is more complicated. If the static radiator model is applied, the existence of closed loop will be neglected. When the dynamic radiator model is applied, one of the following situations are considered:

1. No feedback (direct identification).
2. Feedback simulation (indirect identification). The thermostatic valve is implemented in the model, but the parameters related with the thermostatic valve are considered to be known.

Thus, three formulations are possible with respect to the radiator model.

8.2.5 Test House Model

The dynamic heat transfer models for the two test rooms An and As can be gathered into one model, which simultaneously describes the heat transfer in the two test rooms. From an estimation point of view, such a model has the advantage that some of the parameters are repeated, as e.g. the parameters of the radiator model. Hence, based on the assumption of symmetric test rooms and identical radiators, the following simplifications can be introduced:

$$C_{an} = C_{as} = C_a, \qquad C_{fn} = C_{fs} = C_f$$
$$R_{wn} = R_{ws} = R_a, \qquad R_{fn} = R_{fs} = R_f, \qquad R_{ab} = 2\,R_{aa} = 2\,R_a$$

Thus, the parameter estimation problem is less complicated than the case when the two single room models are used. The model of the symmetric test rooms An and As is illustrated in Figure 8.6.

Based on Figure 8.6, a fourth order model of the test house can be formulated. In order to facilitate the notation, let $\mathcal{M}_a(\underline{\theta}_a)$ denote this model. As presented in the previous section, three formulations are possible with respect to the radiator model. This will of course influence the test house model.

Model Summary 8.1 (Test House Model – Static Radiator)
Let $\mathcal{M}_{a1}(\underline{\theta}_{a1})$ denote the test house model in the case when the static radiator model (8.20) is used in $\mathcal{M}_a(\underline{\theta}_a)$.

Model Summary 8.2 (Test House Model – Dynamic Radiator)
Let $\mathcal{M}_{a2}(\underline{\theta}_{a2})$ denote the test house model in the case when the dynamic radiator model in Model Summary 6.1 (with approximation order $\mathcal{N}=2$) is used in $\mathcal{M}_a(\underline{\theta}_a)$. The submitted radiator power is described by (8.23).

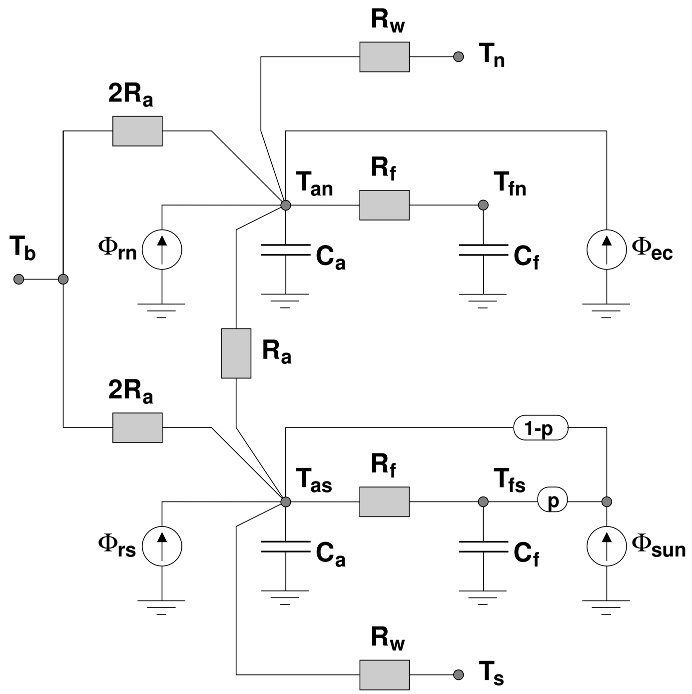

Figure 8.6. *Thermal RC network for the test house model using symmetry considerations.*

Model Summary 8.3 (Test House Model – Closed Loop System)
Let $\mathcal{M}_{a3}(\underline{\theta}_{a3})$ denote the test house model in the case when the dynamic radiator model in Model Summary 6.1 (with approximation order $\mathcal{N}=2$) and with the dynamic thermostatic valve model in Model Summary 7.1 are used in $\mathcal{M}_a(\underline{\theta}_a)$. The submitted radiator power is described by (8.23). For this model prior knowledge for the parameters $T_{set,1}$, $T_{set,2}$, τ_a, τ_w, a and b is assumed.

Model $\mathcal{M}_{a1}(\underline{\theta}_{a1})$ can be characterized by:

4 states : T_{an}, T_{fn}, T_{as} and T_{fs}.
7 inputs : T_b, T_n, T_s, T_{i1}, T_{i2}, Φ_{ec} and Φ_{sun}.
2 outputs : T_{an} and T_{as}.
9 parameters : C_a, C_f, R_a, R_f, R_w, Φ_0, n_1, p and A_w.

where for simplicity T_{i1} and T_{i2} are used directly as radiator mean temperature.

Model $\mathcal{M}_{a2}(\underline{\theta}_{a2})$ can be characterized by:

8 states : T_{an}, T_{fn}, T_{rn1}, T_{rn2}, T_{as}, T_{fs}, T_{rs1} and T_{rs2}.
9 inputs : T_b, T_n, T_s, T_{i1}, T_{i2}, q_1, q_2, Φ_{ec} and Φ_{sun}.
4 outputs : T_{an}, T_{rn2}, T_{as} and T_{rs2}.
11 parameters : C_a, C_f, R_a, R_f, R_w, Φ_0, n_1, p, A_w, C_r and H_q.

Model $\mathcal{M}_{a3}(\underline{\theta}_{a3})$ is an extended versions of $\mathcal{M}_{a2}(\underline{\theta}_{a2})$ and it has two additional state. The number of parameters is not changed, since prior knowledge on $T_{set,1}$, $T_{set,2}$, τ_a, τ_w, a and b are assumed to be available.

The test house models $\mathcal{M}_{a1}(\underline{\theta}_{a1}), \mathcal{M}_{a2}(\underline{\theta}_{a2})$ and $\mathcal{M}_{a3}(\underline{\theta}_{a3})$ represent one particular modelling approach for the test house. Perturbations of the proposed models $\mathcal{M}_{a1}(\underline{\theta}_{a1})$ and $\mathcal{M}_{a2}(\underline{\theta}_{a2})$ (especially for the radiator model), are further analyzed in *(Andersen, 1997)*.

8.3 Experiments

The experimental setup of the test house was described in Section 4.3. The issue is now to perform an experiment in order to estimate the thermal parameters of test house.

8.3.1 Analysis and Input Design

Over the years, the test house has of course been exposed to many thermal experiments, e.g. *(Rasmussen and Saxhof, 1982; Hansen, 1985; Madsen et al., 1990)*. Therefore, the thermal properties of the test house are fairly well-known. In Appendix C, the thermal capacities and thermal resistances, defined in Section 8.2, are computed based on the physical dimensions of the test house, combined with “handbook” knowledge. The computed thermal parameters, summarized in Table 8.1, represent at the same instant a set of expectations.

Table 8.1. *Calculated thermal test house parameters (based on test house dimensions and handbook data).*

Parameter	Unit	Value
C_a, C_{an}, C_{as}	kJ/K	85
C_f, C_{fn}, C_{fs}	MJ/K	4.4
$R_a, R_{aa}, \frac{1}{2}R_{ab}$	K/W	0.15
R_w, R_{wn}, R_{ws}	K/W	0.10
R_f, R_{fn}, R_{fs}	K/W	0.033

The time constants of the heat transfer dynamics can now be assessed. Looking at the linear system formed by (8.16) and (8.17), a set of estimates for the time constant of the air τ_a and of the floor τ_f, can be calculated as follows, using the thermal parameters in Table 8.1:

$$\tau_a \approx \frac{C_{an}}{\frac{1}{R_{fn}} + \frac{1}{R_{aa}} + \frac{1}{R_{ab}} + \frac{1}{R_{wn}}} \approx 28 \text{ minutes} \tag{8.24}$$

$$\tau_f \approx R_{fn}C_{fn} \approx 40 \text{ hours} \tag{8.25}$$

These time constant are quite sensitive to the assumed values of the convective coefficients. The 28 minutes correspond to the 26 minutes reported in *(Madsen et al., 1990)* and the 40 hours compared to the 154 hours is also realistic, since the thermal capacity of floor is not as big as in *(Madsen et al., 1990)*.

The influence of the radiator on the time constant e.g. of temperature zone $\mathcal{Z}_{an}$ is investigated in the following. The thermal resistance R_{rn} between the radiator and zone $\mathcal{Z}_{an}$ can be expressed as:

$$\begin{aligned} \frac{1}{R_{rn}} &= -\frac{d\Phi_{rn}}{dT_{an}} \\ &= \frac{n_1\Phi_0}{2\cdot 60}\left(\left(\frac{T_{rn1,op}-T_{an,op}}{60}\right)^{n_1-1}+\left(\frac{T_{rn2,op}-T_{an,op}}{60}\right)^{n_1-1}\right) \end{aligned} \tag{8.26}$$

where $T_{rn1,op}$, $T_{rn2,op}$ and $T_{an,op}$ denote operation point temperatures. Assume that the water in the radiator is e.g. 60 °C and the room temperature T_{an} is 20 °C, then the thermal resistance R_{rn} is computed to 0.13 K/W, based on the nominal radiator power $\Phi_0 = 395$ W and on the exponent $n_1 = 1.25$, refer to Section 6.1. A new estimate for the time constant of zone $\mathcal{Z}_{an}$ can be calculated as:

$$\tau_a \approx \frac{C_{an}}{\frac{1}{R_{fn}}+\frac{1}{R_{aa}}+\frac{1}{R_{ab}}+\frac{1}{R_{wn}}+\frac{1}{R_{rn}}} \approx 24 \text{ minutes} \tag{8.27}$$

Thus, it can be concluded that a warm radiator yields a faster time constant of the air. The same consideration is also valid for room As.

It should be noted that the calculations for the thermal resistances in Appendix C.1 are based on an ad-hoc procedure. A formalized procedure is defined in *(Dansk Standard, 1986)*.

Input Design

The input signals to the heat transfer dynamic of the test house have been characterized in Section 8.2.5. It was pointed out that the number of inputs

depends on the selected test house model. The task is now to design proper signals for these inputs.

Looking at the model characterization of model $\mathcal{M}_{a2}(\underline{\theta}_{a2})$, in Section 8.2.5, the number of inputs is 9. The temperature T_b of the air in room B is left floating. The two inputs T_{i1} and T_{i2} are not directly design able. They are a result of the actual flow and the water supply temperature T_{hs} from the heating unit (see Figure 4.3). Neither the two input flows q_1 and q_2 are directly design able, as they are a result of the actual pump pressure Δp_s and the state of the thermostatic valves, which further is related to the room temperature. Thus, the number of "real" inputs is reduced to 6 inputs and these input signals can be divided into two groups:

- The climatic inputs: T_n, T_s and Φ_{sun}.
- The controllable inputs: T_{hs}, Δp_s and Φ_{ec}.

The climatic inputs are not controllable (by humans) and therefore they are not relevant for input design. Meanwhile, the behaviour of these inputs is of interest in connection with the controllable inputs. Even though the climatic inputs are of stochastic nature, there is an element of built-in daily and yearly variation. This fact can be used constructive. For example, if the experiment is performed during the winter season, the difference between indoor and outdoor temperature is larger compared to the summer season, hence also the heat demand is larger. All in all, the winter season supports the best noise-signal ratio.

The controllable inputs will now be designed. As discussed in Section 6.4.2, the dynamic of water supply temperature T_{hs} is too slow compared to the dynamic of the radiator. Compared to the time constant e.g. of zone $\mathcal{Z}_{fn}$, the water supply temperature T_{hs} supports a good excitation quantity, as it has a sufficiently faster dynamic. As it was observed in (8.27), the temperature of the radiator has an influence on the dynamic of zone $\mathcal{Z}_{an}$. The temperature of the water supply is influenced by the flow – and the flow is a function of the state of thermostatic valve and of the system pressure Δp_s.

Since the temperature selectors of thermostatic valves are untouched during the experiment, the set point temperatures are constant (neglecting elasticity etc.). Hence, the system pressure Δp_s can be used to excite the dynamic of the radiators and the two zones $\mathcal{Z}_{an}$ and $\mathcal{Z}_{as}$ – a fact which might be quite important from a persistence of excitation point of view (see Section 3.1).

The electric cooker has been introduced in the experiment in order to avoid too much correlation between the temperature in room An and the temperature in room As, in connection with the heat input from the sun. Thus, the design of the heat input Φ_{ec} from the electric cooker should support a dynamic faster than the 24 hours, but not too close to the design for the system pressure Δp_s. As in the previous experiments, PRBS signals are used. The input design is presented in Table 8.2.

Table 8.2. *Input design based on PRBS-signals.*

Input signal type	Symbol	T_0	n
Water supply temperature	T_{hs}	30 hours	6
System pressure	Δp_s	20 minutes	4
Electric cooker	Φ_{ec}	9 hours	3

The levels of the input signals in Table 8.2 were selected as follows. A water supply temperature in the range of $50 - 60$ °C was found adequate in prior testings. Thus, the levels of water supply temperature were selected as 52/58 °C for the low/high levels, respectively. The levels for the pump pressure were selected as minimum/medium for the low/high levels. The electric cooker is an on/off signal. As described in Section 4.3.3, the input power of the electric cooker was selected to be 150 W.

8.3.2 Measurement Data

An experiment has been performed during November-December 1996, based on the input design presented in Table 8.2. The measurement period is approximately 27 days starting from November 22, 1996. The sampling time was 10 seconds.

Not all of the measured signals, described in Section 4.3, are presented below, only those relevant for the modelling of the dynamic heat transfer in room An and room As. The term “relevant” is related to redundancy of some of the measurement signals. As illustrated in Figure 4.8, the room temperature of e.g. room An is represented by the signals: T_{a2}, T_{nw} and T_{ne} – equivalent for room As by: T_{a1}, T_{sw} and T_{se}. The room temperature of room B is represented by the signals: T_{bn} and T_{bs}. The signals in each of these three groups are found to be highly correlated and of the same range. Thus, the basic assumption of the uniform temperature zones is valid.

The problem is now how to reduce the information to one temperature in each zone. There is different possibilities:

- Select a temperature in each zone and discard the rest.
- Select the temperature as the mean value of each group of signals.
- Select the temperature as the principal component of each group of signals.

A principal component analysis is performed in *(Andersen, 1997)*. The analysis shows that the principal component is quite close to T_{nw} and T_{sw}, respectively, of each of the test rooms, while it is close to the mean value of the temperatures in room B.

In Figure 8.7 the first subplot contains the test room temperature T_{an} (measured as T_{nw}), the temperature T_b in room B (measured as the mean of T_{bn} and T_{bs}) and the temperature T_n on the north side of the test house. In the second subplot, the heating unit water supply temperature T_{hs} (indicated by "$--$"), the water supply temperature T_{i2} and return temperature T_{o2} at the outlet of the radiator. The same interpretation can be done for Figure 8.8, where the first subplot contains T_{as}, T_b and T_s, while the second subplot contains T_{as}, T_{i1} and T_{o1}.

In Figure 8.9, the two flows q_1 and q_2 are shown in the first subplot, where flow q_2 from sample 800 is smaller than q_1. The second subplot contains the power input signal Φ_{ec} in Watts, which is identified as the square signal between 0 and 150. The other signal is the solar radiation I_s [W/m^2].

The input design for the system pressure Δp_s is the reason why the two flows in Figure 8.9 and the water temperatures in Figure 8.7 and Figure 8.8 might seem fussy. Furthermore, the effect of Φ_{ec} is reflected in T_{an} (see Figure 8.7), while the heat input from the solar radiation Φ_{sun} can be recognized as the peaks in T_{as} (see Figure 8.8). The effect of the solar radiation is also visible in the flow q_1 of Box 1 (see Figure 8.9) and in the ambient temperature T_n and especially in T_s.

The flow q_2, in Box 2, is approximately 5 l/h, the main part of the experiment time. This small flow results in a quite large heat loss in the water supply temperature, which can be seen by comparison of T_{i2} (second subplot in Figure 8.7) and T_{i1} (second subplot in Figure 8.8). From T_{hs} to T_{i1} the heat loss is a couple of degrees, while from T_{i1} to T_{i2} it is 10-15 degrees. This heat loss from the insulted pipes goes directly into the test rooms.

8.3.3 Alternative Input Design

The input design for the test house experiment was based on time domain design (i.e. PRBS signals). An alternative is to make a frequency domain design. A case study based on the test house is presented in *(Sadegh et al., 1997)*. The considered model is based on $\mathcal{M}_a(\underline{\theta}_a)$ (see Section 8.2.5) with a

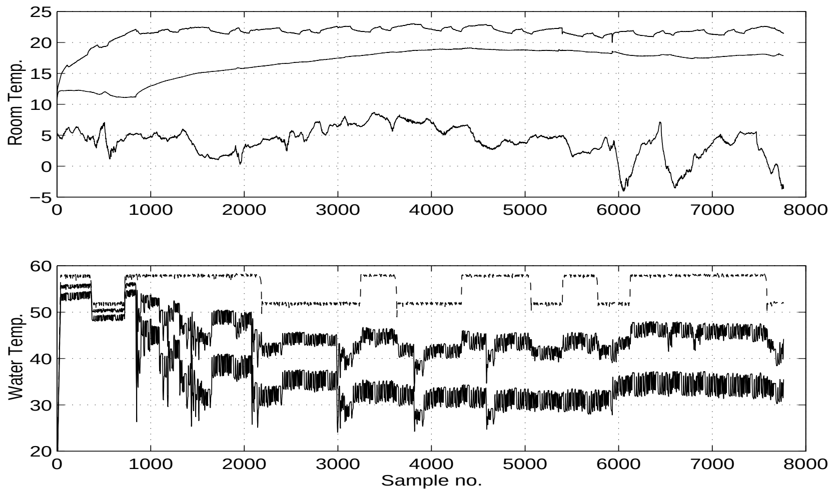

Figure 8.7. *Measurement data for room An (Sample time: 5 minutes).*

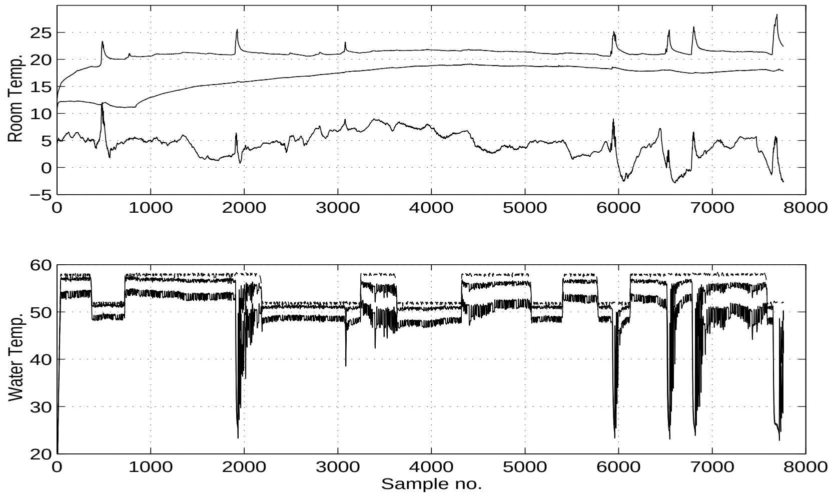

Figure 8.8. *Measurement data for room As (Sample time: 5 minutes).*

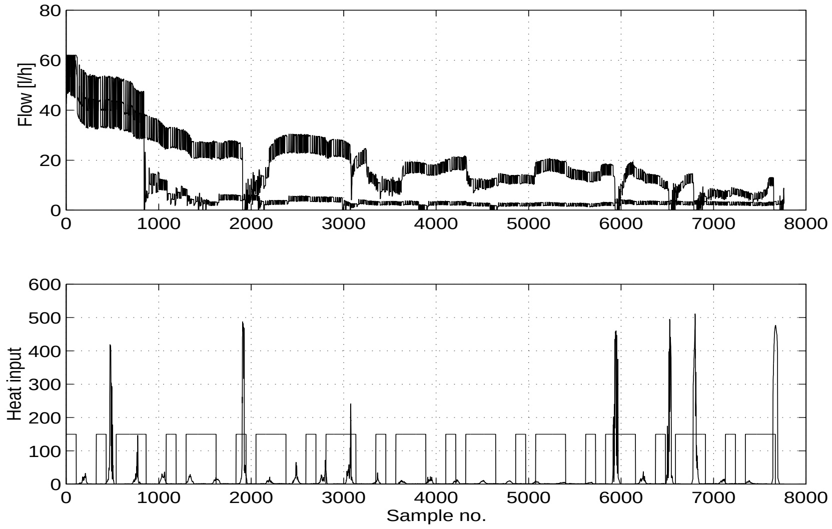

Figure 8.9. *Measurement data for water flows and heat inputs (Sample time: 5 minutes).*

linearized version of the radiator model in Model Summary 6.1 for approximation order $\mathcal{N} = 1$. Furthermore the power from solar radiation and the electric cooker are set to zero.

As mentioned earlier, the calculated parameters in Table 8.1 are sensitive to the assumed values of the convective coefficients. Thus, the goal of the case study is to design an optimal input signal for the circulating pump with respect to the thermal capacities of the floors in room An and room As, i.e. $\underline{\theta} = (C_{fn}, C_{fs})^\top$.

The input is represented as:

$$\Delta p_s(t) = \Delta p_s \sum_j c_j \sin(2\pi f_j t) \tag{8.28}$$

where Δp_s is some desirable system pressure, c_j amplitude coefficients satisfying the power constraint $\sum_j c_j^2 = 1$ and t the time in minutes. The frequencies $f_j, j \in [1, \cdots, 20]$ are selected as $f_j = 1/60/50$. Thus, each sinusoid has a period of $T_j = 50\, j$ hours, which includes a time range of 50 to 1000 hours. It turners out that the optimal frequency is between f_{13} and f_{14} for the considered set of parameter values.

Refer to *(Sadegh et al., 1997)* (or *(Sadegh, 1996)*) for a more profound description of this case study.

8.4 Estimation of Grey Box Models

Based on the experiment described in Section 8.3, the parameters of the model in Model Summary 8.1 will be estimated. Estimation of the parameters of the models in Model Summary 8.2 and Model Summary 8.3 is not performed due to time constraint.

8.4.1 Identifiability

The model $\mathcal{M}_{a_1}(\underline{\theta}_{a_1})$ in Model Summary 8.1 was characterized by 4 states, 7 inputs, 2 outputs and 9 parameters. Consider the model $\mathcal{M}_a(\underline{\theta}_a)$. This linear model is structural identifiable, a fact which can be tested using Laplace transformation and algebraic calculus. $\mathcal{M}_{a1}(\underline{\theta}_{a1})$ contains two parameters more than $\mathcal{M}_a(\underline{\theta}_a)$, i.e. Φ_0 and n_1. Nevertheless, only one of these extra parameters can be identified from data, as the correlation becomes 1.0. Thus, the choice stands between Φ_0 or n_1.

8.4.2 Test House Model with Static Radiator Model

The Grey Box model for the test house in Model Summary 8.1 can be expressed as (where the time argument is left out for notational reasons):

$$dT_{an} = \frac{1}{C_a}\left[\frac{1}{R_f}(T_{fn}-T_{an}) + \frac{1}{R_a}(T_{as}-T_{an}) + \Phi_{ec} + \Phi_{rn} + \frac{1}{2R_a}(T_b-T_{an}) + \frac{1}{R_w}(T_n-T_{an})\right]dt + dW_1 \tag{8.29}$$

$$dT_{fn} = \frac{1}{R_fC_f}(T_{an}-T_{fn})\,dt + dW_2 \tag{8.30}$$

$$dT_{as} = \frac{1}{C_a}\left[\frac{1}{R_f}(T_{fs}-T_{as}) + \frac{1}{R_a}(T_{an}-T_{as}) + \frac{1}{2R_a}(T_b-T_{as}) + \frac{1}{R_w}(T_s-T_{as}) + (1-p)A_wI_s + \Phi_{rs}\right]dt + dW_3 \tag{8.31}$$

$$dT_{fs} = \frac{1}{C_f}\left(\frac{1}{R_f}(T_{as}-T_{fs}) + pA_wI_s\right)dt + dW_4 \tag{8.32}$$

$$\Phi_{rn} = \Phi_0\left(\frac{T_{i2}-T_{an}}{60}\right)^{n1} \tag{8.33}$$

$$\Phi_{rs} = \Phi_0\left(\frac{T_{i1}-T_{as}}{60}\right)^{n1} \tag{8.34}$$

$$\underline{Y}(k) = \begin{bmatrix} 1 & 0 & 0 & 0 \\ 0 & 0 & 1 & 0 \end{bmatrix}\underline{X}(k) + \underline{e}(k) \tag{8.35}$$

where $\underline{X} = (T_{an},\, T_{fn},\, T_{as},\, T_{fs})^\top$, $\underline{Y}$ the measured test room temperatures and $\underline{W} = (W_1,\, W_2,\, W_3,\, W_4)^\top$ the system noise, which is assumed to be a Wiener process with zero mean and incremental covariance matrix $\mathbf{\Sigma}_W$. $\underline{e}$ denotes measurement noise with zero mean and covariance matrix $\mathbf{\Sigma}_e$. $\underline{W}$ are $\underline{e}$ are assumed to be mutually uncorrelated as usual. The thermal resistances, denoted by R in the presented Grey Box, are substituted by heat transmittances, i.e. $H = \frac{1}{R}$, in order to speed up the numerical implementation of the estimation.

A series of estimations have been conducted for $n_1 = 1.25$ (refer to Section 6.1), data subsampled to 20 minutes and different start values for the parameters. Every time, the estimate of parameter p converged to a value close to zero. As a consequence, estimation has been conducted for $n_1 = 1.25$ and $p = 0$, and the estimated parameters and the model performance are presented in Table 8.3 and Table 8.4, respectively.

Table 8.3. *Estimated model parameters for $n_1 = 1.25$ and $p=0$.*

Parameter	Unit	Est.	Std.	$R = 1/H$ K/W
C_a	MJ/K	1.09	$2.14\cdot10^{-4}$	–
C_f	MJ/K	5.01	$3.29\cdot10^{-2}$	–
H_a	W/K	12.8	0.362	$78\cdot10^{-3}$
H_w	W/K	12.0	0.199	$83\cdot10^{-3}$
H_f	W/K	283	0.894	$3.5\cdot10^{-3}$
Φ_0	W	556	0.100	–
A_w	m^2	3.37	$4.52\cdot10^{-3}$	–
$T_{an}(0)$	C	12.0	0.026	–
$T_{fn}(0)$	C	13.6	0.061	–
$T_{as}(0)$	C	12.8	0.063	–
$T_{fs}(0)$	C	15.6	0.165	–
$\sigma^2_{W,1}$	$(C/sec.)^2$	$3.84\cdot10^{-7}$	$1.53\cdot10^{-8}$	–
$\sigma^2_{W,2}$	$(C/sec.)^2$	$6.40\cdot10^{-7}$	$4.40\cdot10^{-8}$	–
$\sigma^2_{W,3}$	$(C/sec.)^2$	$2.23\cdot10^{-6}$	$6.19\cdot10^{-8}$	–
$\sigma^2_{W,4}$	$(C/sec.)^2$	$3.37\cdot10^{-6}$	$8.11\cdot10^{-8}$	–
$\sigma^2_{e,1}$	C^2	$1.03\cdot10^{-6}$	$1.10\cdot10^{-8}$	–
$\sigma^2_{e,2}$	C^2	$1.59\cdot10^{-6}$	$6.94\cdot10^{-7}$	–

Comparing the parameter estimates (see Table 8.3) with the expected values (see Table 8.1), it turns out that the estimated heat capacity of the floor C_f is close to the expectation, while the estimated thermal air capacity C_a is

Table 8.4. *Model performance parameters for* $n_1 = 1.25$ *and* $p = 0$.

	Model performance
$-\log \mathcal{L}$	-6917
Mean(P.E.)	$\mu_1 = -1.84 \cdot 10^{-3}$, $\mu_2 = -10.8 \cdot 10^{-3}$
Var(P.E.)	$\sigma_1^2 = 4.58 \cdot 10^{-4}$ $\sigma_2^2 = 26.1 \cdot 10^{-4}$ $\sigma_{1,2} = 0.192 \cdot 10^{-4}$

12 times larger. This larger value of C_a is not unrealistic, since the expected heat capacity was entirely based on the air in the test room. The larger value of C_a is mainly related to the thermal capacity of the Box, which is a part of the temperature zone, as defined in Section 8.2.1. The thermal resistances are smaller than the expected values, but as it has been mentioned earlier, the thermal resistances are based on an uncertain assessment of the convective coefficients, see Appendix C.1. Therefore the thermal resistances can be considered to be reasonable.

The estimated value $\widehat{\Phi}_0$ is larger than the expected nominal radiator power Φ_0. As mentioned in Section 8.3.2, the heat loss from the pipes is considerably and this aspect explains the larger value for the nominal radiator power Φ_0. Concerning the efficient window area A_w of room A_s, its estimate forms $3.37/4.8 \approx 70$ % of the physical window area, which actually is quite realistic. The estimated variances for the prediction error indicate that the model provides a better modelling of air temperature T_{an} than for T_{as}.

Based on the estimates in Table 8.3, a set of time constants corresponding to (8.25) and (8.27) can be computed:

$$\widehat{\tau}_a \approx 56 \text{ minutes} \quad \text{and} \quad \widehat{\tau}_f \approx 4.9 \text{ hours} \tag{8.36}$$

where $\widehat{\tau}_a$ is evaluated for $T_{rn,op} = 55$ °C and $T_{an,op} = 20$ °C (refer to (8.26)). Thus, the estimated time constant of the air is two times larger than the

expected (8.27), while the time constant of the floor is 10 times smaller the expected value (8.25) – a fact which is mainly due to the small value estimated for R_f.

Statistical tests of the prediction errors for T_{an} are presented in Figure 8.10. The autocorrelation function and the cumulated periodogram almost satisfies the white noise test, while there still exists unmodelled information in the input signals, as indicated by the crosscorrelation functions. The most significant values are found for the crosscorrelation between the water supply temperature T_{i2} and the prediction errors for T_{an}. Thus the part of the model related to the radiator power supply needs to be improved.

The model performance related to T_{an} is presented in Figure 8.11. The first subplot contains measurements and predictions for T_{an}, while the prediction error is plotted in the second subplot. Measurements and simulation are shown in the third subplot. The performance of the model is quite good, but it can be improved as indicated by the statistical tests.

Statistical tests of the prediction errors for T_{as} are presented in Figure 8.12. The autocorrelation function and the cumulated periodogram are not as "good" as for T_{an}. Also for T_{as} there exists unmodelled information in the input signals. The most significant values are found for the crosscorrelation between the solar radiation I_s and the prediction errors for T_{as}. Thus the part of the model related to the solar radiation needs to be improved. The part of the model related to the radiator power supply should also be improved as indicated by the particular crosscorrelation functions.

The model performance related to T_{as} is presented in Figure 8.13. The first subplot contains measurements and predictions for T_{as}, while the prediction error is plotted in the second subplot. Measurements and simulation are shown in the third subplot. The performance of the model for T_{as} is not quite as good as for T_{an}. Looking at prediction errors, the crosscorrelation between the solar radiation I_s and the prediction error is obvious. Furthermore, there is an offset between the measurement and simulation for T_{as}.

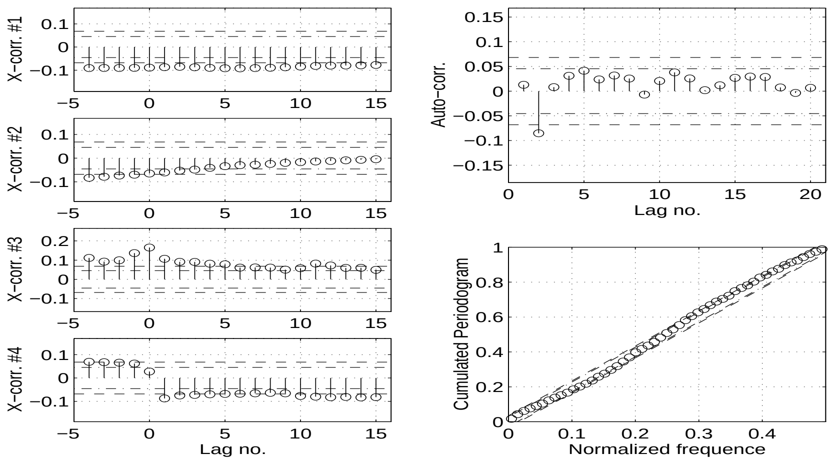

Figure 8.10. *Statistical tests for the prediction error of T_{an}; showing the autocorrelation, cumulated periodogram and the crosscorrelations between* $\#1 : T_b$, $\#2 : T_n$, $\#3 : T_{i2}$, $\#4 : \Phi_{ec}$ *and the prediction error.*

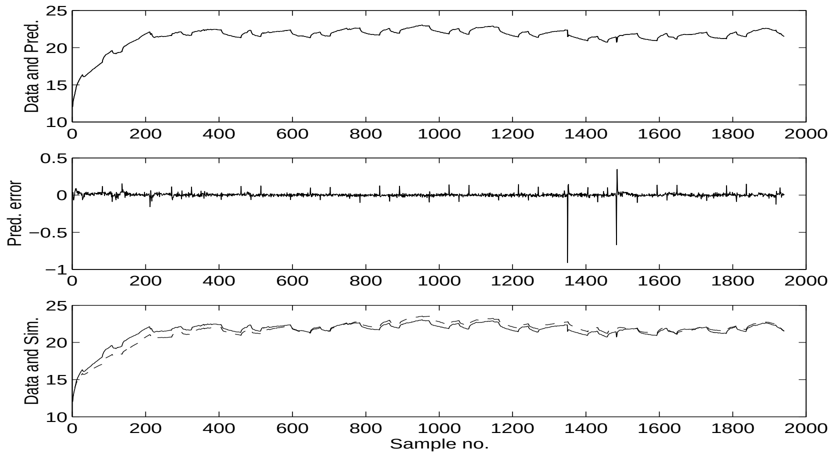

Figure 8.11. *Model performance for T_{an} with $n_1 = 1.25$ and $p = 0$ (Sample time: 20 minutes).*

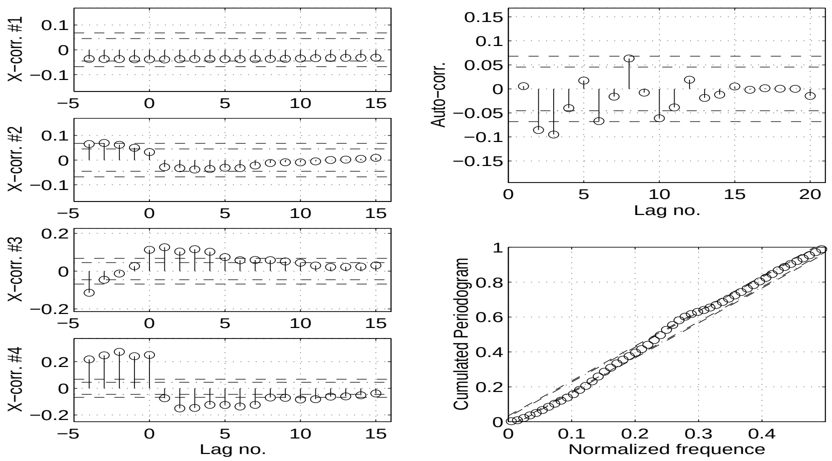

Figure 8.12. *Statistical tests for the prediction error of T_{as}; showing the autocorrelation, cumulated periodogram and the crosscorrelations between* $\#1 : T_b$, $\#2 : T_s$, $\#3 : T_{i1}$, $\#4 : I_s$ *and the prediction error.*

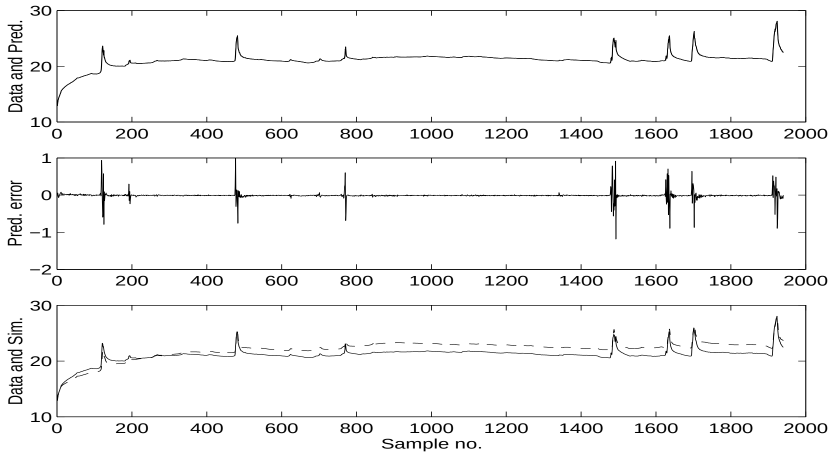

Figure 8.13. *Model performance for T_{as} with $n_1 = 1.25$ and $p = 0$ (Sample time: 20 minutes).*

It can be concluded that based on the statistical tests for the prediction errors, the test house model with the static radiator model cannot be accepted. But the test house model provides a reasonable description of the two room temperatures T_{an} and T_{as}.

8.4.3 Non Symmetric Radiator Power

The estimation result in the previous section can be used to reconsider the proposed test house model. The heat loss in the insulated pipes between Box 1 and Box 2 was originally assumed to be zero. Looking at the measurement data, it can be concluded that this assumption is unrealistic. Hence, the parameter Φ_0 covers both the nominal power of the radiator and the heat loss from the pipes. Since approximately 80 % of the pipes are located in room An, the heat loss from the pipes contributes non symmetric to the two test rooms. In order to model this aspect, the parameter Φ_0 is divide into $\Phi_{0,n}$ and $\Phi_{0,s}$. Applying these parameters to the proposed Grey Box model for the test house, implies replacement of (8.33) and (8.34) as presented in Appendix C.2.

The estimated parameters of the non symmetric radiator power model are presented in Table 8.5, while the model performance parameters are presented in Table 8.6. All the estimates are significant. $\Phi_{0,n}$ is larger than $\Phi_{0,s}$ as expected. Furthermore, $\Phi_{0,s}$ is closer to the data sheet value for the nominal radiator power. The mean values of the prediction error have decreased a factor 10. The other parameter estimates are approximately unchanged.

This alternative model formulation also implies small improvements of the statistical tests and in the model performance, refer to Appendix C.2. For example, no offset is present between the measurements and the simulation, as it is noted for T_{as} in Figure 8.13.

Thus, it can be concluded that the test house model with the non symmetric radiator heat submission provides a better description of data.

Table 8.5. *Estimated model parameters for $n_1 = 1.25$ and $p = 0$.*

Parameter	Unit	Est.	Std.	$R = 1/H$ K/W
C_a	MJ/K	1.13	$7.98 \cdot 10^{-3}$	–
C_f	MJ/K	4.64	$2.08 \cdot 10^{-1}$	–
H_a	W/K	17.4	0.816	$57 \cdot 10^{-3}$
H_w	W/K	12.5	0.333	$80 \cdot 10^{-3}$
H_f	W/K	275	7.53	$3.6 \cdot 10^{-3}$
$\Phi_{0,n}$	W	655	17.8	–
$\Phi_{0,s}$	W	460	10.3	–
A_w	m^2	3.56	$73.3 \cdot 10^{-3}$	–
$T_{an}(0)$	C	12.0	0.035	–
$T_{fn}(0)$	C	13.7	0.084	–
$T_{as}(0)$	C	12.9	0.070	–
$T_{fs}(0)$	C	15.9	0.169	–
$\sigma^2_{W,1}$	$(C/sec.)^2$	$3.89 \cdot 10^{-7}$	$1.65 \cdot 10^{-8}$	–
$\sigma^2_{W,2}$	$(C/sec.)^2$	$5.58 \cdot 10^{-7}$	$3.72 \cdot 10^{-8}$	–
$\sigma^2_{W,3}$	$(C/sec.)^2$	$2.24 \cdot 10^{-6}$	$9.85 \cdot 10^{-8}$	–
$\sigma^2_{W,4}$	$(C/sec.)^2$	$1.84 \cdot 10^{-6}$	$20.1 \cdot 10^{-8}$	–
$\sigma^2_{e,1}$	C^2	$1.06 \cdot 10^{-6}$	$1.75 \cdot 10^{-8}$	–
$\sigma^2_{e,2}$	C^2	$2.20 \cdot 10^{-6}$	$4.10 \cdot 10^{-7}$	–

8.4.4 Cross Validation

In the previous sections, two Grey Box models for the test house have been considered, one based on full symmetry and the other a perturbation of this model allowing asymmetric radiator heat submission. To facilitate the notation, let $\mathcal{M}_{fs}(\underline{\theta}_{fs})$ denote the full symmetric test house model and $\mathcal{M}_{ns}(\underline{\theta}_{ns})$ the other model.

It was concluded that model $\mathcal{M}_{ns}(\underline{\theta}_{ns})$ provided a better description of data than model $\mathcal{M}_{fs}(\underline{\theta}_{fs})$. A cross validation can be performed, in order to determine whether or not this is a general tendency, i.e. if the achieved estimates are locally or globally.

Table 8.6. *Model performance parameters for $n_1 = 1.25$ and $p = 0$.*

	Model performance
$-\log \mathcal{L}$	-7001
Mean(P.E.)	$\mu_1 = -0.140 \cdot 10^{-3}$, $\mu_2 = -0.682 \cdot 10^{-3}$
Var(P.E.)	$\sigma_1^2 = 4.47 \cdot 10^{-4}$ $\sigma_2^2 = 23.9 \cdot 10^{-4}$ $\sigma_{1,2} = 0.234 \cdot 10^{-4}$

The measurement data used for the cross validation are presented in Appendix C.3. The experimental conditions have been altered slightly for these measurements. The operating point is not the same as for the data presented in Section 8.3.2. Thus, the ability of the test house models to generalize is challenged.

The considered cross validation is focused on the covariance of the prediction error only. The results are presented in Table 8.7 and in Table 8.8. From these tables it can be concluded, that both sets of parameter estimates provide a general description of test house. Moreover, model $\mathcal{M}_{ns}(\underline{\theta}_{ns})$ performs slightly better than model $\mathcal{M}_{fs}(\underline{\theta}_{fs})$, as indicated by the smaller variances of the prediction errors.

Table 8.7. *Cross validation based on the variances of the prediction errors for $\mathcal{M}_{fs}(\underline{\theta}_{fs})$ with $n_1 = 1.25$ and $p = 0$.*

Covariance	from estimation	from evaluation
σ_1^2	$4.58 \cdot 10^{-4}$	$4.56 \cdot 10^{-4}$
σ_2^2	$26.1 \cdot 10^{-4}$	$26.1 \cdot 10^{-4}$
$\sigma_{1,2}$	$0.192 \cdot 10^{-4}$	$0.192 \cdot 10^{-4}$

The thermostatic valve is often accused for conducting on/off control of the radiator flow. Inspection of the estimation data in Figure 8.9 and of

Table 8.8. *Cross validation based on the variances of the prediction errors for $\mathcal{M}_{ns}(\underline{\theta}_{ns})$ with $n_1 = 1.25$ and $p = 0$.*

Covariance	from estimation	from evaluation
σ_1^2	$4.47 \cdot 10^{-4}$	$4.44 \cdot 10^{-4}$
σ_2^2	$23.9 \cdot 10^{-4}$	$23.8 \cdot 10^{-4}$
$\sigma_{1,2}$	$0.234 \cdot 10^{-4}$	$0.233 \cdot 10^{-4}$

the validation data in Figure C.7 with respect to the flows in Box 1 and Box 2 indicate active flow control during most of the measurement sequence. Especially for the validation data, it is visible, how the thermostatic valve in room As tries to counteract the changes in the heat input, which are due to changes in the heating unit supply temperature T_{hs} and in the solar radiation Φ_{sun}.

8.5 Summary

In this chapter the dynamic modelling of the thermal dynamics for a house has been considered. In the first section, the modelling approach based on the thermal network approximation technique was presented.

In Section 8.2 dynamic models of the thermal dynamics for the considered test house were established. Due to the closed loop system formed by the thermostatic valve, the radiator and the test room, three model formulations for different radiator models were derived.

An assessment on the time constants for the thermal dynamics of test house based on prior knowledge was presented in Section 8.3. These time constants were used to design the controllable input signals. As an alternative to the performed input design, a case study for a frequency domain design was reviewed.

The first of the proposed models for the considered test house was used for estimation. In order to decrease the number of parameters, the two test rooms, room An and room As, were assumed to be symmetric. The estimated parameters corresponded approximately to the parameters based on prior knowledge. Meanwhile, the time constant for the floor turned out to be 10 times smaller than expected. Validation of the model indicated crosscorrelations between the prediction error and the two inputs, the water supply temperature and the solar radiation. Introduction of an asymmetric heat input from the radiators improved the model performance. Moreover, a cross validation test showed that the estimated models provided reasonable descriptions of new measurement data.

For the considered estimation, the measurement data were subsampled to 20 minutes. When estimations with the two other proposed test house models are conducted, the measurement data should not be subsampled to more than 1 minute, due to the dynamic of the radiator.

Chapter 9

Central Heating System Simulation

The dynamic modelling and identification of the components in the central heating system have two potential applications, i.e. to serve as model for control design or to be used in system simulation.

This chapter is concerned with considerations on the simulation of the central heating system, which of course will be based on the established models of the components for the central heating system presented in the previous chapters. In the first section, some of the numerical challenges related to simulation of the central heating system are presented, while a short introduction of two different simulation approaches is the subject of the second section. The third section describes a solution to a particular simulation problem for the simulation tool Simulink.

9.1 Numerical Challenges

In this section the numerical challenges of conducting system simulation with the central heating system are considered.

The demands to a simulation tool can be formulated through an examination of the central heating system. The basic demand to the simulation tool is of course the ability to handle ordinary differential equations. The numerical implementation must be able to handle the following properties:

D1 stiffness of the central heating system. A stiff system is a dynamic system with considerably difference between the fastest and the slowest dynamic of the system.

D2 smooth nonlinearities of the central heating system. The term "smooth" covers the class of nonlinear functions with continuous gradients. An example of a smooth nonlinearity is the one exponent formula(for $\Delta T \geq 0$.

When these features are fulfilled, it is possible to conduct simulation for simplified system setups. For a complete system simulation, the simulation tool must be able to handle:

D3 discrete events. A discrete event (alias a discontinuous initial-value problem), for e.g. a first order differential equation $dX/dt = f(X(t), t)$, can be characterized as the point X_d for which $df/dX|_{X=X_d}$ is discontinuous. An example of a physical system with this property is a pipe or a thermostatic valve. The discrete events occur, when the flow in the pipe changes from laminar to turbulent or vice-versa, while the discrete event for the thermostatic valve is related to the opening and closing of the valve.

Moreover, to facilitate the implementation of the model, the model interface of the simulation tool should support:

D4 modularity. The implementation of the model is based on a modular structure with a standard interface for all components in the central heating system. In this way, it is easy e.g. to exchange one component with another.

In case of advanced system simulation, the simulation tool must support solution methods for:

D5 partial differential equations.

D6 stochastic differential equations.

9.2 Simulation Tools

As described in Section 8.1, a number of commercial simulation tools already exist for thermal building simulation. The tools are based on finite element techniques (distributed parameter models) with predefined models of the building components. A model established in one of these tools usually is of high order.

The alternative to the finite element technique is lumped parameter modelling. For this purpose, a number of more or less commercial simulation tools can be listed: ACSL, Dymola, Omsim, Simulink. The list is not complete. A model established in one of these tools is of low order compared to a corresponding model established in one of the finite element tools.

The choice of simulation tool depends on the purpose of the simulation. The two approaches, addressed above, have their own advantages and disadvantages, in relation to the imposed demands.

The established component models, presented in Chapter 5, 6, 7 and 8 are all lumped parameter models. As simulation tool, Simulink is selected due to its relative friendly user interface. This tool satisfies only demand D1 and D2. Hence, D4 is the subject of the next section in order to improve the applicability of the tool.

9.3 Hydraulic System Simulations

This section deals with the problem of how to implement a modular model structure in a simulation environment based on transfer function. The considered simulation tool is Simulink ver. 4.2. The presented approach follows the outline of *(Hansen et al., 1995)*.

It is well known that a network solution (i.e. transfer function) can be found for an electrical circuit. A disadvantage of the network solution is that it must be recomputed if the electrical circuit is changed, e.g. by adding or removing a component in the circuit. This drawback can be avoided using a modular model. Another advantage of the modular model is that the modular structure depicts the structure of the modelled physical system. Meanwhile, some basic problems arise if a modular model (i.e. implicit differential equations) is going to be implemented in Simulink. The reason is, that Simulink is constructed to handle transfer functions (i.e. explicit differential equations).

In *(Flinders et al., 1993)* a "Dynamic Node Technique" is suggested. The idea in this technique is to arrange a circuit into functional circuit elements (devices), which are interconnected by circuit nodes, as illustrated in Figure 9.1.

These circuit nodes contain a capacitance, which can be regarded as being a parasitic circuit capacitance lumped at the circuit node. The value of a nodal capacitance can be selected as a tradeoff between a small approximation error and a small simulation time, but also values with physical interpretation can be used.

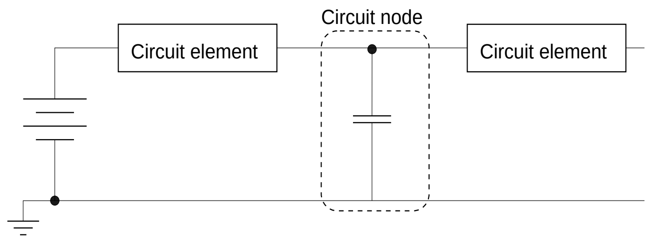

Figure 9.1. *Structure of the Dynamic Node Technique.*

The hydraulic Simulink model approach consists in modelling each component, in e.g. a heating system, as a two port element. The basic idea is to model the pressure drop and the flow in the pipe system, and to use "physical" knowledge about the two port element in the selection of the nodal capacitance.

9.3.1 Two Port Pipe Element

The pipe modelling was described in Chapter 5 and the model for flow in a pipe was presented in Model Summary 5.1. For laminar flow q, the model can be expressed in terms of *(Hansen et al., 1995)*, as follows:

$$\frac{dq}{dt} = K_i(\Delta p - K_l q) \tag{9.1}$$

where $K_i = \frac{1}{L} = \frac{A}{\rho l}$, $K_l = R_l = 32\frac{\rho l \nu}{d^2 A}$ and $\Delta p = p_{in} - p_{out}$. The transfer function from Δp to q is:

$$\frac{Q_i(s)}{\Delta P(s)} = \frac{G_p}{\tau_p s + 1} \tag{9.2}$$

where $G_p = \frac{1}{K_l}$, $\tau_p = \frac{1}{K_i K_l}$, $\omega_p = K_i K_l$ and s the Laplace operator. An electrical equivalent to the laminar case was shown in Figure 5.5.

Now that a simple pipe model is established, the next step is to put two pipe models together, as shown in Figure 9.2.

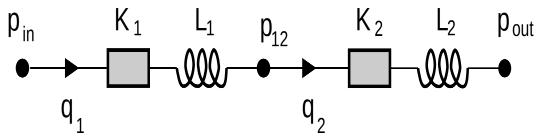

Figure 9.2. *Electrical equivalent for two pipe elements in series.*

The network solution to Figure 9.2 is:

$$\frac{dq}{dt} = \frac{1}{L_1 + L_2}\left(p_{in} - p_{out} - (K_1 + K_2)q\right) \tag{9.3}$$

as $q = q_1 = q_2$. Meanwhile, this system can not be modularly modelled, since there are three variables and only two equations.

To solve this problem, the pipe model for laminar flow (illustrated in Figure 5.5) is expanded with a nodal capacitance and nodal resistance, as illustrated in Figure 9.3.

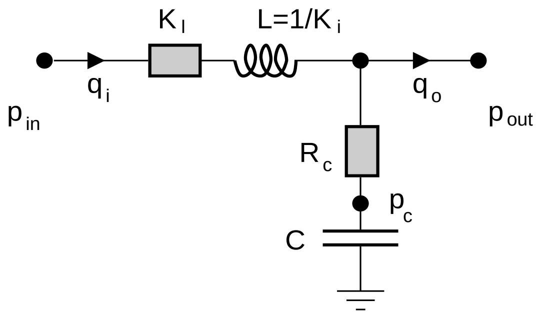

Figure 9.3. *Electrical equivalent of two port element.*

The new parameters, C and R_c, can be physical interpreted: C as the elasticity of the pipe wall, while R_c as a elasticity loss factor. Let p_c denote

the pressure between C and R_c in Figure 9.3. Thus, a network inspection yields the following two differential equations:

$$\frac{dp_c}{dt} = \frac{1}{C}(q_i - q_o) \tag{9.4}$$

$$\frac{dq_i}{dt} = K_i(p_{in} - p_c - (R_c + K_l)q_i + R_c q_o) \tag{9.5}$$

The new model can be considered as a two port element, where the node is placed "inside" the model – instead of outside, as in *(Flinders et al., 1993)*. Thus, selecting p_{in} and q_o as inputs, the following state space equation can be achieved:

$$\frac{d}{dt}\underline{x} = \begin{bmatrix} 0 & \frac{1}{C} \\ -K_i & -K_i(R_c + K_l) \end{bmatrix}\underline{x} + \begin{bmatrix} 0 & -\frac{1}{C} \\ K_i & K_i R_c \end{bmatrix}\underline{u} \tag{9.6}$$

with the output equation:

$$\underline{y} = \begin{bmatrix} 1 & R_c \\ 0 & 1 \end{bmatrix}\underline{x} + \begin{bmatrix} 0 & -R_c \\ 0 & 0 \end{bmatrix}\underline{u} \tag{9.7}$$

where $\underline{x} = (p_c, q_i)^\top$, $\underline{u} = (p_{in}, q_o)^\top$ and $\underline{y} = (p_{out}, q_i)^\top$.

The implementation in Simulink of the hydraulic two port pipe model (9.6) is illustrated in Figure 9.4, using standard components.

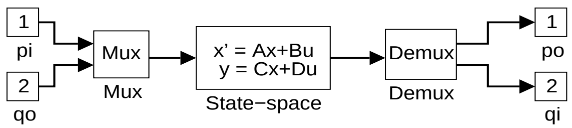

Figure 9.4. *Two port pipe model build of standard components.*

Two Port Radiator Element

From a hydraulic point of view, the radiator can be modelled as just a special pipe, since the sectional area of the radiator is bigger and it is rectangular. A hydraulic diameter d_r, as in (6.12), is used to rescale the radiator to a equivalent pipe:

$$d_r = \frac{4A_r}{P_r} \tag{9.8}$$

where A_r denotes the sectional area of the radiator and P_r the perimeter of this sectional area.

The entering flow (ditto the outgoing) could cause some turbulence in the water, which could invoke an extra pressure drop. This pressure drop p_t due to turbulence can be described as:

$$\Delta p_t = K_t q^2 \tag{9.9}$$

where K_t denotes the turbulent pressure drop factor. The implementation of the hydraulic two port radiator model, sketched in Figure 9.5, is based on the two port pipe model shown in Figure 9.4. Data regarding the radiator is used in the *Pipe* block of Figure 9.5, while the *Fnc* block is introduced for the implementation of (9.9).

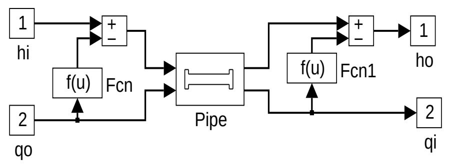

Figure 9.5. *Two port radiator model.*

9.3.2 Model of Circulating Pump

The static relation between the pump pressure Δp_p and the pump flow q can under ideal conditions be modelled as, *(Pfleiderer, 1961)*:

$$\Delta p_p = \Delta p_{\max} \left(\left(\frac{n}{n_{\max}} \right)^2 - \left(\frac{q}{q_{\max}} \right)^2 \right) \tag{9.10}$$

where n denotes the speed of the pump, and $\Delta p_{\max}$, $n_{\max}$ and $q_{\max}$ are characteristic pump data. This static relation is used in the dynamic simulation. The dynamic in the entire pump is introduced through the pump speed. In Figure 9.6 an implementation of (9.10) is presented. The two port structure, (p_{in}, q_o) as inputs and (p_{out}, q_i) as outputs, has been maintained, but an extra input, the pump speed n, has been added.

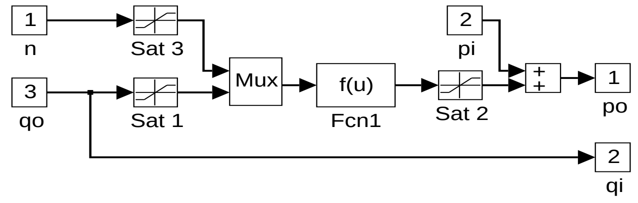

Figure 9.6. *Circulating pump model.*

9.3.3 Nodal Design

The characteristic polynomial of the state space model (9.6) is given by:

$$\det(sI - \boldsymbol{A}) = s^2 + K_i(R_c + K_l)s + \frac{K_i}{C} \tag{9.11}$$

An idea on how to select C and R_c, can be obtained by comparing (9.11) with the well-known characteristic polynomial of a second order system:

$s^2 + 2\zeta\omega_n s + \omega_n^2$, where ω_n denotes the undamped natural frequency and ζ the damping ratio of the system. Thus:

$$\omega_n^2 = \frac{K_i}{C} \quad \text{and} \quad 2\zeta\omega_n = K_i(R_c + K_l) \tag{9.12}$$

It follows that C and R_c can be calculated as:

$$C = \frac{K_i}{\omega_n^2} \quad \text{and} \quad R_c = \frac{2\zeta\omega_n}{K_i} - K_l \tag{9.13}$$

Introducing N as a fitting factor, the undamped natural frequency should be selected N times larger than ω_p the bandwidth of the pipe model. From (9.2) is follows:

$$\omega_n = N\omega_p = NK_iK_l \tag{9.14}$$

The design of the nodal parameters C and R_c is now based on the selection of the fitting factor N and of the damping ratio ζ of the system. The fitting factor N is a tradeoff between fit goodness (a big N-value, i.e. $N \gg 5$, gives a good fit) and simulation time (a small N-value, i.e. $N \approx 5$, yields a short simulation time).

9.3.4 Heating System Simulation

The described elements can now be used to model a simple heating system. An example of such a system is presented in Figure 9.7. In this example, the simulation model consists of: one pump, four pipes and three radiators.

Heating System Data

The considered pump in Figure 9.7 (e.g. a UPS 25-60 180) is characterized by $\Delta p_{\max} = 6$ mWc, $n_{\max} = 1800$ rpm and $q_{\max} = 4.5$ m^3/h.

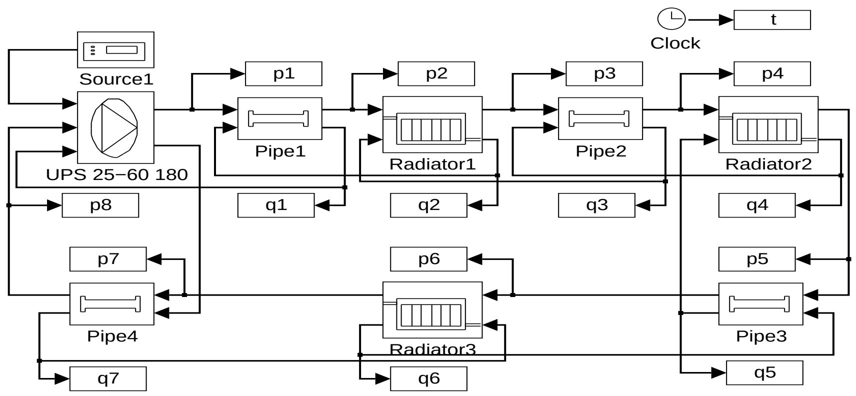

Figure 9.7. *Hydraulic model of a heating system.*

The pipes, 1 and 4, and the pipes, 2 and 3, are considered to be 10 m and 5 m long, respectively. All four pipes have a diameter of 0.015 m. The radiators are considered to be 2 m long with a sectional area of $0.01 \times 0.25 = 0.0025$ m^2, i.e. a volume of 5 liters. The turbulent pressure drop factor is set to $K_t = 2 \cdot 10^{-5}$.

Based on (9.2), the bandwidth of the pipes is about 3.4 Hz. Using the hydraulic diameter (9.8) in model (9.1), the bandwidth of the radiators is found to be about 0.5 Hz.

System Simulation

Before any simulation is started, a pump speed input signal and values for the fitting factor N and the damping ratio ζ have to be selected.

The pump speed signal is chosen as a 1 Hz sinusoidal signal – which forms a tradeoff between the bandwidth of the pipes and the radiators. It is known that a damping ratio value of $\zeta = 0.7$ a good compromise (see e.g.

(Katsuhiko, 1970)). Regarding the fitting factor N, a value of 30 provides a good fit. A simulation with these parameters has been performed and the result is shown in Figure 9.8.

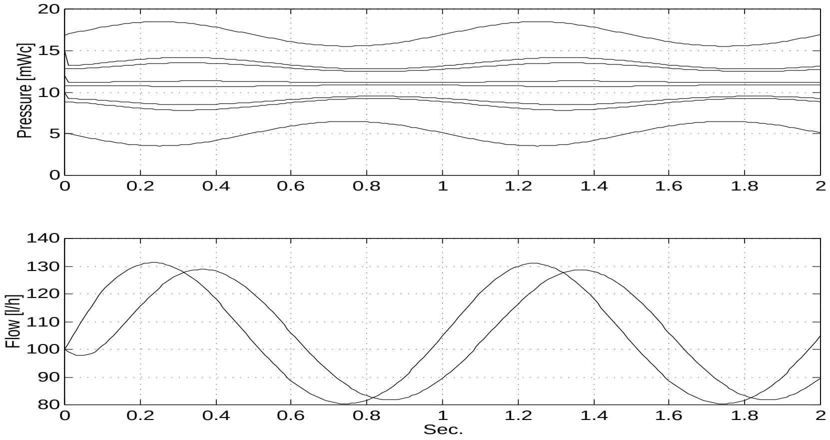

Figure 9.8. *Heating system simulation for* $N=30$ *and* $\zeta=0.7$.

In Figure 9.8, the pressures p1,$\cdots$, p8 and the flows q1,$\cdots$, q7, of the simulation are plotted. A phase shift in the pressures can be noted from p1 (the upper signal) towards p4 and back again from p5 towards p8. The flows in Figure 9.8 are gathered in two groups. The first group contains q1, q2 and q7, i.e. the flows regarding *Pipe1* and *Pipe4*, while the second group contains q3,$\cdots$, q6. In the pipe model the water is assumed to be incompressible. Therefore, a big elasticity of pipe/radiator walls represents the only explanation to the phase between the two groups of flow.

In the design phase, the nodal parameters were determined based on the dynamic upstream the node (see Figure 9.3). It can be argued that the nodal design also must satisfy the dynamic downstream the node, i.e. the fastest of the two adjacent dynamics should be used in the design of the nodal parameters.

Let N_p and N_r denote the fitting factor used in a two port pipe element and in a two port radiator element, respectively. Since the ratio between the bandwidth of the pipe and of the radiator is $3.4/0.5 \approx 7$, N_r should be selected as $N_r = 7N_p$.

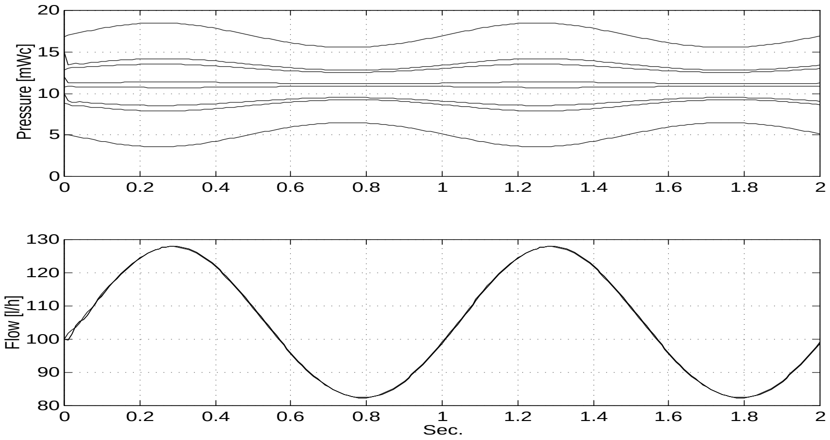

Figure 9.9. *Heating system simulation* $N_p=30$, $N_r=210$ *and* $\zeta=0.7$.

Figure 9.9 shows a new simulation using $N_p = 30$ and $N_r = 210$ as fitting factors. All the flows are now in phase, as they should be. From the second simulation it can be concluded, that a complete modular structure is not possible. It is necessary to apply knowledge from the adjacent elements.

9.4 Summary

Considerations on system simulation of the central heating system have been the issue of this chapter. The central heating system has shown to be quite nonlinear. Hence, a number of demands to the simulation tool has been presented in the first section, while a short description of two simulation approaches was the subject of the second section.

Simulink was selected from the group of simulation tools, adequate for lumped parameter models. This tool did only support the first two demands. Thus, in order to improve the applicability of the tool with respect to support of modular model structures, a dynamic node technique was considered and applied for the hydraulic part of the central heating system, in the third section. As it was exemplified by two simulations, complete modularity was not possible for the considered approach. It was necessary to apply knowledge about the dynamic of the adjacent elements in the nodel design.

A task for the future is to implement the same hydraulic system in ASCL, Dymola and Omsim in order to find the most adequate simulation tool for central heating system simulation.

Chapter 10

Conclusion

The present thesis is concerned with system identification and experimental design for the following components in the water based central heating system: pipe, radiator, thermostatic valve and house. The summary of each chapter may be consulted for more detailed information. The major conclusions are summarized below.

The main objective of this thesis was to enhance the insight into the dynamic properties of water based central heating systems and to contribute to an improved understanding of how this system operates. For the system identification, estimation and validation, the Grey Box modelling method was applied. The goal was to establish a number of dynamic models for individual components in the central heating system. The motivation for the presented modelling was to provide better component models for the complete modelling of the dynamic performance of the central heating system.

In Chapter 2, the mathematical properties of the Grey Box modelling method were presented. The model class of this method was based on stochastic differential equations, thus nonlinear system structure could be preserved in the model. The estimation method was based on the maximum likelihood method. The Kalman filter was used to provide the estimation method with conditional mean and covariance of the one step prediction error. Some validation methods were also described for the validation of the parameter estimates and of the model performance. The Grey Box modelling method is superior to the Black and White Box modelling methods. Meanwhile, the drawback of the Grey Box modelling method is the enhanced computational efforts. The estimation method and some of the validation methods are implemented in the program package CTLSM. This estimation tool has been used throughout thesis.

Experimental design is closely related to system identification. Some of the basic ideas were presented in Chapter 3. Firstly, the problem of identifiability was addressed. Two aspects were found to be important, i.e. informative data and structural identifiability. Secondly, some considerations on sampling, filtering and subsampling were given. Finally, two input design methods were reviewed.

In order to facilitate the experimental design for the system identification of the selected components of the central heating system, two experimental setups were constructed – one of a pipe system and one of a central heating system. The experimental setups and the test house setup were described in Chapter 4. A number of changes and improvements were advised, in order to improve the experimental conditions of these experimental setups.

In Chapter 5, the modelling of the flow in a straight circular water pipe was discussed. The pipe flow model was derived based on one-dimensional incompressible flow and on conservation of mass and momentum. The resulting nonlinear model of the pipe flow was gathered in Model Summary 5.1. The experimental conditions were analyzed and a Grey Box model was formulated for turbulent flow. Estimation results based on data from the pipe setup showed that, the nonlinear model for the pipe flow had to be extended with an instantaneous flow (a direct term), whose physical

interpretation was found to be related to a time delay. The extended model provided an acceptable model performance. Two types of input signals were used in the measurement: PRBS and PRUS signals. Comparing the model performance corresponding to these input signals, the model based on the PRUS signal performed slightly better than based on the PRBS signal.

The modelling of the radiator was considered in Chapter 6. The state of the art, described in the technical literature, concerning this component – as far as the author is aware – is mainly static models. In this thesis the hydraulic and thermal dynamics were investigated. Comparing the expected hydraulic dynamic of the radiator with that of a pipe, it was concluded that the hydraulic radiator dynamic could be neglected. A couple of dynamic thermal radiator models were presented in Model Summary 6.1 and 6.2. These dynamic models were based on a partial differential equation for the cooling of a one dimensional water flow. The experimental conditions were analyzed and it was concluded that the applicability of the experimental setup of the central heating system was limited, regarding system identification of a dynamic radiator model. Furthermore, the theoretical radiator power (i.e. based on the one exponent formula) was compared with the actual submitted radiator power and a significant deviation was notable. It was not determined whether the calibrated nominal power for the applied radiator could be wrong or if the one exponent formula was that misguiding (away from the standard conditions). The world is not ideal and therefore, given the experimental conditions for the radiator - which in this setup reflects reality more than an ideal situation - the modelling was continued and a Grey Box model for the radiator model in Model Summary 6.1 was formulated. The estimation result showed that an approximation of order two had the best performance. In the case of the local operation point data, the radiator model almost provided a satisfying description of the data. For the moving operating point (the general case), the performance was worse. Thus, the investigated radiator model provided an usable (but far from perfect) description of the thermal radiator dynamic.

It is suggested that a dedicated setup is designed for the system identification of the radiator. Moreover, it would be advisable to use a larger radiator in this setup. From an experimental design point of view, the setup should accommodate independent control of the input signals to the radiator model, i.e. for the temperature of the supply water, the flow of the water and the ambient temperature. Furthermore, measurements of the radiator surface temperature would be preferable.

Chapter 7 dealt with the modelling of the gas based thermostatic valve. A relative comprehensive introduction was presented for this components in order to "get acquainted". From the sparse technical literature for this component, it was concluded that the gas based thermostatic valve was quite nonlinear. Two modelling approaches were considered. The first modelling approach was based on the second law of Newton, implying a model with many parametersand the need of very precise knowledge about the geometrical layout of the valve. From a structural identifiability point of view, the resulting model of this approach was very inconvenient. Therefore, a macroscopic modelling approach was applied. The proposed model was gathered in Model Summary 7.1. This thermostatic valve model did not contain the nonlinear effect of hysteresis and elasticity, but it did reflect the non smooth behavior of the thermostatic valve in the closing point. An analysis of the hydraulic interaction between thermostatic valve and the "rest" of the central heating system led to the additional Model Summary 7.2. The experimental conditions for the thermostatic valve setup were analyzed and a Grey Box model was formulated. Due to the non smooth property at the closing point of the thermostatic valve, the input design was constrained to avoid this situation. The large hydraulic resistance of the flow meter made the input design quite complicated. Therefore, a PRBS signal with a very small fundamental time period was applied – supplied with human supervision, in order to avoid the closing situation. Two set of data were presented and used in the estimation of the two models. The estimation results for the first data set showed that both models provided a reasonable description, but the prediction errors were corrupted due to the too fast PRBS signal.

The second data set did not contain the same periodic behaviour as the first data set. Estimation results for the second data set indicated that, both model formulations provided a satisfactory description.

If the experimental conditions for the system identification of the thermostatic valve should be improved, the first aspect would be to decrease the hydraulic resistance of the flow meter or to use a thermostatic valve with a smaller flow capacity. The purpose of this modification is to increase the pressure drop over the thermostatic valve, when it is full open. Moreover, this would increase the relative temperature range, for which the thermostatic valve has influence on the valve flow. This modification would also facilitate the input design. The second aspect would be to accommodate independent control of the water flow and of the temperature of the supply water. When this improvement has been executed, it makes sense to try to identify the time constant from the supply water to the temperature of the gas in the thermostatic head.

The modelling of the test house was described in Chapter 8. The thermal network approximation technique was applied in the modelling. The test house was divided into main temperature zones, where the temperature reasonably was considered uniform. Each zone was characterized by a thermal capacity and a number of thermal resistances describing the heat transport paths to the adjacent zones. A concept of auxiliary zones was also introduced. These auxiliary zones did not have an associated thermal heat capacity. A dynamic model consisting of four main zones and three auxiliary temperature zones was established. Due to the closed loop formed by the thermostatic valve, the radiator and the test room, three model formulations for different radiator models were proposed. The first of these models was used for estimation. The number of parameters of this model was reduced based on the assumption of symmetric test rooms. The validation of the model performance indicated unmodelled dynamics in the two input signals related to the radiator and the solar radiation. Introduction of an asymmetric heat input from the radiators improved the model performance.

System simulation of the central heating system was the issue of Chapter 9. A list of demands to the simulation tool was presented, together with a short introduction of two simulation approaches, one based on a distributed parameter model (finite element method) and one based on a lumped parameter model. The latter approach was relevant for the established component models. Simulink was selected as tool. In order to improve applicability of this tool with respect to support of modular model structures, a dynamic node technique was considered. However, complete modularity was not possible for the considered approach.

Research always leads to new questions and new ideas. For example, assuming that the identification of a pipe flow model for laminar flow is a formality, then the challenging issue for the future work for the pipe modelling is to find a proper model concept for the transition between laminar and turbulent flow. Another project for the future is to perform estimation in the closed loop system of the test house.

Appendix A

Properties of Water

This appendix is concerned with some physical properties of water. In Table A.1 the density ρ, the specific heat c_p, the thermal conductivity λ and the the kinematic viscosity ν are list as function of the water temperature T_w.

In the second section, linear regression is used to describe the relation between the water temperature T_w and the physical properties of water presented in Table A.1.

The third section investigates the product of the specific heat c_p and the density ρ, which is of interest for the pipe and radiator modelling. It is shown that, it is reasonable to consider H_q as a constant.

A.1 Table on Water Properties

The data presented in Table A.1 on thermodynamic properties of water are compiled from *(Raznjević, 1976)*.

Table A.1. *Thermodynamic properties of water at the saturation pressure.*

T_w	ρ	c_p	λ	$\nu \times 10^{-6}$
0	999.9	4.226	0.558	1.789
5	1000.0	4.206	0.568	1.535
10	999.7	4.195	0.577	1.300
15	999.1	4.187	0.587	1.146
20	998.2	4.182	0.597	1.006
25	997.1	4.178	0.606	0.884
30	995.7	4.176	0.615	0.805
35	994.1	4.175	0.624	0.725
40	992.2	4.175	0.633	0.658
45	990.2	4.176	0.640	0.611
50	988.1	4.178	0.647	0.556
55	985.7	4.179	0.652	0.517
60	983.2	4.181	0.658	0.478
65	980.6	4.184	0.663	0.444
70	977.8	4.187	0.668	0.415
75	974.9	4.190	0.671	0.366
80	971.8	4.194	0.673	0.364
85	968.7	4.198	0.676	0.339
90	965.3	4.202	0.678	0.326
95	961.9	4.206	0.680	0.310
100	958.4	4.211	0.682	0.294
°C	kg/m^3	kJ/kg K	W/m K	m^2/s

A.2 Regression

Linear regression is the simplest type of parametric model. The regression concept is quite common in statistics and it is used to describe the static relations. It was initially used for calculating orbits of the planets, by Gauss in 1809.

Consider the linear model:

$$y(k) \;=\; \underline{x}^{\top}(k)\,\underline{\theta} \;+\; e(k) \tag{A.1}$$

where $y(k)$ is a deterministic measurable quantity, also called regressed variable. $\underline{x}(k)$ is the regressor vector, which contains known quantities, while $\underline{\theta}$ is the parameter vector which is desired to be estimate. $e(k)$ denotes the error between the measurement and the model, and it is a stochastic variable. Variable k takes integer values and it denotes a counter variable. The linear model can be written on the following matrix form:

$$\underline{y} \;=\; \boldsymbol{X}\,\underline{\theta} \;+\; \underline{e} \tag{A.2}$$

where:

$$\underline{y} = \begin{bmatrix} y(1) \\ \vdots \\ y(N) \end{bmatrix}, \qquad \boldsymbol{X} = \begin{bmatrix} \underline{x}^{\top}(1) \\ \vdots \\ \underline{x}^{\top}(N) \end{bmatrix},$$
$$\underline{\theta} = \begin{bmatrix} \theta_1 \\ \vdots \\ \theta_{np} \end{bmatrix}, \qquad \underline{e} = \begin{bmatrix} e(1) \\ \vdots \\ e(N) \end{bmatrix} \tag{A.3}$$

where N is the number of measurements and np is the number of parameters which should be estimated.

The problem is to find an estimate $\widehat{\underline{\theta}}$ which minimize the loss function V, the sum of squares of errors:

$$V(\underline{\theta}) = \sum_{k=1}^{N} \underline{e}^\top \underline{e} = \sum_{k=1}^{N} (\underline{y} - \boldsymbol{X}\,\underline{\theta})^\top (\underline{y} - \boldsymbol{X}\,\underline{\theta}) \tag{A.4}$$

Suppose that the matrix $\boldsymbol{X}^\top \boldsymbol{X}$ is positive definite. Than the least square estimator for the parameter vector $\underline{\theta}$ is:

$$\widehat{\underline{\theta}} = (\boldsymbol{X}^\top \boldsymbol{X})^{-1} \boldsymbol{X}^\top \underline{y} \tag{A.5}$$

The covariance matrix $\boldsymbol{P}$ of $\widehat{\underline{\theta}}$ is given by:

$$\boldsymbol{P} = \sigma_e^2 \, (\boldsymbol{X}^\top \boldsymbol{X})^{-1} \tag{A.6}$$

where σ_e^2 denotes the variance of residuals $\underline{e}$. An unbiased estimate of σ_e^2 is given by:

$$\widehat{\sigma}_e^2 = \frac{1}{N - np} V(\widehat{\underline{\theta}}) \tag{A.7}$$

The model is considered valid when the residuals $\underline{e}$ are white noise and the standard deviation $\widehat{\sigma}_e$ is less than 1 % of the difference between maximum and minimum values of measurement data.

A.2.1 On Water Density

Based on water density data, presented in Table A.1, the following linear regression model is suggested:

$$\rho(T_w) = \theta_3 \left(\frac{T_w}{100}\right)^2 + \theta_2 \left(\frac{T_w}{100}\right) + \theta_1 \sin\left(\frac{2\pi}{3}\,\frac{T_w}{100}\right) + \theta_0 \tag{A.8}$$

The estimate of the parameters and of the variance of the residuals are:

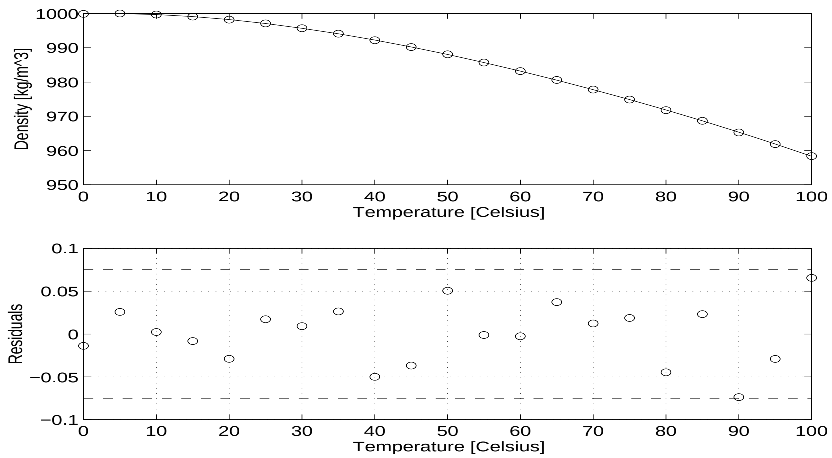

Figure A.1. *Regression's performance on water density.*

$$\begin{aligned}
\widehat{\theta}_3 &= \text{-72.2} && \pm\ 9.1{\cdot}10^{-1}\\
\widehat{\theta}_2 &= 48.9 && \pm\ 1.4\\
\widehat{\theta}_1 &= \text{-21.1} && \pm\ 5.2{\cdot}10^{-1}\\
\widehat{\theta}_0 &= 1000 && \pm\ 3.0{\cdot}10^{-2}\\
\widehat{\sigma}_e^2 &= 1.4\ {\cdot}10^{-3}
\end{aligned}$$

Data and regression between density ρ and temperature of the water T_w are illustrated in the upper half of Figure A.1, while the residuals and the confidence interval 95 % are shown in the lower half of the figure.

A.2.2 On Heat Capacity

Based on heat capacity data, presented in Table A.1, the following linear regression model is suggested:

$$c_p(T_w) \quad = \quad \theta_4 \left(\frac{T_w}{100}\right)^3 + \theta_3 \left(\frac{T_w}{100}\right)^2 + \theta_2 \left(\frac{T_w}{100}\right)$$

$$+\,\theta_1\,\exp\left(-\frac{T_w}{14}\right)\,\sin\left(\frac{2\pi}{3}\,\frac{T_w}{100}\right)+\,\theta_0 \qquad \text{(A.9)}$$

The estimate of the parameters and of the variance of the residuals are:

$$\begin{aligned}
\widehat{\theta}_4 &= \text{-}109 \quad \pm\, 6.4\\
\widehat{\theta}_3 &= 316 \quad \pm\, 9.9\\
\widehat{\theta}_2 &= \text{-}222 \quad \pm\, 3.7\\
\widehat{\theta}_1 &= \text{-}118 \quad \pm\, 5.8\\
\widehat{\theta}_0 &= 4226 \quad \pm\, 0.42\\
\widehat{\sigma}_e^2 &= 0.20
\end{aligned}$$

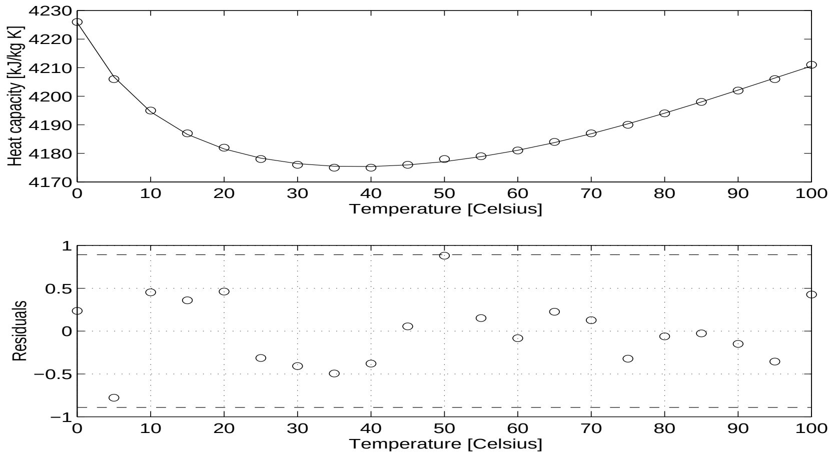

Figure A.2. *Regression's performance on heat capacity.*

Data and regression between heat capacity c_p and temperature of the water T_w are illustrated in the upper half of Figure A.2, while the residuals and the confidence interval 95 % are shown in the lower half of the figure.

A.2.3 On Heat Conductivity

Based on heat conductivity data, presented in Table A.1, the following linear regression model is suggested:

$$\begin{aligned}
\lambda(T_w) \quad = \quad & \theta_4\left(\frac{T_w}{100}\right)^3+\theta_3\left(\frac{T_w}{100}\right)^2+\,\theta_2\left(\frac{T_w}{100}\right)\\
& +\,\theta_1\sin\left(\frac{2\pi}{3}\,\frac{T_w}{100}\right)+\,\theta_0 \qquad \text{(A.10)}
\end{aligned}$$

The estimate of the parameters and of the variance of the residuals are:

$$\begin{aligned}
\widehat{\theta}_4 &= 1.23{\cdot}10^{-1} \quad \pm\, 1.9{\cdot}10^{-2}\\
\widehat{\theta}_3 &= 7.17{\cdot}10^{-2} \quad \pm\, 1.9{\cdot}10^{-2}\\
\widehat{\theta}_2 &= \text{-}2.52{\cdot}10^{-1} \quad \pm\, 6.0{\cdot}10^{-2}\\
\widehat{\theta}_1 &= 2.09{\cdot}10^{-1} \quad \pm\, 2.7{\cdot}10^{-2}\\
\widehat{\theta}_0 &= 5.58{\cdot}10^{-1} \quad \pm\, 0.00\\
\widehat{\sigma}_e^2 &= 2.0\cdot\cdot10^{-7}
\end{aligned}$$

Data and regression between heat conductivity λ and temperature of the water T_w are illustrated in the upper half of Figure A.3, while the residuals and the confidence interval 95 % are shown in the lower half of the figure.

A.2.4 On Kinematic Viscosity

Based on kinematic viscosity data, presented in Table A.1, the following linear regression model is suggested:

$$\begin{aligned}
\nu(T_w) \quad = \quad & \theta_4\left(\frac{T_w}{100}\right)^3+\theta_3\left(\frac{T_w}{100}\right)^2+\,\theta_2\left(\frac{T_w}{100}\right)\\
& +\,\theta_1\,\exp\left(-\frac{T_w}{14}\right)\,\sin\left(\frac{2\pi}{3}\,\frac{T_w}{100}\right)+\,\theta_0 \qquad \text{(A.11)}
\end{aligned}$$

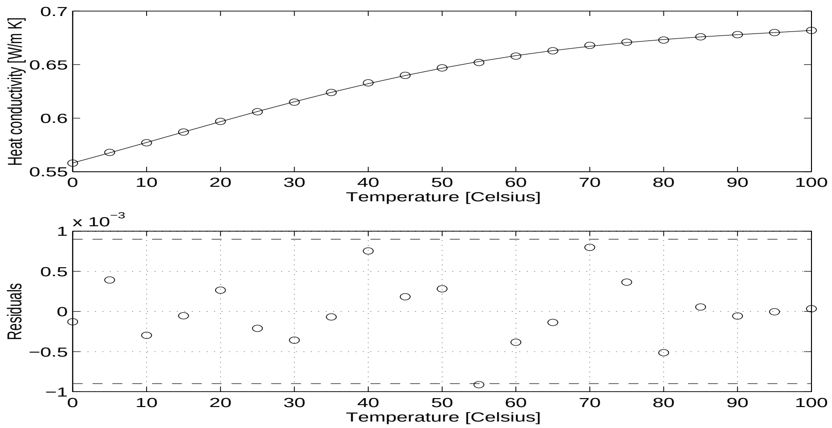

Figure A.3. *Regression's performance on heat conductivity.*

The estimate of the parameters and of the variance of the residuals are:

$$
\begin{aligned}
\widehat{\theta}_4 &= \text{-1.57} \pm 1.5{\cdot}10^{-1}\\
\widehat{\theta}_3 &= \ \ 4.21 \pm 2.3{\cdot}10^{-1}\\
\widehat{\theta}_2 &= \text{-4.15} \pm 8.6{\cdot}10^{-2}\\
\widehat{\theta}_1 &= \text{-1.18} \pm 1.3{\cdot}10^{-1}\\
\widehat{\theta}_0 &= \ \ 1.80 \pm 9.7{\cdot}10^{-2}\\
\widehat{\sigma}_e^2 &= 1.1 \cdot 10^{-4}
\end{aligned}
$$

Data and regression between kinematic viscosity ν and temperature of the water T_w are illustrated in the upper half of Figure A.4, while the residuals and the confidence interval 95 % are shown in the lower half of the figure.

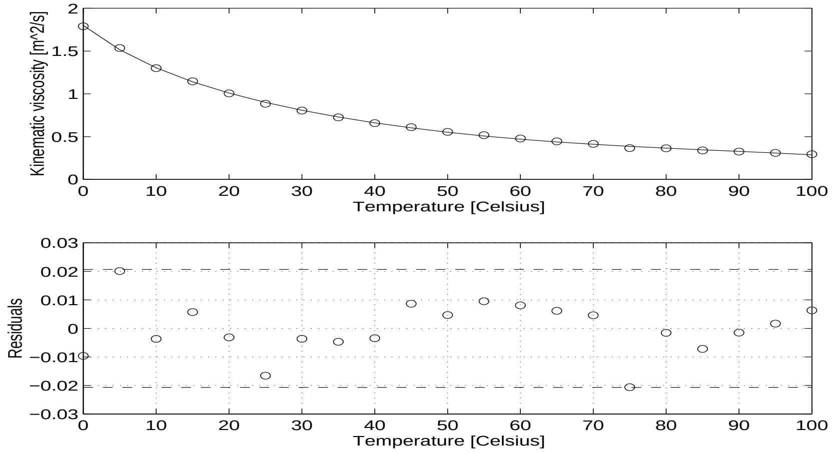

Figure A.4. *Regression's performance on kinematic viscosity.*

A.3 Product of c_p and ρ

In this section an analysis of the product of the specific heat c_p and the density ρ is analyzed. This product is of special interest for the radiator modelling, i.e. whether it is constant or not.

As in Chapter 6, let H_q denote the product of the specific heat c_p and the density ρ, implying that:

$$H_q(T_w) = c_p(T_w)\,\rho(T_w) \tag{A.12}$$

where c_p and ρ are as defined in (A.9) and (A.8), respectively.

Equation (A.12) is illustrated in Figure A.5 for water temperatures in the range of 0 °C to 100 °C.

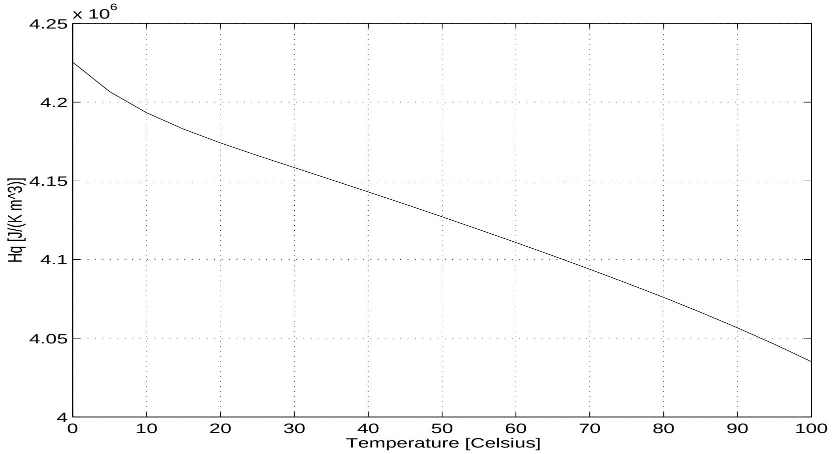

Figure A.5. *Product H_q of the specific heat c_p and the density ρ.*

The mean value of H_q is $\mu_H = 4.1{\cdot}10^6$ and the maximal deviation from the mean value is

$$\frac{H_q(0) - \mu_H}{\mu_H} = 2.4\ \% \tag{A.13}$$

Thus it is reasonable to consider H_q as a constant.

Appendix B

Identifiability

B.1 On the Dynamic One Exponent Formula

In this section the identifiability of the radiator model in Model Summary 6.1 will be investigated. The model of the j'th section is:

$$\frac{C}{\mathcal{N}}\frac{dT_j}{dt} = H_q q((1-\phi)T_{j-1} + (2\phi-1)T_j - \phi T_{j+1}) - \frac{\Phi_0}{\mathcal{N}}\left(\frac{T_j - T_a}{60}\right)^{n_1} \tag{B.1}$$

where $H_q = c_{p,w}\rho_w$ and $\phi \in [0, \frac{1}{2}]$. The model contains five parameters: the heat capacity of the radiator C, the gain factor H_q, the boundary temperature approximation parameter ϕ, the nominal radiator power Φ_0 and the radiator exponent n_1.

For $\mathcal{N} = 1$, the model is reduced to:

$$C\,\frac{dT}{dt} = H_q\,\rho\,(T_i - T)\ -\ \Phi_0\,\left(\frac{T - T_a}{60}\right)^{n_1} \tag{B.2}$$

as $\phi = 0$ for the "last" section, in order to assure the observability of the model, i.e. a first order model with two inputs and four parameters.

In order to investigate the structural identifiability of (B.2), it has to be linearized. The first order Taylor expansion has already been derived in Section 6.4.2 for a stationary operating point:

$$\begin{aligned} C\,\frac{d\overline{T}}{dt} &= -H_q\,q_{op}\,\overline{T} - \frac{n_1\,\Phi_0}{60}\left(\frac{T_{op}-T_{app}}{60}\right)^{n_1-1}\overline{T} \\ &\quad + H_q\,q_{op}\,\overline{T}_i \;+\; H_q\,(T_{i,op}-T_{op})\,\overline{q} \\ &\quad + \frac{n_1\,\Phi_0}{60}\left(\frac{T_{op}-T_{a,op}}{60}\right)^{n_1-1}\overline{T}_a \end{aligned} \tag{B.3}$$

where the index *op* indicates the specific operation point, the "bar" sign denotes a deviation from the operation point, e.g. $\overline{T} = T - T_{op}$. This linearized model is further Laplace transformed and rewritten as:

$$\begin{aligned} \left(\frac{C}{K_{op}}\,s+1\right)T(s) &= \frac{H_q\,q_{op}}{K_{op}}\,T_i(s) \;+\; \frac{H_q\,(T_{i,op}-T_{op})}{K_{op}}\,q(s) \\ &\quad + \frac{n_1\,\Phi_0}{60\,K_{op}}\left(\frac{T_{op}-T_{a,op}}{60}\right)^{n_1-1}T_a(s) \end{aligned} \tag{B.4}$$

where:

$$K_{op} = H_q\,q_{op} \;+\; \frac{n_1\,\Phi_0}{60}\left(\frac{T_{op}-T_{a,op}}{60}\right)^{n_1-1} \tag{B.5}$$

This model will now be compared with the following structure, where the parameters are identifiable:

$$(a_1\;s+1)\,T(s) = b_0\,T_i(s) + b_1\,q(s) + b_2\,T_a(s) \tag{B.6}$$

The task is to determine whether or not it is possible to derive the physical parameters from the identifiable parameters. The answer is no, the model is not structural identifiable. Therefore, one of the physical parameters has to be eliminated, by assuming that it is known. Selection of n_1 as the known parameter is a good choice, but the remaining model is still not identifiable. Hence, another parameter must be selected. H_q is selected this time, as the value of H_q is easy to estimate from the product of c_p and ρ.

In the special case when $q_{op} = 0$, (B.3) is reduced to:

$$\begin{aligned} C\,\frac{d\overline{T}}{dt} &= \frac{n_1\,\Phi_0}{60}\left(\frac{T_{op}-T_{a,op}}{60}\right)^{n_1} - \frac{n_1\,\Phi_0}{60}\left(\frac{T_{op}-T_{a,op}}{60}\right)^{n_1-1}\overline{T} \\ &\quad + \frac{n_1\,\Phi_0}{60}\left(\frac{T_{op}-T_{a,op}}{60}\right)^{n_1-1}\overline{T}_a \end{aligned} \tag{B.7}$$

It is observed that in the stationary operating point $T_{op} = T_{a,op}$, the model is indeed reduced. Therefore, it is necessary to assume that $n_1 = 1$ in this stationary operating point, which yields the proper model (for this situation):

$$C\,\frac{d\overline{T}}{dt} = -\frac{\Phi_0}{60}\,\overline{T} \;+\; \frac{\Phi_0}{60}\,\overline{T}_a \tag{B.8}$$

It is obvious that, for $q_{op} = 0$ it is only possible to identify one parameter, namely the product of $C\,\frac{60}{\Phi_0}$, alias the time constant.

For $\mathcal{N} \geq 2$, the structure of the model becomes more complex, but the number of parameters is still five. As the number of observed section temperature is independent of the approximation order (only the last section output is measured), the observability of the model is not improved, hence the number of identifiable parameters continuous to be two.

B.2 On the Thermostatic Valve

In this section the identifiability of the the models in Model Summary 7.1 and Model Summary 7.2 are investigated below.

B.2.1 Thermostatic Valve Model

The model the thermostatic valve presented in Model Summary 7.1 is summarized below:

$$\frac{dT_g}{dt} = \frac{1}{\tau_a}(T_a - T_g) + \frac{1}{\tau_w}(T_w - T_g) \tag{B.9}$$

$$X_p = T_{set} + 2 - T_g \tag{B.10}$$

$$\mathrm{K}_v(X_p) = \begin{cases} a\tanh(bX_p), & X_p > 0 \\ 0 & \text{otherwise} \end{cases} \tag{B.11}$$

Equation (B.11) can be approximated by the following power series expansion *(Råde and Westergren, 1990)*:

$$\mathrm{K}_v(X_p) \approx a\left(bX_p - \frac{(bX_p)^3}{3} + \frac{2(bX_p)^5}{15} - \cdots\right) \tag{B.12}$$

for $bX_p \in]-\pi/2, \pi/2[$ in general, but here limited to $bX_p \in]0, \pi/2[$.

Using (B.12) instead of (B.11) together with (B.9) and (B.10) the model satisfies the terms of the algorithm presented in *(Ljung and Glad, 1994)*. This model formulation has been tested on the algorithm. Unfortunately, some numerical problems occurred. Therefore, the identifiability of the thermostatic valve model is continued by "hand" calculations.

Consider the power series expansion of "tanh" in (B.12) truncated to the first term. For this case the thermostatic valve model is linear. Hence, applying Laplace transformation the following transfer function from the ambient temperature T_a to the valve constant K_v is derived:

$$\mathrm{K}_v(X_p) = -\frac{a\,b}{\tau_a s + 1} T_a \tag{B.13}$$

and from the set point temperature T_{set} to the valve constant K_v:

$$\mathrm{K}_v(X_p) = a\,b\,T_{set} \tag{B.14}$$

Thus, the two characteristic valve parameters a and b are not structural identifiable. The identifiability of these two parameters is not improved when the transfer function from the water supply temperature T_w is included. Neither including two or more terms in the truncation of (B.12) improves the identifiability of a and b.

B.2.2 Extended Model

The model the thermostatic valve presented in Model Summary 7.2 is summarized below:

$$\frac{dT_g}{dt} = \frac{1}{\tau_a}(T_a - T_g) + \frac{1}{\tau_w}(T_w - T_g) \tag{B.15}$$

$$X_p = T_{set} + 2 - T_g \tag{B.16}$$

$$\mathrm{K}_v(X_p) = \begin{cases} a\tanh(bX_p), & X_p > 0 \\ 0 & \text{otherwise} \end{cases} \tag{B.17}$$

$$q(X_p) = \frac{\mathrm{K}_v(X_p)}{\sqrt{R_s \mathrm{K}_v^2(X_p) + 1}} \sqrt{\Delta p_s} \tag{B.18}$$

For simplicity, consider the first term in the power series expansion (B.12) of "tanh", hence (B.17) is approximated as:

$$\mathrm{K}_v(X_p) \approx a\,b\,(T_{set} + 2 - T_g) \tag{B.19}$$

According to *(Råde and Westergren, 1990)* an inverse square root can be approximated by the power series expansion:

$$\frac{1}{\sqrt{x+1}} \approx 1 - \frac{1}{2}x + \frac{3}{8}x^2 - \frac{5}{16}x^3 - \cdots \tag{B.20}$$

Hence, applying the two first terms in the power series expansion above together with (B.19) and the Laplace transform of (B.15) imply that the transfer function for q can be written as:

$$\begin{aligned} q \quad \approx \quad & a\,b \left(T_{set} + 2 - \frac{1}{\tau_a s + 1} T_a\right) \\ & \left(1 - \frac{1}{2} R_s a^2 b^2 \left(T_{set} + 2 - \frac{1}{\tau_a s + 1} T_a\right)\right) \sqrt{\Delta p_s} \end{aligned} \tag{B.21}$$

From this transfer function it can be observed that a and b again occur as a product pair, thus neither in this case are a and b structural identifiable.

Appendix C

On the Test House

This Appendix describes the calculations of the thermal capacities and thermal resistances in the first section. The second section contains statistical tests and model performance for the non symmetric test house model proposed in Section 8.4.3. Additional measurements for the cross validation in Section 8.4.4, together with statistical tests and model performance are presented in the third section.

C.1 Thermal Test House Parameters

The thermal parameters of the test house are computed in this appendix. The calculations are based on the physical dimensions of the test house and handbook data.

Assuming that the two test rooms are perfectly identical, the following calculations of the thermal parameters are simplified. Hence are related to one test room.

Dimensions of the test house.

Room height: $l_h = 2.4$ m
Floor height (concrete): $l_c = 75$ mm
Floor area: $A_f = 30$ m^2

Length of room An: $l_l = \sqrt{2\,Af}$
Width of room An: $l_w = \frac{1}{2} l_l$

Area of center wall "aa": $A_{aa} = l_l\, l_h$
Area of center wall "ab": $A_{ab} = l_w\, l_h$
Area of outer wall "w": $A_w = A_{aa} + A_{ab}$

Volume of zone $\mathcal{Z}_{an}$: $V_{an} = A_f l_h$
Volume of zone $\mathcal{Z}_{af}$: $V_{af} = A_f l_h$

Handbook data.

The following data are imported from *(Thøgersen, 1992)*.

Density of air (20 °C): $\rho_a = 1.19$ kg/m^3
Density of concrete: $\rho_c = 2200$ kg/m^3

Heat capacity of air (20 °C): $c_{p,a} = 1.01$ kJ/(kg K)
Heat capacity of concrete: $c_{p,c} = 0.879$ kJ/(kg K)

Conductivity of mineral wool: $\lambda_m = 0.04$ W/(m K)

Convective coefficient (natural convection):
Horizontal: $h_h \sim 5$ W/(m^2 K)
Vertical: $h_v \sim 1$ W/(m^2 K)

Thermal heat capacities.

Zone $\mathcal{Z}_{an}$ (and $\mathcal{Z}_{as}$): $C_{an} = c_{p,a}\rho_a V_{an} \approx 85$ kJ/K
Zone $\mathcal{Z}_{af}$ (and $\mathcal{Z}_{fs}$): $C_{af} = c_{p,c}\rho_c V_{af} \approx 4.4$ MJ/K

Thermal resistances.

Thermal resistance R_{aa} between $\mathcal{Z}_{an}$ and $\mathcal{Z}_{as}$:

$$R_{aa} = \left(\frac{1}{h_h} + \frac{s_a}{\lambda_m} + \frac{1}{h_h}\right)/A_{aa} \quad \approx 0.15 \text{ K/W}$$

Thermal resistance R_{ab} between $\mathcal{Z}_{an}$ and $\bar{\mathcal{Z}}_b$:

$$R_{ab} = \left(\frac{1}{h_h} + \frac{s_a}{\lambda_m} + \frac{1}{h_h}\right)/A_{ab} \quad \approx 0.30 \text{ K/W}$$

Thermal resistance R_{wn} between $\mathcal{Z}_{an}$ and $\bar{\mathcal{Z}}_{en}$:

$$R_{wn} = \left(\frac{1}{h_h} + \frac{s_w}{\lambda_m} + \frac{1}{h_h}\right)/A_{wn} \approx 0.10 \text{ K/W}$$

Thermal resistance R_{fn} between $\mathcal{Z}_{an}$ and $\mathcal{Z}_{fn}$:

$$R_{fn} = \left(\frac{1}{h_v}\right)/A_f \qquad \approx 0.033 \text{ K/W}$$

where $s_a = 95$ mm and $s_w = 300$ mm (see Section 4.3).

C.2 Non Symmetric Radiator Power

Grey Box model for the test house with non symmetric radiator power submission:

$$dT_{an} = \frac{1}{C_a}\left[\frac{1}{R_f}(T_{fn}-T_{an}) + \frac{1}{R_a}(T_{as}-T_{an}) + \Phi_{ec} + \Phi_{rn} + \frac{1}{2R_a}(T_b - T_{an}) + \frac{1}{R_w}(T_n - T_{an})\right]dt + dW_1 \quad \text{(C.1)}$$

$$dT_{fn} = \frac{1}{R_f C_f}(T_{an} - T_{fn})\,dt + dW_2 \quad \text{(C.2)}$$

$$dT_{as} = \frac{1}{C_a}\left(\frac{1}{R_f}(T_{fs}-T_{as}) + \frac{1}{R_a}(T_{an}-T_{as}) + \frac{1}{2R_a}(T_b - T_{as}) + \frac{1}{R_w}(T_s - T_{as}) + (1-p)A_w I_s + \Phi_{rs}\right)dt + dW_3 \quad \text{(C.3)}$$

$$dT_{fs} = \left(\frac{1}{R_f C_f}(T_{as} - T_{fs}) + pA_w I_s\right)dt + dW_4 \quad \text{(C.4)}$$

$$\Phi_{rn} = \Phi_{0,n}\left(\frac{T_{i2} - T_{an}}{60}\right)^{n1} \quad \text{(C.5)}$$

$$\Phi_{rs} = \Phi_{0,s}\left(\frac{T_{i1} - T_{as}}{60}\right)^{n1} \quad \text{(C.6)}$$

$$\underline{Y}(k) = \begin{bmatrix} 1 & 0 & 0 & 0 \\ 0 & 0 & 1 & 0 \end{bmatrix}\underline{X}(k) + \underline{e}(k) \quad \text{(C.7)}$$

Statistical tests and model performance for the two test room temperatures are presented in Figure C.1, Figure C.2 and Figure C.3, Figure C.4, respectively.

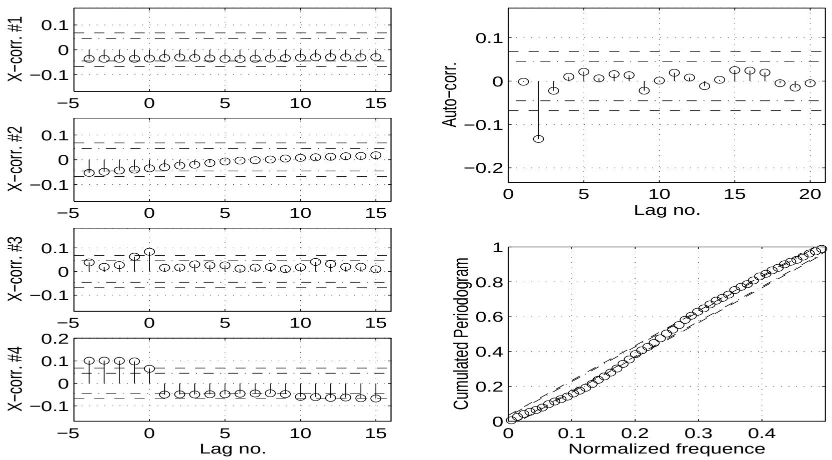

Figure C.1. *Statistical tests for the prediction error of T_{an}; showing the autocorrelation, cumulated periodogram and the crosscorrelations between $\#1 : T_b$, $\#2 : T_n$, $\#3 : T_{i2}$, $\#4 : \Phi_{ec}$ and the prediction error.*

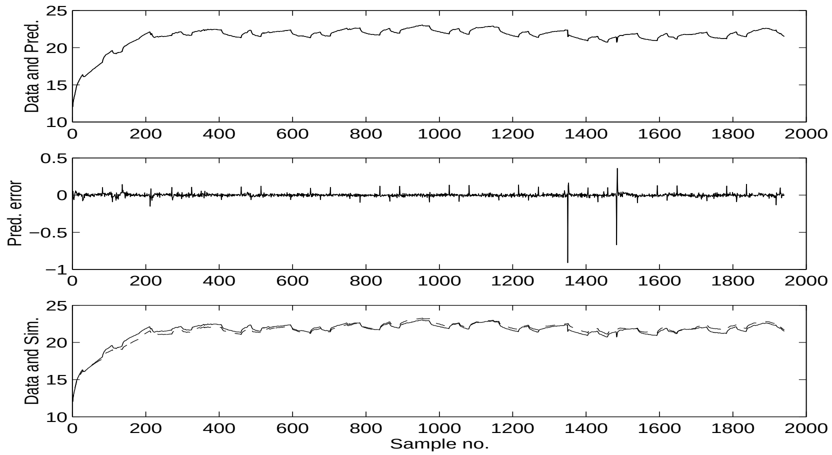

Figure C.2. *Model performance for T_{an} with $n_1 = 1.25$ and $p = 0$ (Sample time: 20 minutes).*

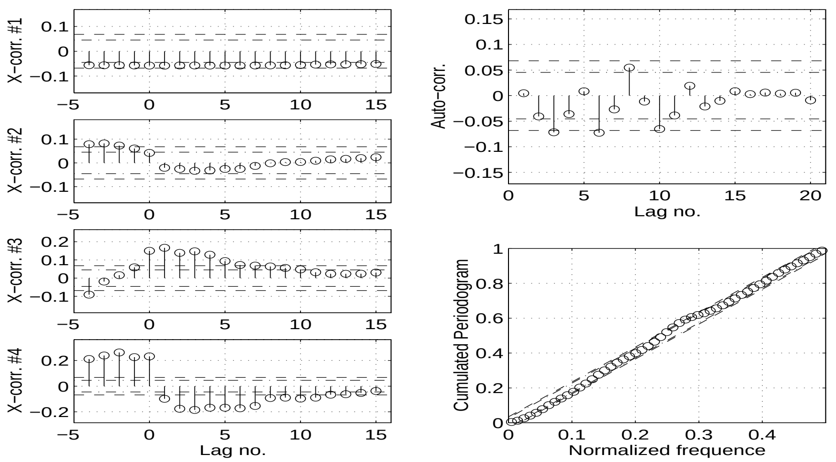

Figure C.3. *Statistical tests for the prediction error of T_{as}; showing the autocorrelation, cumulated periodogram and the crosscorrelations between $\#1 : T_b$, $\#2 : T_s$, $\#3 : T_{i1}$, $\#4 : \Phi_{sun}$ and the prediction error.*

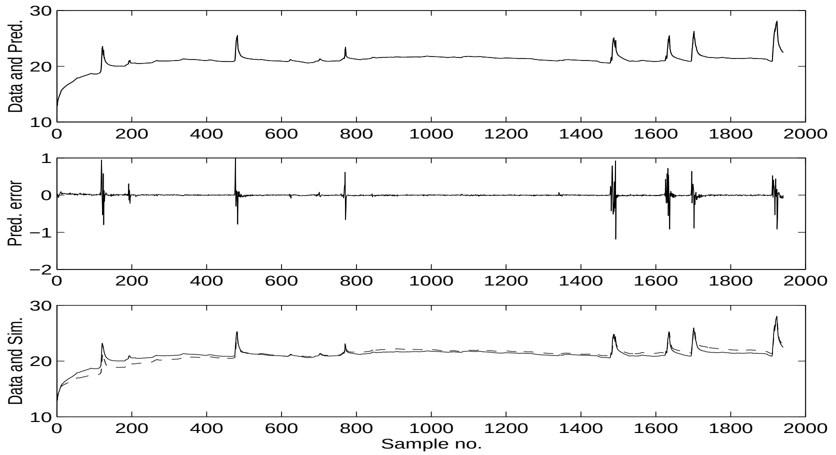

Figure C.4. *Model performance for T_{as} with $n_1 = 1.25$ and $p = 0$ (Sample time: 20 minutes).*

C.3 Cross Validation Data

This section presents the data set used in the cross validation for the test house models. The measurement period is approximately 13 days starting from December 23, 1996. The presented plots in Figure C.5, Figure C.6 and Figure C.7 follow the outline applied in Section 8.3.2. It is noted that $\Phi_{ec} = 0$ and that the levels for T_{hs} were increased to 60/75 °C for the low/high levels. The sampling time was 10 seconds.

Finally, statistical tests and model performance for the cross validation in Section 8.4.4 – for the test house model with the non symmetric radiator power submission – are presented in Figures C.8 to C.11.

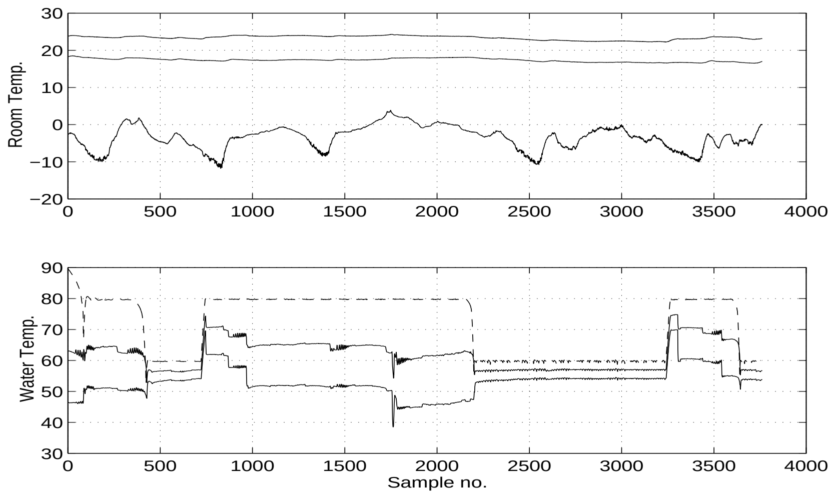

Figure C.5. *Validation data: Measurement data for room An (Sample time: 5 minutes).*

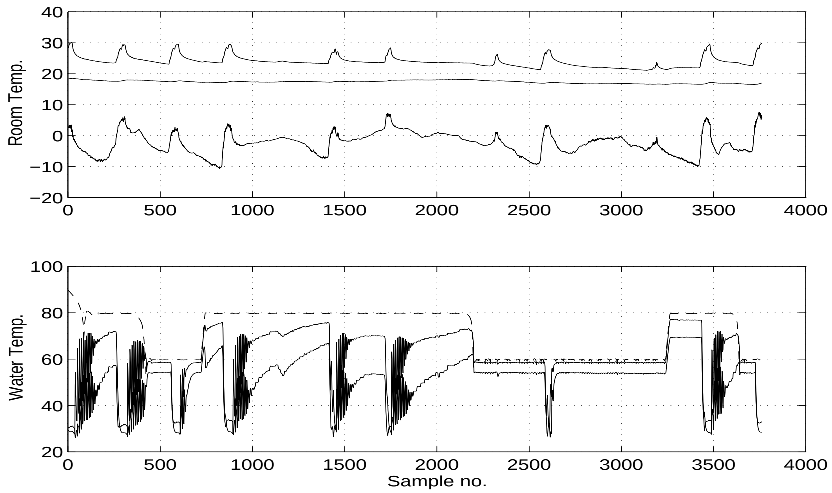

Figure C.6. *Validation data: Measurement data for room As (Sample time: 5 minutes).*

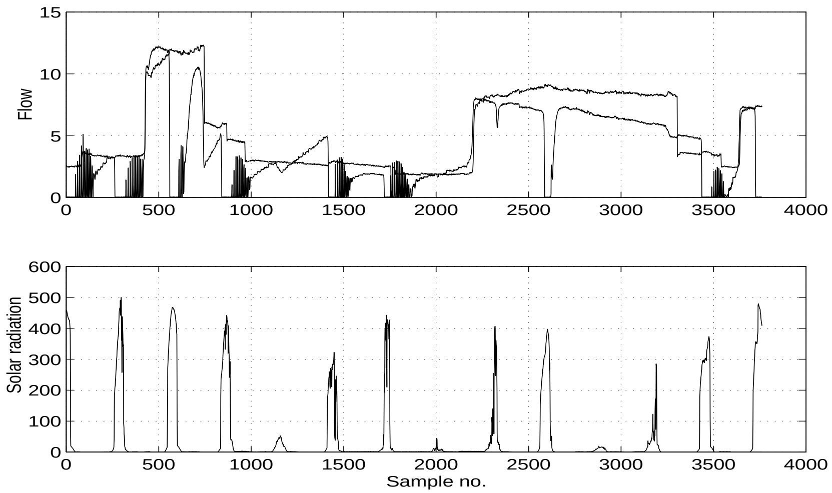

Figure C.7. *Validation data: Measurement data for water flows and solar radiation (Sample time: 5 minutes).*

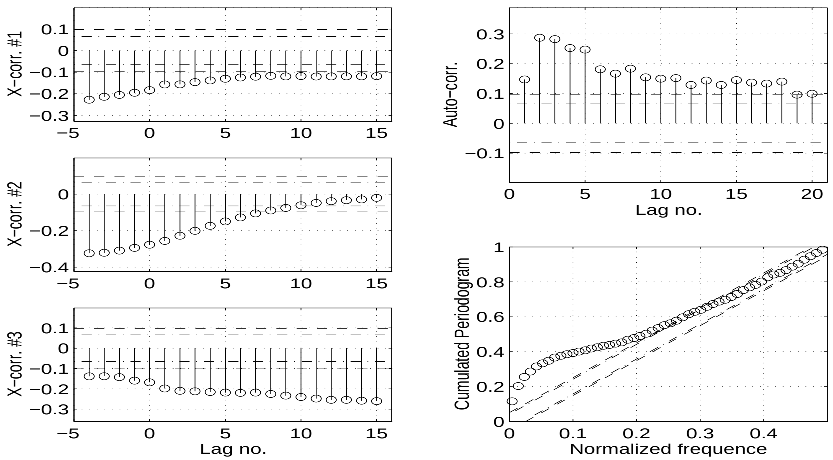

Figure C.8. *Statistical tests for the prediction error of T_{an}; showing the autocorrelation, cumulated periodogram and the crosscorrelations between $\#1 : T_b$, $\#2 : T_n$, $\#3 : T_{i2}$ and the prediction error.*

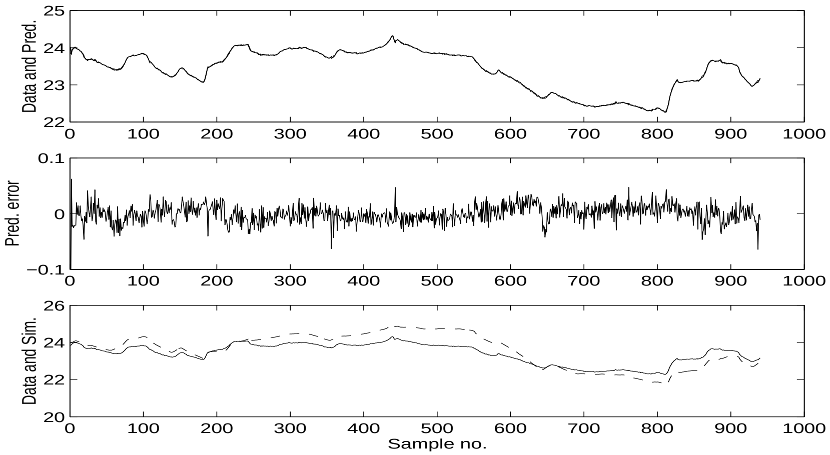

Figure C.9. *Model performance for T_{an} with $n_1 = 1.25$ and $p = 0$ (Sample time: 20 minutes).*

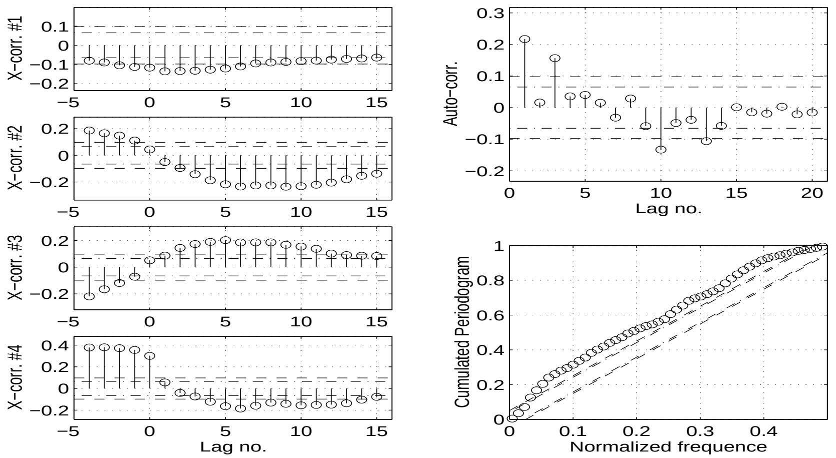

Figure C.10. *Statistical tests for the prediction error of T_{as}; showing the autocorrelation, cumulated periodogram and the crosscorrelations between* $\#1 : T_b$, $\#2 : T_s$, $\#3 : T_{i1}$, $\#4 : \Phi_{sun}$ *and the prediction error.*

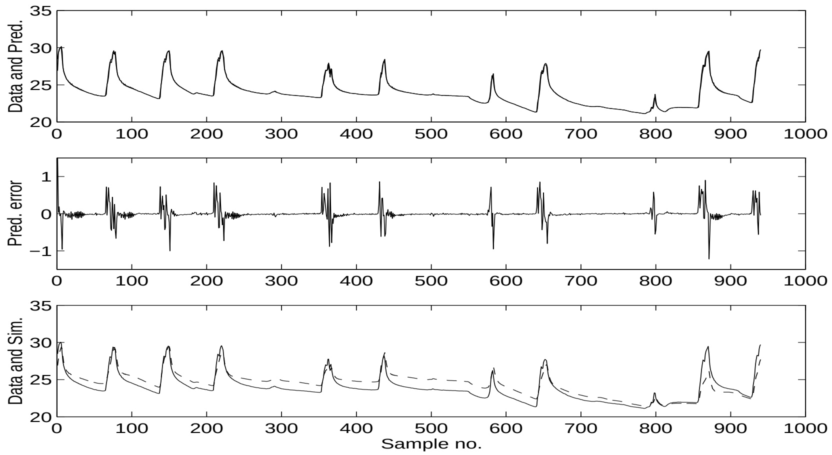

Figure C.11. *Model performance for T_{as} with $n_1 = 1.25$ and $p = 0$ (Sample time: 20 minutes).*

Bibliography

Aggerholm, S. (1983). *Simulation of Heat Installations. (Danish title: Simulering af varmeanlæg).* PhD thesis, Laboratory for Heat and Clima Engineering, the Technical University of Denmark.

Andersen, K. K. (1997). Stochastic Modelling of Energy Systems. (Danish title: Stokastisk modellering af energisystemer). Master's thesis, IMM, the Technical University of Denmark. No. xx/97, August.

Andersson, S. (1993). *Mathematical Models of Heat Exchangers. (Swedish title: Matematiska modeller för värmeväxlare).* PhD thesis, Department of Heat and Power Technology, LTH.

ASHRAE (1989). *Ashrae Handbook 1989, Fundamentals.* Atlanta, GA. SI edition.

Becher, P. (1972). *Heat and Ventilation, Volume 2. (Danish title: Varme og ventilation, Bind 2).* Teknisk Forlag.

Bloem, J. J. (1994). *System Identification applied to Building Performance Data.* Commission of the European Communities, DG XIII.

Box, G. E. P. and Jenkins, G. M. (1976). *Time Series Analysis, Forecasting and Control.* Holden-Day.

Chaudhry, M. H. (1987). *Applied Hydraulic Transients.* Van Nostrand Reinhold Company.

Conradsen, K. (1984). *A Introduction to Statistics, Volume 1B. (Danish title: En introduktion til Statistik, Bind 1B).* IMSOR, the Technical University of Denmark.

Danfoss (1988). *Thermostatic Radiator Valves, RA 2000/RA-FN og RA-G. (Danish title: Radiatortermostat/Ventilhuse, RA 2000/RA-FN og RA-G).* Danfoss A/S, VD.51.A5.01 edition.

Dansk Standard (1986). Rules of the Danish Engineer Association for Calculation of Heat Loss of Buildings. (Danish title: Dansk ingeniørforenings regler for beregning af bygningers varmetab). Technical report, Teknisk Forlag. NP-186-S. DS-418.

Dansk Standard (1988). Thermostatic Radiator Valves. Part 1: Requirements and Test Methods. (Danish title: Termostatiske radiator ventiler. Del 1: Krav og prøvningsmetoder). Technical report, Dansk Standard. DS/EN 215-1.

Data Translation (1995). *How to use DT VEE.* Data Translation, 1 edition.

Enright, W. H., Jackson, K. R., Nørsett, S. P., and Thomsen, P. G. (1988). Effective Solutions of Discontinuous IVPs using a Runga-Kutta Formula Pair with Interpolants. *Applied Mathematics and Computation*, 27:313–335.

Flinders, F., Senini, S., and Oghanna, W. (1993). Power Electronics Simulation Laboratory using "Simulink" Dynamic Systems Analysis Package. In *Proceedings of IMACS-TC1'93*, volume 1, pages 643–650. Ecole Polytechnique de Montréal.

Fox, R. W. and McDonald, A. T. (1985). *Introduction to Fluid Mechanics.* John Wiley & Sons.

Frederiksen, W. (1977). Central Heating Installations with Thermostatic Radiator Valves (Danish title: Varmeanlæg med radiatortermostater). *The Danfoss Journal*, 34(3):2–5.

Gammelby, J. (1974). Heizkörperthermostate. Grundsätze und Eigenschaften. *The Danfoss Journal*, 31(3).

Godfrey, K. R. (1980). Correlations Methods. *Automatica*, 16(2):527–534.

Goodwin, G. C. and Payne, R. L. (1977). *Dynamic System Identification: Experiment Design and Data Analysis.* Academic Press, Inc.

Grundfos (1991). *Pump Catalogue. (Danish title: Pumpekatalog).* Grundfos A/S, 3 edition.

Håkansson, L. (1988). Control Engineering (Control Valves). (Danish title: Reguleringsteknik (Styreventiler)). Technical report, Tour & Andersson Control A/S.

Hallgreen, L. and Paulsen, O. (1982). Low Temperature Heat Installations. (Danish title: Lavtemperatur varmeanlæg – Dimensionering af radiatorer). Technical report, Heat Engineering, Institute of Technology.

Hansen, F. M. (1985). Heat Supply for Buildings – Estimation and Optimal Control. (Danish title: Varmetilførsel til bygninger (Estimation og optimal regulering). Master's thesis, IMSOR, the Technical University of Denmark. No. 2/85.

Hansen, L. H. (1996). Dynamic Analysis of a low Energy Test House and a Central Heating System. Technical Report No. 20, Department of Mathematical Modelling, the Technical University of Denmark.

Hansen, L. H., Bidstrup, N., Madsen, H., Vadstrup, P., and Holst, J. (1995). A Hydraulic Simulink Model of the Heating System in a Single Family House. In Langemyr, L., editor, *Nordic Matlab Conference '95*, volume II, pages 114–118. Computer Solutions Europe AB, Sweden.

Holst, J., Holst, H., Madsen, H., and Melgaard, H. (1992). Validation of Grey-Box Models. In *Symposium on Adaptive Systems in Control and Signal Processing.* IFAC. Grenoble, France.

Johansen, J., Paulsen, O., Svenningsen, N., and Øhrgaard, P. (1979). Heat Contributions of the Heater. (Danish title: Vandvarmeovnens varmeydelser). Technical report, Heat and Installation Engineering, Institute of Technology. Report 2.

Jonsson, G. (1990). *Parameter Estimation in Models of Heat Exchangers and Geothermal Reservoirs*. PhD thesis, Department of Mathematical Statistics, LTH.

Kariž, Z., Bajsić, I., and Dimovski, D. (1989). Local Controlling of Air Temperature with Thermostatic Valves. In *Clima 2000*, pages 251–255.

Katsuhiko, O. (1970). *Modern Control Engineering*. Prentice-Hall International, Inc.

Kloeden, P. E. and Platen, E. (1989). A Survey of Numerical Methods for Stochastic Differential Equations. *Stochastic Hydrology and Hydraulics*, 3:155–178.

Kloeden, P. E., Platen, E., and Schurz, H. (1991). The Numerical Solution of Nonlinear Stochastic Dynamical Systems: A brief Introduction. *International Journal of Bifurcation and Chaos*, 1(2):277–286.

Larsen, P. S. (1984). *Thermodynamics. (Danish title: Termodynamik)*. Polyteknisk Forlag.

Lawaetz, H. (1984). Radiator Dimensioning. (Danish title: Radiatordimensionering). Technical report, Institute of Technology. Notat 2/84.

Lawaetz, H. and Bøhm, B. (1985). Heat Supply Installations. (Danish title: Varmeforsyningsanlæg). Technical report, Institute of Technology.

Lindfors, A. (1994). Frequency domain techniques for estimation of thermal parameters. In *System Identification applied to Building Performance Data*. Commission of the European Communities, DG XIII.

Ljung, L. (1987). *System Identification - Theory for the User*. Prentice-Hall, Englewood Cliffs, New Jersey.

Ljung, L. and Glad, T. (1994). On Global Identification for Arbitrary Model Parametrization. *Automatica*, 30(2):265–276.

Madsen, H. (1995). *Time Series Analysis. (In Danish: Tidsrækkeanalyse)*. IMM, the Technical University of Denmark, 2 edition.

Madsen, H. and Holst, J. (1996). *Modelling Non-Linear and Non-Statinary Time Series*. IMM, the Technical University of Denmark.

Madsen, H. and Melgaard, H. (1991). The Mathematical and Numerical Methods used in CTLSM. Technical Report No. 7, IMSOR, the Technical University of Denmark.

Madsen, H., Melgaard, H., and Holst, J. (1990). Identification of Building Performance Parameters. In Bloem, J. J., editor, *Workshop on Advanced Identification Tools in Solar Energy Research*, Non Nuclear Energy, pages 37–60. Commission of the European Communities, DG XII.

Melgaard, H. (1994). *Identification of Physical Models*. PhD thesis, IMM, the Technical University of Denmark.

Melgaard, H. and Madsen, H. (1993). CTLSM - Continuous Time Linear Stochastic Modeling, Version 2.6. Technical Report No. 1, IMSOR, the Technical University of Denmark.

Nielsen, J. N., Baadsgaard, M., and Madsen, H. (1997). *Statistics in Finance (Lecture Notes)*. IMM, the Technical University of Denmark.

Øksendal, B. (1995). *Stochastic Differential Equations*. Springer-Verlag, 4 edition.

Paulsen, O. and Gundtoft, S. (1985). Dynamical Testing of small Heat Instalations. (Danish title: Dynamisk afprøvning af små varmecentraler).

Technical report, Institute of Technology, Jutlandic Institute of Technology.

Pfleiderer, C. (1961). *Die Kreiselpumpen für Flussigkeiten und Gase.* Springer-Verlag.

Rabl, A. (1994). Application of parameter identification in buildings – an overview. In *System Identification applied to Building Performance Data.* Commission of the European Communities, DG XIII.

Råde, L. and Westergren, B. (1990). *Beta β, Mathematics Handbook.* Chartwell-Bratt, 2 edition.

Rasmussen, N. H. and Saxhof, B. (1982). Simultaneous Testing of Heating Systems. Technical Report No. 128, Thermal Insulation Laboratory, the Technical University of Denmark.

Raznjević, K. (1976). *Handbook of Thermodynamic Tables and Charts.* Hemisphere Publishing Corporation.

Sadegh, P. (1996). *Experiment Design and Optimization in Complex Systems.* PhD thesis, IMM, the Technical University of Denmark.

Sadegh, P., Hansen, L. H., Madsen, H., and Holst, J. (1997). Maxmin Input Design for Linear Dynamic Systems. *Journal of Information & Optimization Sciences.* Accepted and in print.

Söderström, T. and Stoica, P. (1989). *System Identification.* Prentice-Hall Internation, Inc.

Sonderegger, R. C. (1978). *Dynamic Models of House Heating based on Equivalent Thermal Parameters.* PhD thesis, Princeton University, Princeton, N.J. 08540. Report PU/CES 57.

Svensson, A. (1978). Functionality of Thermostatic Radiator Valves. (Swedish title: Radiatortermostatventilors funktion). Technical report, The national Swedish Institute for Building Research. Lägesrapport M78:4.

Thøgersen, L. K. (1992). *Thermal Handbook. (Danish title: Varme ståbi).* Teknisk Forlag, 2 edition.

Thor Eura (1990). *Thor Riffel Radiators. (Danish title: Thor Riffel Radiatorer).* Northor A/S, 1 edition.

Wahlberg, B. and Ljung, L. (1986). Design Variables for Bias Distribution in Transfer Function Estimation. *IEEE, Transactions on Automatic Control*, 31(2):134–144.

Weber, A. P. (1970). *Die Warmwasserheizung.* R. Oldenbourg, München.

Wollerstrand, J. (1993). *District Heating Substations with Counter Flow Heat Exchangers for Hot-Water Production. (Swedish title: Fjärrvärme-abonnentcentraler med genomströmningsberedare för tappvarmvatten).* PhD thesis, Department of Heat and Power Technology, LTH.

Zoebl, H. and Kruschik, J. (1978). *Strömung durch Rohre und Ventile.* Springer-Verlag.

Index

Ph. D. theses from IMM

1. **Larsen, Rasmus.** (1994). *Estimation of visual motion in image sequences. xiv* + 143 pp.
2. **Rygard, Jens Moberg.** (1994). *Design and optimization of flexible manufacturing systems. xiii* + 232 pp.
3. **Lassen, Niels Christian Krieger.** (1994). *Automated determination of crystal orientations from electron backscattering patterns. xv* + 136 pp.
4. **Melgaard, Henrik.** (1994). *Identification of physical models. xvii* + 246 pp.
5. **Wang, Chunyan.** (1994). *Stochastic differential equations and a biological system. xxii* + 153 pp.
6. **Nielsen, Allan Aasbjerg.** (1994). *Analysis of regularly and irregularly sampled spatial, multivariate, and multi-temporal data. xxiv* + 213 pp.
7. **Ersbøll, Annette Kjær.** (1994). *On the spatial and temporal correlations in experimentation with agricultural applications. xviii* + 345 pp.
8. **Møller, Dorte.** (1994). *Methods for analysis and design of heterogeneous telecommunication networks.* Volume 1-2, *xxxviii* + 282 pp., 283-569 pp.
9. **Jensen, Jens Christian.** (1995). *Teoretiske og eksperimentelle dynamiske undersøgelser af jernbanekøretøjer.* ATV Erhvervsforskerprojekt EF 435. *viii* + 174 pp.

10. **Kuhlmann, Lionel.** (1995). *On automatic visual inspection of reflective surfaces.* ATV Erhvervsforskerprojekt EF 385. Volume 1, *xviii* + 220 pp., (Volume 2, *vi* + 54 pp., fortrolig).
11. **Lazarides, Nikolaos.** (1995). *Nonlinearity in superconductivity and Josephson Junctions.* *iv* + 154 pp.
12. **Rostgaard, Morten.** (1995). *Modelling, estimation and control of fast sampled dynamical systems.* *xiv* + 348 pp.
13. **Schultz, Nette.** (1995). *Segmentation and classification of biological objects.* *xiv* + 194 pp.
14. **Jørgensen, Michael Finn.** (1995). *Nonlinear Hamiltonian systems.* *xiv* + 120 pp.
15. **Balle, Susanne M.** (1995). *Distributed-memory matrix computations.* *iii* + 101 pp.
16. **Kohl, Niklas.** (1995). *Exact methods for time constrained routing and related scheduling problems.* *xviii* + 234 pp.
17. **Rogon, Thomas.** (1995). *Porous media: Analysis, reconstruction and percolation.* *xiv* + 165 pp.
18. **Andersen, Allan Theodor.** (1995). *Modelling of packet traffic with matrix analytic methods.* *xvi* + 242 pp.
19. **Hesthaven, Jan.** (1995). *Numerical studies of unsteady coherent structures and transport in two-dimensional flows.* Risø-R-835(EN) 203 pp.
20. **Slivsgaard, Eva Charlotte.** (l995). *On the interaction between wheels and rails in railway dynamics.* *viii* + 196 pp.

21. **Hartelius, Karsten.** (1996). *Analysis of irregularly distributed points.* *xvi* + 260 pp.
22. **Hansen, Anca Daniela.** (1996). *Predictive control and identification - Applications to steering dynamics.* *xviii* + 307 pp.
23. **Sadegh, Payman.** (1996). *Experiment design and optimization in complex systems.* *xiv* + 162 pp.
24. **Skands, Ulrik.** (1996). *Quantitative methods for the analysis of electron microscope images.* *xvi* + 198 pp.
25. **Bro-Nielsen, Morten.** (1996). *Medical image registration and surgery simulation.* *xxvii* + 274 pp.
26. **Bendtsen, Claus.** (1996). *Parallel numerical algorithms for the solution of systems of ordinary differential equations.* *viii* + 79 pp.
27. **Lauritsen, Morten Bach.** (1997). *Delta-domain predictive control and identification for control.* *xxii* + 292 pp.
28. **Bischoff, Svend.** (1997). *Modelling Colliding-pulse mode-locked semiconductor lasers.* *xxii* + 217 pp.
29. **Arnbjerg-Nielsen, Karsten.** (1997). *Statistical analysis of urban hydrology with special emphasis on rainfall modelling.* Institut for Miljøteknik, DTU. *xiv* + 161 pp.
30. **Jacobsen, Judith L.** (1997). *Dynamic modelling of processes in rivers affected by precipitation runoff.* *xix* + 213 pp.
31. **Sommer, Helle Mølgaard.** (1997). *Variability in microbiological degradation experiments. - Analysis and case stydy.* *xiv* + 211 pp.

32. **Ma, Xin.** (1997). *Adaptive extremum control and wind turbine control.* *xix* + 293 pp.

33. **Rasmussen, Kim Ørskov.** (1997). *Nonlinear and stochastic dynamics of coherent structures.* *x* + 215 pp.

34. **Hansen, Lars Henrik.** (1997). *Stochastic modelling of central heating systems.* *xxii* + 301 pp.